frontiers | Research Topics

Added value of 3D imaging in the diagnosis and prognostication of patients with right ventricular dysfunction

Edited by
Attila Kovacs, Márton Tokodi and Elena Surkova

Published in
Frontiers in Cardiovascular Medicine

ISSN 1664-8714
ISBN 978-2-8325-4331-3
DOI 10.3389/978-2-8325-4331-3

About Frontiers

Frontiers is more than just an open access publisher of scholarly articles: it is a pioneering approach to the world of academia, radically improving the way scholarly research is managed. The grand vision of Frontiers is a world where all people have an equal opportunity to seek, share and generate knowledge. Frontiers provides immediate and permanent online open access to all its publications, but this alone is not enough to realize our grand goals.

Frontiers journal series

The Frontiers journal series is a multi-tier and interdisciplinary set of open-access, online journals, promising a paradigm shift from the current review, selection and dissemination processes in academic publishing. All Frontiers journals are driven by researchers for researchers; therefore, they constitute a service to the scholarly community. At the same time, the *Frontiers journal series* operates on a revolutionary invention, the tiered publishing system, initially addressing specific communities of scholars, and gradually climbing up to broader public understanding, thus serving the interests of the lay society, too.

Dedication to quality

Each Frontiers article is a landmark of the highest quality, thanks to genuinely collaborative interactions between authors and review editors, who include some of the world's best academicians. Research must be certified by peers before entering a stream of knowledge that may eventually reach the public - and shape society; therefore, Frontiers only applies the most rigorous and unbiased reviews. Frontiers revolutionizes research publishing by freely delivering the most outstanding research, evaluated with no bias from both the academic and social point of view. By applying the most advanced information technologies, Frontiers is catapulting scholarly publishing into a new generation.

What are Frontiers Research Topics?

Frontiers Research Topics are very popular trademarks of the *Frontiers journals series*: they are collections of at least ten articles, all centered on a particular subject. With their unique mix of varied contributions from Original Research to Review Articles, Frontiers Research Topics unify the most influential researchers, the latest key findings and historical advances in a hot research area.

Find out more on how to host your own Frontiers Research Topic or contribute to one as an author by contacting the Frontiers editorial office: frontiersin.org/about/contact

Added value of 3D imaging in the diagnosis and prognostication of patients with right ventricular dysfunction

Topic editors

Attila Kovacs — Semmelweis University, Hungary

Márton Tokodi — Semmelweis University, Hungary

Elena Surkova — Royal Brompton Hospital, United Kingdom

Citation

Kovacs, A., Tokodi, M., Surkova, E., eds. (2024). *Added value of 3D imaging in the diagnosis and prognostication of patients with right ventricular dysfunction*. Lausanne: Frontiers Media SA. doi: 10.3389/978-2-8325-4331-3

Table of contents

frontiers | Frontiers in Cardiovascular Medicine

TYPE Editorial
PUBLISHED 09 January 2024
DOI 10.3389/fcvm.2023.1356294

OPEN ACCESS

EDITED AND REVIEWED BY
Christos Bourantas,
Queen Mary University of London, United Kingdom

*CORRESPONDENCE
Attila Kovács
attila.kovacs@med.semmelweis-univ.hu

RECEIVED 15 December 2023
ACCEPTED 26 December 2023
PUBLISHED 09 January 2024

CITATION
Kovács A, Tokodi M and Surkova E (2024) Editorial: Added value of 3D imaging in the diagnosis and prognostication of patients with right ventricular dysfunction.
Front. Cardiovasc. Med. 10:1356294.
doi: 10.3389/fcvm.2023.1356294

Editorial: Added value of 3D imaging in the diagnosis and prognostication of patients with right ventricular dysfunction

Attila Kovács[1,2]*, Márton Tokodi[1,2] and Elena Surkova[3]

[1]Heart and Vascular Center, Semmelweis University, Budapest, Hungary, [2]Department of Surgical Research and Techniques, Semmelweis University, Budapest, Hungary, [3]Royal Brompton and Harefield Hospitals, Part of Guy's and St. Thomas' NHS Foundation Trust, London, United Kingdom

KEYWORDS

right ventricle, right ventricular dysfunction, 3D echocardiography, cardiac magnetic resonance imaging, diagnostics, outcomes, prognostication

Editorial on the Research Topic
Added value of 3D imaging in the diagnosis and prognostication of patients with right ventricular dysfunction

Right ventricular (RV) function is an important prognostic factor in various cardiovascular conditions, such as in heart failure with reduced and preserved left ventricular (LV) ejection fraction (EF) or in pulmonary arterial hypertension (1). The quantification of RV function is also a cornerstone of perioperative risk assessment (2) and the management of patients with mechanical circulatory support devices or adults with congenital heart disease (3). Nevertheless, the precise assessment of RV function is challenging due to its complex geometry and mechanics. Three-dimensional (3D) imaging techniques may help clinicians overcome some of these hurdles, allowing them to capture even subtle changes in RV function related to pressure- and volume overload (4), which may be undetectable using conventional imaging parameters. Thus, advanced 3D imaging-based indices of RV function may improve diagnostics and prognostication in numerous diseases (5).

This Research Topic comprises articles providing valuable insights into the intricacies of RV mechanics in both health and disease and showing the added value of 3D imaging in diagnosing RV dysfunction and predicting outcomes.

Using cardiac magnetic resonance (CMR) imaging—the gold-standard imaging modality for assessing RV size and function, a group of investigators analyzed the RV myocardial architecture in two separate articles. In the first one, Kiss et al. described the age- and sex-specific characteristics of RV compacted and trabeculated myocardium using CMR in 200 healthy volunteers. They found that RV compacted (RV-CMi) and trabeculated myocardial mass indices (RV-TMi) were higher in men than in women, and RV-TMi decreased with advancing age in the latter group. Furthermore, LV-CMi and LV-TMi, RV end-systolic volume, and sex were independent predictors of RV-TMi. In the second article, Kiss et al. measured RV volumetric, functional, and feature-tracking strain parameters in 100 patients with LV non-compaction (LVNC) phenotype and normal LVEF and compared them to those of 100 age- and sex-matched healthy controls. They observed that patients with LVNC had higher RV volumes and lower

RV global and septal strain values than controls. Twenty-two percent of the analyzed LVNC patients had an RV-TMi above the reference range, and these patients had higher biventricular volumes, lower biventricular EFs, and worse RV strains than patients with normal RV-TMi. Moreover, there was a strong positive correlation between RV-TMi and LV-TMi, and both showed inverse relationships with RV function.

Besides CMR imaging, 3D echocardiography also has a crucial role in assessing RV size and function. Importantly, 3D echocardiography-derived parameters (e.g., RVEF) have significant prognostic utility, which was also demonstrated by Nabeshima et al. in 392 patients with asymptomatic aortic stenosis. They found that a lower RVEF at baseline was associated with an increased risk of cardiac events. Moreover, RVEF had incremental prognostic value over indexed aortic valve area, LVEF, and two-dimensional echocardiography-derived RV parameters.

In another study, Lan et al. investigated the effects of combined ambrisentan and phosphodiesterase type 5 inhibitor therapy on RV-pulmonary artery coupling (RV-PA coupling, assessed by different echocardiographic parameters, such as the ratio of 3D RV stroke volume and 3D RV end-systolic volume) in a retrospective study including 27 patients with severe pulmonary arterial hypertension. Six months of therapy resulted in significantly improved RV-PA coupling, World Health Organization functional class, 6-min walk distance, N-terminal pro-B-type natriuretic peptide concentration, and reduced pulmonary artery pressures and pulmonary vascular resistance assessed by right heart catheterization.

Beyond the assessment of global RV function, 3D echocardiography, in combination with advanced post-processing software solutions, can also be used for the comprehensive analysis of the RV contraction pattern. One such tool is ReVISION—a thoroughly validated, FDA-cleared, commercially available software solution—which decomposes the motion of the RV along its three orthogonal axes (i.e., longitudinal, radial, and anteroposterior axis), quantifies the contribution of these three motion components to global RV function, and computes 3D RV longitudinal, circumferential, and area strains (6, 7). ReVISION has already been used to characterize the contribution of the three motion components to global RV function in healthy adults (8, 9). However, this software solution has not yet been thoroughly tested in healthy pediatric cohorts. Motivated by this, Valle et al. initiated a two-center study to analyze the RV motion components using ReVISION in healthy children. They demonstrated that assessing the components of RV motion is also feasible in a pediatric population and found that shortening along the anteroposterior axis is the dominant component of RV contractions in healthy children.

To investigate the prognostic value of 3D RV strains measured using ReVISION, Kitano et al. sought to analyze the data of 341 patients with various cardiac diseases. 3D RV strain values (i.e., 3D RV global longitudinal, circumferential, and area strains) were significantly associated with the composite endpoint of cardiac death, ventricular tachyarrhythmia, or heart failure hospitalization, even after adjusting for age, chronic kidney disease, and LV systolic and diastolic parameters. Similarly, Tolvaj et al. also aimed to determine the prognostic power of 3D echocardiography-derived LV and RV strains. In their cohort of 357 patients with different left-sided cardiac diseases, impaired values of 3D LV and RV global circumferential strains were associated with long-term all-cause mortality, emphasizing the prognostic relevance of biventricular circumferential mechanics.

ReVISION was also tested by Evrard et al., who investigated patients ventilated due to moderate-to-severe acute respiratory distress syndrome (ARDS): 21 with ARDS related to SARS-CoV-2, 22 with ARDS unrelated to SARS-CoV-2, and 21 without ARDS. They performed a 3D transesophageal echocardiographic examination on each patient within 24 h after admission and found that RV systolic dysfunction is more pronounced in ARDS unrelated to SARS-CoV-2 than in SARS-CoV-2-related ARDS. Moreover, when analyzing the RV contraction pattern using ReVISION, they observed that the contribution of radial shortening to global RV function was reduced in patients with ARDS unrelated to SARS-CoV-2 compared to the other two groups, whereas the contributions of the other motion components (i.e., shortening along the longitudinal and anteroposterior axes) were unchanged.

Remaining in the realm of intensive care units and operating theatres, Keller et al. analyzed the associations between 3D transesophageal echocardiography-derived parameters of regional RV function and short-term outcomes in 357 patients undergoing elective cardiac surgery. They observed that a higher ratio of apical vs. inflow tract stroke volumes [assessed using their previously published custom-made software solution (10)] was independently associated with the composite of in-hospital mortality and/or the need for extracorporeal life support, underlining the importance of RV evaluation on the segmental level.

Acquiring 3D echocardiographic datasets suitable for 3D analysis might not always be feasible from the apical view. To explore whether 3D datasets can also be acquired from an alternative view, Ferraro et al. measured RV volumes on 3D echocardiographic datasets acquired from apical and subcostal views in pediatric patients and compared these measurements to the corresponding CMR-derived values. RV volumes measured from both echocardiographic views showed similarly good agreement with the CMR-derived RV volumes, confirming that the subcostal view can be an alternative to the apical view in this context.

Last but not least, in a comprehensive review article, Randazzo et al. discussed the current capabilities of 3D echocardiography to enhance RV evaluation and speculated on what the future may hold for the echocardiographic assessment of the RV.

In conclusion, this collection of articles underscores the pivotal role of 3D imaging in assessing RV structure and function across diverse clinical scenarios. Beyond providing a better understanding of the (patho)physiology of the RV, these advanced imaging techniques have true potential to enhance the detection of RV dysfunction and risk stratification, ultimately leading to improved patient care and outcomes.

Author contributions

AK: Conceptualization, Funding acquisition, Supervision, Writing – original draft, Writing – review & editing. MT: Conceptualization, Supervision, Validation, Writing – original draft, Writing – review & editing. ES: Conceptualization, Supervision, Validation, Writing – original draft, Writing – review & editing.

Funding

The author(s) declare financial support was received for the research, authorship, and/or publication of this article.

Project no. RRF-2.3.1-21-2022-00003 has been implemented with the support provided by the European Union. This project was also supported by a grant from the National Research, Development and Innovation Office (NKFIH) of Hungary (FK 142573 to AK). AK was supported by the Janos Bolyai Research Scholarship of the Hungarian Academy of Sciences.

Conflict of interest

AK serves as Chief Medical Officer of Argus Cognitive, Inc., and receives financial compensation for his work. ES is an employee and shareholder of AstraZeneca, and reports speaker honoraria from GE Healthcare and 123sonography, outside of the submitted work. MT reports personal fees from CardioSight, Inc., outside the submitted work.

The author(s) declared that they were an editorial board member of Frontiers, at the time of submission. This had no impact on the peer review process and the final decision.

Publisher's note

References

1. Surkova E, Kovacs A, Tokodi M, Lakatos BK, Merkely B, Muraru D, et al. Contraction patterns of the right ventricle associated with different degrees of left ventricular systolic dysfunction. *Circ Cardiovasc Imaging*. (2021) 14(10):e012774. doi: 10.1161/CIRCIMAGING.121.012774

2. Tokodi M, Nemeth E, Lakatos BK, Kispal E, Toser Z, Staub L, et al. Right ventricular mechanical pattern in patients undergoing mitral valve surgery: a predictor of post-operative dysfunction? *ESC Heart Fail*. (2020) 7(3):1246–56. doi: 10.1002/ehf2.12682

3. Surkova E, Kovacs A, Lakatos BK, Tokodi M, Fabian A, West C, et al. Contraction patterns of the systemic right ventricle: a three-dimensional echocardiography study. *Eur Heart J Cardiovasc Imaging*. (2022) 23(12):1654–62. doi: 10.1093/ehjci/jeab272

4. Bidviene J, Muraru D, Maffessanti F, Ereminiene E, Kovacs A, Lakatos B, et al. Regional shape, global function and mechanics in right ventricular volume and pressure overload conditions: a three-dimensional echocardiography study. *Int J Cardiovasc Imaging*. (2021) 37(4):1289–99. doi: 10.1007/s10554-020-02117-8

5. Sayour AA, Tokodi M, Celeng C, Takx RAP, Fabian A, Lakatos BK, et al. Association of right ventricular functional parameters with adverse cardiopulmonary outcomes: a meta-analysis. *J Am Soc Echocardiogr*. (2023) 36 (6):624–33.e8. doi: 10.1016/j.echo.2023.01.018

6. Lakatos B, Tősér Z, Tokodi M, Doronina A, Kosztin A, Muraru D, et al. Quantification of the relative contribution of the different right ventricular wall motion components to right ventricular ejection fraction: the ReVISION method. *Cardiovasc Ultrasound*. (2017) 15(1):8. doi: 10.1186/s12947-017-0100-0

7. Tokodi M, Staub L, Budai Á, Lakatos BK, Csákvári M, Suhai FI, et al. Partitioning the right ventricle into 15 segments and decomposing its motion using 3D echocardiography-based models: the updated ReVISION method. *Front Cardiovasc Med*. (2021) 8:622118. doi: 10.3389/fcvm.2021.622118

8. Lakatos BK, Nabeshima Y, Tokodi M, Nagata Y, Tősér Z, Otani K, et al. Importance of nonlongitudinal motion components in right ventricular function: three-dimensional echocardiographic study in healthy volunteers. *J Am Soc Echocardiogr*. (2020) 33(8):995–1005.e1. doi: 10.1016/j.echo.2020.04.002

9. Cotella JI, Kovacs A, Addetia K, Fabian A, Asch FM, Lang RM, et al. Three-dimensional echocardiographic evaluation of longitudinal and non-longitudinal components of right ventricular contraction: results from the world alliance of societies of echocardiography study. *Eur Heart J Cardiovasc Imaging*. (2023). doi: 10.1093/ehjci/jead213

10. Nowak-Machen M, Lang T, Schilling A, Mockenhaupt L, Keller M, Rosenberger P, et al. Regional right ventricular volume and function analysis using intraoperative 3-dimensional echocardiography-derived mesh models. *J Cardiothorac Vasc Anesth*. (2019) 33(6):1527–32. doi: 10.1053/j.jvca.2019.02.011

frontiers in Cardiovascular Medicine

ORIGINAL RESEARCH
published: 07 December 2021
doi: 10.3389/fcvm.2021.781393

Age- and Sex-Specific Characteristics of Right Ventricular Compacted and Non-compacted Myocardium by Cardiac Magnetic Resonance

*Anna Réka Kiss, Zsófia Gregor, Ádám Furák, Liliána Erzsébet Szabó, Zsófia Dohy, Béla Merkely, Hajnalka Vágó and Andrea Szűcs**

Heart and Vascular Center of Semmelweis University, Budapest, Hungary

The age and sex-specific characteristics of right ventricular compacted (RV-CMi) and RV-trabeculated myocardial mass (RV-TMi) and the determinants of RV myocardium are less well-studied; however, in different conditions, these might provide additional diagnostic information. We aimed to describe the age- and sex-specific characteristics of RV-CMi, RV-TMi, and RV volumetric and functional parameters and investigate the determinants of RV myocardial mass with cardiac magnetic resonance (CMR). Two hundred healthy Caucasian volunteers free of known cardiovascular or systemic diseases were prospectively enrolled in this study. Four different age groups were established with equal numbers of males and females: Group A (n = 50, 20-29 years, mean age: 24.3 ± 3.2 years), Group B (n = 50, 30-39 years, mean age: 33.6 ± 2.6 years), Group C (n = 50, 40-49 years, mean age: 44.7 ± 2.7 years), and Group D (n = 50, ≥50 years, mean age: 55.1 ± 3.9 years). Left ventricular (LV) and RV volumetric, functional, CMi, and TMi values were measured with a threshold-based post-processing CMR method. The volumetric parameters, RV-CMi, and RV-TMi values were larger, and the ejection fraction (EF) was lower in males. The RV-CMi did not correlate with age in either of the sexes, while the RV-TMi decreased with age in females but remained stable in males. The RV-TMi and RV-CMi correlated positively with RV volumetric parameters, the LV-CMi, the LV-TMi, and each other in both sexes. LV-TMi, LV-CMi, RV end-systolic volume, and sex were independent predictors of RV-TMi. Understanding the characteristics of RV-trabeculated and RV-compacted myocardium might have additive value in diagnosing different conditions with RV hypertrophy or hypertrabeculation.

Keywords: right ventricle, cardiac magnetic resonance, trabeculated myocardium, compacted myocardium, age-related, sex-related, characteristics

OPEN ACCESS

Edited by:
Salah D. Qanadli, University of Lausanne, Switzerland

Reviewed by:
Cezary Szmigielski, Medical University of Warsaw, Poland
Tilman Emrich, Medical University of South Carolina, United States

****Correspondence:***
Andrea Szűcs
szucsand@gmail.com

Specialty section:
This article was submitted to Cardiovascular Imaging, a section of the journal Frontiers in Cardiovascular Medicine

Received: *22 September 2021*
Accepted: *15 November 2021*
Published: *07 December 2021*

Citation:
Kiss AR, Gregor ZS, Furák Á, Szabó LE, Dohy ZS, Merkely B, Vágó H and Szűcs A (2021) Age- and Sex-Specific Characteristics of Right Ventricular Compacted and Non-compacted Myocardium by Cardiac Magnetic Resonance. Front. Cardiovasc. Med. 8:781393. doi: 10.3389/fcvm.2021.781393

INTRODUCTION

The age- and sex-related characteristics of right ventricular (RV) volumetric and functional parameters have already been described in healthy populations (1, 2). In contrast, the characteristics of RV-compacted (RV-CMi) and RV-trabeculated myocardial mass (RV-TMi) and the quantification and determinants of RV myocardium are less well-studied. However, these might

have diagnostic, differential diagnostic, and prognostic relevance in different conditions affecting the right heart (3–8). The segmentation used to measure RV myocardial mass is challenging, and the physiologic presence of the high number of endocardial trabeculae makes its quantification even more difficult. Threshold-based CMR post-processing software can accurately differentiate endocardial trabeculation and papillary muscles from the blood pool and measure the mass of both compacted and trabeculated myocardium (9). This study aimed to describe the age- and sex-specific characteristics of RV volumetric and functional parameters and RV-compacted and RV-trabeculated myocardial masses and investigate the relationship between RV trabeculation and RV volumetric and functional parameters and LV trabeculation using threshold-based CMR post-processing software.

MATERIALS AND METHODS

Study Population

One hundred male and one hundred female Caucasian volunteers free of known diseases were prospectively enrolled between January 2019 and September 2020. Each participant completed a questionnaire including demographic data, cardiovascular symptoms, medical history, medication use, and sport activity. The inclusion criteria were as follows: the absence of cardiac diseases (congenital abnormality, ischemic heart disease, arrhythmia, valvular heart disease, cardiomyopathy), lack of sudden cardiac death in the family history, absence of other systemic disorders (hypertension-related, pulmonary, renal, gastrointestinal, metabolic, autoimmune, endocrine, psychiatric, oncological, neuromuscular, or other hereditary diseases), and sport activity <6 h per week (10). CMR examination without an injection of contrast agent, blood pressure measurement, 12-lead resting electrocardiography, and echocardiography were performed on the same day, and no abnormalities were found.

The study population was divided into four different age groups, which were set up with equal numbers of males and females: Group A ($n = 50$, 20-29 years, mean age: 24.3 ± 3.2 years), Group B ($n = 50$, 30-39 years, mean age: 33.6 ± 2.6 years), Group C ($n = 50$, 40-49 years, mean age: 44.7 ± 2.7 years), and Group D ($n = 50$, 50-66 years, mean age: 55.1 ± 3.9 years). The male and female participants' baseline demographic, morphometric, and left and right ventricular parameters are shown in **Tables 2**, **3**. The sports activities of the studied groups are presented in **Supplementary Table 1**.

All procedures performed in this study were under the 1964 Helsinki Declaration and its later amendments or comparable ethical standards. Ethics approval was obtained from the Central Ethics Committee of Hungary, and all participants provided informed consent.

Image Acquisition and Analysis

The CMR examinations were performed with 1.5 T MRI scanners (Achieva, Philips Medical System, Eindhoven, the Netherlands and Magnetom Aera, Siemens Healthineers, Erlangen, Germany). Functional imaging was performed with balanced steady-state free precession cine sequences in 2-, 3-, and 4-chamber long-axis views and breath-hold short-axis views from base to apex with complete coverage of the LV and RV according to current recommendations (11, 12). The scan parameters acquired with the Philips Achieva and with the Siemens Aera scanners were the following: repetition time: 2.7 and 2.5 ms respectively, echo time: 1.3 and 1.15 ms, respectively, flip angle: 60° and 58°, respectively, spatial resolution: 1.5 × 1.5 mm in both scanners, temporal resolution: 25 frames per cardiac cycle in both scanners. The slice thickness was 8 mm with no interslice gap, the field of view 350 mm on average adapted to body size. A contrast agent was not administered.

Medis Suite version 3.0 was used for the segmentation (Medis Medical Imaging Systems, Leiden, the Netherlands). Automatic tracing with manual correction of the endo- and epicardial contours of the LV and RV was performed by two observers (ASz with 10 years of experience and ARK with 5 years of experience). Inter-and-intraobserver agreement values are presented in **Table 1**. The LV and RV volumetric and functional values and the myocardial mass values were calculated with the MassK module of the software. This module performs a threshold-based papillary muscle and trabeculated myocardium quantification analysis that differentiates endocardial trabeculation from the blood pool based on the differing signal intensities of the blood and myocardium. Each voxel within the epicardial contour was classified as either blood or myocardium according to the chosen threshold, which was set to 50% (**Figure 1**) (9). Manual correction of the threshold was not applied. Voxels classified as myocardium within the endocardial contour were calculated as trabeculated myocardial mass, while compacted myocardial mass was calculated as the difference between the total detected and trabeculated myocardial mass. The following LV and RV parameters were calculated: left and right ventricular end-diastolic volume (LV-EDV, RV-EDV),

TABLE 1 | Intraclass correlation coefficient (ICC) of the measured left and right ventricular parameters to describe inter-and intraobserver agreement.

	Interobserver agreement (ICC)	Intraobserver agreement (ICC)
LV-EDVi	0.98 (0.86-0.99)	0.99 (0.99-0.99)
LV-ESVi	0.96 (0.90-0.98)	0.95 (0.90-0.98)
LV-SVi	0.95 (0.85-0.98)	0.99 (0.98-0.99)
LV-EF	0.95 (0.89-0.98)	0.98 (0.95-0.99)
LV-TMi	0.99 (0.95-0.99)	0.98 (0.95-0.99)
LV-CMi	0.99 (0.98-0.99)	0.99 (0.98-0.99)
RV-EDVi	0.99 (0.97-0.99)	0.99 (0.98-0.99)
RV-ESVi	0.96 (0.93-0.99)	0.95 (0.87-0.97)
RV-SVi	0.99 (0.97-0.99)	0.99 (0.98-0.99)
RV-EF	0.98 (0.95-0.99)	0.92 (0.82-0.97)
RV-CMi	0.98 (0.95-0.99)	0.83 (0.62-0.92)
RV-TMi	0.99 (0.97-0.99)	0.98 (0.96-0.99)

CMi, end-diastolic compacted myocardial mass index; EDVi, end-diastolic volume index; EF, ejection fraction; ESVi, end-systolic volume index; LV, left ventricle; RV, right ventricle; SVi, stroke volume index; TMi, end-diastolic trabeculated myocardial mass index.

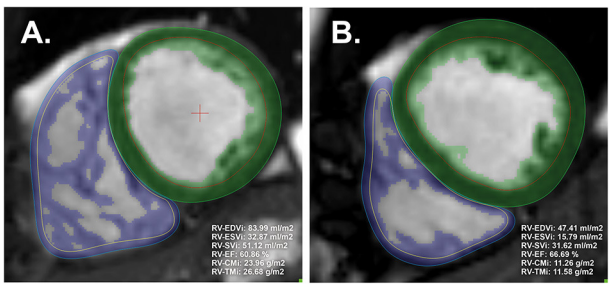

FIGURE 1 | Representative image analysis with threshold-based papillary and trabeculated muscle quantification software and the calculated right ventricular parameters of male **(A)** and female **(B)** participants. The green and blue areas represent the myocardial mass, including the left and right ventricles' endocardial trabeculation (included in the endocardial contours). The threshold was set to the default (50%). CMi, end-diastolic compacted myocardial mass index; EDVi, end-diastolic volume index; EF, ejection fraction; ESVi, end-systolic volume index; LV, left ventricle; RV, right ventricle; SVi, stroke volume index; TMi, end-diastolic trabeculated myocardial mass index.

TABLE 2 | Baseline demographic and left ventricular characteristics of the studied male and female participants.

	Male	Female	*P*
Number of participants	100	100	–
Age	39.5 (29.3, 49.8)	40.0 (29.2, 49.5)	0.833
BSA (m^2)	2.1 (2.0, 2.2)	1.7 (1.6, 1.8)	**<0.0001**
BMI (kg/m^2)	25.5 (24.1, 27.5)	22.2 (20.3, 24.3)	**<0.0001**
LV-EDVi (ml/m^2)	69.5 ± 10.8	64.4 ± 8.5	**0.0003**
LV-ESVi (ml/m2)	23.0 ± 5.3	19.3 ± 4.1	**<0.0001**
LV-SVi (ml/m^2)	46.5 ± 7.9	45.1 ± 6.2	0.164
LV-EF (%)	67.0 ± 5.6	70.1 ± 4.4	**<0.0001**
LV-CMi (g/m^2)	51.2 ± 8.0	40.5 ± 5.6	**<0.0001**
LV-TMi (g/m2)	22.8 ± 4.4	18.2 ± 3.3	**<0.0001**

For the comparison between sexes, Mann-Whitney U-test was used in age, BSA, and BMI; otherwise, Student's t-test was used.
BMI, body mass index; BSA, body surface area; CMi, end-diastolic compacted myocardial mass index; EDVi, end-diastolic volume index; EF, ejection fraction; ESVi, end-systolic volume index; LV, left ventricle; SVi, stroke volume index; TMi, end-diastolic trabeculated myocardial mass index.
Bold values are statistically significant ($p < 0.05$).

end-systolic volume (LV-ESV, RV-ESV), stroke volume (LV-SV, RV-SV), ejection fraction (LV-EF, RV-EF), end-diastolic compacted myocardial mass (LV-CM, RV-CM), and end-diastolic trabeculated myocardial mass (LV-TM, RV-TM). The parameters were indexed (i) to body surface area. The following additional ratios were generated to study the relationship of volumetric parameters and myocardial mass: RV-trabeculated myocardial mass-to-compact myocardial mass (RV-TMi/RV-CMi), RV-trabeculated myocardial mass-to-end-diastolic volume (RV-TMi/RV-EDVi), and RV-compacted myocardial mass-to-end-diastolic volume (RV-CMi/RV-EDVi).

Statistical Analysis

The intra-and interobserver agreement of the two observers was tested using the intraclass correlation coefficient (ICC). An ICC <0.4, between 0.4 and 0.75, and >0.75 indicates poor, fair to good, and excellent interobserver agreement. The Shapiro-Wilk test was used to assess the normality of each distribution. Normally distributed continuous variables are presented as the mean and standard deviation (SD), while median and interquartile range (IQR) is shown in the case of non-normal distribution. An unpaired Student's *t*-test or the Mann-Whitney U-test was used to compare male and female groups appropriately. The Pearson or Spearman test was used for correlation analysis as appropriate. Multiple linear regression analysis was applied to determine independent predictors for RV-compacted and RV-trabeculated myocardial mass. A p-value < 0.05 was considered statistically significant. IBM SPSS Statistics (Version 25.0, Armonk, NY) was used for calculations.

RESULTS

The inter- and intraobserver agreement of the two observers was tested on 25 randomly selected participants. All of the measured parameters showed excellent inter-and intraobserver agreement.

Studying the LV and RV parameters in the total population, we found significant differences between males and females: both LV and RV EDVi, ESVi, CMi, and TMi values were significantly larger, while the EF was significantly lower in males (**Tables 2**, **3**).

We further described the sex-related differences in each age group (**Table 3**). The volumetric, functional, and myocardial mass values significantly differed between males and females in each age group, similar to the total population. However, the RV-EDVi value was not significantly different between the sexes in Group D. The RV-SVi value was larger in males; still, the difference was significant only in Group C (**Table 3**).

Regarding sex-related differences of the studied ratios, the RV-TMi/RV-CMi ratio was comparable in the youngest age group between males and females, but it was higher in males than in females in Group B, Group C, and D and was significantly different between sexes in Group C**.** The RV-CMi/RV-EDVi and RV-TMi/RV-EDVi ratios were larger in males. The former was significantly different in Group C, and the latter was significant in Group C and Group (**Table 3**).

Age-related changes in the studied parameters were as follows (**Figures 2**, **3**). The RV-EDVi, RV-ESVi, and RV-SVi showed a significant negative correlation with age in both sexes. The RV-EF was positively correlated with age in females but not in males. The RV-CMi value was not associated with age in either of the sexes, while the RV-TMi value negatively correlated with age in females.

The RV-TMi/RV-CMi did not correlate with age in either males or females, while the RV-CMi/RV-EDVi ratio positively correlated with age in both sexes, and the RV-TMi/RV-EDVi ratio showed a positive correlation only in males.

Linear relationships were studied between RV-TMi, RV-CMi, RV volumetric and functional parameters, and LV myocardial mass values (**Table 4**). RV-TMi was positively correlated with

TABLE 3 | Right ventricular volumetric, functional, and myocardial mass values and the studied myocardial mass-to-volume ratios of the total population and the different age groups stratified by sex; and its comparison between sexes.

	Group		Male	Female	*P*
RV- EDVi (ml/m^2)	Total population	Mean ± SD	70.3 ± 14.1	61.3 ± 9.4	**<0.0001**
	A	Mean ± SD	74.8 ± 11.8	66.5 ± 8.5	**0.006**
	B	Mean ± SD	71.5 ± 12.4	61.8 ± 8.5	**0.02**
	C	Mean ± SD	73.2 ± 13.4	61.9 ± 9.1	**0.001**
	D	Mean ± SD	61.7 ± 15.6	55.1 ± 8.5	0.068
RV-ESVi (ml/m^2)	Total population	Mean ± SD	27.1 ± 6.0	21.2 ± 4.8	**<0.0001**
	A	Mean ± SD	29.3 ± 5.0	24.7 ± 4.4	**0.001**
	B	Mean ± SD	27.9 ± 6.2	21.4 ± 4.2	**<0.0001**
	C	Mean ± SD	27.6 ± 5.8	21.1 ± 15.5	**<0.0001**
	D	Mean ± SD	23.4 ± 5.7	17.6 ± 3.8	**<0.0001**
RV-SVi (ml/m^2)	Total population	Mean ± SD	43.2 ± 9.8	40.1 ± 6.4	**0.007**
	A	Mean ± SD	45.6 ± 8.0	41.9 ± 6.4	0.086
	B	Mean ± SD	43.5 ± 8.9	40.4 ± 5.8	0.142
	C	Mean ± SD	45.6 ± 9.2	40.4 ± 6.7	**0.029**
	D	Mean ± SD	38.3 ± 11.4	37.5 ± 6.2	0.77
RV-EF (%)	Total population	Mean ± SD	61.4 ± 4.8	65.5 ± 5.1	**<0.0001**
	A	Mean ± SD	60.8 ± 3.4	63.2 ± 4.7	**0.048**
	B	Mean ± SD	60.8 ± 5.7	65.4 ± 4.4	**0.002**
	C	Mean ± SD	62.1 ± 4.9	65.3 ± 5.4	**0.034**
	D	Mean ± SD	62.0 ± 5.0	68.2 ± 4.8	**<0.0001**
RV-CMi (g/m^2)	Total population	Mean ± SD	16.4 (15.0, 19.1)	13.4(12.0, 14.8)	**<0.0001**
	A	Mean ± SD	16.8 ± 3.4	13.4 (12.1, 15.3)	**0.002**
	B	Mean ± SD	16.6 ± 2.7	13.7 ± 1.8	**<0.0001**
	C	Mean ± SD	18.0 ± 3.5	13.4 (12.5, 15.3)	**<0.0001**
	D	Mean ± SD	17.0 ± 3.1	13.4 ± 2.0	**<0.0001**
RV-TMi (g/m^2)	Total population	Mean ± SD	20.1 ± 4.2	15.3 ± 3.3	**<0.0001**
	A	Mean ± SD	19.9 ± 3.7	17.1 ± 3.6	**0.009**
	B	Mean ± SD	19.3 ± 3.8	14.9 ± 3.0	**<0.0001**
	C	Mean ± SD	21.8 ± 5.2	13.9 (11.9, 19.3)	**<0.0001**
	D	Mean ± SD	19.5 ± 3.6	14.3 ± 2.8	**<0.0001**
RV-TMi/RV-CMi	Total population	Mean ± SD	1.21 ± 0.29	1.12 ± 0.27	**0.029**
	A	Mean ± SD	1.23 ± 0.30	1.24 ± 0.30	0.889
	B	Mean ± SD	1.18 ± 0.25	1.10 ± 0.25	0.217
	C	Mean ± SD	1.24 ± 0.35	1.05 ± 0.24	**0.032**
	D	Mean ± SD	1.18 ± 0.26	1.09 ± 0.24	0.181
RV-TMi/RV-EDVi	Total population	Mean ± SD	0.28 (0.24, 0.33)	0.24 (0.21, 0.28)	**<0.0001**
	A	Mean ± SD	0.27 (0.22, 0.31)	0.25 (0.22, 0.30)	0.527
	B	Mean ± SD	0.27 (0.24, 0.30)	0.24 (0.21, 0.28)	0.062
	C	Mean ± SD	0.28 (0.25, 0.33)	0.23 (0.21, 0.26)	**0.001**
	D	Mean ± SD	0.32 (0.28, 0.39)	0.26 (0.23, 0.30)	**0.008**
RV-CMi/RV-EDVi	Total population	Mean ± SD	0.24 (0.21, 0.28)	0.22 (0.20, 0.25)	**0.018**
	A	Mean ± SD	0.22 (0.20, 0.24)	0.21 (0.19, 0.24)	0.445
	B	Mean ± SD	0.23 (0.21, 0.26)	0.22 (0.19, 0.25)	0.75
	C	Mean ± SD	0.24 (0.22, 0.30)	0.23 (0.21, 0.25)	0.139
	D	Mean ± SD	0.27 (0.24, 0.31)	0.25 (0.22, 0.28)	**0.025**

For the comparison between sexes, Mann-Whitney U-test was used in case of the following parameters: RV-CMi in the total population and Group A and C in females, in the total population and Group C in males; RV-TMi in Group C in females; RV-TMi/RV-EDVi in every group in both males and females; RV-CMi/RV-EDVi in every group in both males and females. Otherwise, Student's t-test was used.

CMi, end-diastolic compacted myocardial mass index; EDVi, end-diastolic volume index; EF, ejection fraction; ESVi, end-systolic volume index; RV, right ventricle; RV-CMi/RV-EDVi, right ventricular end-diastolic compacted myocardial mass index-to-right ventricular end-diastolic volume index ratio; RV-TMi/RV-CMi, right ventricular end-diastolic trabeculated myocardial mass index-to-right ventricular end-diastolic compacted myocardial mass index ratio; RV-TMi/RV-EDVi, right ventricular end-diastolic trabeculated myocardial mass index-to-right ventricular end-diastolic volume index ratio; SVi, stroke volume index; TMi, end-diastolic trabeculated myocardial mass index.

Bold values are statistically significant ($p < 0.05$).

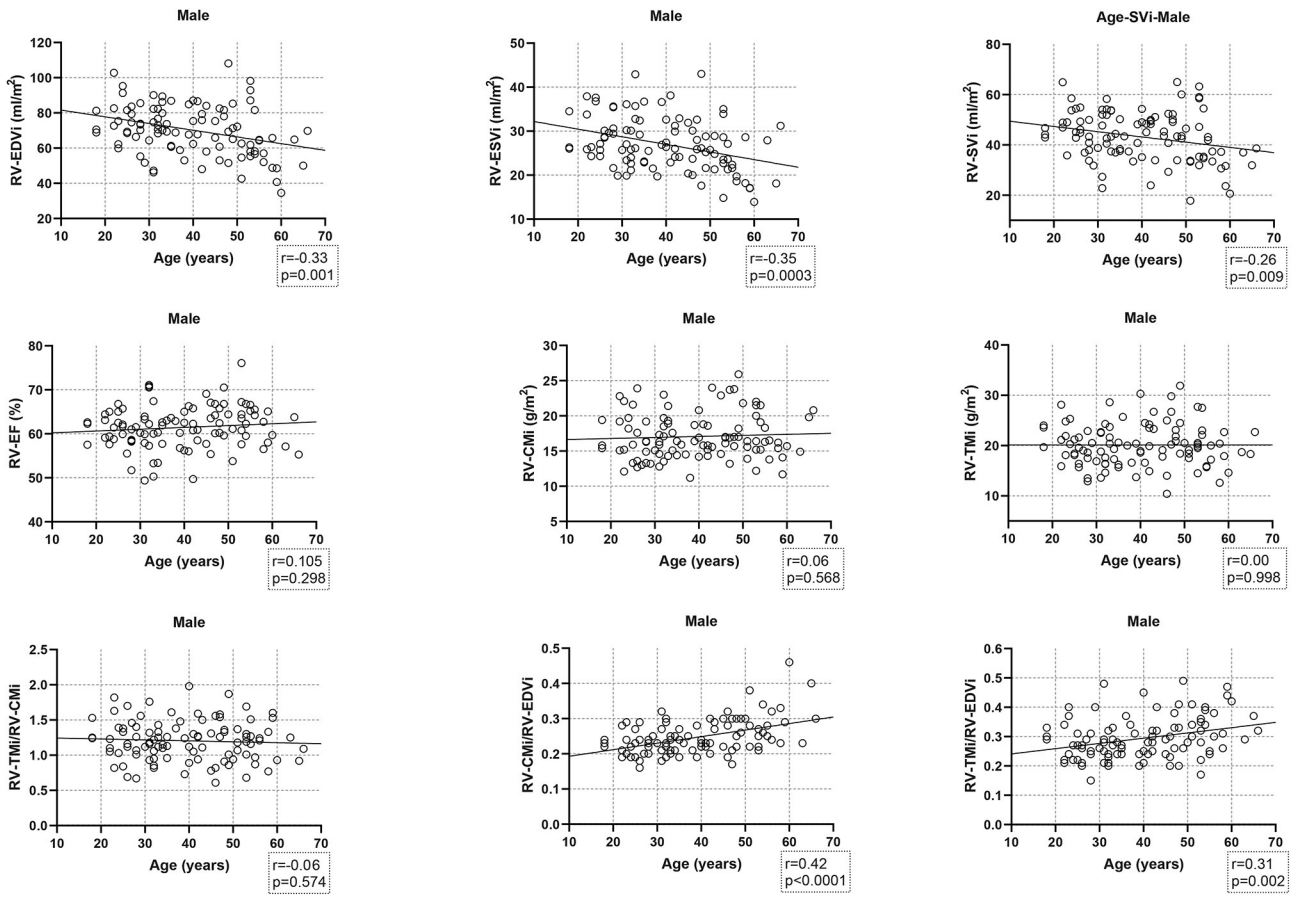

FIGURE 2 | Correlation between age and right ventricular volumetric, functional, and myocardial mass values, and the studied ratios in males. CMi, end-diastolic compacted myocardial mass index; EDVi, end-diastolic volume index; EF, ejection fraction; ESVi, end-systolic volume index; RV, right ventricle; SVi, stroke volume index; TMi, end-diastolic trabeculated myocardial mass index.

RV-ESVi, RV-EDVi, RV-CMi, LV-TMi, and LV-CMi in both sexes and negatively correlated with age and RV-EF in females. In both sexes, the RV-CMi significantly correlated with the RV-EDVi, RV-TMi, LV-CMi, and LV-TMi; however, it correlated significantly with the RV-ESVi and RV-EF only in males.

Multiple regression analysis was performed on the total population to find independent predictors of RV-TMi and RV-CMi (**Table 5**). RV-TMi was independently associated with sex, RV-ESVi, LV-TMi, and LV-CMi, with a cumulative *R*-value of 0.701 ($p < 0.0001$). Independent predictors of RV-CMi were age, sex, RV-EDVi, and LV-CMi, with a cumulative *R*-value of 0.728 ($p < 0.0001$).

DISCUSSION

In this study, we assessed the characteristics of RV in different age groups stratified by sex. We described smaller RV volumes and higher RV-EF, while the RV compact myocardial mass values were similar to those published (2, 13). During conventional contour-based post-processing techniques, trabeculae are included in the endocardial contours and are calculated as blood volume; however, they contribute approximately 50% to the RV myocardial mass (14). The threshold-based software used in our study is a highly reproducible technique with an excellent inter-and intraobserver agreement that enables us to measure both total and trabeculated myocardial mass values accurately. However, volumetric parameters are significantly lower compared to conventional techniques (9, 14). Average RV total myocardial mass values have already been established, but the reference ranges of compacted and trabeculated RV myocardial mass are less well-studied. We found only one publication that quantified RV trabeculation; however, they used manual contouring and defined myocardium volumes (15). After converting these RV trabeculated myocardium values from volume to mass, we found that Andre et al. described higher RV trabeculated mass values than those in our results. It might be due to the different post-processing techniques; namely, they used manual contouring of the endo- and epicardial borders compared to the threshold-based software applied in our study (15, 16). The use of normal ranges of RV compacted and trabeculated myocardial mass might have diagnostic, differential diagnostic, and prognostic relevance

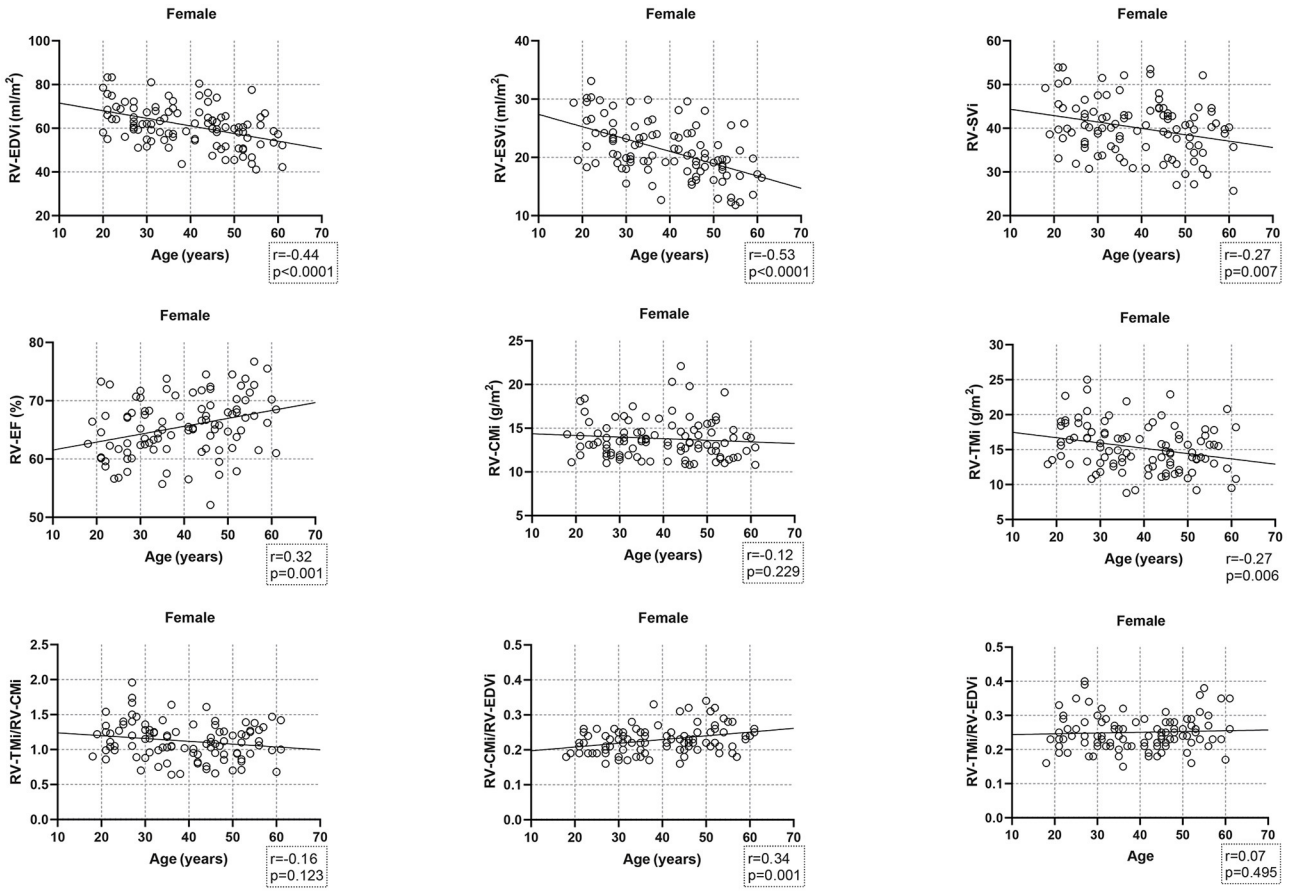

FIGURE 3 | Correlation between age and right ventricular volumetric, functional, and myocardial mass values, and the studied ratios in females. CMi, end-diastolic compacted myocardial mass index; EDVi, end-diastolic volume index; EF, ejection fraction; ESVi, end-systolic volume index; RV, right ventricle; SVi, stroke volume index; TMi, end-diastolic trabeculated myocardial mass index.

in cases where RV hypertrabeculation or RV hypertrophy is present (5–8). Furthermore, our study's myocardial mass ratios and the myocardial mass-to-volume ratios might also help in the differential diagnosis of physiological (e.g., athletes' heart, pregnancy) and pathological conditions resulting in volume or pressure overload of the RV. Our study's presented age- and sex-specific values could be used as standard reference ranges for this threshold-based software with the same threshold setting as in our study.

Assessing the sex-related differences in the studied RV parameters, we found higher compacted and trabeculated myocardial mass values, higher volumetric parameters, and smaller RV-EF in males. These were consistent with the literature and could be explained by biometric and hormonal differences between sexes (1, 15, 17). Previous studies described the age-related decrease in RV functional parameters, which is in line with our results; however, there are inconsistent data about the changes in RV myocardial mass (18, 19). Kawut et al. and Maceira et al. described a significant decrease in RV myocardial mass over time, although they studied wider age ranges with older participants than ours (1, 18). Sandstede et al. studied similar age groups and found unchanged RV mass values with age, similar to our compacted myocardial mass results (19). The relatively stable RV-compacted mass values might be explained by the age-related changes in the myocardium characterized by the loss of myocytes with an increase in cell volume, resulting in compensatory hypertrophy. This mechanism could be the cause of unchanged compacted myocardial mass values (20).

Regarding the trabeculated myocardial mass, we found a slight decrease with age in females, and this negative age dependency is in line with Andre's results, although the mechanism is unknown (15, 21). In contrast to previous results, the RV trabeculated mass was not different between the age groups and was higher in older males than in females of the same age in our study (15). A possible explanation for these altering results could be the abovementioned difference in post-processing techniques. We did not find information about the sex- or age-related factors and mechanisms influencing RV trabeculation; however, we hypothesize that physical activity might play a role. It is known that excessive LV and RV trabeculation can be found in athletes as part of the process of adaptation to intense physical activity (22, 23). Woodbridge et al. studied the relationship

TABLE 4 | Correlation between right ventricular compacted and trabeculated myocardial mass values and right ventricular volumetric and functional and left ventricular myocardial mass values.

			RV-ESVi	RV-EDVi	RV-EF	RV-TMi	RV-CMi	LV-TMi	LV-CMi
RV-TMi	Male	r	0.32	0.35	0.03	1.00	0.27	0.35	0.38
		P	**0.001**	**0.0004**	0.799	–	**0.007**	**0.0003**	**0.0001**
	Female	r	0.532	0.45	−0.37	1.00	0.24	0.32	0.36
		P	**<0.0001**	**<0.0001**	**0.0002**	–	**0.018**	**0.001**	**0.0003**
RV-CMi	Male	r	0.39	0.58	0.24	0.27	1.00	0.27	0.46
		P	**<0.0001**	**<0.0001**	**0.015**	**0.007**	–	**0.006**	**<0.0001**
	Female	r	0.30	0.48	0.04	0.24	1.00	0.22	0.47
		P	0.002	**<0.0001**	0.686	**0.018**	–	**0.026**	**<0.0001**

Spearman test was used to correlate RV-CMi to the other parameters; otherwise, Pearson test was used.
CMi, end-diastolic compacted myocardial mass index; EDVi, end-diastolic volume index; EF, ejection fraction; ESVi, end-systolic volume index; LV, left ventricle; RV, right ventricle; TMi, end-diastolic trabeculated myocardial mass index.
Bold values are statistically significant ($p < 0.05$).

TABLE 5 | Multivariate linear regression analysis and the independent predictors of right ventricular compacted and trabeculated myocardial mass.

	RV-TMi			RV-CMi	
Covariate	**β**	***P***	**Covariate**	**β**	***P***
Age	0.002	0.978	Age	0.175	**0.001**
Sex	0.152	**0.030**	Sex	0.219	**0.001**
RV-EDVi	−0.061	0.552	RV-EDVi	0.490	**<0.0001**
RV-ESVi	0.264	**<0.0001**	RV-ESVi	−0.159	0.106
RV-SVi	−0.048	0.475	RV-SVi	0.214	0.102
RV-EF	−0.057	0.425	RV-EF	0.082	0.134
RV-CMi	−0.006	0.934	RV-TMi	0.014	0.825
LV-CMi	0.225	**0.002**	LV-CMi	0.186	**0.014**
LV-TMi	0.253	**<0.0001**	LV-TMi	0.086	0.152
Cumulative R	0.701		Cumulative R	0.728	
Standard error	3.24		Standard error	2.22	
Cumulative P	**<0.0001**		Cumulative P	**<0.0001**	

CMi, end-diastolic compacted myocardial mass index; EDVi, end-diastolic volume index; EF, ejection fraction; ESVi, end-systolic volume index; LV, left ventricle; RV, right ventricle; SVi, stroke volume index; TMi, end-diastolic trabeculated myocardial mass index.
Bold values are statistically significant ($p < 0.05$).

between physical activity and the extent of LV trabeculation in a community-based cohort and found no linear relationship (24). They propose that there might be a threshold in physical activity that must be exceeded to manifest an increase in LV trabeculation. It is also known that there is a slight difference between LV and RV sport adaptation, as the right ventricle shows slightly stronger morphological changes (25). Thus, we hypothesize that RV trabeculation develops more easily than LV trabeculation and might be more sensitive to physical activity that does not exceed the training hours of competitive athletes and does not result in changes in RV volumes (10). A possible mechanism is that regular exercise increases the circulating level of testosterone, which might lead to muscle growth through increased protein synthesis and decreased protein degradation in males (26). This hypothesis might explain the comparable RV trabeculated myocardial mass value between the studied age groups in males; however, the cause of the slight age-related decrease in RV-TMi in females remains unanswered.

The RV-EF was positively correlated with age in females but not in males. The data are controversial about the age-related changes in the RV-EF: Petersen et al. found an age-related increase in females only, which is similar to our results, while Maceira et al. described an increase in the RV-EF in males as well. However, the RV-EF did not change significantly over time in either males or females in Sandstede's study (2, 18, 19).

The RV trabeculated myocardial mass-to-compact myocardial mass ratio did not show sex-related differences and was not correlated with age. To the best of our knowledge, there is no information about the RV trabeculated myocardial mass-to-compact myocardial mass ratio in healthy male and female populations. However, previous studies found no significant association between sex and non-compacted-to-compacted myocardial thickness of the LV (27, 28). The results of Gregor et al. might also strengthen this; namely, there is no significant difference between the LV trabeculated myocardial mass-to-compact myocardial mass ratio in males and females in either younger or older age groups measured with threshold-based software (29). However, we need to mention that physiological mechanisms affecting RV and LV trabeculation might be different.

Different myocardial mass-to-volume ratios have been previously studied in the left ventricle but not in the right ventricle. Czimbalmos et al. described the high diagnostic accuracy of LV muscle-to-volume ratios in the differential diagnosis of hypertrophic cardiomyopathy and athletes' hearts (30). The RV-TMi/RV-EDVi and RV-CMi/RV-RDVi ratios in our study correlated positively with age. They might help identify the early stages of different pathological conditions that affect the RV.

In studying the relationship between RV and LV myocardial mass values and RV volumetric parameters, we found that compacted RV myocardial mass correlated with trabeculated RV myocardial mass and vice versa. Furthermore, both compacted and trabeculated RV masses correlated with LV compacted and trabeculated myocardial masses, and LV trabeculation was

an independent predictor of RV trabeculation. We did not find previous studies about the connection between either RV or LV compacted and trabeculated myocardial masses. Some researchers suggest that left and right ventricular myocardial mass is genetically determined; however, the degree of trabeculation might vary between the ventricles due to the different physiological mechanisms and stimulating factors (15). RV volumetric parameters showed a strong relationship with compacted and trabeculated RV myocardial mass values. Moreover, the RV-ESVi was an independent predictor of RV trabeculation, while the RV-EDVi was an independent predictor of RV-compacted myocardium. Previous studies conducted in a healthy population, pregnant women, patients with chronic anemia, patients with heart failure, and high-level athletes suggest that LV trabeculation is strongly related to LV volumes. Furthermore, excessive LV trabeculation is a normal response to increased cardiac preload and ventricular volume (21, 27, 31–33). We did not find previous publications about the impact of RV volumes on RV trabeculation, but the relationship might not be surprising. RV-compacted myocardial mass was previously described to correlate with RV volumes positively, LV compacted myocardial mass, and pulmonary artery pressure, which is in line with our results (34).

To summarize, the RV-compacted myocardial mass remained stable over time in both sexes, but the RV trabeculated myocardial mass decreased with age in females. RV trabeculated myocardial mass correlated significantly with RV-compacted myocardial mass and vice versa. Furthermore, LV compacted, and trabeculated myocardial mass values and RV volumetric parameters were independent predictors of RV-compacted and trabeculated myocardial mass. The age- and sex-related characteristics of RV compacted and trabeculated myocardial masses described in a healthy population have not been previously studied; however, this additional information might help differentiate conditions with RV hypertrophy or hypertrabeculation.

We need to mention the limitations of this study. It was conducted on a large cohort; however, the subgroups were relatively small after dividing by age. This study did not cover elderly populations as we needed to exclude these participants due to cardiovascular or other systemic diseases (mainly hypertension). The CMR cine images were acquired using two different CMR scanners, and although the scan parameters were similar, this might be considered a limitation. We need to mention a few limitations regarding the threshold-based software as well. The current ejection fraction and volume quantification use a stack of thick short-axis slices, and 8 mm is common for Z-direction spatial resolution. In the meantime, trabeculae and papillary muscles do not cross the slice in an exactly perpendicular fashion, which creates partial volume effects. Depending on the actual path of the trabeculae, this will influence the threshold-based quantification (9, 16). The reported values in this study were measured with the threshold set to 50%. However, altering the threshold might change the measured myocardial mass values. Papillary muscles were counted as trabeculation in our study because of the nature of this technique. Previous studies on LV trabeculation excluded the papillary muscles from trabeculation, making the comparison of the different results more challenging. However, researchers suggest that the segmentation of papillary muscles does not make a significant difference (15).

DATA AVAILABILITY STATEMENT

The raw data supporting the conclusions of this article will be made available by the authors, without undue reservation.

ETHICS STATEMENT

Ethical review and approval was not required for the study on human participants in accordance with the local legislation and institutional requirements. The patients/participants provided their written informed consent to participate in this study.

AUTHOR CONTRIBUTIONS

AK: methodology, formal analysis, investigation, resources, data curation, writing—original draft, and visualization. ZG: data curation. ÁF: data curation. LS: writing—review and editing. ZD: writing—review and editing. BM: supervision. HV: writing—review and editing and supervision. AS: conceptualization, methodology, investigation, resources, writing—review and editing, supervision, and project administration. All authors contributed to the article and approved the submitted version.

FUNDING

This research was financed by the Thematic Excellence Programme (Tématerületi Kiválósági Program, 2020-4.1.1.-TKP2020) of the Ministry for Innovation and Technology in Hungary within the framework of the Therapeutic Development and Bioimaging Programs of Semmelweis University; by the Development of Scientific Workshops of Medical, Health Sciences and Pharmaceutical Education (Project identification number: EFOP-3.6.3-VEKOP-16-2017-00009); and by the Ministry of Innovation and Technology NRDI Office within the framework of the Artificial Intelligence National Laboratory Program. Project no. NVKP_16-1–2016-0017 (National Heart Program) has been implemented with the support provided by the National Research, Development, and Innovation Fund of Hungary, financed under the NVKP_16 funding scheme.

ACKNOWLEDGMENTS

We thank the technicians who helped perform the cardiac magnetic resonance imaging examinations.

SUPPLEMENTARY MATERIAL

The Supplementary Material for this article can be found online at: https://www.frontiersin.org/articles/10.3389/fcvm.2021.781393/full#supplementary-material

REFERENCES

1. Kawut SM, Lima JA, Barr RG, Chahal H, Jain A, Tandri H, et al. Sex and race differences in right ventricular structure and function: the multi-ethnic study of atherosclerosis-right ventricle study. *Circulation.* (2011) 123:2542-51. doi: 10.1161/CIRCULATIONAHA.110.985515
2. Petersen SE, Aung N, Sanghvi MM, Zemrak F, Fung K, Paiva JM, et al. Reference ranges for cardiac structure and function using cardiovascular magnetic resonance (CMR) in Caucasians from the UK Biobank population cohort. *J Cardiovasc Magn Reson.* (2017) 19:18. doi: 10.1186/s12968-017-0327-9
3. Marcus JT, Vonk Noordegraaf A, De Vries PM, Van Rossum AC, Roseboom B, Heethaar RM, et al. MRI evaluation of right ventricular pressure overload in chronic obstructive pulmonary disease. *J Magn Reson Imaging.* (1998) 8:999-1005. doi: 10.1002/jmri.1880080502
4. Hagger D, Condliffe R, Woodhouse N, Elliot CA, Armstrong IJ, Davies C, et al. Ventricular mass index correlates with pulmonary artery pressure and predicts survival in suspected systemic sclerosis-associated pulmonary arterial hypertension. *Rheumatology.* (2009) 48:1137-42. doi: 10.1093/rheumatology/kep187
5. Saba TS, Foster J, Cockburn M, Cowan M, Peacock AJ. Ventricular mass index using magnetic resonance imaging accurately estimates pulmonary artery pressure. *Eur Respir J.* (2002) 20:1519-24. doi: 10.1183/09031936.02.00014602
6. Stacey RB, Andersen M, Haag J, Hall ME, McLeod G, Upadhya B, et al. Right ventricular morphology and systolic function in left ventricular noncompaction cardiomyopathy. *Am J Cardiol.* (2014) 113:1018-23. doi: 10.1016/j.amjcard.2013.12.008
7. Song ZZ. A combination of right ventricular hypertrabeculation/noncompaction and arrhythmogenic right ventricular cardiomyopathy: a syndrome? *Cardiovasc Ultrasound.* (2008) 6:63. doi: 10.1186/1476-7120-6-63
8. Yamamura K, Yuen D, Hickey EJ, He X, Chaturvedi RR, Friedberg MK, et al. Right ventricular fibrosis is associated with cardiac remodelling after pulmonary valve replacement. *Heart.* (2019) 105:855-63. doi: 10.1136/heartjnl-2018-313961
9. Jaspers K, Freling HG, van Wijk K, Romijn EI, Greuter MJ, Willems TP. Improving the reproducibility of MR-derived left ventricular volume and function measurements with a semi-automatic threshold-based segmentation algorithm. *Int J Cardiovasc Imaging.* (2013) 29:617-23. doi: 10.1007/s10554-012-0130-5
10. Pelliccia A, Sharma S, Gati S, Back M, Borjesson M, Caselli S, et al. 2020 ESC Guidelines on sports cardiology and exercise in patients with cardiovascular disease. *Eur Heart J.* (2021) 42:17-96. doi: 10.1093/eurheartj/ehaa605
11. Kramer CM, Barkhausen J, Bucciarelli-Ducci C, Flamm SD, Kim RJ, Nagel E. Standardized cardiovascular magnetic resonance imaging (CMR) protocols: 2020 update. *J Cardiovasc Magn Reson.* (2020) 22:17. doi: 10.1186/s12968-020-00607-1
12. Kramer CM, Barkhausen J, Flamm SD, Kim RJ, Nagel E, Society for Cardiovascular Magnetic Resonance Board of Trustees Task Force on Standardized P. Standardized cardiovascular magnetic resonance (CMR) protocols 2013 update. *J Cardiovasc Magn Reson.* (2013) 15:91. doi: 10.1186/1532-429X-15-91
13. Hudsmith LE, Petersen SE, Francis JM, Robson MD, Neubauer S. Normal human left and right ventricular and left atrial dimensions using steady state free precession magnetic resonance imaging. *J Cardiovasc Magn Reson.* (2005) 7:775-82. doi: 10.1080/10976640500295516
14. Csecs I, Czimbalmos C, Suhai FI, Mikle R, Mirzahosseini A, Dohy Z, et al. left and right ventricular parameters corrected with threshold-based quantification method in a normal cohort analyzed by three independent observers with various training-degree. *Int J Cardiovasc Imaging.* (2018) 34:1127-33. doi: 10.1007/s10554-018-1322-4
15. Andre F, Burger A, Lossnitzer D, Buss SJ, Abdel-Aty H, Gianntisis E, et al. Reference values for left and right ventricular trabeculation and noncompacted myocardium. *Int J Cardiol.* (2015) 185:240-7. doi: 10.1016/j.ijcard.2015.03.065
16. Espe EKS, Bendiksen BA, Zhang L, Sjaastad I. Analysis of right ventricular mass from magnetic resonance imaging data: a simple post-processing algorithm for correction of partial-volume effects. *Am J Physiol Heart Circ Physiol.* (2021) 320:H912-22. doi: 10.1152/ajpheart.00494.2020
17. Ventetuolo CE, Ouyang P, Bluemke DA, Tandri H, Barr RG, Bagiella E, et al. Sex hormones are associated with right ventricular structure and function: The MESA-right ventricle study. *Am J Respir Crit Care Med.* (2011) 183:659-67. doi: 10.1164/rccm.201007-1027OC
18. Maceira AM, Prasad SK, Khan M, Pennell DJ. Reference right ventricular systolic and diastolic function normalized to age, gender and body surface area from steady-state free precession cardiovascular magnetic resonance. *Eur Heart J.* (2006) 27:2879-88. doi: 10.1093/eurheartj/ehl336
19. Sandstede J, Lipke C, Beer M, Hofmann S, Pabst T, Kenn W, et al. age- and gender-specific differences in left and right ventricular cardiac function and mass determined by cine magnetic resonance imaging. *Eur Radiol.* (2000) 10:438-42. doi: 10.1007/s003300050072
20. Olivetti G, Melissari M, Capasso JM, Anversa P. Cardiomyopathy of the aging human heart. Myocyte loss and reactive cellular hypertrophy. *Circ Res.* (1991) 68:1560-8. doi: 10.1161/01.RES.68.6.1560
21. Gati S, Papadakis M, Papamichael ND, Zaidi A, Sheikh N, Reed M, et al. Reversible *de novo* left ventricular trabeculations in pregnant women: implications for the diagnosis of left ventricular noncompaction in low-risk populations. *Circulation.* (2014) 130:475-83. doi: 10.1161/CIRCULATIONAHA.114.008554
22. Abela M, D'Silva A. Left ventricular trabeculations in athletes: epiphenomenon or phenotype of disease? *Curr Treat Options Cardiovasc Med.* (2018) 20:100. doi: 10.1007/s11936-018-0698-8
23. D'Andrea A, Morello A, Iacono AM, Scarafile R, Cocchia R, Riegler L, et al. Right ventricular changes in highly trained athletes: between physiology and pathophysiology. *J Cardiovasc Echogr.* (2015) 25:97-102. doi: 10.4103/2211-4122.172486
24. Woodbridge SP, Aung N, Paiva JM, Sanghvi MM, Zemrak F, Fung K, et al. Physical activity and left ventricular trabeculation in the UK Biobank community-based cohort study. *Heart.* (2019) 105:990-8. doi: 10.1136/heartjnl-2018-314155
25. Major Z, Csajagi E, Kneffel Z, Kovats T, Szauder I, Sido Z, et al. comparison of left and right ventricular adaptation in endurance-trained male athletes. *Acta Physiol Hung.* (2015) 102:23-33. doi: 10.1556/APhysiol.102.2015.1.2
26. Barnes JN, Fu Q. Sex-specific ventricular and vascular adaptations to exercise. *Adv Exp Med Biol.* (2018) 1065:329-46. doi: 10.1007/978-3-319-77932-4_21
27. Kawel N, Nacif M, Arai AE, Gomes AS, Hundley WG, Johnson WC, et al. Trabeculated (noncompacted) and compact myocardium in adults: the multi-ethnic study of atherosclerosis. *Circ Cardiovasc Imaging.* (2012) 5:357-66. doi: 10.1161/CIRCIMAGING.111.971713
28. Dawson DK, Maceira AM, Raj VJ, Graham C, Pennell DJ, Kilner PJ. Regional thicknesses and thickening of compacted and trabeculated myocardial layers of the normal left ventricle studied by cardiovascular magnetic resonance. *Circ Cardiovasc Imaging.* (2011) 4:139-46. doi: 10.1161/CIRCIMAGING.110.960229
29. Gregor Z, Kiss AR, Szabó LE, Tóth A, Grebur K, Horváth M, et al. sex- and age- specific normal values of left ventricular functional and myocardial mass parameters using threshold-based trabeculae quantification. *PLoS ONE.* (2021) 16:e0258362. doi: 10.1371/journal.pone.0258362
30. Czimbalmos C, Csecs I, Toth A, Kiss O, Suhai FI, Sydo N, et al. The demanding grey zone: sport indices by cardiac magnetic resonance imaging differentiate hypertrophic cardiomyopathy from athlete's heart. *PLoS ONE.* (2019) 14:e0211624. doi: 10.1371/journal.pone.0211624
31. Kohli SK, Pantazis AA, Shah JS, Adeyemi B, Jackson G, McKenna WJ, et al. Diagnosis of left-ventricular non-compaction in patients with left-ventricular systolic dysfunction: time for a reappraisal of diagnostic criteria? *Eur Heart J.* (2008) 29:89-95. doi: 10.1093/eurheartj/ehm481
32. Gati S, Chandra N, Bennett RL, Reed M, Kervio G, Panoulas VF, et al. Increased left ventricular trabeculation in highly trained athletes: do we need more stringent criteria for the diagnosis of left ventricular non-compaction in athletes? *Heart.* (2013) 99:401-8. doi: 10.1136/heartjnl-2012-303418
33. Gati S, Papadakis M, Van Niekerk N, Reed M, Yeghen T, Sharma S. Increased left ventricular trabeculation in individuals with sickle cell anaemia: physiology or pathology? *Int J Cardiol.* (2013) 168:1658-60. doi: 10.1016/j.ijcard.2013.03.039

34. Vormbrock J, Liebeton J, Wirdeier S, Meissner A, Butz T, Trappe HJ, et al. Determinants of right ventricular muscle mass in idiopathic dilated cardiomyopathy: impact of left ventricular muscle mass and pulmonary hypertension. *Int J Med Sci.* (2014) 11:834-40. doi: 10.7150/ijms.6961

Conflict of Interest: The authors declare that the research was conducted in the absence of any commercial or financial relationships that could be construed as a potential conflict of interest.

Publisher's Note: All claims expressed in this article are solely those of the authors and do not necessarily represent those of their affiliated organizations, or those of the publisher, the editors and the reviewers. Any product that may be evaluated in this article, or claim that may be made by its manufacturer, is not guaranteed or endorsed by the publisher.

frontiers in Cardiovascular Medicine

ORIGINAL RESEARCH
published: 13 December 2021
doi: 10.3389/fcvm.2021.795016

Prognostic Value of the Three-Dimensional Right Ventricular Ejection Fraction in Patients With Asymptomatic Aortic Stenosis

Yosuke Nabeshima[1], Tetsuji Kitano[2] and Masaaki Takeuchi[3]*

[1] Second Department of Internal Medicine, School of Medicine, University of Occupational and Environmental Health, Kitakyushu, Japan, [2] Department of Cardiology and Nephrology, Wakamatsu Hospital of University of Occupational and Environmental Health, Kitakyushu, Japan, [3] Department of Laboratory and Transfusion Medicine, School of Medicine, Hospital of University of Occupational and Environmental Health, Kitakyushu, Japan

Background: The right ventricular (RV) function is an important prognostic marker of asymptomatic aortic stenosis (AS). However, previous publications have not addressed the additive value of conventional RV parameters over left heart parameters. Whether three-dimensional echocardiography (3DE)-derived RV ejection fraction (RVEF) has prognostic utility independent of 3DE derived left heart parameters is also unknown. We investigated the prognostic utility of 3DE RVEF in patients with asymptomatic AS.

Methods: We retrospectively selected 392 asymptomatic AS patients. RVEF, left ventricular ejection fraction (LVEF) and left atrial volumes (LAVs) were measured using 3DE datasets. We determined the association of those parameters, as well as of aortic valve replacement (AVR), and Charlson's comorbidity index with cardiac events. We also analyzed whether RVEF has incremental value over two-dimensional echocardiography (2DE) RV parameters.

Results: During a median follow-up of 27 months, 57 patients developed cardiac events, and 68 patients received AVR. Univariate Cox proportional hazard analysis revealed that RVEF was associated with cardiac events ($p < 0.001$). Multivariate analysis revealed that RVEF was significantly associated with cardiac events ($p < 0.001$) even after adjusting for AVR, Charlson's comorbidity index, LVEF, LAV, E/e', and indexed aortic valve area (iAVA). An incremental value of RVEF over left heart parameters was also demonstrated using a nested regression model. Classification and regression-tree analysis selected RVEF first with a cut-off value of 41%. RVEF had incremental value over iAVA, LVEF, and 2DE conventional RV parameters for its association with future outcomes.

Conclusions: 3DE RVEF had significant prognostic value even after adjusting for comorbidities, left heart parameters, and conventional 2DE RV parameters in asymptomatic aortic stenosis.

Keywords: asymptomatic aortic stenosis, prognosis, 3DE, RVEF, CART analysis

OPEN ACCESS

Edited by:
Elena Surkova, Royal Brompton Hospital, United Kingdom

Reviewed by:
Andrea Agnes Molnar, Semmelweis University, Hungary
Ali Hosseinsabet, Tehran University of Medical Sciences, Iran

****Correspondence:***
Yosuke Nabeshima
y.nabeshima1016@gmail.com

Specialty section:
This article was submitted to Cardiovascular Imaging, a section of the journal Frontiers in Cardiovascular Medicine

Received: *14 October 2021*
Accepted: *22 November 2021*
Published: *13 December 2021*

Citation:
Nabeshima Y, Kitano T and Takeuchi M (2021) Prognostic Value of the Three-Dimensional Right Ventricular Ejection Fraction in Patients With Asymptomatic Aortic Stenosis. Front. Cardiovasc. Med. 8:795016. doi: 10.3389/fcvm.2021.795016

INTRODUCTION

The number of patients with aortic stenosis (AS) has been increasing rapidly due to the aging of society, especially in developed countries (1). This change has resulted in an exponential increase of heart failure (HF) hospitalizations and surgical or transcatheter aortic valve replacements (AVRs) (2). Due to the socioeconomic impact of AS, optimization of surgical intervention is urgently required. Current guidelines recommend AVR for patients with symptomatic severe AS (3). However, management of asymptomatic AS with preserved left ventricular ejection fraction (LVEF) has not been clarified (3–6). When considering AVR in asymptomatic AS patients (6, 7), we have to assess not only valve condition, but also myocardial function, because of the non-negligible rate of sudden cardiac death and relatively higher risk of HF (8–10). The prognostic impact of right ventricular (RV) function has garnered increased interest in this parameter in recent years. RV dysfunction can affect the risk of HF via a negative impact on cardiac output and ventricular interactions in various heart diseases (11). Genereux and colleagues have proposed a new concept called "cardiac damage stage" for risk stratification of asymptomatic AS patients (12, 13). According to their findings, patients with RV dysfunction had worse prognoses than those with left ventricular (LV) dysfunction with preserved RV function. Galli et al. also indicated the importance of tricuspid annular plane systolic excursion (TAPSE) to predict cardiovascular death in severe AS (14). However, those publications used 2D or Doppler echocardiography to analyze RV function, irrespective of complex RV geometry. Three-dimensional echocardiography (3DE) does not rely on geometric assumptions and can provide more accurate and reliable information regarding RV function (15). Left atrial (LA) function is also reported as a useful marker to stratify the risk of asymptomatic AS patients (16). We hypothesized that RV ejection fraction (RVEF) is the most robust predictor for future outcomes among LV, LA, and RV function parameters assessed with 3DE in asymptomatic AS. Accordingly, we sought to investigate the prognostic utility of 3DE-derived RVEF in patients with asymptomatic AS.

MATERIALS AND METHODS

Study Population

This was a single-center observational study. Using a 3DE database, we retrospectively selected 3DE datasets of Japanese patients with AS who had undergone transthoracic echocardiography in the University of Occupational and Environmental Health hospital from April 2008 to December 2018. Individuals who had no AS-related symptoms were selected from the database. Patients with fewer than 30 days of follow-up after echocardiography were excluded. We also collected several clinical parameters to calculate Charlson's comorbidity index (17). The study was approved by the ethics committee at the University of Occupational and Environmental Health. As this was a retrospective study, the Institutional Review Board waved the requirement for informed consent.

Echocardiography

3DE was performed immediately after standard transthoracic 2D echocardiography (2DE) and Doppler echocardiography. 3DE images were acquired using an apical approach and commercially available ultrasound machines (iE33 or Epic7G, Philips Healthcare, Andover, MA; Vivid7 or Vivid E95, GE Healthcare, Horten, Norway) equipped with a 3DE transducer (X3-1 or X5-1, Philips Healthcare, Andover, MA; 4V, GE Healthcare, Horten, Norway). Trans-mitral flow velocity was recorded at the coaptation point of both leaflets. Mitral annular velocities were recorded at septal and lateral sides of the mitral annulus, and average e' was calculated. Peak aortic flow velocity was recorded in multiple transducer positions, and the highest value was used for the measurements of the mean pressure gradient (PG) and velocity-time integral (VTI). RV fractional area change (RVFAC) was calculated by standard formula. 2DE RV speckle tracking analysis was performed using commercially available, vendor-independent, fully automated strain analysis software (AutoStrain RV, TomTec Imaging Systems, Unterschleissheim, Germany). The software automatically determined the RV endocardial border and performed speckle tracking analysis during a single cardiac cycle. The endocardial border was manually corrected as required. RV free-wall longitudinal strain (RVfwLS) and global longitudinal strain (RVGLS) were calculated.

3D Speckle Tracking Analysis

LV and RV 3DE speckle tracking analyses were performed using commercially available, vendor-independent, 3DE quantification software (4D LV ANALYSIS-3 and 4D RV FUNCTION 3, TomTec Imaging Systems). These methods have been described in detail previously, and their accuracy and reliability are recognized (18). For LV analysis, after selecting a specific 3DE dataset, the software automatically detected the LV endocardial border. Manual correction of the endocardial border was performed as needed. After confirming the tracing line, 3D speckle-tracking analysis was performed through a single cardiac cycle, generating LV volume curves, from which LV end-diastolic volume (LVEDV), end-systolic volume (LVESV), and LVEF were calculated. LV mass was calculated by manually drawing the epicardium of end-diastolic frames of three standard apical views extracted from 3DE datasets. LVEDV index (LVEDVI), LVESV index (LVESVI), and LV mass index (LVMI) were calculated by body surface area (BSA). For the RV analysis, LV-focused end-diastolic apical four-, two-, and three-chamber views, and RV-focused two-orthogonal views were extracted from a 3DE dataset. After specifying anatomical landmarks (center points of the mitral and tricuspid annular planes and the apex), the software automatically determined the RV endocardial cast. Following manual correction of the endocardial border, 3D speckle tracking analysis was performed. RV end-diastolic volume index (RVEDVI), end-systolic volume index (RVESVI), and RVEF were calculated (**Figure 1**).

3D Left Atrial Volume

3D maximal and minimal left atrial volumes (LAVs) were calculated using vendor-specific software (QLAB 13.0, Philips

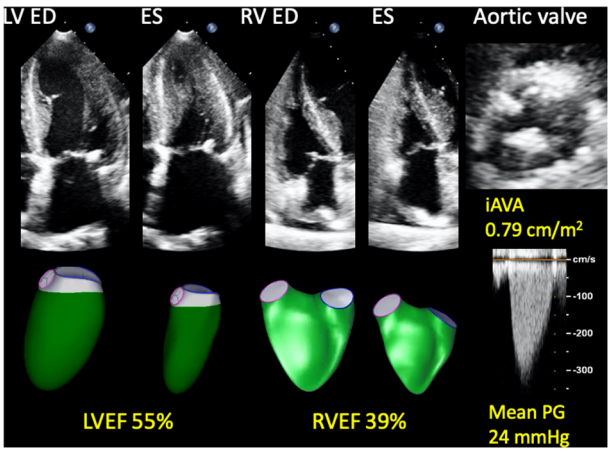

FIGURE 1 | Representative 3D RV and LV analyses in a patient with asymptomatic AS who developed a cardiac event. A 74-year-old woman who developed heart failure three months after baseline echocardiography. AS was moderate and LVEF was preserved; however, RVEF was reduced. She also had hypertension, chronic kidney disease, and chronic obstructive pulmonary disease. 3D, three-dimensional; AS, aortic stenosis; ED, end-diastole; ES, end-systole; iAVA, indexed aortic valve area; LV, left ventricular; LVEF, left ventricular ejection fraction; PG, pressure gradient; RV, right ventricular; RVEF, right ventricular ejection fraction.

TABLE 1 | Patient characteristics ($n = 367$).

Variables	
Age (y.o)	77.1 ± 10.0
Sex (Male)	168 (46%)
Body mass index (kg/m^2)	22.7 ± 3.9
Body surface area (m^2)	1.52 ± 0.21
Systolic blood pressure (mmHg)	147.5 ± 23.5
Diastolic blood pressure (mmHg)	75.0 ± 13.5
Heat Rate (bpm)	69.5 ± 12.6
Rhythm (SR/Af/PM)	338/25/4
Comorbidities	
Hypertension	295 (80%)
Diabetes mellitus	115 (31%)
Coronary artery disease	79 (22%)
Chronic kidney disease	174 (47%)
Chronic pulmonary disease	62 (17%)
Medications	
Calcium channel blocker	185 (52%)
β-blocker	76 (21%)
ACEi or ARB	208 (58%)
Digitalis	7 (2%)
Diuretics	107 (30%)
Warfarin/DOAC	58 (16%)
Charlson's index	5.22 ± 1.94

Data are shown as mean ± standard deviations or n (%).
ACEi, angiotensin converting enzyme inhibitor; Af, atrial fibrillation; ARB, angiotensin receptor blocker; DOAC, direct oral anticoagulant; SR, sinus rhythm; PM, pacemaker.

Healthcare, Andover, MA; EchoPAC version 203, GE Healthcare, Horten, Norway). Detailed methods have been described previously (19). Briefly, we calculated LAVs using Simpson's biplane method with the anterior-posterior and medial-lateral 2D views extracted from 3DE datasets. LAVs were indexed to BSA yielding maximal LAV index (LAVIx) and minimal LAV index (LAVIn). This is a manual method, and we did not use 3D LA speckle tracking software.

AS Severity

Stroke volume (SV) was calculated as the difference of LVEDV and LVESV measured by 3DE. Stroke volume index (SVi) was calculated as SV divided by BSA. Indexed aortic valve area (iAVA) was calculated as SV divided by AV VTI times BSA. We defined more-than-moderate-to-severe AS as AVA <1.0 cm^2 or iAVA <0.6 cm^2/m^2. The patients were classified as high-gradient (peak velocity ≥ 4.0 m/s or mean PG ≥ 40 mmHg) AS (HG-AS), and low-gradient (peak velocity <4.0 m/s and mean PG <40 mmHg) AS (LG-AS) according to the current ESC guideline (20). LG-AS was further classified into 3 categories: low-flow (SVi <35 mL/m^2) low-gradient AS (LFLG-AS) with preserved LVEF, LFLG-AS with reduced LVEF, and normal-flow low-gradient AS (NFLG-AS).

Follow-Up

Patients were followed up in an outpatient clinic. Prognostic information was obtained by interviewing attending physicians or by searching digital medical records. If patients were followed up in other hospitals, we also contacted corresponding physicians to obtain prognostic information. The primary endpoint was defined as a composite adverse cardiac event, including cardiac death, hospitalization due to heart failure, ventricular tachycardia/fibrillation, or non-fatal myocardial infarction.

Statistical Analysis

Continuous data were expressed as means ± SDs or as medians and interquartile ranges (IQR; 25th to 75th percentiles). Categorical variables were presented as absolute numbers or percentages. Student's *t*-test was used to compare continuous variables between two groups when data were normally distributed. Wilcoxon sum rank test was used when data were not normally distributed. Fisher's exact test or a chi-square test were used to compare categorical variables. Cox proportional hazards analysis was used to calculate hazard ratios and 95% confidence intervals. Univariate and multivariate Cox proportional hazard analyses were used to assess the prognostic utility of echocardiographic parameters. AVR was treated as a time-dependent covariate. Survival analysis was performed using the Kaplan-Meier method, and differences in survival rates between groups were analyzed by the log-rank test. Net-reclassification improvement (NRI) analysis and DeLong's test were used to compare risk prediction utility between the two models. Classification and regression-tree (CART) analyses were conducted to predict cardiac events. A two-sided p-value < 0.05 was considered statistically significant. All statistical analyses were performed using commercial software (JMP version 14.0, SAS Institute Inc., Cary, NC; R version 3.6.3, The R foundation for Statistical Computing, Vienna).

RESULTS

Patient Characteristics

Using a 3DE database, we found 392 asymptomatic AS patients. Of those patients, 25 were excluded because their follow-up duration after baseline echocardiography was <30 days. Finally, first-time echocardiographic datasets from 367 patients were selected for the analysis. We could not analyze 3DE datasets of twelve patients due to a low volume rate or extremely poor image quality. We performed 3DE LV and RV analysis in the other 355 patients, resulting in feasibility of 97% for both LV and RV analyses. Image quality of LV was good in 35%, fair in 53%, and poor in 12%. Corresponding RV values were good in 13%, fair in 57%, and poor in 30%. It was impossible to analyze 3D LAVs due to the fact that datasets failed to encompass all of the LA wall in 10 patients, and the feasibility of 3D LA analysis was 94%. LA image quality was good in 35%, fair in 53%, and poor in 11%. Clinical characteristics are summarized in **Table 1**.

Two- and Three-Dimensional Echocardiographic Parameters

Severe AS was observed in 43% (152/354) of the study population. Median values of LVEF and RVEF by 3DE analysis were 52 and 48%, respectively. 30% (107/355) of patients had reduced LVEF (LVEF <50%), and 32% (112/355) had reduced RVEF (RVEF <45%). 53% (189/355) of patients had preserved both ventricular EFs, and 15% (53/355) of patients had reduced bilateral ventricular EFs. **Table 2** presents echocardiography parameters.

TABLE 2 | Echocardiographic parameters ($n = 367$).

Variables	Number	Median (25th to 75th percentiles)
E-wave (cm/s)	367	77.0 (62.0–98.0)
E/A	335	0.71 (0.59–0.90)
E/e'	363	16.9 (12.8–22.1)
MR (severe/moderate/mild)	318	3/5/219
TR (severe/moderate/mild)	274	3/12/218
SPAP (mmHg)	326	33.0 (27.9–39.2)
PH (SPAP > 50 mmHg)	326	20 (6%)
RVFAC (%)	342	40.1 (36.1–44.8)
RVfwLS (%)	342	24.6 (20.7–27.8)
RVGLS (%)	342	19.4 (16.6–21.8)
Peak velocity (m/s)	366	3.04 (2.53–3.59)
Mean PG (mmHg)	366	19.4 (13.8–29.8)
Indexed AVA (cm^2/m^2)	354	0.64 (0.51–0.80)
AS classification	354	
HG-AS		44 (12%)
LFLG-AS with preserved LVEF		24 (7%)
LFLG-AS with reduced LVEF		21 (6%)
NFLG-AS		108 (30%)
Mild to moderate AS		158 (45%)
SVi (mL/m^2)	355	42.5 (37.0–49.1)
3D LVEDVI (mL/m^2)	355	83.3 (72.1–97.3)
3D LVESVI (mL/m^2)	355	39.9 (33.1–49.2)
3D LVEF (%)	355	52.5 (47.9–55.6)
3D LVMI (g/m^2)	355	98.8 (83.9–113.6)
3D LAVIx (mL/m^2)	345	50.1 (39.7–61.3)
3D LAVIn (mL/m^2)	345	26.9 (21.1–36.1)
3D RVEDVI (mL/m^2)	355	55.9 (48.4–66.4)
3D RVESVI (mL/m^2)	355	29.4 (24.2–34.1)
3D RVEF (1%)	355	48.0 (43.7–52.7)

Data are shown as medians (25th to 75th percentiles) or n (%).
3D, three-dimensional; AVA, aortic valve area; LAEF, left atrial emptying fraction; LAVIn, minimum left atrial volume index; LAVIx, maximum left atrial volume index; LVEDVI, left ventricular end-diastolic volume index; LVEF, left ventricular ejection fraction; LVESVI, left ventricular end-systolic volume index; LVMI, left ventricular mass index; MR, mitral regurgitation; PG, pressure gradient; PH, pulmonary hypertension; RVEDVI, right ventricular end-diastolic volume index; RVEF, right ventricular ejection fraction; RVESVI, right ventricular end-systolic volume index; RVFAC, right ventricular fractional area change; RVfwLS, right ventricular free-wall longitudinal strain; RVGLS, right ventricular global longitudinal strain; SPAP, systolic pulmonary artery pressure; SVi, stroke volume index; TR, tricuspid regurgitation.

Outcomes

During a median follow-up of 26.7 months (IQR, 15.4–56.6 months), 57 patients reached a primary endpoint, including 19 cardiac deaths, 32 HFs requiring hospital admission, four myocardial infarctions, and two ventricular tachyarrhythmias. Notably, four cardiac deaths and three HFs occurred after AVR. Sixty-eight patients received AVR during the follow-up. The median interval from baseline echocardiography to AVR was 20.5 months. Univariate Cox proportional hazard analysis revealed that mean PG, iAVA, E/e', SVi, Charlson's comorbidity index, LVEF, RVEF, and LAVIs were associated with cardiac events (**Table 3**).

Table 4 depicts the results of multivariate Cox proportional hazard analyses. According to results from univariate analysis and clinical importance, we created five models for multivariate analyses. LVEF and RVEF were significantly associated with cardiac events after adjusting Charlson's comorbidity index, AVR, and one of either echocardiographic parameter. DeLong's test revealed a significant increase of c-statistics after adding RVEF to LVEF, LAVIn, E/e', and mean PG (**Figure 2**). NRI analysis revealed that the logistic regression model that included RVEF showed a significant improvement of outcome classification compared with the logistic regression model including LVEF, LAVIn, E/e', and mean PG (NRI = 0.655; $p < 0.001$).

For survival CART analysis, we entered 18 variables including age, sex, Charlson's comorbidity index, LVEDVI, LVESVI, LVEF, LVMI, SVi, LAVIx, LAVIn, peak velocity, mean PG, iAVA, E wave, E/e', RVEDVI, RVESVI, and RVEF. CART first selected RVEF (with a cut-off of 41%), followed by LVEF (with a cut-off of 39%), Charlson's cormorbidity index, LAVIn, and mean PG (**Figure 3**). Generated Kaplan-Meier curves indicated that only 4% of patients (9/212) having more than cut-off values of LVEF, RVEF, and Charlson's comorbidity index ≤6 developed cardiac events. Corresponding values of patients with ≤41% of RVEF and ≤ 39% of LVEF were 58% (30/52) and 43% (6/14), respectively.

For the Kaplan-Meier analysis, we divided patients into four groups according to cut-off values of LVEF (50%) and RVEF (45%) (**Figure 4**). There was a significant difference between the

TABLE 3 | Univariate Cox regression analyses of predictors of cardiac events.

	HR	95% CI	*Z*-score	*P*-value
Age (per 1 y.o increase)	1.025	0.994–1.058	1.569	0.117
Sex (Male)	1.237	0.735–2.083	0.801	0.423
BMI (per 1 kg/m^2 increase)	0.956	0.888–1.030	−1.181	0.238
BSA (per 1 m^2 increase)	0.738	0.196–2.787	−0.448	0.654
SBP (per 1 mmHg increase)	0.993	0.982–1.004	−1.318	0.188
DBP (per 1mmHg increase)	0.996	0.977–1.015	−0.419	0.675
Heat Rate (per 1 bpm increase)	1.030	1.010–1.051	2.899	0.004
E-wave (per 1 cm/s increase)	1.010	1.003–1.017	2.809	0.005
E/A (per 1-unit increase)	1.298	0.808–2.087	1.078	0.281
E/e' (per 1-unit increase)	1.031	1.013–1.049	3.349	<0.001
MR (moderate or severe)	2.303	0.557–0.529	1.152	0.250
TR (moderate or severe)	2.301	0.700–7.569	1.372	0.170
SPAP (per 1 mmHg increase)	1.015	0.989–1.042	1.117	0.264
PH (yes)	2.874	1.222–6.757	2.420	0.016
RVFAC (per 1% increase)	0.916	0.884–0.949	−4.866	<0.001
RVfwLS (per 1% increase)	0.887	0.841–0.936	−4.399	<0.001
RVGLS (per 1% increase)	0.820	0.765–0.880	−5.535	<0.001
Peak velocity (per 1 m/s increase)	1.283	0.911–1.081	1.427	0.153
Mean PG (per 1 mmHg increase)	1.020	1.002–1.039	2.163	0.030
Indexed AVA (per 1 cm^2/m^2 increase)	0.065	0.013–0.317	−3.384	<0.001
SVi (per 1 mL/m^2 increase)	0.945	0.916–0.975	−3.598	<0.001
AVR (yes)	0.539	0.272–1.335	−1.335	0.182
Charlson's index (per 1-point increase)	1.296	1.137–1.487	3.876	<0.001
3D LVEDVI (per 1 mL/m^2 increase)	1.006	0.994–1.017	0.965	0.335
3D LVESVI (per 1 mL/m^2 increase)	1.027	1.014–1.039	4.215	<0.001
3D LVEF (per 1% increase)	0.894	0.868–0.920	−7.559	<0.001
3D LVMI (per 1 g/m^2 increase)	1.012	1.004–1.020	2.979	0.003
3D LAVIx (per 1 mL/m^2 increase)	1.023	1.011–1.036	3.812	<0.001
3D LAVIn (per 1 mL/m^2 increase)	1.034	1.022–1.046	5.508	<0.001
3D LAEF (per 1% increase)	0.941	0.921–0.960	−5.790	<0.001
3D RVEDVI (per 1 mL/m^2 increase)	1.017	1.003–1.032	2.435	0.015
3D RVESVI (per 1 mL/m^2 increase)	1.060	1.041–1.079	6.437	<0.001
3D RVEF (per 1% increase)	0.891	0.864–0.917	−7.669	<0.001

3D, three-dimensional; AVA, aortic valve area; AVR, aortic valve replacement; BMI, body mass index; BSA, body surface area; CI, confidence interval; DBP, diastolic blood pressure; LAEF, left atrial emptying fraction; LAVIn, minimum left atrial volume index; LAVIx, maximum left atrial volume index; LVEDVI, left ventricular end-diastolic volume index; LVEF, left ventricular ejection fraction; LVESVI, left ventricular end-systolic volume index; LVMI, left ventricular mass index; HR, hazard ratio; PG, pressure gradient; RVEDVI, right ventricular end-diastolic volume index; RVEF, right ventricular ejection fraction; RVESVI, right ventricular end-systolic volume index; SBP, systolic blood pressure; SPAP, systolic pulmonary artery pressure; SVi, stroke volume index.

group of patients who had preserved LVEF with impaired RVEF and the group of patients with both EFs preserved ($p < 0.001$).

RVEF and Conventional 2D RV Parameters

RVGLS was significantly associated with cardiac events even after being adjusted for AVR, Charlson's comorbidity index, LVEF, and either mean PG, iAVA, E/e', LAVIn, or SVi (**Supplementary Tables S1–S3**). RVfwLS had no significant association with outcome when LAVIn was included in the multivariate model. However, when we added RVEF to the multivariate model, the prognostic significance of all of three 2D RV parameters disappeared (**Supplementary Table S4**). To determine the independent and incremental prognostic value of RVEF, we generated a nested regression model, sequentially adding iAVA, LVEF, conventional 2D RV parameters (either FAC of RVGLS), and RVEF. Chi-square values increased in stepwise fashion upon adding each parameter. Addition of RVEF to the model including iAVA, LVEF and RVFAC further increased the chi-square value from 57.7 to 71.7 ($p < 0.001$), whereas adding it to the model containing iAVA, LVEF and RVGLS increased it from 61.5 to 72.7 ($p < 0.001$), respectively (**Supplementary Figure S1**).

Patients With Preserved LVEF

For sensitivity analysis, we performed subgroup analyses in a subset of patients who had ≥50% of LVEF. Among 248 patients

TABLE 4 | Multivariate Cox regression analyses after adjusting Charlson index and AVR as time-dependent covariates.

	Mean PG model		iAVA model		SVi model		E/e' model		LAVIn model	
	HR (95% CI)	*P*-value	HR (95% CI)	*P*-value	HR (95% CI)	*P*-value	HR (95% CI)	*P*-value	HR (95% CI)	*P*-value
LVEF	0.933 (0.900–0.968)	<0.001	0.944 (0.910–0.978)	0.002	0.945 (0.908–0.983)	0.005	0.951 (0.916–0.988)	0.010	0.954 (0.917–0.993)	0.021
RVEF	0.918 (0.887–0.949)	<0.001	0.924 (0.893–0.956)	<0.001	0.918 (0.884–0.954)	<0.001	0.913 (0.881–0.947)	<0.001	0.926 (0.892–0.961)	<0.001
Mean PG	1.038 (1.020–1.055)	<0.001								
iAVA			0.073 (0.015–0.357)	0.001						
SVi					0.999 (0.971–1.029)	0.981				
E/e'							1.035 (1.009–1.062)	0.009		
LAVIn									1.024 (1.008–1.039)	0.002

AVR, aortic valve replacement; CI, confidence interval; HR, hazard ratio; iAVA, indexed aortic valve area; LAVIn, minimal left atrial volume index; LVEF, left ventricular ejection fraction; RVEF, right ventricular ejection fraction; SVi, stroke volume index.

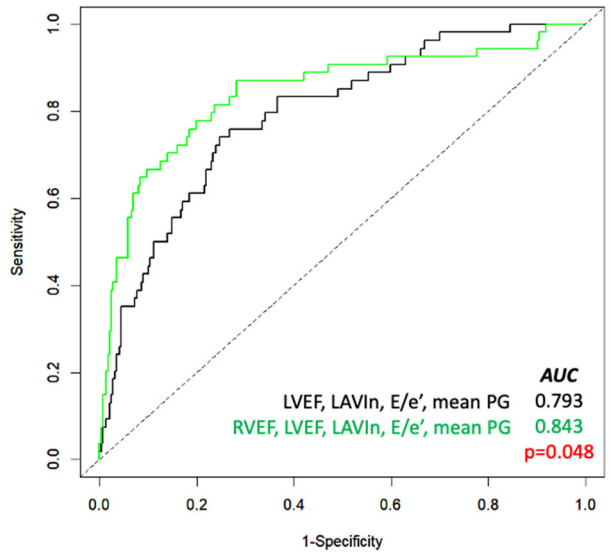

FIGURE 2 | Receiver-operating characteristic curve analysis for prediction of cardiac events. Comparison of the area under the curve (AUC) of several parameters (black line) and with RVEF added (green line). LAVIn, minimum left atrial volume index; LVEF, left ventricular ejection fraction; PG, pressure gradient; RVEF, right ventricular ejection fraction.

with LVEF ≥50%, 23 patients developed cardiac events during a median of 32 months follow-up. Multivariate Cox analysis, revealed that RVEF was a significant marker even after adjusting for LVEF ($p < 0.001$). **Supplementary Figure S2** shows the results of the CART analysis. As with the results for all patients, CART selected RVEF first.

Patients With "More-Than-Moderate-to-Severe AS"

Among 196 "more-than-moderate-to-severe" AS patients, 40 developed cardiac events during a median of 30 months follow-up. Univariate Cox regression analysis indicated that RVEF and conventional 2DE RV parameters were significantly associated with cardiac events (**Supplementary Table S5**). The results of multivariate Cox regression analyses revealed that RVEF was significantly associated with cardiac events, even after adjusting for AVR, Charlson index, and LVEF / iAVA/ LVMI /E/e' /LAVIn (**Supplementary Table S6**). We constructed a nested regression model incorporating iAVA, LVEF, RVFAC or RVLS, and RVEF in stepwise manner to determine the independent and incremental prognostic value of RVEF. RVEF had a significant incremental value over iAVA, LVEF, and RVFAC (**Supplementary Figure S3**, left panel) and over iAVA, LVEF, and RVGLS (**Supplementary Figure S3**, right panel). **Supplementary Figure S4** shows the CART analysis indicating that LVEF was selected first with a cut-off value of 47%, followed by RVESVI with a cut-off value of 39 mL/m^2.

Patients With "Less-Than-Moderate-to-Severe AS"

Among 158 "less-than-moderate-to-severe" AS patients, 16 developed cardiac events during a median of 28 months follow-up. Univariate Cox regression analysis revealed that RVEF and RVGLS were significantly associated with cardiac events (**Supplementary Table S7**). CART analysis selected RVEF at first with a cut-off value of 42% (**Supplementary Figure S5**).

Factors Associated With Reduced RVEF

We performed logistic regression analysis to determine which parameter was associated with reduced RVEF, which was defined as RVEF < 40%. Univariate logistic regression analysis revealed that heart rate, E/e', iAVA, SVi, LVEF, LAVIn, coronary artery disease (CAD), chronic kidney disease (CKD), and atrial fibrillation (AF) were significantly associated with reduced RVEF. Multivariate logistic regression analyses revealed that iAVA, SVi, LVEF, and LAVIn were significantly associated with reduced RVEF, even after adjusting for CAD, CKD, and AF (**Supplementary Table S8**).

DISCUSSION

To the best of our knowledge, this is the first study to demonstrate the prognostic utility of 3DE determined RVEF in patients with asymptomatic AS.

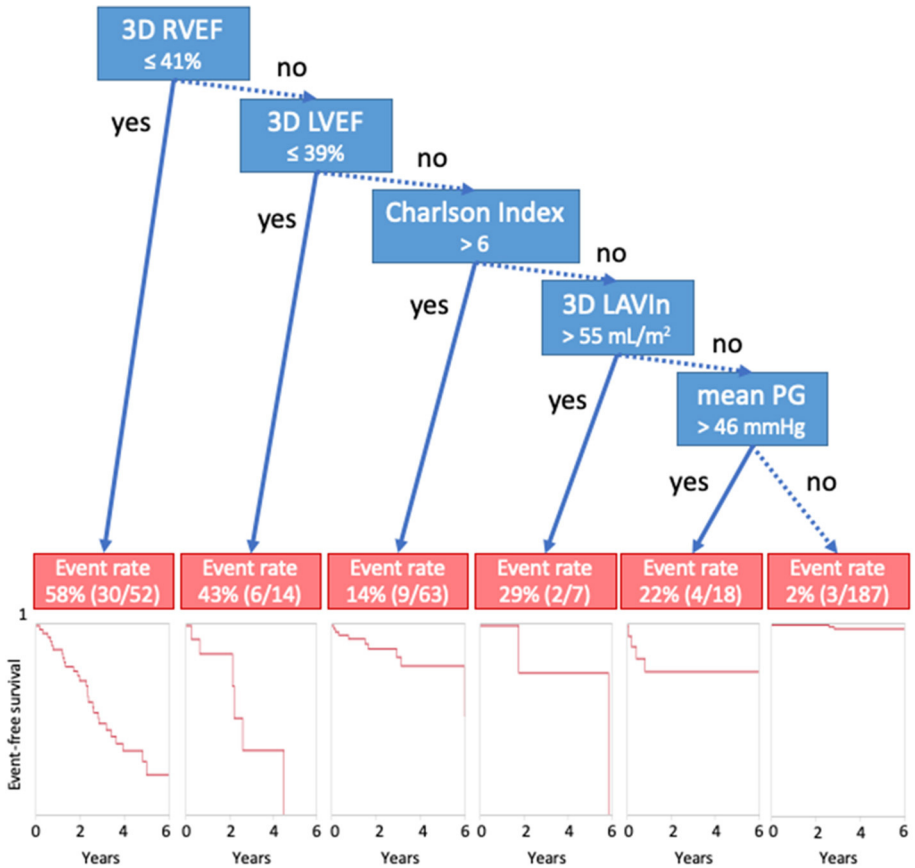

FIGURE 3 | Classification and regression-tree analysis for cardiac events. Blue boxes denote cut-offs, and red boxes describe event rates. 3D, three-dimensional; AVR, aortic valve replacement; LAVIn, minimum left atrial volume index; LVEF, left ventricular ejection fraction; PG, pressure gradient; RVEF, right ventricular ejection fraction.

Previous Studies

Indications and best timing of AVR for patients with asymptomatic AS are not clearly defined. Some studies suggest that early elective AVR improves the prognosis of patients with asymptomatic severe AS (21). Genereux et al. proposed the "cardiac damage" concept, which claims that damage to each heart chamber regulates the prognosis of patients with severe AS who received AVR, and their results suggest that when RV damage has occurred, it is too late to intervene (12). Moreover, Tastes et al. reported that the cardiac damage system has significant prognostic utility for patients with moderate to severe asymptomatic AS, independent of AVR (13). Because of its reduced invasiveness and lower perioperative risk, the advent of transcatheter AVR could increase the frequency of valve replacement in patients who are at high risk for surgical AVR. For this reason, pre-operative risk stratification of patients with asymptomatic AS is vital for optimal use of health resources.

Some reports have explained the prognostic utility of RV functional parameters in AS. Galli et al. reported the prognostic importance of RV function among 200 patients with severe AS (14). The subjects were predominantly asymptomatic (87%). They found that 24% of severe AS patients had impaired RV function, and biventricular dysfunction was a strong prognostic indicator of future cardiac events. Zilberszac et al. reported the prognostic value of RV dysfunction in 76 patients with low-flow, low-gradient severe AS (22). Only seven patients were asymptomatic. RV dysfunction was assessed by TAPSE, the systolic lateral tricuspid annulus velocity or 2D RV free-wall strain. RV dysfunction was a significant prognostic marker for overall survival in univariate Cox proportional hazard analysis. However, this utility was no longer significant after adjusting EuroSCORE II. Those two papers used only RV parameters that represent longitudinal motion. This limitation may explain why in those studies, RV parameters were not such strong markers compared with other factors, because the RV moves three-dimensionally, and regional and longitudinal motion may not represent global RV function in some cases (23).

Current Study

We found that 3D RVEF had significant utility in predicting future cardiac events, even after adjusting for LVEF, AS severity, LV diastolic function, AVR, and comorbidities. Statistical analysis revealed that RVEF had incremental value over comorbidities, left heart parameters, and AS severity to predict cardiac events.

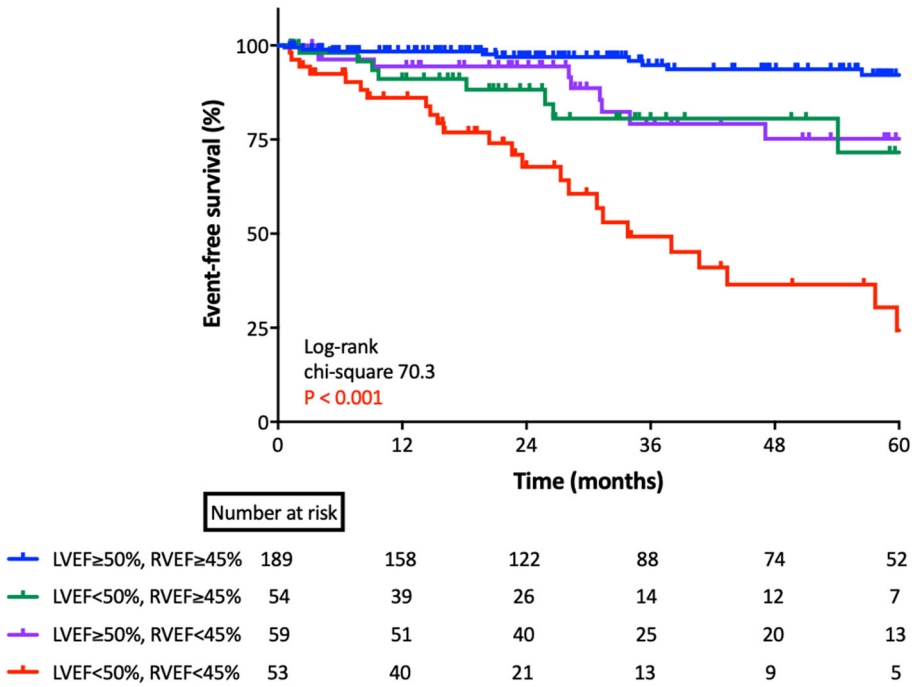

FIGURE 4 | Kaplan-Meier survival analysis for cardiac events based upon RVEF and LVEF. Kaplan-Meier analysis for cardiac events, according to group, as classified by lower limits of normal LVEF and RVEF. LVEF, left ventricular ejection fraction; RVEF, right ventricular ejection fraction.

Kaplan-Meier analysis indicated that both LVEF and RVEF were useful for risk stratification of patients with asymptomatic AS.

In our cohort, 73% of asymptomatic AS patients had some non-cardiac comorbidities. Not only AS severity and left heart function, but also other comorbidities that develop RV volume or pressure overload, such as pulmonary disease and CKD can affect RV function. Thus, RV function may represent status of the whole heart. In fact, reduced RVEF was significantly associated with echocardiographic parameters, CKD, CAD, and atrial fibrillation. We cannot determine the causal relationship because of the cross sectional nature of the study; however, optimal medical therapy or intervention targeting HF, ischemia, and AF have potential to improve management of AS patients with reduced RVEF.

Our results are consistent with previous publications. Previously, we determined the prognostic utility of 3D RVEF in 446 patients with diverse backgrounds (18). 3D RVEF had an incremental value over 3D LVEF, E/e', and CKD to predict future adverse events. CART analysis selected RVEF first with a cut-off of 41%. The value was equivalent to observed value in this study (**Figure 3**). Muraru et al. also reported the prognostic utility of 3D RVEF in patients with various cardiac diseases (24). They stressed that 3D RVEF showed higher predictive power for cardiac events than TAPSE or RVFAC, which was in agreement with our results. Kaplan-Meier analysis indicated that patients with RVEF <40% showed a high incidence of cardiac death, cardiac events, and all-cause mortality. Those results are consistent with our RVEF cut-off values derived from CART analysis. Unlike those two previous studies, our intent was to determine prognostic value of RVEF in a specific group of patients, asymptomatic AS, and we clearly showed its prognostic utility.

In a subset of patients with "more-than-moderate-to-severe" AS, CART analysis selected LVEF first. The current AHA/ACC guideline (3) recommends aortic valve surgery as class I indication for asymptomatic severe AS patients with LVEF <50%. Therefore, we believe that assessing LVEF at first is reasonable in asymptomatic severe AS. CART secondly selected RVESVI. However, we must note that 7 of 28 more-than-moderate-to-severe AS patients with LVEF ≥50%, who also had RVEF <45% developed cardiac events. Of those 7 patients who had cardiac events, two developed heart failure after AVR. Thus, when we manage asymptomatic severe AS patients, we should assess LV function for indications of AVR first. However, we should carefully manage patients with preserved LVEF, but impaired RVEF. On the other hand, for patients with asymptomatic mild/moderate AS, the prognostic importance of RVEF may be greater than that of left heart function and valve condition.

Clinical Implications

Assessment of RVEF using 3DE provides robust information for predicting future outcomes in patients with asymptomatic AS. Overall, 3D RVEF was significantly associated with cardiac events regardless of AS severity or left chamber function. 3DE determined that RVEF is a much more useful parameter than 2DE-derived RV parameters for predicting future outcome. Thus, combined 3DE assessment of left and right chamber function

might be the best way for appropriate management of patients with asymptomatic AS.

LIMITATIONS

This study has several limitations. First, it includes not only severe AS patients, but also mild to moderate AS patients. However, because AS is a progressive disease, predicting future outcomes of patients with mild to moderate AS using baseline echocardiography is essential for appropriate management. In fact, RV systolic functions were significant prognostic parameters, independent of AS severity. Second, 3D LAV analysis was based on manual tracing, even though 3D LV and RV analyses were performed using semi-automated 3D speckle tracking software. This difference could underrepresent the prognostic value of LAVs in this study, and further studies using 3D LA speckle tracking analysis are required. Third, we did not include 3D global strain values. It is crucial to determine whether 3D global strain values are superior to EFs and volumetric parameters. However, there are few commercial software packages that can incorporate 3D RV and LA strains. Fourth, although we demonstrated that 3D RVEF is better than 2D RV parameters, its accuracy and reliability depend on the expertise of the examiner. 3DE data acquisition was not always possible in every AS patient. In such situations, 2D RVFAC and RVGLS are a potential alternative. Fifth, although significant tricuspid regurgitation (TR) and mitral regurgitation (MR) have potential to affect the prognosis of patients with AS, there were not significant association with cardiac events in this study. This may be due to the small sample size in more than moderate TR and MR. Finally, this was a single-center retrospective study. To validate our concepts, a multi-center prospective study is required.

CONCLUSIONS

3D RVEF had significant prognostic value, even after adjusting 3D left heart parameters and comorbidities in patients with asymptomatic AS. A cut-off value of RVEF $\leq$40% should be considered for better management in asymptomatic AS patients.

DATA AVAILABILITY STATEMENT

The raw data supporting the conclusions of this article will be made available by the authors, without undue reservation.

ETHICS STATEMENT

The studies involving human participants were reviewed and approved by the Ethics Committee at the University of Occupational and Environmental Health. Written informed consent for participation was not required for this study in accordance with the national legislation and the institutional requirements.

AUTHOR CONTRIBUTIONS

YN: data curation, data analysis, and writing—draft. TK: data curation. MT: conceptualization, methodology, supervision, writing—review, and editing. All authors contributed to the article and approved the submitted version.

SUPPLEMENTARY MATERIAL

The Supplementary Material for this article can be found online at: https://www.frontiersin.org/articles/10.3389/fcvm.2021.795016/full#supplementary-material

REFERENCES

1. Benjamin EJ, Virani SS, Callaway CW, Chamberlain AM, Chang AR, Cheng S, et al. Heart disease and stroke statistics-2018 update: a report from the American Heart Association. *Circulation.* (2018) 137:e67–492. doi: 10.1161/CIR.0000000000000558
2. Goldsweig AM, Tak HJ, Chen LW, Aronow HD, Shah B, Kolte DS, et al. The evolving management of aortic valve disease: 5-year trends in SAVR, TAVR, and medical therapy. *Am J Cardiol.* (2019) 124:763–71. doi: 10.1016/j.amjcard.2019.05.044
3. Nishimura RA, Otto CM, Bonow RO, Carabello BA, Erwin JP, Fleisher LA, et al. 2017 AHA/ACC focused update of the 2014 AHA/ACC guideline for the management of patients with valvular heart disease: a report of the American College of Cardiology/American Heart Association Task Force on Clinical Practice Guidelines. *Circulation.* (2017) 135:e1159–95. doi: 10.1161/CIR.0000000000000503
4. Pai RG, Kapoor N, Bansal RC, Varadarajan P. Malignant natural history of asymptomatic severe aortic stenosis: benefit of aortic valve replacement. *Ann Thorac Surg.* (2006) 82:2116–22. doi: 10.1016/j.athoracsur.2006.07.043
5. Pellikka PA, Nishimura RA, Bailey KR, Tajik AJ. The natural history of adults with asymptomatic, hemodynamically significant aortic stenosis. *J Am Coll Cardiol.* (1990) 15:1012–7. doi: 10.1016/0735-1097(90)90234-G
6. Pellikka PA, Sarano ME, Nishimura RA, Malouf JF, Bailey KR, Scott CG, et al. Outcome of 622 adults with asymptomatic, hemodynamically significant aortic stenosis during prolonged follow-up. *Circulation.* (2005) 111:3290–5. doi: 10.1161/CIRCULATIONAHA.104.495903
7. Rosenhek R, Binder T, Porenta G, Lang I, Christ G, Schemper M, et al. Predictors of outcome in severe, asymptomatic aortic stenosis. *N Engl J Med.* (2000) 343:611–7. doi: 10.1056/NEJM200008313430903
8. Dal-Bianco JP, Khandheria BK, Mookadam F, Gentile F, Sengupta PP. Management of asymptomatic severe aortic stenosis. *J Am Coll Cardiol.* (2008) 52:1279–92. doi: 10.1016/j.jacc.2008.07.020
9. Lancellotti P, Magne J, Dulgheru R, Clavel MA, Donal E, Vannan MA, et al. Outcomes of patients with asymptomatic aortic stenosis followed up in heart valve clinics. *JAMA Cardiol.* (2018) 3:1060–8. doi: 10.1001/jamacardio.2018.3152
10. Otto CM. Valvular aortic stenosis: disease severity and timing of intervention. *J Am Coll Cardiol.* (2006) 47:2141–51. doi: 10.1016/j.jacc.2006.03.002
11. Purmah Y, Lei LY, Dykstra S, Mikami Y, Cornhill A, Satriano A, et al. Right ventricular ejection fraction for the prediction of major adverse cardiovascular and heart failure-related events: a cardiac MRI based study of 7131 patients with known or suspected cardiovascular disease. *Circ Cardiovasc Imaging.* (2021) 14:3. doi: 10.1161/CIRCIMAGING.120.011337
12. Genereux P, Pibarot P, Redfors B, Mack MJ, Makkar RR, Jaber WA, et al. Staging classification of aortic stenosis based on the extent of cardiac damage. *Eur Heart J.* (2017) 38:3351–8. doi: 10.1093/eurheartj/ehx381

13. Tastet L, Tribouilloy C, Marechaux S, Vollema EM, Delgado V, Salaun E, et al. Staging cardiac damage in patients with asymptomatic aortic valve stenosis. *J Am Coll Cardiol.* (2019) 74:550–63. doi: 10.1016/j.jacc.2019.04.065
14. Galli E, Guirette Y, Feneon D, Daudin M, Fournet M, Leguerrier A, et al. Prevalence and prognostic value of right ventricular dysfunction in severe aortic stenosis. *Eur Heart J Cardiovasc Imaging.* (2015) 16:531–8. doi: 10.1093/ehjci/jeu290
15. Lang RM, Badano LP, Mor-Avi V, Afilalo J, Armstrong A, Ernande L, et al. Recommendations for cardiac chamber quantification by echocardiography in adults: an update from the American Society of Echocardiography and the European Association of Cardiovascular Imaging. *J Am Soc Echocardiogr.* (2015) 28:1–39. doi: 10.1016/j.echo.2014.10.003
16. Todaro MC, Carerj S, Khandheria B, Cusma-Piccione M, La Carrubba S, Antonini-Canterin F, et al. Usefulness of atrial function for risk stratification in asymptomatic severe aortic stenosis. *J Cardiol.* (2016) 67:71–9. doi: 10.1016/j.jjcc.2015.04.010
17. Charlson ME, Pompei P, Ales KL, MacKenzie CR. A new method of classifying prognostic comorbidity in longitudinal studies: development and validation. *J Chronic Dis.* (1987) 40:373–83. doi: 10.1016/0021-9681(87)90171-8
18. Nagata Y, Wu VC, Kado Y, Otani K, Lin FC, Otsuji Y, et al. Prognostic value of right ventricular ejection fraction assessed by transthoracic 3D echocardiography. *Circ Cardiovasc Imaging.* (2017) 10:2. doi: 10.1161/CIRCIMAGING.116.005384
19. Iwataki M, Takeuchi M, Otani K, Kuwaki H, Haruki N, Yoshitani H, et al. Measurement of left atrial volume from transthoracic three-dimensional echocardiographic datasets using the biplane Simpson's technique. *J Am Soc Echocardiogr.* (2012) 25:1319–26. doi: 10.1016/j.echo.2012.08.017
20. Vahanian A, Beyersdorf F, Praz F, Milojevic M, Baldus S, Bauersachs J, et al. 2021 ESC/EACTS Guidelines for the management of valvular heart disease. *Eur Heart J.* (2021) 28:ehab395. doi: 10.1093/eurheartj/ehab626
21. Miyake M, Izumi C, Taniguchi T, Morimoto T, Amano M, Nishimura S, et al. Early surgery vs. surgery after watchful waiting for asymptomatic severe aortic stenosis. *Circ J.* (2018) 82:2663–71. doi: 10.1253/circj.CJ-18-0416
22. Zilberszac R, Gleiss A, Schweitzer R, Bruno P, Andreas M, Stelzmuller M, et al. Prognostic value of right ventricular dysfunction and tricuspid regurgitation in patients with severe low-flow low-gradient aortic stenosis. *Sci Rep.* (2019) 9:1. doi: 10.1038/s41598-019-51166-0
23. Lakatos BK, Nabeshima Y, Tokodi M, Nagata Y, Toser Z, Otani K, et al. Importance of nonlongitudinal motion components in right ventricular function: three-dimensional echocardiographic study in healthy volunteers. *J Am Soc Echocardiogr.* (2020) 33:995–1005. doi: 10.1016/j.echo.2020.04.002
24. Muraru D, Badano LP, Nagata Y, Surkova E, Nabeshima Y, Genovese D, et al. Development and prognostic validation of partition values to grade right ventricular dysfunction severity using 3D echocardiography. *Eur Heart J Cardiovasc Imaging.* (2020) 21:10–21. doi: 10.1093/ehjci/jez233

Conflict of Interest: The authors declare that the research was conducted in the absence of any commercial or financial relationships that could be construed as a potential conflict of interest.

Publisher's Note: All claims expressed in this article are solely those of the authors and do not necessarily represent those of their affiliated organizations, or those of the publisher, the editors and the reviewers. Any product that may be evaluated in this article, or claim that may be made by its manufacturer, is not guaranteed or endorsed by the publisher.

frontiers in Cardiovascular Medicine

ORIGINAL RESEARCH
published: 25 February 2022
doi: 10.3389/fcvm.2022.837584

Prognostic Value of Right Ventricular Strains Using Novel Three-Dimensional Analytical Software in Patients With Cardiac Disease

Tetsuji Kitano[1], Attila Kovács[2], Yosuke Nabeshima[3], Márton Tokodi[2], Alexandra Fábián[2], Bálint Károly Lakatos[2] and Masaaki Takeuchi[4]*

[1] Department of Cardiology and Nephrology, Wakamatsu Hospital of the University of Occupational and Environmental Health, Kitakyushu, Japan, [2] Heart and Vascular Center, Semmelweis University, Budapest, Hungary, [3] Second Department of Internal Medicine, School of Medicine, University of Occupational and Environmental Health, Kitakyushu, Japan, [4] Department of Laboratory and Transfusion Medicine, University of Occupational and Environmental Health Hospital, Kitakyushu, Japan

Background: Right ventricular (RV) three-dimensional (3D) strains can be measured using novel 3D RV analytical software (ReVISION). Our objective was to investigate the prognostic value of RV 3D strains.

Methods: We retrospectively selected patients who underwent both 3D echocardiography (3DE) and cardiac magnetic resonance from January 2014 to October 2020. 3DE datasets were analyzed with 3D speckle tracking software and the ReVISION software. The primary end point was a composite of cardiac events, including cardiac death, heart failure hospitalization, or ventricular tachyarrhythmia.

Results: 341 patients were included in this analysis. During a median of 20 months of follow-up, 49 patients reached a composite of cardiac events. In univariate analysis, 3D RV ejection fraction (RVEF) and three 3D strain values [RV global circumferential strain (3D RVGCS), RV global longitudinal strain (3D RVGLS), and RV global area strain (3D RVGAS)] were significantly associated with cardiac death, ventricular tachyarrhythmia, or heart failure hospitalization (Hazard ratio: 0.88 to 0.93, $p < 0.05$). Multivariate analysis revealed that 3D RVEF, three 3D strain values were significantly associated with cardiac events after adjusting for age, chronic kidney disease, and left ventricular systolic/diastolic parameters. Kaplan-Meier survival curves showed that 3D RVEF of 45% and median values of 3D RVGCS, 3D RVGLS, and 3D RVGAS stratified a higher risk for survival rates. Classification and regression tree analysis, including 22 clinical and echocardiographic parameters, selected 3D RVEF (cut-off value: 34.5%) first, followed by diastolic blood pressure (cut-off value: 53 mmHg) and 3D RVGAS (cut-off value: 32.4%) for stratifying two high-risk group, one intermediate-risk group, and one low-risk group.

Conclusions: RV 3D strain had an equivalent prognostic value compared with 3D RVEF. Combining these parameters with 3D RVEF may allow more detailed stratification of patient's prognosis in a wide array of cardiac diseases.

Keywords: right ventricular (RV), right ventricular ejection fraction, three-dimensional strain (3D strain), prognosis, ReVISION, cardiac disease

OPEN ACCESS

Edited by:
Daniel A. Morris, Charité-Universitätsmedizin Berlin, Campus Virchow-Klinikum, Germany

Reviewed by:
You-Bin Deng, Huazhong University of Science and Technology, China
Navin Nanda, University of Alabama at Birmingham, United States

****Correspondence:***
Tetsuji Kitano
syuukyuu1986@gmail.com

Specialty section:
This article was submitted to Cardiovascular Imaging, a section of the journal Frontiers in Cardiovascular Medicine

Received: *16 December 2021*
Accepted: *03 February 2022*
Published: *25 February 2022*

Citation:
Kitano T, Kovács A, Nabeshima Y, Tokodi M, Fábián A, Lakatos BK and Takeuchi M (2022) Prognostic Value of Right Ventricular Strains Using Novel Three-Dimensional Analytical Software in Patients With Cardiac Disease. Front. Cardiovasc. Med. 9:837584. doi: 10.3389/fcvm.2022.837584

INTRODUCTION

For the last decade, the right ventricle has gained increasing attention for morphological and functional assessment. Although tricuspid annular plane systolic excursion (TAPSE), right ventricular (RV) fractional area change, systolic tricuspid annular velocity (RVs'), and longitudinal strains are commonly used for assessment of RV function with two-dimensional (2D) and tissue Doppler echocardiography, these measurements do not cover all aspects of RV function and 2D echocardiographic assessment of RV function has several limitations due to the complex morphology of the right ventricle. Three-dimensional echocardiography (3DE) provides accurate and reproducible values of RV volumes and ejection fraction (RVEF) (1, 2) and current guidelines recommend its use to examiners who are familiar with 3DE (3). We have previously reported that RVEF by 3DE is useful for predicting future prognosis in various cardiac diseases (4–6).

The ReVISION (Right VentrIcular Separate wall motion quantificatiON) software was recently introduced, enabling comprehensive 3D echocardiographic analysis of the right ventricle (7). With this method, strain values such as 3D RV global circumferential strain (RVGCS), 3D RV global longitudinal strain (RVGLS), and 3D RV global area strain (RVGAS) could also be calculated from 3DE datasets. Area strain was defined as the percentage change of the regional area of the endocardium, which can be regarded as the product of both longitudinal strain and circumferential strain. Although reference values of 3D RVGCS, 3D RVGLS, and 3D RVGAS were established using ReVISION software (8), there are no studies indicating whether 3D RV strains have prognostic value over 3DE-derived RVEF in patients with cardiac disease.

We hypothesized that 3D RV strains would provide incremental prognostic information over 3D RVEF. Accordingly, we sought to investigate the prognostic value of RV 3D strains in a diverse group of subjects.

MATERIALS AND METHODS

Study Subjects

This was a single-center, retrospective, observational study. Using a cardiac magnetic resonance (CMR) database, we retrospectively selected patients who underwent both CMR and transthoracic echocardiography on the same day at the University of Occupational and Environmental Health Hospital from January 2014 to October 2020. Exclusion criteria were repeat examinations, age <20 years, patients with <30 days of follow-up, patients without echocardiographic datasets, and patients with extremely poor image quality. Clinical characteristics such as anthropometric data, risk factors, and medication information on the day of the echocardiography were collected. This study protocol was approved by the local Ethics Committee of the University of Occupational and Environmental Health (IRB No: UOEHCRB20-181). The requirement for written informed consent was waived because of the retrospective nature of the study.

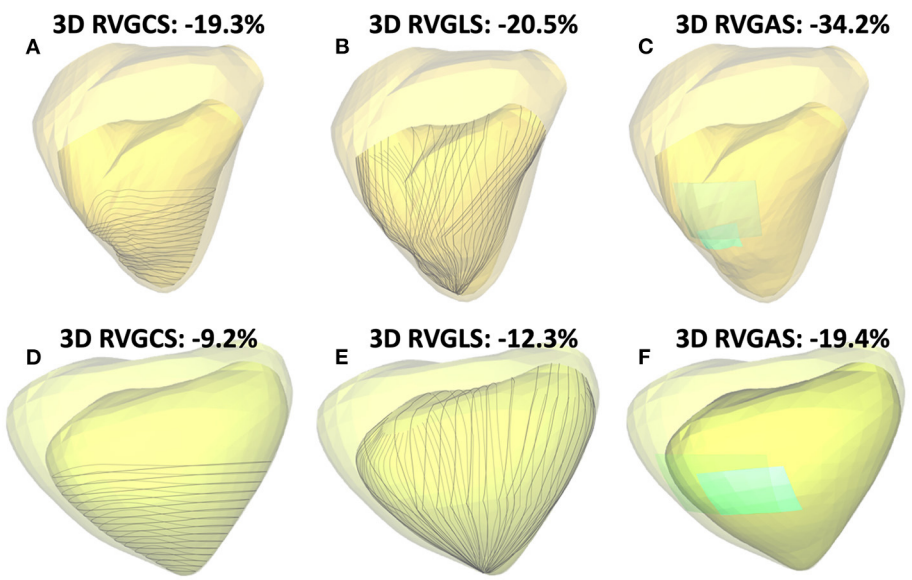

FIGURE 1 | Two representative cases of three-dimensional (3D) right ventricular (RV) analysis using ReVISION software: One case of normal RV function (3D RVEF: 49%, **A–C**) and another case of severe RV dysfunction (3D RVEF: 28%, **D–F**). Transparent light-yellow and light-green represents the end-diastolic endocardial boundary, and darker yellow and darker green represents the end-systolic endocardial boundary. Gray lines indicate contours used for 3D RV global circumferential strain (RVGCS) **(A,D)**, and 3D RV global longitudinal strain (RVGLS) **(B,E)** assessment, respectively. Light-blue segmental areas and their change from end-diastole to end-systole represent the rationale behind area strain calculations [3D RV global area strain (RVGAS) is calculated using entire RV endocardial areas, **C,F**].

Echocardiographic Acquisition

Comprehensive transthoracic two-dimensional and Doppler echocardiographic examination were performed using a commercially available ultrasound system (iE33 or Epic7G, Philips Medical System, Andover, Massachusetts; Vivid E95, GE Healthcare, Horten, Norway).

3DE was performed according to guidelines of the American Society of Echocardiography (ASE) using an iE33, Epic7G, or Vivid E95 equipped with a 3DE transducer (X5-1, Philips Medical System, Andover, Massachusetts; 4V or 4Vc, GE Healthcare, Horten, Norway) (3). 3DE datasets that focused on the left heart chamber were acquired from the apical approach in one- or multi-beat acquisition mode. In addition, 3DE datasets that focused on the right heart chamber were acquired from more lateral transducer positions. In order to increase the volume rate, the width of the image sector size was reduced as narrow as possible, keeping orthogonal 2D echocardiographic images encompassing the entire right ventricle. Datasets were transferred to a separate workstation for off-line analysis.

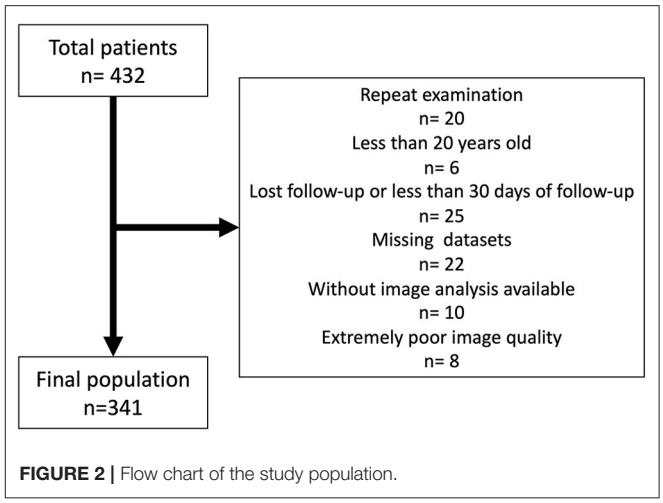

FIGURE 2 | Flow chart of the study population.

Echocardiographic Analysis

Echocardiographic analysis was performed by an experienced examiner (MT). Traditional transthoracic 2D and Doppler echocardiographic parameters were measured according to current guidelines of the ASE and the European Association of Cardiovascular Imaging (9).

Image quality of 3DE datasets was subjectively evaluated by visibility of the endocardium in 2D echocardiography images extracted from 3DE datasets (apical four-chamber, two-chamber, and long-axis view for the left ventricle, and in apical four-chamber view, coronal view, and basal short-axis view for the right ventricle). Each view was divided into six segments, and each segment was scored as 0 (no endocardial visualization), 0.5 (partial endocardial visualization during one cardiac cycle), or 1 (complete endocardial visualization throughout one cardiac cycle). These scores were summed to calculate the total image score (range: 0–18). Results were categorized as good (defined as a total score $\geq$ 16), fair (13 $\leq$ score $<$ 16), poor (10 $\leq$ score $<$ 13), or extremely poor (score $<$ 10) (5).

For 3DE analysis of the left ventricle (LV), 3DE datasets that focused on the left heart chamber were analyzed using vendor-independent 3D speckle tracking software (4D LV analysis, TomTec Imaging System, Unterschleissheim, Germany). The software automatically extracted apical four-chamber, two-chamber, long-axis, and short-axis views from 3DE datasets and detected endocardial surface at LV end-diastole. Endocardial borders at LV end-diastole and end-systole were manually corrected as required. After endocardial boundaries were determined, the software conducted 3D speckle tracking analysis over the entire cardiac cycle and automatically measured LV end-diastolic volume (LVEDV), LV end-systolic volume (LVESV), LV ejection fraction (LVEF), and LV global longitudinal strain (LVGLS).

For RV analysis, we used commercially available 3D speckle tracking software (4D RV function 3, TomTec Imaging system, Unterschleissheim, Germany) and ReVISION software (Argus Cognitive, Inc., Lebanon, New Hampshire, USA, www.revisionmethod.com). First, 3D models of the right ventricle were created with 4D RV function 3. After selecting a 3DE dataset that focused on the right heart chamber, the software automatically extracted two orthogonal views of the left and right ventricles from the 3DE datasets. After aligning each view and determining several anatomic landmarks (the LV apex and the middle of the mitral annulus, the RV apex and the middle of the tricuspid annulus), RV endocardial boundaries were automatically drawn by the software. RV endocardial borders at end-diastole were manually corrected as required. The software performed speckle tracking analysis resulting in calculation of RV volumes and RVEF. 3D RV models were exported throughout the cardiac cycle as a 3D object file series and transferred to ReVISION software. The detailed analytical method of ReVISION software has been described elsewhere (10). Briefly, the software calculates conventional volumetric parameters, i.e., RV end-diastolic volume (RVEDV), RV end-systolic volume (RVESV), and RV ejection fraction (RVEF). To evaluate 3D RVGCS, 15 circumferential contours were created by slicing the 3D model with horizontal planes at equal distances along the longitudinal axis and were tracked throughout the cardiac cycle. The length of the latitudes (C) can be calculated by subdividing the curve and calculating it as the sum of the straight lines. RVGCS can be calculated by multiplying the sum of $(C^{end-systole}\text{-}C^{end-diastole}/C^{end-diastole})$ of the 15 latitudes by 100. To evaluate 3D RVGLS, 45 longitudinally oriented contours were generated by connecting the RV apex and predefined points of the RV base and were tracked throughout the cardiac cycle. The length of the longitude (L) can be calculated as the sum of the apex-middle section of the RV and middle section of the RV-RV base geodesic distances. RVGLS can be calculated by multiplying the sum of $(L^{end-systole}\text{-}L^{end-diastole}/L^{end-diastole})$ of 45 longitudes by 100. RVGAS was calculated from the relative change of the endocardial surface between end-diastole and end-systole. The surface is divided into a triangular mesh and its surface area

TABLE 1 | Clinical characteristics in the study population.

Number	$n = 341$
Age (year)	68 (58, 76)
Male	226 (66)
Sinus	310 (91)
AFib	31 (9)
Risk factor	
HT	191 (56)
DM	101 (30)
HL	149 (44)
CAD	143 (42)
CKD	149 (44)
Etiology	
Myocardial infarction	71 (21)
Ischemic heart disease	57 (17)
Dilated cardiomyopathy	45 (13)
Secondary cardiomyopathy	84 (25)
Hypertrophic cardiomyopathy	10 (3)
Valvular heart disease	42 (12)
Pulmonary hypertension	12 (3)
Other causes	20 (6)
Medication	
Calcium channel blocker	72 (21)
Beta blocker	236 (69)
ACEi/ARB	253 (74)
Diuretics	170 (50)
Mineralocorticoid blocker	113 (33)
Vitamin K antagonist	42 (12)
Direct oral anticoagulant	42 (12)
Echo image quality (good/fair/poor) (LC)	68/160/113
Echo image quality (good/fair/poor) (RC)	45/144/152

Data are expressed as numbers (percentages). ACEi/ARB, angiotensin converting enzyme inhibitor/angiotensin receptor blocker; AFib, atrial fibrillation; CAD, coronary artery disease; CKD, chronic kidney disease; DM, diabetes mellitus; HL, hyperlipidemia; HT, hypertension; LC, left chamber; RC, right chamber. Secondary cardiomyopathy includes cardiac sarcoidosis in 28, hypertensive cardiomyopathy in 16, cardiac amyloidosis in 14, tachycardia cardiomyopathy in 4, arrhythmogenic right ventricular cardiomyopathy in 2, cancer therapy-related cardiac dysfunction in 6, alcoholic cardiomyopathy in 4, ampulla cardiomyopathy in 2, peripartum cardiomyopathy in 2, myocarditis in 2, Loeffler endocarditis in 2, eosinophilic myocarditis in 1, hypothyroidism in 1. Valvular heart disease includes mitral valve regurgitation in 9, mitral valve stenosis in 3, aortic valve regurgitation in 9, aortic valve stenosis in 16, pulmonary valve stenosis in 1, post prosthetic valve replacement in 2, infective endocarditis in 2. Other causes include atrial fibrillation in 3, aortic dissection in 2, abdominal aortic aneurysm in 1, pulmonary thromboembolism in 2, Brugada syndrome in 1, torsade de pointes in 1, cardiac tumor in 4, pericarditis in 2, constrictive pericarditis in 1, patent ductus arteriosus in 1, atrial septal defect in 1, left ventricular aneurysm in 1.

(A) is calculated. The sum of the surface areas at the end of systole ($A^{end-systole}$) and at the end of diastole ($A^{end-diastole}$) is calculated, and the RVGAS is calculated by multiplying ($A^{end-systole}$-$A^{end-diastole}$/$A^{end-diastole}$) by 100 (**Figure 1**). RV volumes, RVEF and 3D RV strains (RVGCS, RVGLS, and RVGAS) with ReVISION software were used for the main analysis, while RV volumes and RVEF derived from TomTec software (4D RV function 3) were also presented and used for some analysis.

Follow-Up

Follow-up information was obtained by two researchers (TK, YN), who were not involved in the echocardiographic analysis. Patients were followed up regularly in the outpatient clinic. For patients attending our hospital, prognostic information, such as whether and when a cardiac event occurred, was obtained from the attending physician or the electronic medical record. For patients undergoing treatment at other hospitals, we called the patient at home. If consent was obtained, we asked the patient or family about their current health status and whether and when a cardiac event had occurred. The day of echocardiography was defined as day 0, and final follow-up data were obtained in February 2021. The primary endpoint was a composite of cardiac events, including cardiac death, sustained ventricular tachyarrhythmia, or heart failure (HF) hospitalization. If patient developed multiple events, we selected hardest one as following order (HF hospitalization < sustained ventricular tachyarrhythmia < cardiac death). The secondary endpoint was HF hospitalization.

Reproducibility Analysis

Intra-observer variability of 3D RV volumes and 3D RVEF by 4D RV function 3 was evaluated by repeating measurements taken by the examiner on 35 randomly selected patients at interval of at least one-month, inter-observer variability was evaluated by a second examiner taking these measurements on the same 35 patients.

Statistical Analysis

Commercially available statistical software was used for statistical analysis (JMP Version 14.3.0, SAS Institute, Cary, North Carolina, USA; R Version 4.1.2, The R foundation for Statistical Computing, Vienna). Continuous variables were represented as medians and interquartile ranges (IQR). Categorical variables were expressed as frequencies or percentages. Comparisons between the two groups were analyzed using *t*-tests or Mann-Whitney U tests for continuous variables, and Fisher's exact test or the chi-square test for categorical variables. A correlation analysis was performed with the r value of the Spearman rank correlation coefficient. Numbers needed to treat (NNTs) were calculated as indicators of effect size (11). Survival time analysis was evaluated using the Kaplan-Meier method, and differences between groups were determined using the log-rank test. A cox proportional hazards model was built to calculate hazard ratio (HR) and 95% confidence interval (CI). The nested regression model was used to assess the incremental prognostic value. A decision tree model was created using classification and regression tree (CART) analysis, which divided patients into binary groups with the highest outcome contrasts and also estimated appropriate cutoff values to predict time-to-event outcomes (12).

RESULTS

Of 432 patients enrolled in the CMR database from January 2014 to October 2020, 341 patients were included as a final study population (**Figure 2**). Feasibilities of 3D LV and RV analysis

TABLE 2 | Clinical and echocardiography parameters in patients with and without a composite of cardiac events (cardiac death, sustained ventricular arrhythmia, or HF hospitalization).

	Overall ($n = 341$)	CE (+) ($n = 49$)	CE (-) ($n = 292$)	*P*-value	NNT
Age (year)	68 [58, 76]	74 [64, 80]	67 [57, 75]	0.005	4.1
Sex (male)	226 (66%)	26 (53%)	200 (68%)	0.034	6.5
BSA (/m^2)	1.62 [1.50, 1.75]	1.55 [1.44, 1.74]	1.63 [1.51, 1.75]	0.061	5.1
HT	191 (56%)	29 (59%)	162 (55%)	0.6	27.0
DM	101 (30%)	19 (39%)	82 (28%)	0.13	9.4
HL	149 (44%)	22 (45%)	127 (43%)	0.9	71.2
CAD	143 (42%)	19 (39%)	124 (42%)	0.6	27.1
CKD	149 (44%)	29 (59%)	120 (41%)	0.018	5.5
HR (beat/minute)	67 (59, 76)	69 [60, 82]	66 [59, 75]	0.2	8.4
SBP (mmHg)	127 [112, 145]	115 [107, 130]	129 [114, 146]	0.001	3.8
DBP (mmHg)	71 [63, 79]	67 [58, 74]	72 [64, 80]	<0.001	3.1
3D LVEDVI (mL/m^2)	90 [71, 124]	105 [90, 131]	87 [69, 123]	0.005	5.2
3D LVESVI (mL/m^2)	52 [36, 85]	68 [52, 102]	49 [33, 83]	<0.001	3.9
3D LVEF (%)	41 [28, 50]	31 [24, 43]	43 [31, 51]	<0.001	2.8
3D LVGLS (%)	12.2 [7.8, 15.5]	8.6 [5.9, 12.3]	12.6 [8.7, 15.9]	<0.001	2.9
3D LAVI max (mL/m^2)	48 [35, 66]	64 [52, 77]	45 [33, 61]	<0.001	2.7
3D LAVI min (mL/m^2)	31 [20, 47]	49 [34, 57]	27 [19, 41]	<0.001	2.5
E (cm/sec)	66 [49, 85]	78 [63, 93]	64 [49, 82]	0.007	5.2
A (cm/sec)	70 [51, 90]	79 [41, 96]	69 [52, 89]	0.9	26.7
Average mitral E/e'	11.4 [8.4, 15.2]	13.9 [10.5, 19.1]	10.9 [8.2, 14.6]	<0.001	2.7
SPAP (mmHg)	31 [25, 38]	37 [31, 43]	31 [25, 37]	0.004	3.9
TAPSE (mm)	16.7 [13, 20.6]	14 [11, 18.8]	17 (13, 21)	0.001	3.4
RV s' velocity (cm/sec)	10.6 [8.8, 12.3]	9.6 [8.5, 11.4]	10.7 [8.8, 12.4]	0.074	6.6
TomTec					
3D RVEDVI (mL/m^2)	61 [51, 76]	75 [58, 89]	60 [50, 73]	<0.001	3.9
3D RVESVI (mL/m^2)	32 [25, 42]	44 [34, 57]	30 [23, 40]	<0.001	2.6
3D RVEF (%)	48 [40, 54]	40 [31, 48]	49 [41, 55]	<0.001	2.1
ReVISION					
3D RVEDVI (mL/m^2)	61 [51, 76]	75 [58, 89]	61 [50, 73]	<0.001	3.9
3D RVESVI (mL/m^2)	33 [25, 42]	44 [34, 57]	31 [24, 41]	<0.001	2.7
3D RVEF (%)	47 [39, 54]	39 [32, 46]	48 [41, 54]	<0.001	2.1
3D RVGCS (%)	19.5 [15.7, 23.3]	15.9 [12.1, 20.3]	20.0 [16.5, 23.7]	<0.001	2.4
3D RVGLS (%)	15.2 [12.1, 18.4]	12.4 [9.7, 15.4]	15.7 [12.8, 18.8]	<0.001	2.5
3D RVGAS (%)	30.0 [24.2, 35.4]	23.3 [17.8, 30.2]	30.5 [25.4, 36.0]	<0.001	2.2

*Data are expressed as numbers (percentages) or medians [interquartile ranges]. 3D, three-dimensional; BSA, body surface area; CE, a composite of cardiac event (cardiac death, sustained ventricular arrhythmia, or heart failure hospitalization); DBP, diastolic blood pressure; HF, heat failure; HR, heart rate; LAVI max (min), left atrial maximum (minimum) volume index; LVED(S)VI, left ventricular end-diastolic (systolic) volume index, LVEF, left ventricular ejection fraction; LVGLS, left ventricular global longitudinal strain; NNT, number needed to treat; RV, right ventricular; RVED(S)VI, right ventricular end-diastolic (systolic) volume index; RVEF, right ventricular ejection fraction; RVGAS, right ventricular global area strain; RVGCS, right ventricular global circumferential strain; RVGLS, right ventricular global longitudinal strain; SBP, systolic blood pressure; SPAP, systolic pulmonary arterial pressure; TAPSE, tricuspid annular plane systolic excursion. Other abbreviations are the same as in **Table 1**.*

were 99% (340/341), and 100% (341/341). Image quality of the left ventricle was good in 20% (68/341), fair in 47% (160/341), and poor in 33% (113/341), respectively. Corresponding values of the right ventricle were 14% (45/341), 42% (144/341), and 44% (152/341) respectively. The median volume rate was 23 Hz (IQR: 20–27 Hz, range: 15–58 Hz). **Table 1** shows clinical characteristics of study subjects.

Echocardiographic Parameters

For 3DE LV parameters, median values of LVEDV index, LVESV index, LVEF, and LVGLS were 90 mL/m^2 (IQR: 71–124 mL/m^2), 52 mL/m^2 (36–85 mL/m^2), 41% (28–50%), and 12.2% (7.8–15.5 %), respectively. For 3DE RV parameters, the median values of RVEDV index, RVESV index, RVEF by TomTec software were 61 mL/m^2 (51–76 mL/m^2), 32 mL/m^2 (25–42 mL/m^2), 48% (40–54%), respectively. The median values of RVEDV index, RVESV index, RVEF, RVGCS, RVGLS, and RVGAS by ReVISION software were 61 mL/m^2 (51–76 mL/m^2), 33 mL/m^2 (25–42 mL/m^2), 47% (39–54%), 19.5% (15.7–23.3%), 15.2% (12.1–18.4%), and 30.0% (24.2–35.4%), respectively. 3D LVEF had a significant correlation with 3D LVGLS ($r = 0.92$) and 3D RVEF ($r = 0.64$). 3D RVEF also had a significant strong

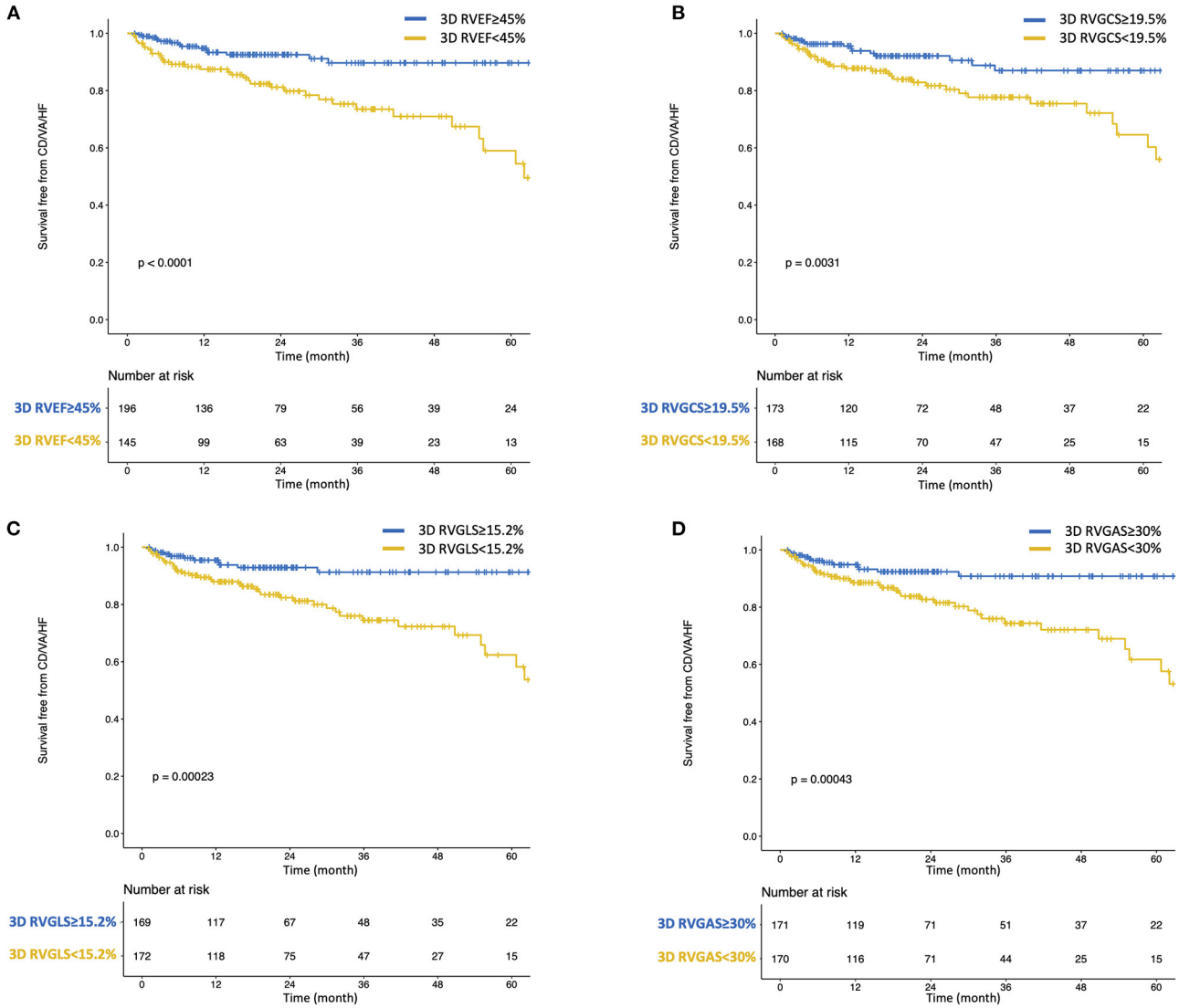

FIGURE 3 | Kaplan-Meier survival curves for cardiac death, ventricular tachyarrhythmia, or heart failure hospitalization stratified by predefined cut-off value of 3D RVEF **(A)** and median values of 3D RVGCS **(B)**, 3D RVGLS **(C)**, and 3D RVGAS **(D)**. CD, cardiac death; HF, heart failure; VA, ventricular tachyarrhythmia.

correlation with 3D RVGCS ($r = 0.90$), 3D RVGLS ($r = 0.87$), and 3D RVGAS ($r = 0.93$). Echocardiographic parameters are presented in **Table 2**.

Association With "Cardiac Death, Ventricular Tachyarrhythmia, or HF Hospitalization"

During a median of 19.8 (IQR: 9.0–38.5) months of follow-up, 49 patients reached a composite of cardiac events, 14 of whom suffered cardiac death. Thirty patients were HF hospitalization, and 5 patients developed sustained ventricular tachyarrhythmia. Of the 14 patients with cardiac death, worsened heart failure was the cause of death in eight patients, ventricular tachyarrhythmia was the cause of death in three, sudden cardiac death was the cause in two, and myocardial infarction was the cause of death in one patient. **Table 2** presents clinical and echocardiographic parameters between patients with and without cardiac events, and their NNTs. NNT was smallest in 3D RVEF (2.1), followed by 3D RVGAS (2.2), 3D RVGCS (2.4), 3D RVGLS (2.5), 3D minimum LA volume index (2.5), and 3D RVESV index (2.7). Kaplan-Meier survival analysis of 3D RVEF which were divided into binary groups using predefined cut-off value of 45% and that of 3D RVGCS, 3D RVGLS, and 3D RVGAS, which were divided into binary groups using median values showed that all four parameters had significant discriminatory power for "cardiac death, ventricular tachyarrhythmia, or HF hospitalization" (**Figure 3**). In univariate

Cox proportional hazard analysis, 3D RVEF (HR: 0.93, 95%CI: 0.91–0.96), 3D RVGCS (HR: 0.88, 95%CI: 0.83–0.93), 3D RVGLS (HR: 0.85, 95%CI: 0.79–0.91), and 3D RVGAS (HR: 0.91, 95%CI: 0.88–0.94) were significantly associated with "cardiac death, ventricular tachyarrhythmia, or HF hospitalization" (**Supplementary Table 1**). The corresponding values of C-Statistic were 0.71 (95%CI: 0.63–0.78), 0.68 (0.60–0.76), 0.68 (0.60–0.76), and 0.70 (0.62–0.77), respectively. There were no statistically significant differences in C-Statics between 3D RVEF and 3D RV strain parameters. We also performed a dichotomous univariate analysis using the cutoff values based on previous reports (3, 13) (**Table 3**). 3D RVGLS < 15% had a similar hazard ratio compared with 3D RVEF < 45%. Multivariate Cox proportional hazard analysis showed that 3D RVEF and 3D RV strains were associated with future cardiac events, after adjusting age, chronic kidney disease (CKD), 3D LVEF, and average mitral E/e', 3D maximal left atrial volume index (LAVI), or TAPSE (**Supplementary Table 2**). Incremental values of 3D RVEF and three RV 3D strains are shown in **Figure 4**. When 3D RVEF, 3D RVGCS, or 3D RVGAS were added to the model including age, CKD, 3D LVEF and average mitral E/e', chi-squared values increased significantly. When either of four parameters were added to the model including age, CKD, 3D LVEF and 3D maximal LAVI, the chi-square value increased significantly. **Figure 5** shows results of CART analysis. When 22 clinical and echocardiographic parameters were used, including age, gender, body surface area, CKD, heart rate, systolic blood pressure, diastolic blood pressure (DBP), 3D LVEDVI, 3D LVESVI, 3D LVEF, 3D LVGLS, 3D maximal LAVI, 3D minimal LAVI, E/e', TAPSE, RV s', 3D RVEDVI, 3D RVESVI, 3D RVEF, 3D RVGCS, 3D RVGLS, and 3D RVGAS. CART selected 3D RVEF (cut-off value: 34.5%) first, followed by DBP at the time of echocardiography examination (cut-off value: 53 mmHg) and 3D RVGAS (cut-off value: 32.4%), resulting in classification into two high-risk groups, one intermediate-risk group, and one low-risk group (**Figure 5A**). If we included 15 echocardiography parameters, CART selected 3D RVEF (cut-off value: 34.5%) first, followed by average mitral E/e' (cut-off value: 25.6) and 3D LVESVI (cut-off value: 51.5 mL/m^2), resulting in classification into two high-risk groups, one intermediate-risk group, and one low-risk group (**Figure 5B**).

TABLE 3 | Univariate cox proportional hazards analysis with dichotomous variables for "cardiac death, sustained ventricular arrhythmia, or HF hospitalization."

Variables	Hazard ratio	95% CI	*P*-value
3D LVEF < 50 %	5.66	1.75–18.3	0.004
3D LVEF < 40 %	2.71	1.47–4.99	0.001
3D LVEF < 30 %	2.11	1.20–3.73	0.010
3D LVGLS < 16 %	2.92	1.15–7.37	0.024
3D LVGLS < 13 %	3.05	1.55–6.00	0.001
3D LVGLS < 10 %	3.48	1.91–6.34	<0.001
3D LAVI max > 34 mL/m^2	4.82	1.91–12.2	<0.001
Average mitral E/e' > 14	1.78	1.01–3.15	0.046
TR > 2.8 m/s	2.60	1.36–4.98	0.004
TAPSE < 17 mm	2.15	1.18–3.90	0.012
TAPSE < 13 mm	2.62	1.48–4.64	<0.001
TAPSE < 10 mm	2.38	1.11–5.09	0.025
RV s' < 9.5 cm/sec	1.98	1.05–3.72	0.034
RV s' < 7.5 cm/sec	1.07	0.42–2.73	0.9
RV s' < 5 cm/sec	2.26	0.31–16.5	0.4
3D RVEF < 45 %	3.22	1.75–5.92	<0.001
3D RVEF < 40 %	3.09	1.76–5.42	<0.001
3D RVEF < 35 %	3.91	2.20–6.95	<0.001
3D RVEF < 30 %	3.81	1.94–7.47	<0.001
3D RVGCS < 19 %	2.70	1.49–4.92	<0.001
3D RVGLS < 15 %	3.22	1.70–6.08	<0.001
3D RVGAS < 30 %	2.97	1.57–5.61	<0.001

CI, confidence interval; TR, tricuspid regurgitation velocity. Other abbreviations are the same as in ***Table 2****.*

Association With HF Hospitalization

During a median of 19.7 (IQR: 8.7–37.7) months of follow-up, 37 patients reached HF hospitalization. **Supplementary Table 3** presents clinical and echocardiographic parameters between patients with and without HF hospitalization, and their NNTs. **Figure 6** showed Kaplan-Meier survival analysis of 3D RVEF, 3D RVGCS, 3D RVGLS, and 3D RVGAS divided into binary groups using the aforementioned cutoff values. In univariate analysis, 3D RVEF (HR: 0.93, 95%CI: 0.90–0.96), 3D RVGCS (HR: 0.88, 95%CI: 0.83–0.94), 3D RVGLS (HR: 0.84, 95%CI: 0.78–0.91), 3D RVGAS (HR: 0.91, 95%CI: 0.87–0.95) were significantly associated with HF hospitalization (**Supplementary Table 4**). **Table 4** shows a dichotomous univariate analysis for several echocardiographic parameters using the cutoff values based on previous reports (3, 13). 3D RVGLS < 15% had a similar hazard ratio for HF hospitalization compared with 3D RVEF < 45%.

Reliability of the ReVISION Method

To evaluate the reliability of the ReVISION method, 3D RVEF values by the ReVISION method were compared to corresponding values obtained from TomTec software or CMR. The prognostic value was also evaluated among three RVEFs. A correlation coefficient of RVEF between the ReVISION method and TomTec software was 0.99 and that between the ReVISION method and CMR was 0.67 (**Supplementary Figure 1**). The prognostic values of primary and secondary endpoints were comparable among RVEFs assessed by the three methods (**Table 5**).

Reproducibility

The intra- and inter-observer variability of 3D RVEDV, 3D RVESV and 3D RVEF was 4.5–5.4% [intraclass correlation coefficients (ICC): 0.92–0.97] and 7.4–9.2% (ICC: 0.86–0.93), respectively (**Supplementary Table 5**).

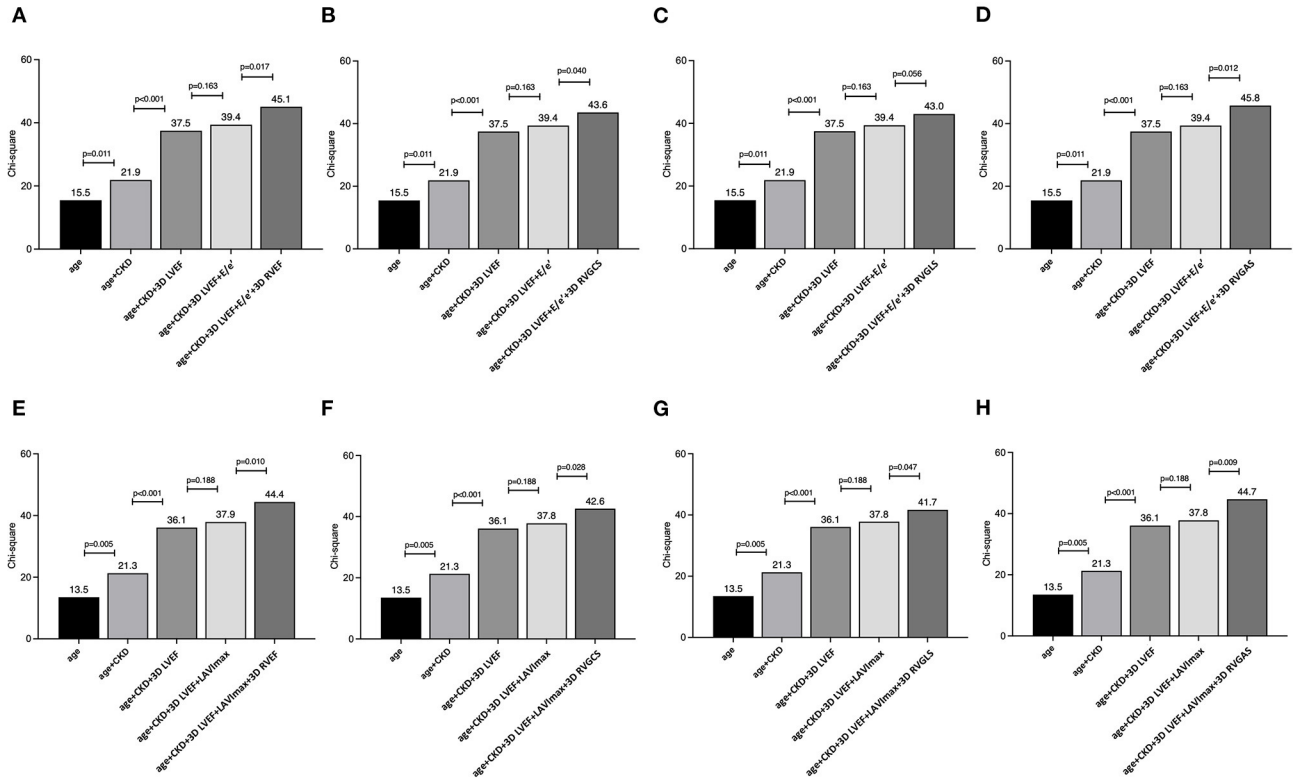

FIGURE 4 | The nested regression model to evaluate the incremental value of 3D RVEF, 3D RVGCS, 3D RVGLS, and 3D RVGAS for cardiac death, ventricular tachyarrhythmia, or HF hospitalization. χ^2 scores show that 3D RVEF, 3D RVGCS, and 3D RVGAS have significant incremental value for prediction of a composite of cardiac events in addition to models, including age, chronic kidney disease, left ventricular ejection fraction, and average mitral E/e' **(A–D)**. χ^2 scores show that 3D RVEF, all 3D global strains have significant incremental value for prediction over the models, including age, chronic kidney disease, left ventricular ejection fraction, and maximum 3D left atrial volume index **(E–H)**.

DISCUSSION

To the best of our knowledge, this is the first report of the prognostic utility of RV 3D strains in patients with diverse cardiac diseases. The major findings of our study can be summarized as follows:, (i) Univariate analysis showed that 3D RVEF and RV 3D strains were associated with future outcomes, (ii) Multivariate analysis revealed that 3D RVEF, 3D RVGCS and 3D RVGAS are independently associated with cardiac events after adjusting for age, CKD, 3D LVEF, and average mitral E/e'. 3D RVEF and all 3D RV global strains are independently associated with cardiac events after adjusting for age, CKD, 3D LVEF, and 3D maximum LAVI, (iii) CART selected 3D RVEF first, followed by DBP and 3D RVGAS, which divided the patients into four groups stratified for risk of cardiac events of different degrees.

Previous Studies

Echocardiographic cardiac function analysis has focused mainly on left cardiac chambers, including LVEF, LVGLS, and left atrial volumes and function. The right ventricle, on the other hand, has been regarded for many years as the neglected or forgotten chamber of the heart, with less relevance to RV disease as a primary cardiac disease (14). However, the importance of RV function, especially RVEF, has been recently demonstrated in management and prognostication of cardiac disease (4–6). It has also been reported that patients who had preserved LVEF and reduced RVEF had significantly worse prognoses than patients with reduced LVEF, but preserved RVEF (4, 15), and more attention is now being paid to the right heart chambers.

RV pump function consists of three main mechanisms: (i) shortening of the longitudinal axis with traction of the tricuspid annulus toward the apex; (ii) inward (radial) movement of the RV free wall; (iii) bulging of the interventricular septum into the RV during LV contraction and stretching of the free wall over the septum (7, 16). Impairment of these mechanisms may vary depending on cardiac diseases or conditions. Hence, Lakatos et al. (8) developed the ReVISION method, a 3DE-based solution for quantification of the relative contributions of longitudinal, radial, and antero-posterior shortening to global RVEF. Assessments of RVGCS, RVGLS, and RVGAS have also been implemented. Atsumi et al. (17) first demonstrated the reliability and clinical feasibility of RV 3D strains in animal studies. Ishizu et al. (18) showed that RV 3D strains are associated with impaired RV function in adult patients with a wide array of cardiovascular problems. In these studies, a 3D wall motion tracking algorithm for the RV was used. We reported normal values of RV 3D strains

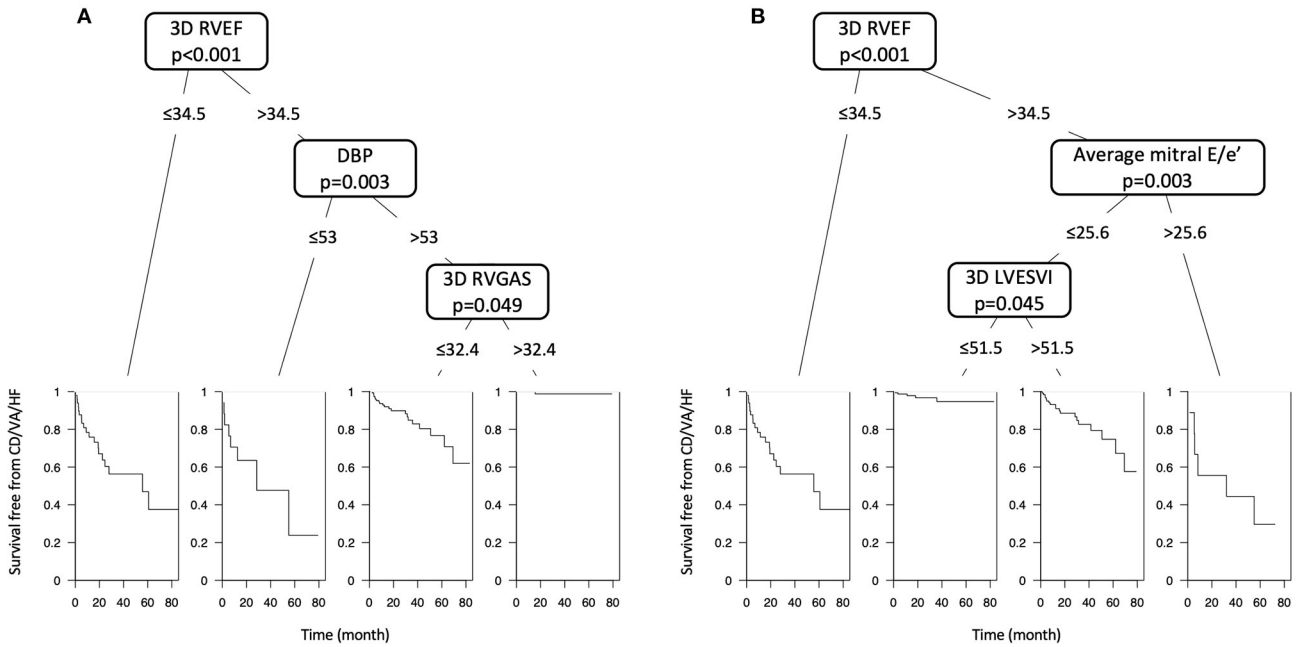

FIGURE 5 | (A) Classification and regression tree (CART) analysis, including twenty-two clinical and echocardiographic parameters. CART selected 3D RVEF (cut-off value: 34.5%) first, followed by DBP (cut-off value: 53 mmHg) and 3D RVGAS (cut-off value: 32.4%), resulting in classification into two high-risk groups ($n = 67$), one intermediate-risk group ($n = 154$), and one low-risk group ($n = 120$). **(B)** CART analysis, including fifteen echocardiographic parameters. CART selected 3D RVEF (cut-off value: 34.5%) first, followed by average mitral E/e' (cut-off value: 25.6) and 3D LVESVI (cut-off value: 51.5 mL/m^2), resulting in classification into two high-risk groups ($n = 59$), one intermediate-risk group ($n = 126$), and one low-risk group ($n = 156$).

in healthy volunteers using the ReVISION software (8). Recently, RV 3D strains were shown to be associated with short-term outcomes in patients undergoing cardiac surgery (19). However, no studies have investigated whether RV 3D strains provide prognostic information in patients with cardiovascular disease.

Current Study

Univariate and multivariate Cox proportional hazard analysis revealed that not only 3D RVEF but also 3D RV global strains were significantly associated with a composite of cardiac events as well as HF hospitalization. However, because of the collinearity of 3D RVEF and RV 3D strains, multivariate analyses including both 3D RVEF and RV 3D strains were not conducted in this study.

In the CART analysis, 3D RVEF was selected first, followed by DBP, and finally 3D RVGAS, when we included clinical and echocardiography parameters. Selection of 3D RVGAS makes sense because of its smaller NNT next to that of 3D RVEF and because its value reflects strain values in both longitudinal and circumferential directions. Previous publications have reported that lower DBPs are associated with worse prognoses (20–22). In addition, low systolic and mean blood pressures are associated with increased mortality in heart failure patients (22, 23). When we included 15 echocardiography parameters, CART selected 3D RVEF first, followed by LV diastolic function parameter (mitral E/e') and LV systolic function parameter (3D LVESVI). The results suggest that among echocardiographic parameters, 3D RVEF is more important than LV diastolic and systolic parameters to predict future outcome, which agreed with the previous study in patients with asymptomatic aortic stenosis (24).

In the present study, RV 3D strain had prognostic value equivalent to that of 3D RVEF, but not better than 3D RVEF. This may be due to the inclusion of left-sided heart disease of various etiologies and the inclusion of patients with preserved or impaired LV function, which may have resulted in different mechanisms of RV dysfunction among patients. Left-sided heart disease was also thought to diffusely impair the right ventricle. As a result, 3D RV strain, which is an indicator of one or two directional motion components, was equivalent but not superior to 3D RVEF, which is a global indicator. This was also consistent with the fact that for RV 3D strain values, 3D RVGAS, a multidimensional index, was a better parameter for prognosis than 3D RVGCS or 3D RVGLS. Combining these parameters with RVEF may allow more detailed stratification of patient prognosis, especially in a specific type of cardiovascular diseases.

The cut-off values of 3D RVGCS, 3D RVGLS, and 3D RVGAS found for outcome analysis in this study were 19.5, 15.2, and 30.0%, respectively. These values were correctly below the lower limit of normality (LLN) of 3D RVGCS (LLN: 21.3%), 3D RVGLS (LLN: 24.7%), and 3D RVGAS (LLN: 34.8%) reported by Lakatos et al. (8), which is in agreement with the prognostic cut-off value for LVGLS that is also below the LLN for LVGLS (i.e., <16%) (25–27), since cut-off values to estimate worse outcomes

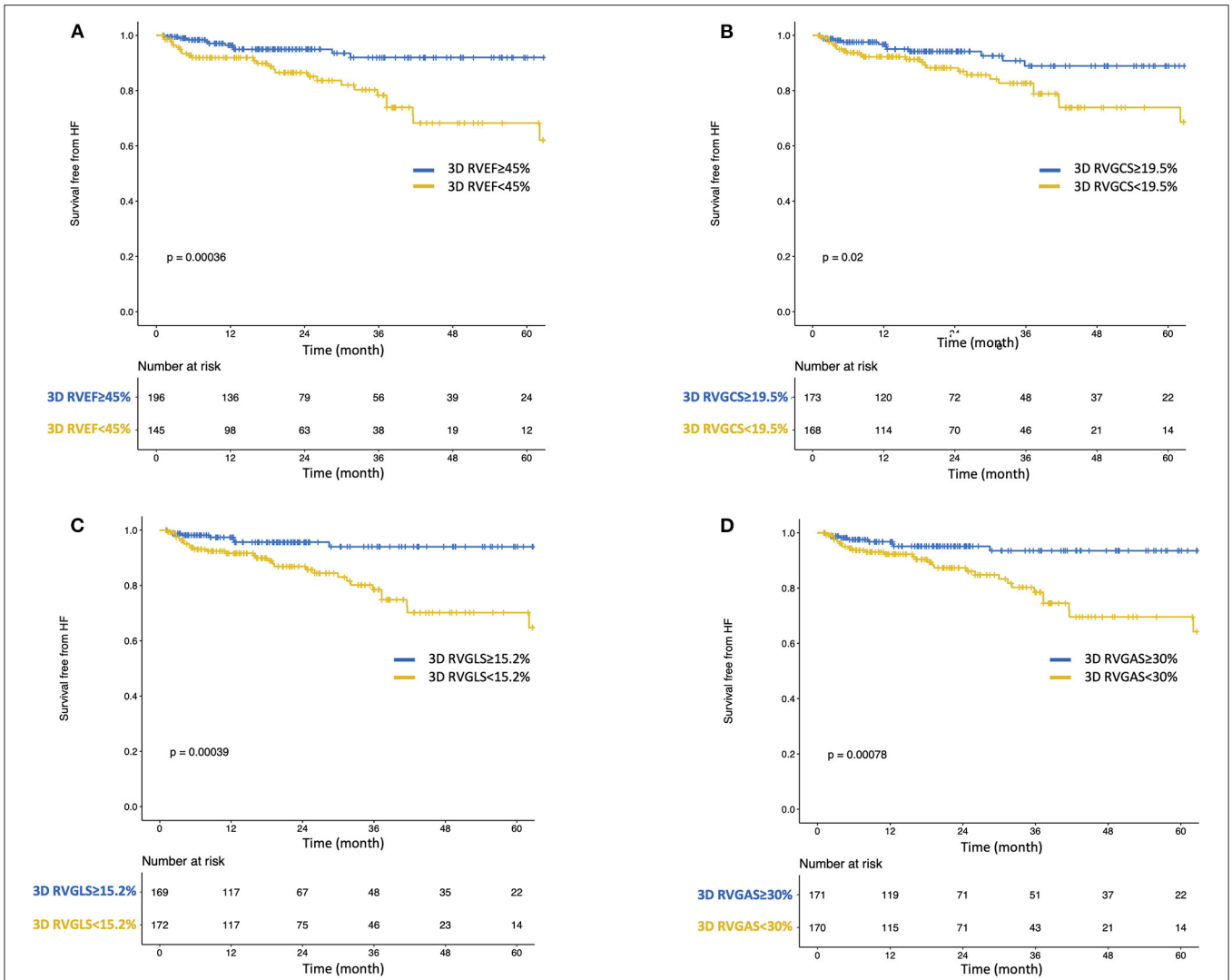

FIGURE 6 | Kaplan-Meier survival curves for heart failure hospitalization stratified by predefined cut-off value of 3D RVEF **(A)** and median values of 3D RVGCS **(B)**, 3D RVGLS **(C)**, and 3D RVGAS **(D)**.

should be below the LLN of the parameter analyzed. 3D RVGLS < 15% had a similar hazard ratio compared with 3D RVEF < 45% for the association of a composite of cardiac events as well as HF hospitalization. Further study should be required to validate whether 3D RVGLS of 15% is an optimal cut-off value for prognostication. It is also important to determine whether 3D RVGLS provides useful prognostic information in patients whose 3D RVEF is preserved.

Study Limitations

Some limitations must be acknowledged. This study was single-center, retrospective, observational study that included patients selected from the CMR database. Selection bias should be recognized because only patients undergoing CMR were included, which might be biased toward certain left-sided cardiac conditions. Some echocardiographic parameters and information on the severity of valvular heart disease were not used for the analysis. ReVISION software relies on 3D RV endocardial meshes generated using vendor-independent, commercially available 3DE speckle tracking software. The relatively small number of events in this study did not allow for extensive subgroup analysis. Further studies are needed to investigate the potential usefulness of RV 3D strains in specific cardiac diseases. The decision tree obtained from the CART analysis has been optimized for our population and needs to be externally validated in future studies.

Conclusions

RV 3D strains provided equivalesnt prognostic usefulness compared with 3D RVEF in patients with diverse cardiac diseases. Combining these parameters with 3D RVEF may allow for a more detailed stratification of patient prognoses.

TABLE 4 | Univariate cox proportional hazards analysis with dichotomous variables for HF hospitalization.

Variables	Hazard ratio	95% CI	*P*-value
3D LVEF < 50 %	4.15	1.27–13.6	0.019
3D LVEF < 40 %	2.85	1.40–5.80	0.004
3D LVEF < 30 %	2.02	1.04–3.89	0.037
3D LVGLS < 16 %	3.96	1.18–12.6	0.025
3D LVGLS < 13 %	3.82	1.67–8.75	0.001
3D LVGLS < 10 %	4.01	1.97–8.15	<0.001
3D LAVI max > 34 mL/m^2	6.08	1.86–19.8	0.003
Average mitral E/e' > 14	1.73	0.90–3.34	0.10
TR > 2.8 m/s	3.19	1.51–6.77	0.002
TAPSE < 17 mm	2.16	1.08–4.30	0.028
TAPSE < 13 mm	2.38	1.22–4.63	0.011
TAPSE < 10 mm	1.94	0.75–4.99	0.2
RV s' < 9.5 cm/sec	1.68	0.82–3.33	0.2
RV s' < 7.5 cm/sec	0.79	0.24–2.59	0.7
RV s' < 5 cm/sec	0.00	0.00–Inf	0.9
3D RVEF < 45 %	3.36	1.66–6.82	<0.001
3D RVEF < 40 %	2.85	1.49–5.43	0.001
3D RVEF < 35 %	3.50	1.78–6.89	<0.001
3D RVEF < 30 %	4.32	2.03–9.22	<0.001
3D RVGCS < 19 %	2.40	1.22–4.73	0.011
3D RVGLS < 15 %	3.61	1.70–7.67	<0.001
3D RVGAS < 30 %	3.37	1.59–7.16	0.002

*Abbreviations are the same as in **Tables 2**, **3**.*

TABLE 5 | Comparison of the prognostic value of RVEF among ReVISION method and the other methods.

Variables	Hazard ratio	95% CI	*P*-value
"Cardiac death, sustained ventricular arrhythmia, or HF hospitalization"			
3D RVEF by ReVISION method	0.93	0.91–0.96	<0.001
3D RVEF by TomTec software	0.93	0.91–0.96	<0.001
RVEF by CMR	0.96	0.94–0.99	0.002
HF hospitalization			
3D RVEF by ReVISION method	0.93	0.90–0.96	<0.001
3D RVEF by TomTec software	0.93	0.90–0.96	<0.001
RVEF by CMR	0.96	0.93–0.98	0.002

*CMR, cardiac magnetic resonance. TomTec software was 4D RV function 3. Other abbreviations are the same as in **Tables 2**, **3**.*

DATA AVAILABILITY STATEMENT

The raw data supporting the conclusions of this article will be made available by the authors, without undue reservation.

ETHICS STATEMENT

The studies involving human participants were reviewed and approved by the Ethics Committee at the University of Occupational and Environmental Health. Written informed consent for participation was not required for this study in accordance with the national legislation and the institutional requirements.

AUTHOR CONTRIBUTIONS

TK: conceptualization, data curation, data analysis, investigation, methodology, and writing-original draft. AK: investigation, methodology, and writing-original draft. YN: data curation. MT, AF, and BL: investigation and methodology. MT: conceptualization, data analysis, investigation, methodology, writing-original draft, and supervision. All authors contributed to the article and approved the submitted version.

SUPPLEMENTARY MATERIAL

The Supplementary Material for this article can be found online at: https://www.frontiersin.org/articles/10.3389/fcvm.2022.837584/full#supplementary-material

Supplementary Figure 1 | Correlation plot between RVEF by ReVISION method and 4D RV Function 3 or CMR.

Supplementary Table 1 | Univariate Cox proportional hazard analysis for "cardiac death, ventricular tachyarrythmia, or HF hospitalization." 3D, three-dimensional; BSA, body surface area; CAD, coronary artery disease; CI, confidence interval; CKD, chronic kidney disease; DBP, diastolic blood pressure; DM, diabetes mellitus; HF, heart failure; HL, hyperlipidemia; HR, heart rate; HT, hypertension; LAVI, left atrial volume index; LVED(S)VI, left ventricular end-diastolic (systolic) volume index, LVEF, left ventricular ejection fraction; LVGLS, left ventricular global longitudinal strain; RV, right ventricular; RVED(S)VI, right ventricular end-diastolic (systolic) volume index; RVEF, right ventricular ejection fraction; RVGAS, right ventricular global area strain; RVGCS, right ventricular global circumferential strain; RVGLS, right ventricular global longitudinal strain; SBP, systolic blood pressure; SPAP, systolic pulmonary arterial pressure; TAPSE, tricuspid annular plane systolic excursion.

Supplementary Table 2 | Multivariable Cox proportional hazard analysis for "cardiac death, ventricular tachyarrhythmia, or HF hospitalization." HR, hazard ratio. Other abbreviations are the same as in **Supplementary Table 1**.

Supplementary Table 3 | Clinical and echocardiography parameters in patients with and without HF hospitalization. Data are expressed as numbers (percentages) or medians [interquartile ranges]. NNT, number needed to treat. Other abbreviations are the same as in **Supplementary Table 1**.

Supplementary Table 4 | Univariate Cox proportional hazard analysis for HF hospitalization. Abbreviations are the same as in **Supplementary Table 1**.

Supplementary Table 5 | Result of reproducibility analysis for right ventricular volumes and right ventricular ejection fraction. ICC, intraclass correlation coefficients; IQR, interquartile ranges. Other abbreviations are the same as in **Supplementary Table 1**.

REFERENCES

1. Muraru D, Spadotto V, Cecchetto A, Romeo G, Aruta P, Ermacora D, et al. New speckle-tracking algorithm for right ventricular volume analysis from three-dimensional echocardiographic data sets: validation with cardiac magnetic resonance and comparison with the previous analysis tool. *Eur Heart J Cardiovasc Imaging.* (2016) 17:1279–89. doi: 10.1093/ehjci/jev309
2. Medvedofsky D, Addetia K, Patel A, Sedlmeier A, Baumann R, Mor-Avi V, et al. Novel approach to three-dimensional echocardiographic quantification of right ventricular volumes and function from focused

views. *J Am Soc Echocardiogr.* (2015) 28:1222–31. doi: 10.1016/j.echo.2015.06.013
3. Lang R, Badano L, Mor-Avi V, Afilalo J, Armstrong A, Ernande L, et al. Recommendations for cardiac chamber quantification by echocardiography in adults: an update from the American society of echocardiography and the European association of cardiovascular imaging. *J Am Soc Echocardiogr.* (2015) 28:1–39. doi: 10.1016/j.echo.2014.10.003
4. Nagata Y, Wu V, Kado Y, Otani K, Lin F, Otsuji Y, et al. Prognostic value of right ventricular ejection fraction assessed by transthoracic 3D echocardiography. *Circ Cardiovasc Imaging.* (2017) 10:e005384. doi: 10.1161/CIRCIMAGING.116.005384
5. Namisaki H, Nabeshima Y, Kitano T, Otani K, Takeuchi M. Prognostic value of the right ventricular ejection fraction, assessed by fully automated three-dimensional echocardiography: a direct comparison of analyses using right ventricular-focused views versus apical four-chamber views. *J Am Soc Echocardiogr.* (2021) 34:117–26. doi: 10.1016/j.echo.2020.09.016
6. Muraru D, Badano L, Nagata Y, Surkova E, Nabeshima Y, Genovese D, et al. Development and prognostic validation of partition values to grade right ventricular dysfunction severity using 3D echocardiography. *Eur Heart J Cardiovasc Imaging.* (2020) 21:10–21. doi: 10.1093/ehjci/jez233
7. Lakatos B, Tosér Z, Tokodi M, Doronina A, Kosztin A, Muraru D, et al. Quantification of the relative contribution of the different right ventricular wall motion components to right ventricular ejection fraction: the ReVISION method. *Cardiovasc Ultrasound.* (2017) 15:8. doi: 10.1186/s12947-017-0100-0
8. Lakatos B, Nabeshima Y, Tokodi M, Nagata Y, Toser Z, Otani K, et al. Importance of nonlongitudinal motion components in right ventricular function: three-dimensional echocardiographic study in healthy volunteers. *J Am Soc Echocardiogr.* (2020) 33:995–1005. doi: 10.1016/j.echo.2020.04.002
9. Mitchell C, Rahko P, Blauwet L, Canaday B, Finstuen J, Foster M, et al. Guidelines for performing a comprehensive transthoracic echocardiographic examination in adults: recommendations from the American society of echocardiography. *J Am Soc Echocardiogr.* (2019) 32:1–64. doi: 10.1016/j.echo.2018.06.004
10. Tokodi M, Staub L, Budai A, Lakatos B, Csakvari M, Suhai F, et al. Partitioning the right ventricle into 15 segments and decomposing its motion using 3D echocardiography-based models: the updated ReVISION method. *Front Cardiovasc Med.* (2021) 8:622118. doi: 10.3389/fcvm.2021.622118
11. Furukawa T, Leucht S. How to obtain NNT from Cohen's d: comparison of two methods. *PLoS ONE.* (2011) 6:e19070. doi: 10.1371/journal.pone.0019070
12. Podgorelec V, Kokol P, Stiglic B, Rozman I. Decision trees: an overview and their use in medicine. *J Med Syst.* (2002) 26:445–63. doi: 10.1023/A:1016409317640
13. Nagueh SF, Smiseth OA, Appleton CP, Byrd BF, Dokainish H, Edvardsen T, et al. Recommendations for the evaluation of left ventricular diastolic function by echocardiography: an update from the american society of echocardiography and the European association of cardiovascular imaging. *J Am Soc Echocardiogr.* (2015) 4:277–314. doi: 10.1016/j.echo.2016.01.011
14. Kossaify A. Echocardiographic assessment of the right ventricle, from the conventional approach to speckle tracking and three-dimensional imaging, and insights into the "Right Way" to explore the forgotten chamber. *Clin Med Insights Cardiol.* (2015) 9:65–75. doi: 10.4137/CMC.S27462
15. Doesch C, Dierks D, Haghi D, Schimpf R, Kuschyk J, Suselbeck T, et al. Right ventricular dysfunction, late gadolinium enhancement, and female gender predict poor outcome in patients with dilated cardiomyopathy. *Int J Cardiol.* (2014) 177:429–35. doi: 10.1016/j.ijcard.2014.09.004
16. Buckberg G, Hoffman J. Right ventricular architecture responsible for mechanical performance: unifying role of ventricular septum. *J Thorac Cardiovasc Surg.* (2014) 148:3166–71. doi: 10.1016/j.jtcvs.2014.05.044
17. Atsumi A, Seo Y, Ishizu T, Nakamura A, Enomoto Y, Harimura Y, et al. Right ventricular deformation analyses using a three-dimensional speckle-tracking echocardiographic system specialized for the right ventricle. *J Am Soc Echocardiogr.* (2016) 29:402–11 e2. doi: 10.1016/j.echo.2015.12.014
18. Ishizu T, Seo Y, Atsumi A, Tanaka Y, Yamamoto M, Machino-Ohtsuka T, et al. Global and regional right ventricular function assessed by novel three-dimensional speckle-tracking echocardiography. *J Am Soc Echocardiogr.* (2017) 30:1203–13. doi: 10.1016/j.echo.2017.08.007
19. Keller M, Heller T, Duerr MM, Schlensak C, Nowak-Machen M, Feng YS, et al. Association of 3d mesh-derived right ventricular strain with short-term outcome in patients undergoing cardiac surgery. *J Am Soc Echocardiogr.* (2021) S0894-7317(21)00823-3. doi: 10.1016/j.echo.2021.11.008
20. McEvoy J, Chen Y, Rawlings A, Hoogeveen R, Ballantyne C, Blumenthal R, et al. Diastolic blood pressure, subclinical myocardial damage, and cardiac events: implications for blood pressure control. *J Am Coll Cardiol.* (2016) 68:1713–22. doi: 10.1016/j.jacc.2016.07.754
21. Sandesara P, O'Neal W, Kelli H, Topel M, Samman-Tahhan A, Sperling L. Diastolic blood pressure and adverse outcomes in the TOPCAT (treatment of preserved cardiac function heart failure with an aldosterone antagonist) trial. *J Am Heart Assoc.* (2018) 7:e007475. doi: 10.1161/JAHA.117.007475
22. Lee TT, Chen J, Cohen DJ, Tsao L. The association between blood pressure and mortality in patients with heart failure. *Am Heart J.* (2006) 151:76–83. doi: 10.1016/j.ahj.2005.03.009
23. Domanski MJ, Mitchell GF, Norman JE, Exner DV, Pitt B, Pfeffer MA. Independent prognostic information provided by sphygmomanometrically determined pulse pressure and mean arterial pressure in patients with left ventricular dysfunction. *J Am Coll Cardiol.* (1999) 33:951–8. doi: 10.1016/S0735-1097(98)00679-2
24. Nabeshima Y, Kitano T, Takeuchi M. Prognostic value of the three-dimensional right ventricular ejection fraction in patients with asymptomatic aortic stenosis. *Front Cardiovasc Med.* (2021) 8:795016. doi: 10.3389/fcvm.2021.795016
25. Magne J, Cosyns B, Popescu BA, Carstensen HG, Dahl J, Desai MY, et al. Distribution and prognostic significance of left ventricular global longitudinal strain in asymptomatic significant aortic stenosis. an individual participant sata meta-analysis. J *Am coll Cardiol Img.* (2019) 12:84–92. doi: 10.1016/j.jcmg.2018.11.005
26. Thellier N, Altes A, Appert L, Binda C, Leman B, Marsou W, et al. Prognostic importance of left ventricular global longitudinal strain in patients with severe aortic stenosis and preserved ejection fraction. *J Am Soc Echocardiogr.* (2020) 33:1454–64. doi: 10.1016/j.echo.2020.07.002
27. Otani K, Higa Y, Kitano T, Nabeshima Y, Takeuchi M. Prediction of cardiac events using fully automated GLS and BNP titers in patients with known or suspected heart failure. *PLoS ONE.* (2020) 15:e0234294. doi: 10.1371/journal.pone.0234294

Conflict of Interest: The authors declare that the research was conducted in the absence of any commercial or financial relationships that could be construed as a potential conflict of interest.

Publisher's Note: All claims expressed in this article are solely those of the authors and do not necessarily represent those of their affiliated organizations, or those of the publisher, the editors and the reviewers. Any product that may be evaluated in this article, or claim that may be made by its manufacturer, is not guaranteed or endorsed by the publisher.

frontiers in Cardiovascular Medicine

ORIGINAL RESEARCH
published: 22 March 2022
doi: 10.3389/fcvm.2022.821831

Regional Right Ventricular Function Assessed by Intraoperative Three-Dimensional Echocardiography Is Associated With Short-Term Outcomes of Patients Undergoing Cardiac Surgery

Marius Keller[1], Marcia-Marleen Duerr[1†], Tim Heller[1†], Andreas Koerner[1], Christian Schlensak[2], Peter Rosenberger[1] and Harry Magunia[1]*

[1] Department of Anesthesiology and Intensive Care Medicine, University Hospital Tuebingen, Eberhard-Karls-University, Tuebingen, Germany, [2] Department of Thoracic and Cardiovascular Surgery, University Hospital Tuebingen, Eberhard-Karls-University, Tuebingen, Germany

OPEN ACCESS

Edited by:
Márton Tokodi,
Semmelweis University, Hungary

Reviewed by:
Csilla Czimbalmos,
Semmelweis University, Hungary
Alina Nicoara,
Duke University, United States

***Correspondence:**
Marius Keller
marius.keller@med.uni-tuebingen.de

[†] These authors have contributed equally to this work

Specialty section:
This article was submitted to Cardiovascular Imaging, a section of the journal Frontiers in Cardiovascular Medicine

Received: *24 November 2021*
Accepted: *11 February 2022*
Published: *22 March 2022*

Citation:
Keller M, Duerr M-M, Heller T, Koerner A, Schlensak C, Rosenberger P and Magunia H (2022) Regional Right Ventricular Function Assessed by Intraoperative Three-Dimensional Echocardiography Is Associated With Short-Term Outcomes of Patients Undergoing Cardiac Surgery. Front. Cardiovasc. Med. 9:821831. doi: 10.3389/fcvm.2022.821831

Background: The assessment of right ventricular (RV) function in patients undergoing elective cardiac surgery is paramount for providing optimal perioperative care. The role of regional RV function assessment employing sophisticated state-of-the-art cardiac imaging modalities has not been investigated in this cohort. Hence, this study investigated the association of 3D echocardiography-based regional RV volumetry with short-term outcomes.

Materials and Methods: In a retrospective single-center study, patients undergoing elective cardiac surgery were included if they underwent 3D transesophageal echocardiography prior to thoracotomy. A dedicated software quantified regional RV volumes of the inflow tract, apical body and RV outflow tract employing meshes derived from 3D speckle-tracking. Echocardiographic, clinical and laboratory data were entered into univariable and multivariable logistic regression analyses to determine association with the endpoint (in-hospital mortality or the need for extracorporeal circulatory support).

Results: Out of 357 included patients, 25 (7%) reached the endpoint. Inflow RV ejection fraction (RVEF, 32 ± 8% vs. 37 ± 11%, $p = 0.01$) and relative stroke volume (rel. SV) were significantly lower in patients who reached the endpoint (44 ± 8 vs. 48 ± 9%, $p = 0.02$), while the rel. SV of the apex was higher (38 ± 10% vs. 33 ± 8%, $p = 0.01$). Global left and right ventricular function including RVEF and left ventricular global longitudinal strain did not differ. In univariable logistic regression, tricuspid regurgitation grade ≥ 2 [odds ratio (OR) 4.24 (1.66–10.84), $p < 0.01$], inflow RVEF [OR 0.95 (0.92–0.99), $p = 0.01$], inflow rel. SV [OR 0.94 (0.90–0.99), $p = 0.02$], apex rel. SV [OR 1.07 (1.02–1.13), $p < 0.01$] and apex to inflow rel. SV ratio [OR 5.81 (1.90–17.77), $p < 0.01$] were significantly associated with the endpoint. In a multivariable model, only the presence of tricuspid regurgitation [OR 4.24 (1.66–10.84), $p < 0.01$] and apex to inflow rel. SV ratio [OR 6.55 (2.09–20.60), $p < 0.001$] were independently associated with the endpoint.

Conclusions: Regional RV function is associated with short-term outcomes in patients undergoing elective cardiac surgery and might be helpful for optimizing risk stratification.

Keywords: right ventricle, ejection fraction, cardiac surgery, outcome research, three-dimensional echocardiography

INTRODUCTION

Perioperative right ventricular (RV) dysfunction dramatically limits patient outcomes following cardiac surgery (1, 2). While most current risk stratification scores disregard baseline RV function, even subclinical preoperative RV dysfunction has been shown to be associated with increased postoperative mortality (3). However, as the RV is of a complex anatomical and physiological nature, detecting subtle deviations from normal RV function is challenging. Hence, the hunt for novel non-invasive parameters that could yield further insight into RV pathophysiology is thriving. Echocardiography can be considered the most important non-invasive diagnostic method for quantifying RV function. In perioperative medicine, it is mainly applied by cardiologists via transthoracic acoustic windows distinctively before referral to surgery and by cardiac anesthesiologists in the operating room using transesophageal echocardiography (TEE). Intraoperative TEE has the potential to influence surgical decision-making, and its application is associated with improved outcomes (4, 5). Due to the ability to generate high-resolution images under general anesthesia, TEE facilitates the acquisition of 3D datasets that are advantageous over 2D recordings in the assessment of baseline RV function (6, 7). 3D volumetric analyses of the RV, especially 3D-derived RV ejection fraction (RVEF), carry incremental prognostic information in various chronic cardiac diseases (8). Depicting global into regional systolic RV function is a promising approach for unveiling contraction patterns associated with early pathological remodeling or abnormal loading conditions and hence increasing sensitivity in detecting RV dysfunction (7, 9–11). Literature on regional RV systolic function using 3D echocardiography regarding short-term prognosis after cardiac surgery is sparse (12). Therefore, the present study investigated the association of regional systolic function of the right ventricle with short-term outcome in patients undergoing cardiac surgery using mesh models derived from intraoperative transesophageal 3D-STE and a previously reported software approach (13). The performances of the novel parameters were compared to established clinical and echocardiographic measures that are routinely utilized for risk stratification. To our knowledge, this is the first study to investigate sophisticated 3D-derived intraoperative regional RV volumetry in patients undergoing cardiac surgery.

Abbreviations: 3D, three-dimensional; CI, confidence interval; ECLS, extracorporeal life support; EDV(i), end-diastolic volume (index); ESV(i), end-systolic volume (index); eGFR, estimated glomerular filtration rate; FAC, fractional area change; ICC, intraclass correlation coefficient; LVAD, left ventricular assist device; LVEF, left ventricular ejection fraction; LV-GLS, left ventricular global longitudinal strain; NYHA, New York Heart Association; OPCAB, off-pump coronary artery bypass surgery; OR, odds ratio; rel., relative; RV, right ventricle/right ventricular; RVEDV(i), right ventricular end-diastolic volume (index); RVEF, right ventricular ejection fraction; RVESV(i), right ventricular end-systolic volume index; RVOT, right ventricular outflow tract; STE, speckle-tracking echocardiography; SV, stroke volume; TAPSE, tricuspid annular plane systolic excursion; TEE, transesophageal echocardiography/echocardiograms.

MATERIALS AND METHODS

Patients

Ethical approval for retrospective patient inclusion was granted by the Ethics Committee of the Medical School at the University of Tuebingen (Trial Registration # IRB 350/2015R) and the study was conducted in accordance with the Declaration of Helsinki. Patients were screened for inclusion to this single-center cohort study if they underwent one of the following elective cardiac surgery procedures between November 2013 and October 2018: on-pump coronary artery bypass grafting, off-pump coronary artery bypass grafting (OPCAB), left-sided valve surgery, thoracic aortic surgery or left ventricular assist device (LVAD) implantation. Surgeries were categorized as "mixed" if one of the major procedures (except LVAD implantation) was combined with other procedures, or a combination of two or more major procedures (except LVAD implantation) was performed. Of the screened patients, only those with standardized intraoperative 3D transesophageal echocardiograms available in the institutional database were included in the study. Patients were excluded if they were underage (<18 years) at the time of surgery, needed extracorporeal circulatory support preoperatively or electronic patient records were incomplete for clinical data analysis.

Anesthesia and Intraoperative Echocardiography

The institutional regimen for standardized anesthesia during cardiac surgery and intraoperative echocardiography was described previously (14, 15). Briefly, anesthesia was induced with midazolam, sufentanil and rocuronium. After endotracheal intubation, anesthesia was maintained with sevoflurane and continuous administration of sufentanil. A norepinephrine infusion was titrated, if necessary, to maintain a mean arterial pressure above 65 mmHg. No additional sympathomimetics were used between anesthesia induction and thoracotomy. Inotropic therapies initiated prior to anesthesia induction were maintained unaltered.

The institutional standard for intraoperative TEE requires recordings after the establishment of hemodynamic stability following anesthesia induction but prior to thoracotomy. TEE was performed by specially trained cardiac anesthesiologists using commercially available 3D-compatible probes (Philips X7-2t Matrix, Philips Healthcare, Inc., Andover, MA, USA and Siemens Z6Ms TEE probe, Siemens Healthineers AG, Erlangen,

Germany). Representative 3D loops of the fully projected right and left ventricles at a frame rate above 20 fps were acquired.

Established Echocardiographic Parameters of LV and RV Function

All functional parameters were derived offline from the intraoperatively acquired 3D TEE studies using commercially available 3D-STE software packages. Left ventricular volumes, ejection fraction (LVEF) and global longitudinal strain (LV-GLS) were calculated using 4D LV-ANALYSIS software (Tomtec Imaging Systems GmbH, Unterschleissheim, Germany). If 3D LV datasets of sufficient quality were not available, left ventricular volumes, LVEF and LV-GLS were derived from two-dimensional recordings using appropriate speckle-tracking software. RV volumes, RVEF, fractional area change (FAC) and tricuspid annular plane systolic excursion (TAPSE) were calculated with the widely used 4D RV-Function software (version 2.0, Tomtec Imaging Systems GmbH, Unterschleissheim, Germany). Image acquisition and measurements were carried out in accordance with guideline recommendations (16–18).

Regional Right Ventricular Volumetry

After exporting the endocardial RV mesh files derived from 3D-STE (UCD file format), offline regional volumetry was performed using custom-made post-processing software as previously reported (13). The software algorithm is written in C++ based on the Visualization Toolkit (Ver. 7.1.1, Kitware, Inc., Clifton Park, New York, USA) and automatically performs regional volumetry of three RV regions:

- "inflow"—comprising mainly the anatomic region of the tricuspid annulus leaflets, also referred to as the "inlet."
- "apex"—comprising the apical trabecular region.
- "RVOT"—comprising the right ventricular outflow tract, also referred to as the "outlet."

Virtual cutting surfaces derived from an annular set of mesh points around the border of two regions served as the borders to divide the RV into the three regions. A set of two neighboring mesh points and the common center point each formed a triangle, all of which formed the cutting surface. The cutting points were manually defined and evaluated on a set of exemplary meshes, and the same set of cutting points was applied to all meshes analyzed for the study (13). Regional volumetric analysis yielded the *RVEF* (difference between maximum and minimum volume divided by the maximum volume of a region within the cardiac cycle, given in %), *end-diastolic volume (EDV*, maximum volume of a region within the cardiac cycle, given in ml), *end-diastolic volume index* (*EDVi*, normalized to body surface), *stroke volume* (*SV*, difference between maximum and minimum volume of a region within the cardiac cycle) and the *relative stroke volume* (*rel. SV*, relative contribution to the global RV stroke volume, given in %) individually for each region.

Clinical Data and Outcome

Epidemiologic, laboratory, clinical and outcome data were extracted from electronic patient records. The following baseline parameters were recorded: age, body mass index, body surface, estimated glomerular filtration rate (eGFR), hematocrit, lactate, the presence of chronic lung disease (defined as long-term use of bronchodilators or steroids for lung disease), the presence of pulmonary hypertension (defined as systolic pulmonary artery pressure > 30 mmHg assessed by Doppler echocardiography), the presence of tricuspid regurgitation (defined as grade 2 or 3 measured by color Doppler echocardiographic jet size and RA dimensions), the presence of diabetes (defined as insulin-dependent), the New York Heart Association (NYHA) functional class and the European System for Cardiac Operative Risk Evaluation II (EuroSCORE II). For short-term outcome analysis, the combined endpoint reflecting short-term outcome was defined as a composite of in-hospital mortality and/or the need for extracorporeal life support (ECLS, by venoarterial extracorporeal membrane oxygenation) within the postoperative hospital period.

TABLE 1 | Baseline clinical data of the complete patient cohort ($n = 357$).

Parameter	Result
Age, years	66 ± 13
Male, *n*	259 (73)
Body mass index, kg/m²	27 ± 5
Chronic lung disease*, *n*	29 (8)
Pulmonary hypertension†, *n*	57 (16)
Tricuspid regurgitation‡, *n*	45 (13)
Diabetes§, *n*	36 (10)
NYHA functional class	
I	67 (19)
II	105 (29)
III	118 (33)
IV	67 (19)
eGFR, ml/min	80 (61–102)
Lactate, mmol/l	0.90 ± 0.48
Hematocrit, %	37 ± 6
EuroSCORE II, %	3.4 (1.5–7.8)
Type of surgery	
On-pump coronary artery bypass grafting, *n*	51 (14)
OPCAB, *n*	69 (19)
Left-sided valve surgery, *n*	96 (27)
Thoracic aortic surgery, *n*	17 (5)
LVAD implantation, *n*	25 (7)
Mixed procedures, *n*	99 (28)

Values are means ± standard deviations, medians (interquartile ranges) or n (%).
ECLS, extracorporeal life support; eGFR, estimated glomerular filtration rate; LVAD, left ventricular assist device; NYHA, New York Heart Association; OPCAB, off-pump coronary artery bypass surgery.
**Long term use of bronchodilators or steroids for lung disease.*
†Systolic pulmonary artery pressure > 30 mmHg.
‡Grade ≥ 2.
§Insulin-dependent.

Statistical Analysis

Normally distributed continuous variables are presented as the mean ± standard deviation, and non-normally distributed continuous variables are presented as the median (interquartile

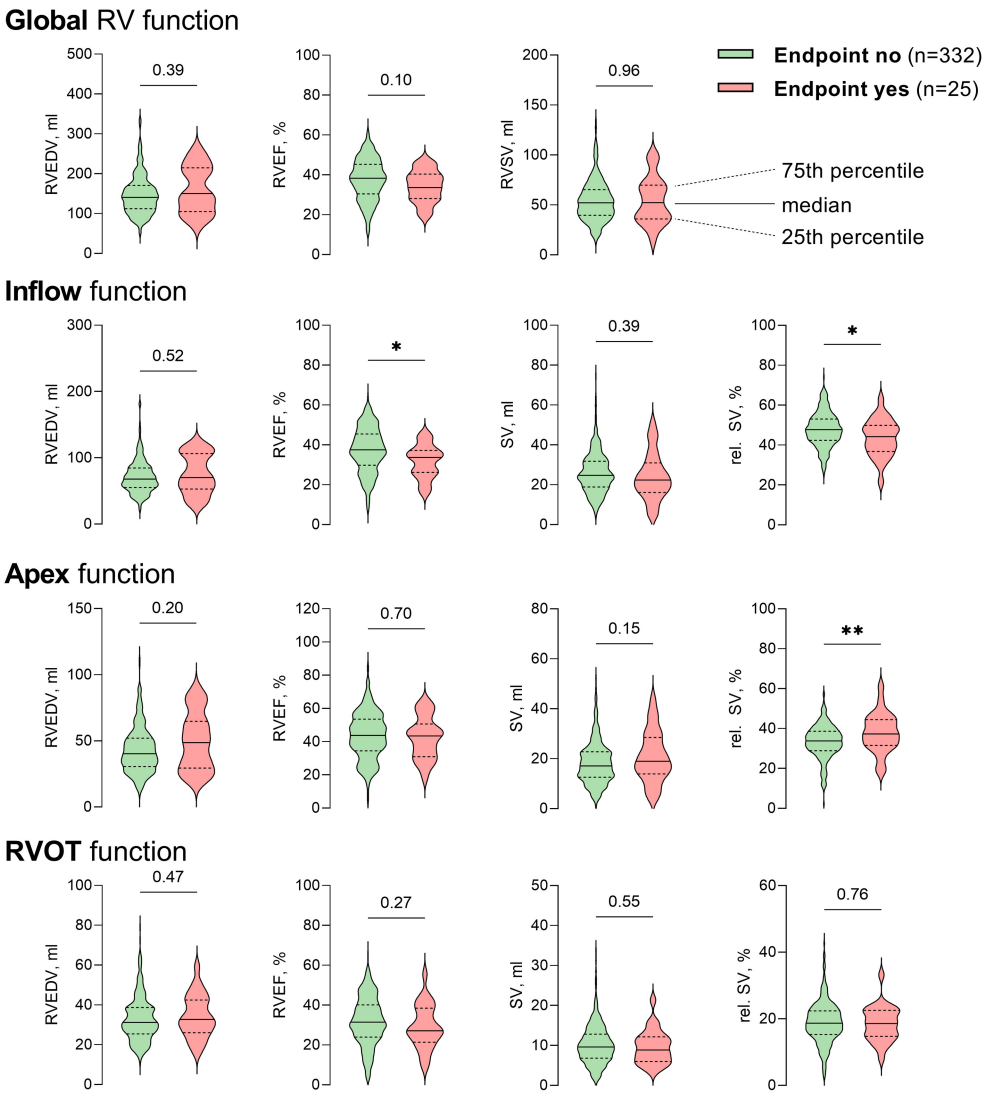

FIGURE 1 | Violin plots of global and regional RV volumetry parameters using 3D-STE-derived mesh models. Global RV function of patients who reached the endpoint (red) did not differ significantly from patients with an uncomplicated postoperative course (green). However, patients who died postoperatively or required extracorporeal circulatory support had lower inflow ejection fraction and inflow relative stroke volume, while relative stroke volume of the apex was significantly higher. *P*-values are derived from unpaired Student's *t*-tests. Rel., relative; RVEDV, right ventricular end-diastolic volume; RVEF, right ventricular ejection fraction; STE, speckle-tracking echocardiography; (RV)SV, (right ventricular) stroke volume; *$p < 0.05$; **$p < 0.01$.

range). Categorial variables are displayed as absolute numbers and percentages. Normally distributed samples were compared with unpaired Student's *t*-tests, while non-normally distributed samples were compared using Mann–Whitney U tests. Proportions were compared using chi-square tests. Binomial logistic regression was used to examine risk factors that could influence the endpoint, which are depicted with odds ratios (ORs) and their 95% confidence intervals (CIs). Variables that were significantly associated with the endpoint in univariable logistic regression were considered for inclusion in multivariable analysis. Multivariable logistic regression was performed with a forward stepwise conditional selection method (entry inclusion if $p < 0.05$, exclusion if $p > 0.1$) with respect to collinearity and the number of events per variable (19). The omnibus test of model coefficients was used to compare chi-square values of logistic regression models. Reproducibility of global and regional RVEF analyses was evaluated on 25 randomly selected patients. The same investigator reanalyzed those patients at least 3 months after the initial measurements for intraobserver reproducibility analysis, while a second investigator performed measurements for interobserver reproducibility analysis; both were blinded to the initial results. Intraclass correlation coefficients (ICCs) from a two-way random model for absolute agreement on average, Pearson's correlation coefficient r, Bland–Altman bias, and 95% limits of agreement were calculated to quantify reproducibility. *P*-values of <0.05 were regarded

as significant. Prism (GraphPad Software, San Diego, CA), MedCalc (MedCalc Software Ltd., Ostend, Belgium) and SPSS (IBM Corp., Armonk, NY) were used for statistical calculations and data presentation.

RESULTS

Clinical Data

Out of 3,561 patients in the institutional database screened for inclusion, $n = 357$ patients could be included. Baseline clinical data are displayed in **Table 1**. On average, patients were 66 ± 13 years old, moderately overweight (mean body mass index 27 ± 5 kg/m²) and predominantly male (73%). Chronic lung disease, pulmonary hypertension, tricuspid regurgitation or diabetes were only present in a small number of patients (8, 16, 13, and 10%, respectively). Mixed procedures were most common (28%, details listed in **Supplementary Table 1**), followed by isolated left-sided valve surgery (27%) and off-pump (19%) and on-pump (14%) coronary artery revascularizations. Isolated surgery of the thoracic aorta (5%) or LVAD implantations (7%) were less common. Thoracic aortic surgery was performed for aneurysm repair ($n = 16$) or resection of an intramural hematoma ($n = 1$) by performing supracoronary ascending aortic replacement ($n = 8$), hybrid frozen elephant trunk procedures ($n = 4$), aortic root and ascending aorta replacement ($n = 4$) or resection of ascending aorta intramural hematoma ($n = 1$). Overall, baseline lactate levels, hematocrit, and eGFR were within the normal ranges.

Echocardiographic Data

Echocardiographic parameters of LV and RV systolic function, including mesh-derived regional RV volumetric data (**Figure 1**) of patients who reached the endpoint compared to patients who did not reach the endpoint, are listed in **Table 2**. Global left and right ventricular volumes did not differ significantly between the outcome groups. The same relationship was observed for global RV and LV functional parameters derived from 3D-STE (LVEF, LV-GLS, RVEF, RV SV, TAPSE, and FAC). Of note, the percentage of patients with severely decreased LVEF or RVEF (<20% each) was similar in both groups. As a simple measure of longitudinal function of the basal inflow region, 3D-derived TAPSE correlated moderately with inflow RVEF ($r = 0.50$, 95% CI 0.42–0.58, $p < 0.001$). Global and regional RVEF decreased with increased systolic pulmonary artery pressures (**Supplementary Table 2**). Regional RV volumetry was feasible in all included patients. Patients who reached the endpoint had significantly lower systolic function in the inflow region (reflected by inflow RVEF and rel. SV) and higher rel. SV in the apex region than patients who did not reach the endpoint (**Figure 2**). Interestingly, the end-diastolic volumes of the three RV regions did not differ significantly. The opposite changes in the rel. SV of the inflow and the rel. SV of the apex comprised a statistically significant difference in the *apex to inflow rel. SV ratio* between the different outcome groups. This parameter was not defined a priori but based on the analysis' findings.

TABLE 2 | Conventional and novel echocardiographic parameters derived from transesophageal echocardiography of patients who reached the endpoint (in-hospital mortality or the need for ECLS) and patients who did not reach the endpoint.

Parameter	Endpoint yes ($n = 25$)	Endpoint no ($n = 332$)	*p*-value
LV and RV systolic function parameters (derived from 3D-STE)			
LVEDV, ml	176 (134–213)	150 (117–203)	0.30
LVEDVi, ml/m²	91 (74–121)	78 (62–106)	0.23
LVESV, ml	106 (58–143)	90 (65–137)	0.54
LVESVi, ml/m²	54 (31–75)	46 (34–70)	0.41
LVEF, %	38 ± 15	38 ± 14	0.47
LVEF < 20%, *n*	4 (16)	36 (11)	0.66
LV-GLS, %	−11.6 ± 6.5	−12.6 ± 5.6	0.38
RVEDV, ml	150 (108–213)	141 (112–171)	0.39
RVEDVi, ml/m²	78 (55–99)	73 (61–87)	0.25
RVESV, ml	94 (73–139)	87 (65–110)	0.15
RVESVi, ml/m²	51 (38–67)	44 (34–57)	0.08
RVEF, %	34 ± 8	38 ± 10	0.10
RVEF < 20%, *n*	1 (4)	16 (5)	0.76
RV SV global, ml	54 ± 23	54 ± 20	0.96
TAPSE, mm	11 ± 6	12 ± 6	0.58
FAC, %	27 ± 8	31 ± 10	0.08
Mesh-derived regional RV volumetry			
RVEF inflow, %	32 ± 8	37 ± 11	**0.01**
EDV inflow, ml	70 (54–106)	68 (55–85)	0.52
EDVi inflow, ml/m²	40 (28–51)	35 (29–43)	0.35
SV inflow, ml	24 ± 12	26 ± 10	0.39
rel. SV inflow, %	44 ± 8	48 ± 9	**0.02**
RVEF apex, %	42 ± 13	44 ± 14	0.70
EDV apex, ml	49 (29–65)	40 (31–52)	0.20
EDVi apex, ml/m²	27 (17–32)	21 (16–26)	0.11
SV apex, ml	21 ± 10	18 ± 8	0.15
rel. SV apex, %	38 ± 10	33 ± 8	**0.01**
RVEF RVOT, %	29 ± 11	32 ± 12	0.27
EDV RVOT, ml	33 (26–42)	32 (26–39)	0.47
EDVi RVOT, ml/m²	17 (15–21)	16 (14–19)	0.46
SV RVOT, ml	10 ± 4	10 ± 5	0.55
rel. SV RVOT, %	18 ± 5	19 ± 6	0.76
Apex/inflow rel. SV ratio	0.97 ± 0.51	0.74 ± 0.29	**0.04**

Values are means ± standard deviations, medians (interquartile ranges) or n (%). p-values are derived from unpaired t-tests, Mann–Whitney U tests or chi-square tests where appropriate. Significant p-values are highlighted in bold.

3D-STE, three-dimensional speckle-tracking echocardiography; ECLS, extracorporeal life support; EDV(i), end-diastolic volume (index); FAC, fractional area change derived from 3D-STE; eGFR, estimated glomerular filtration rate; LV-GLS, left ventricular global longitudinal strain; LVAD, left ventricular assist device; LVEDV(i), left ventricular end-diastolic volume (index); LVESV(i), left ventricular end-systolic volume (index); LVEF, left ventricular ejection fraction; OPCAB, off-pump coronary artery bypass surgery; rel., relative; RVEDV(i), right ventricular end-diastolic volume (index); RVESV(i), right ventricular end-systolic volume (index); RVEF, right ventricular ejection fraction; RVOT, right ventricular outflow tract; SV, stroke volume; TAPSE, tricuspid annular plane systolic excursion derived from 3D-STE.

Association With Outcome

A total of $n = 25$ patients (7%) reached the endpoint. Nineteen patients died during the primary hospital stay (5%), and 11 of

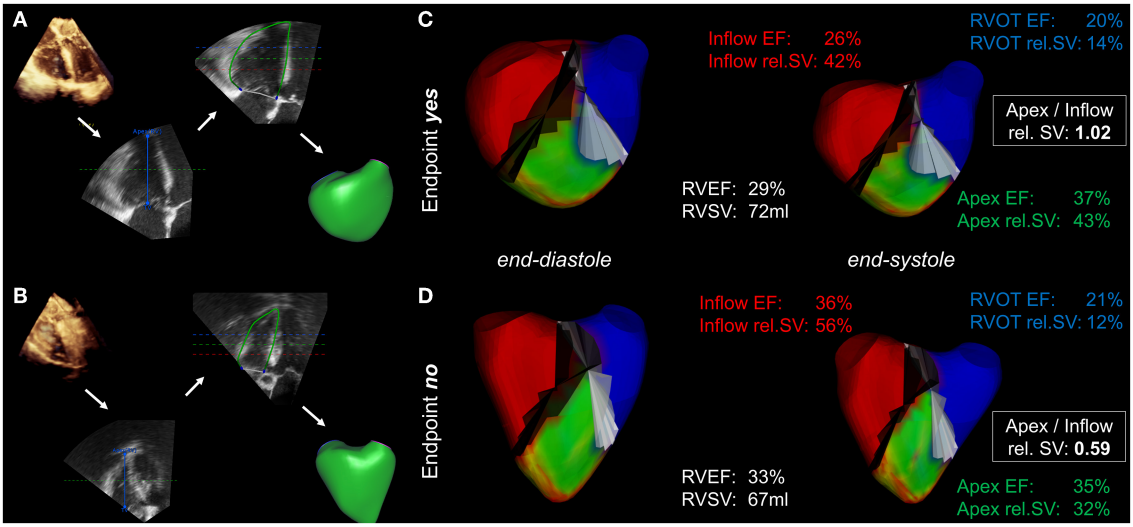

FIGURE 2 | Mesh-derived regional RV volumetry. Visualization of regional RV volumetry in a patient who reached the endpoint **(A,C)** compared with that in a patient with an uneventful postoperative course **(B,D)**. **(A,B)** The intraoperative 3D datasets undergo segmentation and endocardial borders are tracked using speckle-tracking technology, resulting in the generation of mesh models (workflow indicated by the white arrows). **(C,D)** Mesh-derived regional volumetry of the inflow (red), apex (green) and RVOT (blue). The displayed results include regional ejection fractions (EF), relative stroke volumes (rel. SV) and the apex to inflow rel. SV ratio. The cutting planes between the regions are colored black and white.

those required postoperative ECLS (3%). Six patients required postoperative ECLS but were successfully discharged (2%). The endpoint incidence was 6% (3/51) among on-pump coronary artery bypass grafting patients, 7% (5/69) among OPCAB patients, 8% (8/96) among left-sided valve surgery patients, 6% (1/17) among thoracic aortic surgery patients, 4% (1/25) among LVAD patients and 7% (7/99) among mixed procedure patients. In univariable logistic regression of the investigated clinical and conventional echocardiographic parameters, only tricuspid regurgitation grade $\geq$ 2 was significantly associated with the endpoint (OR 3.75, 95% CI 1.52–9.30, $p < 0.01$). The odds ratio of a binary variable defines the relative risk change of reaching the endpoint in case the variable is present: e.g., 375% increased risk of patients with tricuspid regurgitation grade $\geq$ 2 to reach the endpoint compared with patients with tricuspid regurgitation grade 0 or 1. The surgical categories were not significantly associated with the endpoint in univariable logistic regression (**Supplementary Table 3**). Strikingly, inflow RVEF (OR 0.95, 95% CI 0.92–0.99, $p = 0.01$), rel. SV of the inflow (OR 0.94, 95% CI 0.90–0.99, $p = 0.02$), rel. SV of the apex (OR 1.07, 95% CI 1.02–1.13, $p < 0.01$) and apex to inflow rel. SV ratio (OR 5.81, 95% CI 1.90–17.77, $p < 0.01$) showed a significant association with short-term outcome (**Table 3**). The OR of a continuous variable defines the relative risk change of reaching the endpoint if the variable increases by one unit: e.g., an increase of inflow RVEF by 1% decreases the risk by 5%, while an increase of apex rel. SV by 1% increases the risk by 7%. In a multivariable regression model including tricuspid regurgitation, inflow RVEF and apex to inflow rel. SV ratio, only tricuspid regurgitation (OR 4.24, 95% CI 1.66–10.84, $p < 0.01$) and apex to inflow rel. SV ratio (OR 6.55, 95% CI 2.09–20.60, $p < 0.001$) remained independently associated with the endpoint. In this model, apex to inflow rel. SV ratio carried incremental value and added significantly to the model fit (**Figure 3**).

Reproducibility

Figure 4 and **Table 4** summarize the results of the reproducibility analysis of the double measured patients ($n = 25$). Reproducibility was better for global RVEF analysis than for regional RVEF analysis. While intraobserver and interobserver variability was fairly low for inflow and apex RVEF measurements, RVOT RVEF showed the poorest comparability, with wide 95% limits of agreement (−10 to 21) and an ICC of 0.840 (95% CI: 0.524–0.937). Interobserver variability of apex to inflow rel. SV ratio was moderate [$r = 0.75$, $p < 0.0001$; ICC 0.820 (0.591–0.920); bias −0.02; 95% limits of agreement −0.34 to −0.30].

DISCUSSION

Key Findings

In a mixed cohort of elective cardiac surgery patients, most baseline clinical and intraoperative echocardiographic parameters showed no significant association with short-term outcome, including sophisticated measures such as 3D-derived RVEF and LV-GLS. Strikingly, an established score for perioperative risk assessment (EuroSCORE II) did not correlate with adverse outcomes in these patients. Using a simple approach to quantify regional systolic function in three anatomically different regions of the RV, a novel parameter incorporating the relative contributions of the apex and the inflow tract to volume ejection (apex to inflow rel. SV ratio) was

TABLE 3 | Univariable and multivariable logistic regression analysis for the association with the endpoint (in-hospital mortality or the need for ECLS).

Parameter	Univariable OR (95% CI)	*p*-value	Multivariable OR (95% CI)	*p*-value
Age, years	1.00 (0.97–1.04)	0.91		
Body mass index, kg/m²	1.02 (0.95–1.10)	0.62		
Chronic lung disease*	2.21 (0.29–16.96)	0.45		
Pulmonary hypertension†	0.00 (–)	0.99		
Tricuspid regurgitation‡	3.75 (1.52–9.30)	**<0.01**	4.24 (1.66–10.84)	**<0.01**
Diabetes§	0.56 (0.18–1.73)	0.31		
NYHA class IV	0.71 (0.27–1.86)	0.49		
eGFR, ml/min	0.99 (0.98–1.01)	0.30		
Lactate, mmol/l	1.84 (0.96–3.52)	0.07		
Hematocrit, %	0.96 (0.90–1.03)	0.23		
EuroSCORE II, %	1.01 (0.96–1.06)	0.79		
LVEDVi, ml/m²	1.00 (0.99–1.01)	0.45		
LVEF, %	1.00 (0.97–1.03)	0.94		
LV-GLS, %	1.03 (0.96–1.11)	0.38		
RVESVi, ml/m²	1.01 (0.99–1.03)	0.16		
RVEF, %	0.97 (0.93–1.01)	0.10		
FAC, %	0.97 (0.93–1.00)	0.08		
RVEF inflow, %	0.95 (0.92–0.99)	**0.01**	Excluded	0.32
rel. SV inflow, %	0.94 (0.90–0.99)	**0.02**		
RVEF apex, %	0.99 (0.97–1.02)	0.70		
rel. SV apex, %	1.07 (1.02–1.13)	**<0.01**		
RVEF RVOT, %	0.98 (0.95–1.02)	0.27		
rel. SV RVOT, %	0.99 (0.93–1.06)	0.76		
Apex/inflow rel. SV ratio	5.81 (1.90–17.77)	**<0.01**	6.55 (2.09–20.60)	**<0.001**

CI, confidence interval; eGFR, estimated glomerular filtration rate; FAC, fractional area change; LV-GLS, left ventricular global longitudinal strain; LVEDV(i), left ventricular end-diastolic volume (index); LVEF, left ventricular ejection fraction; NYHA, New York Heart Association; OR, odds ratio; rel., relative; RVESV(i), right ventricular end-systolic volume (index); RVEF, right ventricular ejection fraction; RVOT, right ventricular outflow tract; SV, stroke volume.

**Long term use of bronchodilators or steroids for lung disease.*

† Systolic pulmonary artery pressure > 30 mmHg.

‡ Grade ≥ 2.

§ Insulin-dependent.

Significant p-values are highlighted in bold.

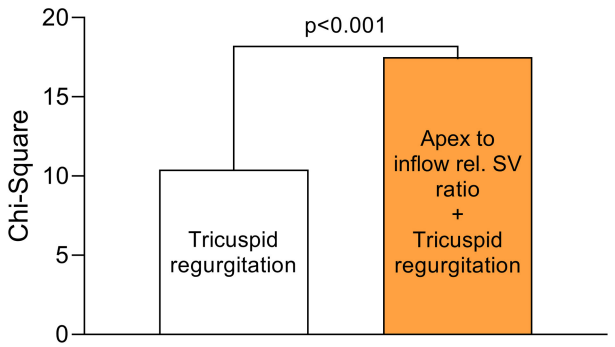

FIGURE 3 | Incremental value of apex to inflow rel. SV ratio over the presence of tricuspid regurgitation. In a multivariable logistic regression model ($n = 357$) for the combined endpoint (in-hospital mortality/ECLS), apex to inflow rel. SV ratio added incrementally to the model over the presence of tricuspid regurgitation (grade ≥ 2). The chi-square values were compared using the omnibus test of model coefficients.

significantly and independently associated with the combined endpoint of in-hospital death and life-threatening hemodynamic failure requiring ECLS. Only the presence of significant tricuspid regurgitation (grade ≥ 2) showed similar associations in logistic regression. Furthermore, the novel technique for regional RV analysis is feasible and reproducible, with higher observer variabilities in the RVOT region, potentially because of its complex anatomy and relatively small volume. Reproducibility was further warranted by an identical definition of the segmental borders in all meshes, avoiding errors due to manual border determination. Overall, parameters of cardiac function acquired intraoperatively using novel 3D techniques were lower than conventional reference ranges, a phenomenon that has been discussed previously (20).

Perioperative Right Ventricular Function

Assessment of systolic RV function by intraoperative TEE is crucial. The induction of general anesthesia and positive pressure

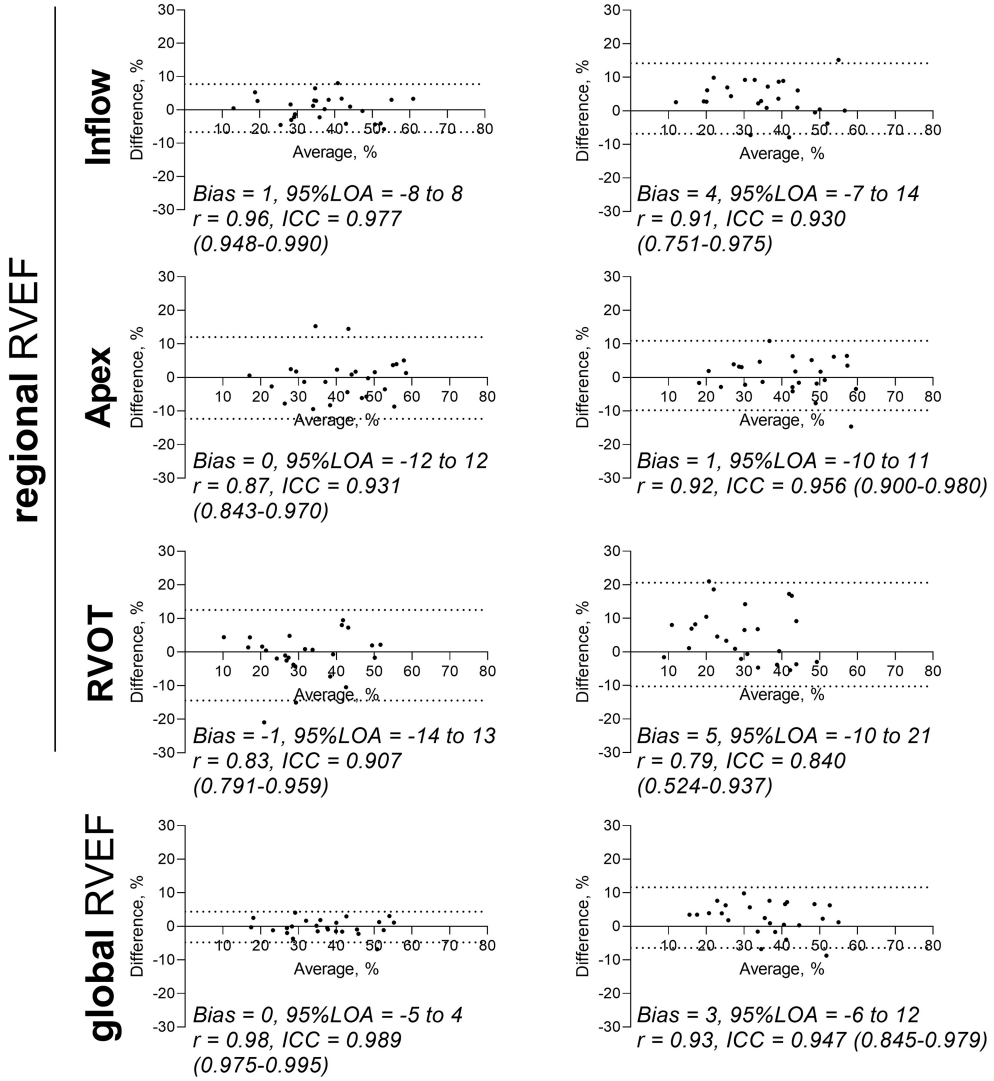

FIGURE 4 | Reproducibility analysis of global and regional RVEF measurements. Intraobserver and interobserver analysis of $n = 25$ patient meshes. Bland–Altman diagrams are displayed for global and regional RVEFs with biases, 95% limits of agreement (95% LOA), correlation coefficients r and intraclass correlation coefficients (ICCs) with 95% confidence intervals. ICC, intraclass correlation coefficient; LOA, limits of agreement; r, Pearson correlation coefficient; RVEF, right ventricular ejection fraction; RVOT, right ventricular outflow tract.

ventilation have distinct effects on RV function (21), and the application of goal-directed therapies by the anesthesiologist—such as vasopressor infusions to achieve predefined mean arterial pressures—could help to equilibrate loading conditions. Baseline reductions in RV function are associated with perioperative RV dysfunction and adverse outcomes following cardiac surgery (22), but the sensitivities of traditional echocardiographic measures are potentially insufficient (23). TAPSE, e.g., quantifies longitudinal function of the basal inflow segment but did not correlate with the endpoint, in contrast to the novel inflow parameters. Preoperative TTE-derived 2D TAPSE measurements might yield different results. The paradigm of disease-induced RV enlargement and dilation with increased EDVs has existed for decades. However, RVEDV showed no independent association with short-term outcomes in a previous investigation from our institution (20). Another possible phenotype of pathological RV remodeling could be reflected by altered regional EDVs in the absence of global enlargement, e.g., increased apical EDVs vs. decreased inlet EDVs. In conditions of pressure or volume overload, regionally different adaptive reactions according to the heterogeneous structure within the right ventricular myocardium appear plausible (24). However, in our retrospective analysis, regional EDVs did not differ significantly between patients with good and unfavorable outcomes. Instead, our data stress the hypothesis that a deterioration of RV function precedes enlargement of the RV,

TABLE 4 | Intra- and interobserver reproducibility analysis for global and regional RVEF.

Parameter	*r*	ICC (95% CI)	Bias (%)	95% LOA (%)
Intraobserver reproducibility				
RVEF inflow, %	0.96	0.977 (0.948–0.990)	1	−8 to 8
RVEF apex, %	0.87	0.931 (0.843–0.970)	0	−12 to 12
RVEF RVOT, %	0.83	0.907 (0.791–0.959)	−1	−14 to 13
RVEF, %	0.98	0.989 (0.975–0.995)	0	−5 to 4
Interobserver reproducibility				
RVEF inflow, %	0.91	0.930 (0.751–0.975)	4	−7 to 14
RVEF apex, %	0.92	0.956 (0.900–0.980)	1	−10 to 11
RVEF RVOT, %	0.79	0.840 (0.524–0.937)	5	−10 to 21
RVEF, %	0.93	0.947 (0.845–0.979)	3	−6 to 12

CI, confidence interval; ICC, intraclass correlation coefficient; LOA, limits of agreement; r, Pearson correlation coefficient; RVEF, right ventricular ejection fraction; RVOT, right ventricular outflow tract.

as regional functional parameters (e.g., rel. SV) of the regions showed distinct differences between the outcome groups. Rel. SV is further affected by the volume of a segment and should be considered as a parameter associated with RV remodeling. Consequently, the assessment of static parameters or the quantification of altered shapes might be less favorable than novel functional measures in the context of elective cardiac surgery. During the analysis of our findings, we intuitively linked them to a historic echocardiographic finding named McConnell's sign: during acute pressure overload or ischemia, the stressed RV in some cases reacts with a distinct contraction pattern (25, 26). While the apex shows normal or even hyperdynamic contractility, the basomidventricular free wall myocardium appears hypo- or akinetic (27). Even though McConnell's sign is usually observed during acute RV failure, the shift from inflow to apical relative stroke volume ejection in our patients with adverse short-term outcomes could point to a mild or chronic form of a *McConnell-esque* contraction pattern, indicating subclinical RV dysfunction.

Risk Stratification in Cardiac Surgery and Clinical Implications

The prediction of postoperative outcomes following cardiac surgery is important but challenging. If the onset or progression of cardiovascular disease indicates surgery, interdisciplinary teams involving cardiac surgeons, cardiologists and anesthesiologists need to decide for or against the procedure based on the individual benefit-risk assessment. Currently, a wide variety of clinical features are available, but their interpretation and integration are complex. Established current risk scores, such as the EuroSCORE II or the Society of Thoracic Surgeons Risk Score, have been shown to predict unfavorable postoperative outcomes but do not incorporate a direct measure of RV systolic function (28, 29). Therefore, these scoring systems are prone to severely underestimating patients' risks in cases of RV dysfunction. In the context of cardiac anesthesia, the interpretation of intraoperative TEE-derived functional parameters—among other parameters of respiratory function or invasive hemodynamics, for example—is paramount for evaluating the patients' needs regarding postoperative care (30). While the course of an operation and its surgical success can be similar, patient outcomes can vary dramatically depending on their ability to recover from major surgical trauma, extracorporeal circulation or altered loading conditions. Hence, modern perioperative strategies focus on the individual patient's needs and range from fast-track regimens to extensive ICU protocols. While short durations of mechanical ventilation and early mobilization decrease the risk for postoperative complications in eligible patients (31), the identification of patients at risk for hemodynamic failure is important and should lead to a continuous evaluation of diagnostic measures and subsequent therapies—such as inotropic support or ECLS—if necessary (32). Our results indicate that sophisticated measures of RV function, measured via intraoperative TEE by the anesthesiologist, have the potential to predict adverse short-term outcomes. As these parameters, e.g., apex to inflow rel. SV ratio, are not part of current and established risk scores, their assessment should be considered during the planning and initiation of the postoperative regimen. Future studies should attempt to unveil the potential of this parameter in preoperative risk assessment prior to cardiac surgery employing awake transthoracic echocardiography. Technical optimizations of regional RV volumetry to warrant online, bedside applicability are needed to facilitate clinical implementation.

Limitations

Naturally, there are some limitations to the interpretation of the results and their generalizability. The investigated patients were retrospectively included, resulting in a strictly observational study design. As not all patients underwent intraoperative 3D echocardiography, a potential inclusion bias needs to be considered during interpretation of the results. Furthermore, incidence of the endpoint is low resulting in a limited number of events. Prospective randomized trials are necessary to fully characterize the association between the reported parameters and patient outcomes following cardiac surgery. Baseline cardiac function was not characterized by other techniques, such as invasive hemodynamics, awake transthoracic echocardiography

or cardiac magnetic resonance imaging. Hence, a comparison of the novel measures with reference methods cannot be provided. Awake pulmonary artery pressures and the underlying cause of present pulmonary hypertension might be associated with the outcome but were not systematically available in this cohort. The severity of tricuspid regurgitation was a variable of interest in regression analysis but the reproducibility of the assessment of tricuspid regurgitation was not investigated systematically in this cohort. Since only the association of clinical and echocardiographic parameters with short-term outcome was studied, the report does not allow for conclusions regarding long-term prognosis.

Conclusions

Regional right ventricular systolic function assessed by intraoperative three-dimensional transesophageal speckle-tracking echocardiography is feasible. The apex to inflow relative stroke volume ratio is associated with increased in-hospital mortality and life-threatening postoperative hemodynamic failure. These findings might be useful to improve perioperative risk estimation in patients with baseline RV dysfunction in which conventional echocardiographic parameters are within normal range.

DATA AVAILABILITY STATEMENT

The raw data supporting the conclusions of this article will be made available by the authors, without undue reservation.

ETHICS STATEMENT

The studies involving human participants were reviewed and approved by Ethics Committee of the Medical School at the University of Tuebingen, Gartenstraße 47 72074 Tuebingen, Germany. Written informed consent for participation was not required for this study in accordance with the national legislation and the institutional requirements.

AUTHOR CONTRIBUTIONS

MK and HM contributed to conception and design of the study. MK, M-MD, and TH performed data acquisition. MK and HM performed the statistical analysis. MK, AK, CS, PR, and HM performed data interpretation. MK wrote the first draft of the manuscript. AK, CS, and PR critically revised the manuscript. HM contributed substantially to the final revision of the manuscript. All authors read and approved the submitted version.

FUNDING

This work was supported by Deutsche Forschungsgemeinschaft (DFG) (Grant DFG-INST 2388/71–1 FUGG) and funded by departmental funds.

ACKNOWLEDGMENTS

We thank Tobias Lang for his help and expertise throughout the coding process of the software algorithm.

SUPPLEMENTARY MATERIAL

The Supplementary Material for this article can be found online at: https://www.frontiersin.org/articles/10.3389/fcvm.2022.821831/full#supplementary-material

REFERENCES

1. Peyrou J, Chauvel C, Pathak A, Simon M, Dehant P, Abergel E. Preoperative right ventricular dysfunction is a strong predictor of 3 years survival after cardiac surgery. *Clin Res Cardiol.* (2017) 106:734–42. doi: 10.1007/s00392-017-1117-y
2. Haddad F, Denault AY, Couture P, Cartier R, Pellerin M, Levesque S, et al. Right ventricular myocardial performance index predicts perioperative mortality or circulatory failure in high-risk valvular surgery. *J Am Soc Echocardiogr.* (2007) 20:1065–72. doi: 10.1016/j.echo.2007.02.017
3. Ternacle J, Berry M, Cognet T, Kloeckner M, Damy T, Monin JL, et al. Prognostic value of right ventricular two-dimensional global strain in patients referred for cardiac surgery. *J Am Soc Echocardiogr.* (2013) 26:721–6. doi: 10.1016/j.echo.2013.03.021
4. MacKay EJ, Zhang B, Heng S, Ye T, Neuman MD, Augoustides JG, et al. Association between transesophageal echocardiography and clinical outcomes after coronary artery bypass graft surgery. *J Am Soc Echocardiogr.* (2021) 34:571–81. doi: 10.1016/j.echo.2021.01.014
5. Eltzschig HK, Rosenberger P, Loffler M, Fox JA, Aranki SF, Shernan SK. Impact of intraoperative transesophageal echocardiography on surgical decisions in 12,566 patients undergoing cardiac surgery. *Ann Thorac Surg.* (2008) 85:845–52. doi: 10.1016/j.athoracsur.2007.11.015
6. Zhang Y, Sun W, Wu C, Zhang Y, Cui L, Xie Y, et al. Prognostic value of right ventricular ejection fraction assessed by 3D echocardiography in COVID-19 patients. *Front Cardiovasc Med.* (2021) 8:641088. doi: 10.3389/fcvm.2021.641088
7. Ishizu T, Seo Y, Atsumi A, Tanaka YO, Yamamoto M, Machino-Ohtsuka T, et al. Global and regional right ventricular function assessed by novel three-dimensional speckle-tracking echocardiography. *J Am Soc Echocardiogr.* (2017) 30:1203–13. doi: 10.1016/j.echo.2017.08.007
8. Nagata Y, Wu VC, Kado Y, Otani K, Lin FC, Otsuji Y, et al. Prognostic value of right ventricular ejection fraction assessed by transthoracic 3D echocardiography. *Circ Cardiovasc Imaging.* (2017) 10:e005384. doi: 10.1161/CIRCIMAGING.116.005384
9. Greiner S, Heimisch M, Aurich M, Hess JA, Katus HA, Mereles D. Multiplane two-dimensional strain echocardiography for segmental analysis of right ventricular mechanics: new-RV study. *Clin Res Cardiol.* (2014) 103:817–24. doi: 10.1007/s00392-014-0723-1
10. Bidviene J, Muraru D, Maffessanti F, Ereminiene E, Kovács A, Lakatos B, et al. Regional shape, global function and mechanics in right ventricular volume and pressure overload conditions: a three-dimensional echocardiography study. *Int J Cardiovasc Imaging.* (2021) 37:1289–99. doi: 10.1007/s10554-020-02117-8
11. Moriyama H, Kawakami T, Kataoka M, Hiraide T, Kimura M, Endo J, et al. Regional right ventricular abnormalities implicate distinct pathophysiological conditions in patients with chronic thromboembolic pulmonary hypertension. *J Am Heart Assoc.* (2020) 9:e018096. doi: 10.1161/JAHA.120.018096

12. Magunia H, Dietrich C, Langer HF, Schibilsky D, Schlensak C, Rosenberger P, et al. 3D echocardiography derived right ventricular function is associated with right ventricular failure and mid-term survival after left ventricular assist device implantation. *Int J Cardiol.* (2018) 272:348–55. doi: 10.1016/j.ijcard.2018.06.026
13. Nowak-Machen M, Lang T, Schilling A, Mockenhaupt L, Keller M, Rosenberger P, et al. Regional right ventricular volume and function analysis using intraoperative 3-dimensional echocardiography-derived Mesh models. *J Cardiothorac Vasc Anesth.* (2019) 33:1527–32. doi: 10.1053/j.jvca.2019.02.011
14. Keller M, Heller T, Lang T, Patzelt J, Schreieck J, Schlensak C, et al. Acute changes of global and longitudinal right ventricular function: an exploratory analysis in patients undergoing open-chest mitral valve surgery, percutaneous mitral valve repair and off-pump coronary artery bypass grafting. *Cardiovasc Ultrasound.* (2020) 18:32. doi: 10.1186/s12947-020-00218-x
15. Keller M, Lang T, Schilling A, Nowak-Machen M, Rosenberger P, Magunia H. Novel mesh-derived right ventricular free wall longitudinal strain analysis by intraoperative three-dimensional transoesophageal speckle-tracking echocardiography: a comparison with conventional parameters. *Int J Cardiovasc Imaging.* (2019) 35:2177–88. doi: 10.1007/s10554-019-01669-8
16. Hahn RT, Abraham T, Adams MS, Bruce CJ, Glas KE, Lang RM, et al. Guidelines for performing a comprehensive transesophageal echocardiographic examination: recommendations from the American Society of Echocardiography and the Society of Cardiovascular Anesthesiologists. *J Am Soc Echocardiogr.* (2013) 26:921–64. doi: 10.1016/j.echo.2013.07.009
17. Lang RM, Badano LP, Mor-Avi V, Afilalo J, Armstrong A, Ernande L, et al. Recommendations for cardiac chamber quantification by echocardiography in adults: an update from the American Society of Echocardiography and the European Association of Cardiovascular Imaging. *J Am Soc Echocardiogr.* (2015) 28:1–39.e14. doi: 10.1016/j.echo.2014.10.003
18. Lang RM, Badano LP, Tsang W, Adams DH, Agricola E, Buck T, et al. EAE/ASE recommendations for image acquisition and display using three-dimensional echocardiography. *J Am Soc Echocardiogr.* (2012) 25:3–46. doi: 10.1016/j.echo.2011.11.010
19. van Smeden M, de Groot JAH, Moons KGM, Collins GS, Altman DG, Eijkemans MJC, et al. No rationale for 1 variable per 10 events criterion for binary logistic regression analysis. *BMC Med Res Methodol.* (2016) 16:163. doi: 10.1186/s12874-016-0267-3
20. Keller M, Heller T, Duerr M-M, Schlensak C, Nowak-Machen M, Feng Y-S, et al. Association of 3D Mesh-derived right ventricular strain with short-term outcome in patients undergoing cardiac surgery. *J Am Soc Echocardiogr.* (2021). doi: 10.1016/j.echo.2021.11.008. [Epub ahead of print].
21. Magunia H, Jordanow A, Keller M, Rosenberger P, Nowak-Machen M. The effects of anesthesia induction and positive pressure ventilation on right-ventricular function: an echocardiography-based prospective observational study. *BMC Anesthesiol.* (2019) 19:199. doi: 10.1186/s12871-019-0870-z
22. Maslow AD, Regan MM, Panzica P, Heindel S, Mashikian J, Comunale ME. Precardiopulmonary bypass right ventricular function is associated with poor outcome after coronary artery bypass grafting in patients with severe left ventricular systolic dysfunction. *Anesthesia Analgesia.* (2002) 95:1507–18. doi: 10.1097/00000539-200212000-00009
23. Carluccio E, Biagioli P, Alunni G, Murrone A, Zuchi C, Coiro S, et al. Prognostic value of right ventricular dysfunction in heart failure with reduced ejection fraction: superiority of longitudinal strain over tricuspid annular plane systolic excursion. *Circ Cardiovasc Imaging.* (2018) 11:e006894. doi: 10.1161/CIRCIMAGING.117.006894
24. Sanz J, Sánchez-Quintana D, Bossone E, Bogaard HJ, Naeije R. Anatomy, function, and dysfunction of the right ventricle: JACC state-of-the-art review. *J Am Coll Cardiol.* (2019) 73:1463–82. doi: 10.1016/j.jacc.2018.12.076
25. Sosland RP, Gupta K. Images in cardiovascular medicine: McConnell's Sign. *Circulation.* (2008) 118:e517–8. doi: 10.1161/CIRCULATIONAHA.107.746602
26. Casazza F, Bongarzoni A, Capozi A, Agostoni O. Regional right ventricular dysfunction in acute pulmonary embolism and right ventricular infarction. *Eur J Echocardiogr.* (2005) 6:11–4. doi: 10.1016/j.euje.2004.06.002
27. Brenes-Salazar JA. McConnell's echocardiographic sign in acute pulmonary embolism: still a useful pearl. *Heart Lung Vessels.* (2015) 7:86–8.
28. Nashef SA, Roques F, Sharples LD, Nilsson J, Smith C, Goldstone AR, et al. EuroSCORE II. *Eur J Cardiothorac Surg.* (2012) 41:734–44. doi: 10.1093/ejcts/ezs043
29. Shahian DM, O'Brien SM, Filardo G, Ferraris VA, Haan CK, Rich JB, et al. The Society of Thoracic Surgeons 2008 cardiac surgery risk models: part 1–coronary artery bypass grafting surgery. *Ann Thorac Surg.* (2009) 88 (1 Suppl.):S2–22. doi: 10.1016/j.athoracsur.2009.05.053
30. Click RL, Abel MD, Schaff HV. Intraoperative transesophageal echocardiography: 5-year prospective review of impact on surgical management. *Mayo Clin Proc.* (2000) 75:241–7. doi: 10.1016/S0025-6196(11)65027-1
31. Fleming IO, Garratt C, Guha R, Desai J, Chaubey S, Wang Y, et al. Aggregation of marginal gains in cardiac surgery: feasibility of a perioperative care bundle for enhanced recovery in cardiac surgical patients. *J Cardiothorac Vasc Anesth.* (2016) 30:665–70. doi: 10.1053/j.jvca.2016.01.017
32. Guru V, Tu JV, Etchells E, Anderson GM, Naylor CD, Novick RJ, et al. Relationship between preventability of death after coronary artery bypass graft surgery and all-cause risk-adjusted mortality rates. *Circulation.* (2008) 117:2969–76. doi: 10.1161/CIRCULATIONAHA.107.722249

Conflict of Interest: The authors declare that the research was conducted in the absence of any commercial or financial relationships that could be construed as a potential conflict of interest.

Publisher's Note: All claims expressed in this article are solely those of the authors and do not necessarily represent those of their affiliated organizations, or those of the publisher, the editors and the reviewers. Any product that may be evaluated in this article, or claim that may be made by its manufacturer, is not guaranteed or endorsed by the publisher.

frontiers | Frontiers in Cardiovascular Medicine

ORIGINAL RESEARCH
published: 12 April 2022
doi: 10.3389/fcvm.2022.843952

Impact of Right Ventricular Trabeculation on Right Ventricular Function in Patients With Left Ventricular Non-compaction Phenotype

*Anna Réka Kiss, Zsófia Gregor, Adrián Popovics, Kinga Grebur, Liliána Erzsébet Szabó, Zsófia Dohy, Attila Kovács, Bálint Károly Lakatos, Béla Merkely, Hajnalka Vágó and Andrea Szűcs**

Heart and Vascular Center of Semmelweis University, Budapest, Hungary

Right ventricular (RV) involvement in left ventricular (LV) non-compaction (LVNC) remains unknown. We aimed to describe the RV volumetric, functional, and strain characteristics and clinical features of patients with LVNC phenotype and good LV ejection fraction (EF) using cardiac magnetic resonance to characterize RV trabeculation in LVNC and to study the relationships of RV and LV trabeculation with RV volume and function. This retrospective study included 100 Caucasian patients with LVNC phenotype and good LV-EF and 100 age- and sex-matched healthy controls. Patients were further divided into two subgroups according to RV indexed trabecular mass [RV-TMi; patients with RV hypertrabeculation (RV-HT) vs. patients with normal RV trabeculation (RV-NT)]. We measured the LV and RV volumetric, functional, and TMi values using threshold-based postprocessing software and the RV and LV strain values using feature tracking and collected the patients' LVNC-related clinical features. Patients had higher RV volumes, lower RV-EF, and worse RV strain values than controls. A total of 22% of patients had RV-TMi values above the reference range; furthermore, RV-HT patients had higher RV and LV volumes, lower RV- and LV-EF, and worse RV strain values than RV-NT patients. We identified a strong positive correlation between RV- and LV-TMi and between RV-TMi and RV volumes and a significant inverse relationship of both RV- and LV-TMi with RV function. The prevalence of LVNC-related clinical features was similar in the RV-HT and RV-NT groups. These results suggest that some patients with LVNC phenotype might have RV non-compaction with subclinical RV dysfunction and without more severe clinical features.

Keywords: right ventricle (RV), right ventricular function, cardiac magnetic resonance (CMR), left ventricular non-compaction, non-comaption, trabecula, trabeculation

OPEN ACCESS

Edited by:
Alessandro Zorzi,
University Hospital of Padua, Italy

Reviewed by:
Anna Baritussio,
University of Padua, Italy
Alberto Cipriani,
University Hospital of Padua, Italy

****Correspondence:***
Andrea Szűcs
szucsand@gmail.com

Specialty section:
This article was submitted to Cardiovascular Imaging, a section of the journal Frontiers in Cardiovascular Medicine

Received: *27 December 2021*
Accepted: *22 February 2022*
Published: *12 April 2022*

Citation:
Kiss AR, Gregor Z, Popovics A, Grebur K, Szabó LE, Dohy Z, Kovács A, Lakatos BK, Merkely B, Vágó H and Szűcs A (2022) Impact of Right Ventricular Trabeculation on Right Ventricular Function in Patients With Left Ventricular Non-compaction Phenotype. Front. Cardiovasc. Med. 9:843952. doi: 10.3389/fcvm.2022.843952

INTRODUCTION

Left ventricular non-compaction (LVNC) has become a well-known clinical entity, and the amount of research on this topic is increasing. Nevertheless, right ventricular (RV) involvement in LVNC remains a controversial issue with little available data. Compared with those of the left ventricle (LV), the unique shape of the RV and its physiologically greater quantity of endocardial trabeculae

make it difficult to evaluate RV hypertrabeculation. Despite the lack of established diagnostic criteria, case reports suggest the existence of isolated RV non-compaction (1–3). The negative relationship between LV trabeculation and LV ejection fraction (EF) has prompted questions about whether RV trabeculation is similarly associated with RV function, which has been shown to be an important prognostic parameter in several cardiac diseases, including LVNC (4–7). The impact of LVNC on RV trabeculation and RV function and the presence of RV dysfunction have not been described. Furthermore, the possibility of RV involvement raises further questions regarding affected patients' morphologic diagnosis, clinical features, incidence, and prognosis.

Our study aimed to describe the RV volumetric, functional and feature-tracking strain parameters of patients with LVNC phenotype and good LV-EF and compare them to those of a healthy control group using cardiac magnetic resonance (CMR); to characterize RV trabeculation in patients with LVNC phenotype; and to describe the relationships of RV and LV trabeculation with RV volume and function. Furthermore, we studied the connection between clinical features and the extent of RV trabeculation in patients with LVNC phenotype.

MATERIALS AND METHODS

Study Population

This retrospective study included 100 Caucasian patients with the LVNC phenotype and 100 age- and sex-matched healthy volunteers (**Table 1**, **Figure 1**). CMR examinations were performed at the same institute, and all patients completed a questionnaire for collection of demographic data, cardiovascular symptoms, medical history, medication use, and sports activity. The diagnosis of the LVNC phenotype was established when the CMR-based criteria of both Petersen et al. (non-compacted/compacted ratio > 2.3) and Jaquier et al. (trabeculated LV mass >20% of total LV mass) were fulfilled (8, 9). The presence of other LVNC related clinical features described by others or positive family history was not part of the inclusion criteria (10, 11). Patients with a reduced LV ejection fraction (EF; <50%); ischemic, valvular, or other myocardial or congenital heart disease; or other significant comorbidities (e.g., diabetes, hypertension, chronic kidney disease, or chronic liver failure) and patients whose CMR short-axis and long-axis cine images contained artifacts or were performed after the injection of contrast agent were excluded (12, 13). Clinical features of LVNC, including data about the patients' family history (cardiomyopathies, sudden cardiac death or congenital cardiac abnormalities), symptoms (e.g., syncope, palpitation, atypical chest pain), previous diagnosis of arrhythmia (supraventricular or ventricular extrasystoles, atrioventricular reentry tachycardia, atrioventricular nodal reentry tachycardia, or ventricular tachycardia), previously described non-ischemic electrocardiography (ECG) abnormalities (depolarization and repolarization abnormalities), history of embolic events (stroke, transient ischemic attack, or pulmonary embolism) or sudden cardiac death, were collected retrospectively by reviewing the

TABLE 1 | Baseline characteristics of the study population.

	LVNC	Control	*p*
Number of participants (male)	100 (58)	100 (58)	-
Age (years)	37.5 ± 14.9	37.7 ± 13.4	0.678
BMI (kg/m^2)	25.3 ± 4.0	24.4 ± 3.9	0.077
LV-EDVi (ml/m^2)	76.8 ± 14.6	66.5 ± 10.5	**<0.001**
LV-ESVi (ml/m^2)	26.4 ± 7.4	21.0 ± 5.4	**<0.001**
LV-SVi (ml/m^2)	50.4 ± 9.4	45.5 ± 7.3	**<0.001**
LV-EF (%)	65.8 ± 5.6	68.7 ± 5.3	**<0.001**
LV-TMi (g/m^2)	26.5 ± 7.3	20.7 ± 4.5	**<0.001**
LV-CMi (g/m^2)	50.2 ± 12.4	46.3 ± 8.5	0.052
LV-GLS (%)	−21.9 ± 3.0	−23.5 ± 2.6	**<0.001**
LV-GCS (%)	−29.6 ± 5.0	−34.6 ± 4.9	**<0.001**
RV-EDVi (ml/m^2)	72.2 ± 15.1	65.5 ± 12.7	**0.001**
RV-ESVi (ml/m^2)	27.3 ± 7.7	24.3 ± 5.9	**0.005**
RV-SVi (ml/m^2)	45.0 ± 9.0	41.2 ± 8.2	**0.002**
RV-EF (%)	62.4 ± 6.2	63.0 ± 4.9	0.528
RV-TMi (g/m^2)	21.4 ± 6.2	17.9 ± 4.3	**<0.001**
RV-CMi (g/m^2)	15.0 ± 4.5	15.5 ± 3.3	0.102
RV-GLS (%)	−25.2 ± 4.3	−27.3 ± 4.4	**<0.001**
RV-FWS (%)	−29.1 ± 5.0	−29.3 ± 6.4	0.830
RV-SS (%)	−16.3 ± 4.8	−19.1 ± 6.2	**<0.001**

Bold values indicate statistical significance ($p < 0.05$). BMI, body mass index; CMi, compacted myocardial mass index; EDVi, end-diastolic volume index; EF, ejection fraction; ESVi, end-systolic volume index; FWS, free-wall strain; GCS, global circumferential strain; GLS, global longitudinal strain; LV, left ventricle; LVNC, left ventricular non-compaction; RV, right ventricle; SS, septal strain; SVi, stroke volume index; TMi, trabeculated myocardial mass index.

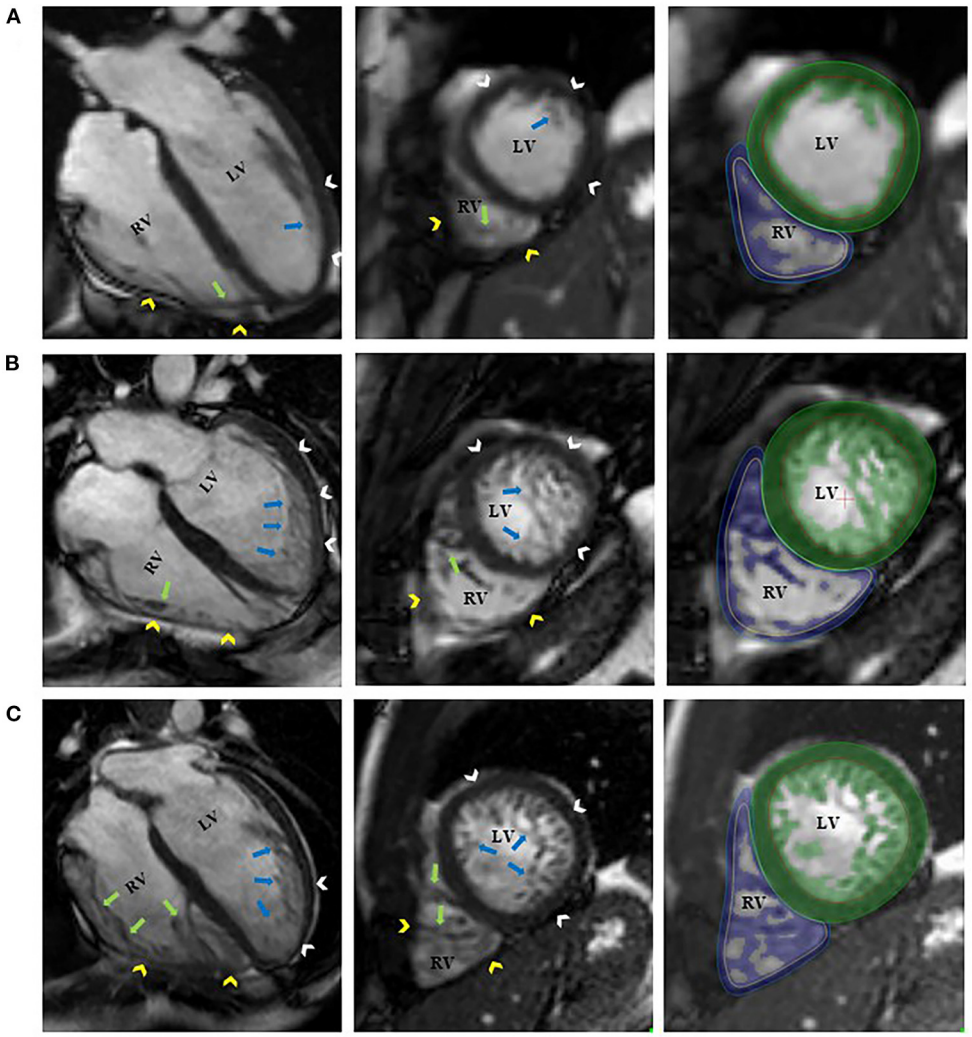

FIGURE 1 | Representative 4-chamber long-axis and short-axis images of a control participant [**(A)**, RV-TMi = 12.6 g/m^2, age and sex-specific reference: 13.9 (11.9, 19.3) g/m^2]; a patient with left ventricular non-compaction phenotype and normal amount of right ventricular trabeculation [**(B)**, RV-TMi = 25.2 g/m^2, age and sex-specific reference: 21.8 ± 5.2 g/m^2]; and a patient with left ventricular non-compaction phenotype and right ventricular hypertrabeculation [**(C)**, RV-TMi = 32.9 g/m^2, age and sex-specific reference: 19.9 ± 3.7 g/m^2]. The white and yellow arrowheads represent the left and right ventricular compacted myocardium. The blue and green arrows represent the left and right ventricular endocardial trabeculation. The green and blue areas represent the myocardial mass, including the endocardial trabeculation of the left and right ventricles, respectively. LV, left ventricle; LVNC, left ventricular non-compaction; RV, right ventricle; RV-TMi, right ventricular trabeculated myocardial mass index.

patients' medical records and the completed questionnaires (10, 11). Patients were divided into two subgroups by the amount of RV trabecular mass indexed to body surface area (RV-TMi): those who exceeded the upper limit of the age and sex-specific RV-TMi reference range were assigned to the LVNC phenotype with RV hypertrabeculation (RV-HT, $n = 22$) subgroup, and those who were within the reference range were assigned to the LVNC phenotype with normal RV trabeculation (RV-NT, $n = 78$) subgroup (**Figure 1**) (14). The value of RV-TMi of each participant was individually checked and compared to the age and sex-related reference values (14). These reference values were set up previously on a large healthy cohort (100 male and 100 female participants) free of known disease using CMR and a threshold-based segmentation method, further described in the "Image Acquisition and Analysis" section. The population was divided into four different age groups set up with equal numbers of males and females (14). The mean and standard deviation or median and 95% confidence interval values of the used RV-TMi age- and sex-specific reference ranges are as follows: male: 20–29 years = 19.9 ± 3.7 g/m^2, 30–39 years = 19.3 ± 3.8 g/m^2, 40–49 years = 21.8 ± 5.2 g/m^2, 50–66 years = 19.5 ± 3.6 g/m^2, female: 20–29 years = 17.1 ± 3.6 g/m^2, 30–39 years = 14.9 ± 3.0 g/m^2, 40–49 years = 13.9 (11.9, 19.3) g/m^2, and 50–66 years = 14.3 ± 2.8 g/m^2 (14).

Age- and sex-matched healthy volunteers who were free of known cardiovascular or other systemic diseases and who did not take medication were selected from our database as the control group. The average sports activity for both the patients and controls was <6 h/week (15). All procedures in this study were performed in accordance with the 1964 Helsinki Declaration and its later amendments or comparable ethical standards. Ethical approval was obtained from the Central Ethics Committee of Hungary, and all participants provided informed consent.

Image Acquisition and Analysis

CMR examinations were performed on a 1.5 T MRI machine (Achieva, Philips Medical System, Eindhoven, the Netherlands). Balanced steady-state free precession cine images were obtained in 2-, 3-, and 4-chamber long-axis views and breath-hold short-axis views from base to apex with full coverage of the LV and RV before the administration of contrast agent (gadobutrol, 0.15 ml/kg). The scan parameters were as follows: repetition time, 2.7 ms; echo time, 1.3 ms; flip angle, 60°; spatial resolution, 1.5 × 1.5 mm; temporal resolution, 25 frames per cardiac cycle; slice thickness, 8 mm without interslice gap; and field of view, 350 mm on average adapted to body size.

Segmentation analysis was performed with Medis Suite QMass version 3.0 software (Medis Medical Imaging Systems, Leiden, the Netherlands). Automatic tracing with manual correction of the LV and RV endo- and epicardial contours was performed by one observer as described previously (16). Inter-and intraobserver agreement values were good-to-excellent and are presented in **Supplementary Table 1**. The MassK module of the QMass software was used to calculate the LV and RV volumetric and functional values and the myocardial mass values. This is a threshold-based papillary and trabeculated muscle quantification analysis software module that differentiates myocardial trabeculation from the blood pool based on differences in the signal intensity (16). Each voxel was classified as either blood or myocardium according to the chosen threshold (50%). Manual correction of the threshold was not applied. Papillary muscles and ventricular trabeculation were included in the endocardial contours and defined as trabeculated myocardial mass, while compacted myocardial mass was calculated as the difference between the total detected and trabeculated myocardial mass. LV and RV end-diastolic volume (LV-EDV, RV-EDV), end-systolic volume (LV-ESV, RV-ESV), stroke volume (LV-SV, RV-SV), ejection fraction (LV-EF, RV-EF), end-diastolic compacted myocardial mass (LV-CM, RV-CM), and end-diastolic trabeculated myocardial mass (LV-TM, RV-TM) were measured. The parameters were indexed (i) to body surface area using the Mosteller formula.

The QStrain module of Medis Suite version 3.0 was used for the feature-tracking strain analysis (Medis Medical Imaging Systems, Leiden, the Netherlands). To assess subendocardial strain, the endocardial contours were drawn in end-diastole and end-systole in the 2-, 3-, and 4-chamber long-axis and short-axis views of the LV and in the 4-chamber view of the RV, including endocardial trabeculation. The LV global longitudinal strain (LV-GLS), LV global circumferential strain (LV-GCS), RV-GLS, RV free-wall strain (RV-FWS), and RV septal strain (RV-SS) were measured.

Statistical Analysis

Continuous parameters are described as the mean and standard deviation (SD), and discrete parameters are expressed as percentages. The intra-and interobserver agreement of the two observers was tested using the intraclass correlation coefficient (ICC). Distribution normality was assessed with the Shapiro–Wilk test. An unpaired Student's *t*-test or the Mann–Whitney test was used to compare the studied groups. Differences in normally distributed, variables with equal variance between the control and patient subgroups were analyzed with one-way analysis of variance (ANOVA) and Tukey's *post-hoc* test, while the Welch test and Games-Howell *post-hoc* test were used for variables with unequal variance; all other data were compared with the Kruskal–Wallis test with Bonferroni correction for multiple comparisons. Pearson's or Spearman's correlation was performed to describe the linear relationship between the parameters. The chi-squared test was used to compare discrete data. A p-value < 0.05 was considered indicative of statistical significance. IBM SPSS Statistics (Version 25.0, Armonk, NY) was used for calculations.

RESULTS

The baseline LV characteristics of the studied patients with the LVNC phenotype and the control subjects were compared (**Table 1**). Patients had significantly higher values of LV-EDVi, LV-ESVi, LV-SVi, and LV-TMi and significantly lower LV-EF, LV-GLS, and LV-GCS values (i.e., less negative strain values).

The comparison of the RV parameters yielded similar results: the RV-EDVi, RV-ESVi, RV-SVi, and RV-TMi values were significantly larger, and the RV-GLS and RV-SS values were significantly lower in the patient group, while the RV-EF, RV-CMi, and RV-FWS values were similar between the groups. Sixty-nine patients received contrast agent, but none demonstrated late gadolinium enhancement. Wall motion abnormalities were not visible in either the LV or RV in any patients.

Next, the patients were divided into two subgroups by the amount of RV-TMi. Twenty-two patients had RV-TMi values that were higher than the age- and sex-specific reference values, forming the RV-HT subgroup (male: $n = 15$, mean age: 36.8 ± 3.8 years), while those whose RV-TMi values were within the normal reference range formed the RV-NT subgroup ($n = 78$, male: $n = 43$, mean age: 37.7 ± 1.6 years). None of the healthy control participants exceeded the upper normal limit for RV-TMi. We found significant differences between the two subgroups and the control group: the LV-ESVi, LV-TMi, RV-ESVi, RV-TMi, and RV-CMi values were significantly larger in the RV-HT group than in the RV-NT and control groups, the LV-EF, RV-GLS, and RV-SS values were significantly lower in the RV-HT group than in the RV-NT and control groups, and RV-EF values were significantly lower in the RV-HT group than in the RV-NT group (**Table 2**, **Figure 2**).

The linear relationship between RV-TMi, LV-TMi, and RV volumetric and functional parameters and left and right

TABLE 2 | Comparison of the left and right ventricular volumetric and functional (A) and strain (B) parameters of LVNC patients with right ventricular hypertrabeculation, patients with normal right ventricular trabeculation, and controls.

	Control	RV-NT	RV-HT	*p*
Age (years)	37.7 ± 13.4	37.7 ± 14.1	36.8 ± 17.9	**0.733**
LV-EDVi (ml/m^2)	66.5 ± 10.5$^{¶\#}$	75.0 ± 13.2†	83.2 ± 17.9†	**<0.001**
LV-ESVi (ml/m^2)	21.0 ± 5.4$^{¶\#}$	25.2 ± 6.9$^{\#\dagger}$	31.0 ± 7.7¶†	**<0.001**
LV-SVi (ml/m^2)	45.5 ± 7.3$^{¶\#}$	49.9 ± 8.7†	52.2 ± 11.6†	**<0.001**
LV-EF (%)	68.7 ± 5.3$^{¶\#}$	66.7 ± 5.6†	62.7 ± 4.7†	**<0.001**
LV-TMi (g/m^2)	20.7 ± 4.5$^{¶\#}$	25.2 ± 6.6$^{\#\dagger}$	31.0 ± 7.9¶†	**<0.001**
LV-CMi (g/m^2)	46.3 ± 8.5$^{\#}$	48.7 ± 11.8	55.3 ± 13.4†	**0.013**
LV-GLS (%)	−23.5 ± 2.6$^{¶\#}$	−22.0 ± 3.2†	−21.6 ± 2.3†	**<0.001**
LV-GCS (%)	−34.9 ± 4.9$^{¶\#}$	−29.5 ± 4.9†	−29.9 ± 5.7†	**<0.001**
RV-EDVi (ml/m^2)	65.5 ± 12.7$^{\#}$	70.5 ± 14.0	78.2 ± 17.7†	**<0.001**
RV-ESVi (ml/m^2)	24.3 ± 5.9$^{¶\#}$	26.0 ± 6.5†	32.0 ± 9.8†	**<0.001**
RV-SVi (ml/m^2)	41.2 ± 8.2¶	44.6 ± 8.9†	46.3 ± 9.5	**0.007**
RV-EF (%)	63.0 ± 4.9	63.1 ± 6.2$^{\#}$	59.6 ± 5.2¶	**0.023**
RV-TMi (g/m^2)	17.9 ± 4.3$^{\#}$	19.2 ± 4.4$^{\#}$	29.3 ± 5.1¶†	**<0.001**
RV-CMi (g/m^2)	15.5 ± 3.3$^{\#}$	14.3 ± 4.2$^{\#\dagger}$	17.6 ± 4.5¶	**0.001**
RV-GLS (%)	−27.3 ± 4.4$^{¶\#}$	−25.7 ± 4.5$^{\#\dagger}$	−23.3 ± 2.7¶†	**<0.001**
RV-FWS (%)	−29.3 ± 6.4	−29.4 ± 5.2	−28.0 ± 4.1	0.608
RV-SS (%)	−19.1 ± 6.2$^{¶\#}$	−17.0 ± 5.0$^{\#\dagger}$	−13.8 ± 3.4¶†	**<0.001**

Bold values indicate statistical significance. CMi, compacted myocardial mass index; EDVi, end-diastolic volume index; EF, ejection fraction; ESVi, end-systolic volume index; FWS, free-wall strain; GCS, global circumferential strain; GLS, global longitudinal strain; LV, left ventricle; LVNC, left ventricular non-compaction; RV, right ventricle; RV-HT, patients with right ventricular hypertrabeculation; RV-NT, patients with normal right ventricular trabeculation; SS, septal strain; SVi, stroke volume index; TMi, trabeculated myocardial mass index.

$^{¶}p < 0.05$ vs. RV-NT.

$^{\#}p < 0.05$ vs. RV-HT.

$^{\dagger}p <$. vs. Control.

ventricular strain values were studied in the patient population (**Table 3**). A significant positive correlation was found between RV-TMi and LV-TMi, between RV-TMi and RV volumetric parameters, and between LV-TMi and RV volumetric parameters, while a larger RV-TMi value was associated with a lower RV-EF and worse RV-GLS, RV-SS, RV-FWS, and LV-GLS values. Furthermore, a higher LV trabecular mass was associated with worse RV-EF, RV-GLS, LV-GLS, and LV-GCS values.

We studied the frequency of the clinical features and family history of LVNC in the patients with the LVNC phenotype. Patients with multiple findings were found in each category (**Table 4**). Sixty-eight percent of patients had at least one clinical feature of LVNC. Documented arrhythmia was present in 22%, while 13% of the patients had palpitations without documented arrhythmia. Almost one-quarter (23%) of the patients had a positive family history, and in 10% of these patients, at least one other clinical feature of LVNC was present. Atypical chest pain was described in 11 cases, non-ischemic ECG abnormalities in nine patients, syncope in eight patients, thromboembolic events in three patients, and a non-fatal episode of cardiac arrest in one patient. No significant difference in the frequency of clinical features was found between the RV-HT and RV-NT subgroups.

We also compared the LV and RV parameters of the patients with LVNC phenotype with at least one clinical feature ($n = 68$) and without any clinical features ($n = 32$). The LV-CMi and RV-ESVi values were significantly lower in the patient with at least one clinical feature subgroup. However, all of the other measured RV and LV parameters were comparable between the groups (**Table 5**).

DISCUSSION

This study described the RV volumetric, functional, and strain characteristics and clinical features of patients with LVNC phenotype and good LV function using CMR. We also identified differences between LVNC phenotype patients with RV hypertrabeculation and those with normal RV trabeculation.

We observed higher LV and RV volumes, lower LV-EF, and lower LV and RV strain values in LVNC phenotype patients than in controls. These might be related to excessive trabeculation, but the clinical relevance is controversial. We also need to mention that all of these parameters were in the normal range. Kawel et al. found that more prominent LV trabeculation was associated with lower LV-EF and higher LV volumes in a population with no known cardiovascular disease or diagnosed LVNC but presenting with LV hypertrabeculation (4). A geometric model might address the physiologic explanation for these observations: a ventricle with trabeculation can maintain the SV with less deformation than a smooth-walled ventricle, which needs to generate much more deformation to keep the SV (17). However, trabeculation occupies space of its own. Thus, the ventricle needs to be dilated, suggesting that the presence of excessive RV trabeculation causes increased RV volumes (17). In our study, almost one-quarter of the patients with LVNC phenotype had

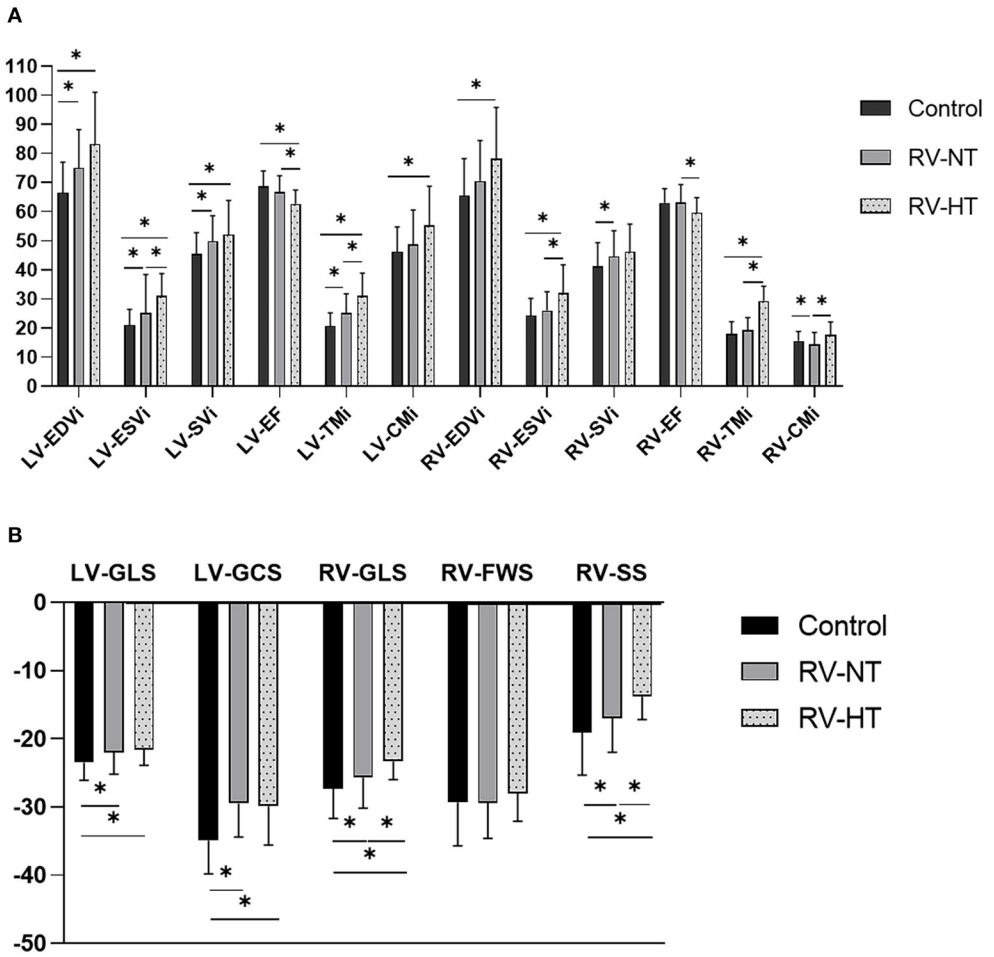

FIGURE 2 | Graphic representation of **Table 2**. Comparison of the left and right ventricular volumetric and functional **(A)** and strain **(B)** parameters of LVNC patients with right ventricular hypertrabeculation, patients with normal right ventricular trabeculation, and controls. CMi, compacted myocardial mass index; EDVi, end-diastolic volume index; EF, ejection fraction; ESVi, end-systolic volume index; FWS, free-wall strain; GCS, global circumferential strain; GLS, global longitudinal strain; LV, left ventricle; LVNC, left ventricular non-compaction; RV, right ventricle; RV-HT, patients with right ventricular hypertrabeculation; RV-NT, patients with normal right ventricular trabeculation; SS, septal strain; SVi, stroke volume index; TMi, trabeculated myocardial mass index. *$p < 0.05$.

RV trabecular mass that exceeded the upper value of the age and sex-specific reference range (14). These patients had higher LV and RV volumetric values, lower RV and LV-EF, and worse RV-GLS and RV-SS values than patients whose RV trabecular mass values were within the reference range. The positive correlation between RV volumetric parameters and RV trabecular mass, and the inverse relationship between RV trabecular mass and RV strain values further strengthen the hypothesis that excessive RV trabeculation might be the cause of these alterations. According to these results, the volumetric and functional characteristics in a hypertrabeculated RV are similar to those in LV non-compaction, suggesting RV non-compaction in some patients with LVNC.

However, the clinical importance of these findings and RV hypertrabeculation in the setting of good LV and RV function are difficult to evaluate due to the lack of follow-up studies in this patient population. One study found no relation between the presence of RV non-compaction and RV dysfunction; furthermore, LV-EF was the only independent predictor of RV-EF in patients with LVNC (18). The most common cause of RV dysfunction is LV dysfunction in non-ischemic cardiomyopathy due to several factors, including ventricular interdependence with septal dysfunction (19). The ventricular septum accounts for the major force of RV ejection due to its twisting and shortening during systole, which is caused by the oblique fiber orientation of the septum (20). In the case of ventricular dilatation, the oblique fibers of the septum become more transverse, resulting in a decrease in septal twisting and shortening and causing decreased RV ejection (20, 21). We described an association between a higher LV trabecular mass value and a higher RV trabecular mass, higher RV volumes, lower RV-EF, and a worse RV-GLS value, which might strengthen the hypothesis that LV involvement affects RV function. Furthermore, we found that a higher RV-TMi value was associated with a worse RV-SS value. It supports the

TABLE 3 | Correlation between right and left ventricular trabecular mass index and right ventricular parameters and left ventricular global strains.

	RV-TMi		LV-TMi	
	r	*p*	*r*	*p*
RV-EDVi	0.54	**<0.001**	0.48	**<0.001**
RV-ESVi	0.66	**<0.001**	0.53	**<0.001**
RV-SVi	0.34	**0.001**	0.34	**0.001**
RV-EF	−0.49	**<0.001**	−0.30	**0.002**
RV-TMi	1	0	0.59	**<0.001**
RV-CMi	0.69	**<0.001**	0.44	**<0.001**
RV-GLS	0.37	**<0.001**	0.22	**0.035**
RV-FWS	0.25	**0.014**	0.09	0.383
RV-SS	0.21	**0.038**	0.10	0.314
LV-GLS	0.24	**0.018**	0.38	**<0.001**
LV-GCS	0.03	0.809	0.28	**0.006**

Bold values indicate statistical significance ($p < 0.05$). Pearson's or Spearman's correlation was performed to describe the linear relationship between the parameters. CMi, compacted myocardial mass index; EDVi, end-diastolic volume index; EF, ejection fraction; ESVi, end-systolic volume index; FWS, free wall strain; GCS, global circumferential strain; GLS, global longitudinal strain; LV, left ventricle; LVNC, left ventricular non-compaction; r, correlation coefficient; RV, right ventricle; SS, septal strain; SVi, stroke volume index; TMi, trabeculated myocardial mass index.

TABLE 4 | Prevalence of clinical features in the total patient population and patient subgroups.

A.	Clinical features	LVNC total ($n = 100$)	RV-HT ($n = 22$)	RV-NT ($n = 78$)	RV-HT vs. RV-NT *p*
	Palpitation	20%	23%	19%	0.717
	Palpitation with documented arrhythmia	7%	9%	6%	0.663
	Palpitation without documented arrhythmia	13%	14%	13%	0.920
	Arrhythmia	22%	27%	21%	0.499
	Non-sustained ventricular arrhythmia	3%	5%	3%	0.630
	Ventricular extrasystoles	15%	14%	15%	0.839
	Supraventricular extrasystoles	4%	9%	3%	0.168
	Atrioventricular reentry tachycardia	2%	5%	1%	0.334
	Bradycardia	1%	5%	0%	0.058
	Syncope	8%	14%	6%	0.270
	Non-ischemic ECG abnormalities	9%	5%	10%	0.408
	Previous thromboembolic event	3%	5%	3%	0.630
	Transient ischemic attack	1%	0%	1%	0.594
	Stroke	1%	5%	0%	0.058
	Pulmonary microembolism	1%	0%	1%	0.594
	Sudden cardiac death	1%	0%	1%	0.594
	Positive family history	23%	18%	24%	0.543
	Positive family history and other clinical features	10%	14%	9%	0.520
	Atypical chest pain	11%	9%	12%	0.746
	No symptoms or family history	32%	32%	32%	0.983

LVNC, left ventricular non-compaction; RV-HT, patients with right ventricular hypertrabeculation; RV-NT, patients with normal right ventricular trabeculation.

theory that RV dysfunction arises from septal dysfunction, both of which can be observed even in cases of good LV function in patients with LVNC phenotype.

Previous studies have suggested that myocardial mass, including ventricular trabeculation, is genetically determined (22, 23). The strong relationship between LV and RV trabecular mass further indicates that the genetic mutations underlying LV non-compaction might also affect RV trabeculation, causing RV non-compaction in some cases.

None of the healthy control participants exceeded the upper limit of the age and sex-specific reference values in this study. Stämpfli et al. studied the RV end-diastolic trabeculated area and trabeculated volume in LVNC patients and controls (24). However, they described a significant overlap in RV trabeculation of patients and controls, which several factors might cause. First, they used manual contouring to measure RV trabeculated volume, which is different from ours. Second, they did not use age and sex-specific normal reference ranges to differentiate between

TABLE 5 | Comparison of the left and right ventricular parameters of the patients with LVNC phenotype and at least one clinical feature and the patients with LVNC phenotype and no clinical features.

	Patients with LVNC phenotype and at least one clinical feature ($n = 68$)	Patients with LVNC phenotype and no clinical features ($n = 32$)	p
Age (years)	34.8 ± 12.3	38.8 ± 16.0	0.212
LV-EDVi (ml/m^2)	75.1 ± 14.5	80.3 ± 14.5	0.094
LV-ESVi (ml/m^2)	25.7 ± 7.9	28.0 ± 6.2	0.152
LV-SVi (ml/m^2)	49.5 ± 9.2	52.3 ± 9.7	0.164
LV-EF (%)	66.1 ± 6.2	65.5 ± 4.2	0.455
LV-TMi (g/m^2)	26.1 ± 7.6	27.2 ± 6.8	0.504
LV-CMi (g/m^2)	48.2 ± 11.7	54.4 ± 13.0	**0.019**
LV-GLS (%)	−22.3 ± 3.0	−21.1 ± 3.0	0.051
LV-GCS (%)	−30.1 ± 5.2	−28.6 ± 4.6	0.163
RV-EDVi (ml/m^2)	70.2 ± 15.1	76.5 ± 14.5	0.052
RV-ESVi (ml/m^2)	26.1 ± 7.9	29.9 ± 6.8	**0.022**
RV-SVi (ml/m^2)	44.2 ± 9.1	46.6 ± 8.8	0.211
RV-EF (%)	63.0 ± 6.9	61.0 ± 4.2	0.146
RV-TMi (g/m^2)	20.8 ± 6.0	22.9 ± 6.5	0.111
RV-CMi (g/m^2)	14.5 ± 4.5	16.2 ± 4.3	0.067
RV-GLS (%)	−25.5 ± 4.0	−24.4 ± 4.8	0.23
RV-FWS (%)	−29.7 ± 4.8	−27.7 ± 5.2	0.059
RV-SS (%)	−16.0 ± 4.4	−17.0 ± 5.7	0.344

Bold values indicate statistical significance ($p < 0.05$). CMi, compacted myocardial mass index; EDVi, end-diastolic volume index; EF, ejection fraction; ESVi, end-systolic volume index; FWS, free wall strain; GCS, global circumferential strain; GLS, global longitudinal strain; LV, left ventricle; LVNC, left ventricular non-compaction; RV, right ventricle; SS, septal strain; SVi, stroke volume index; TMi, trabeculated myocardial mass index.

normal and excessive RV trabeculation. Third, the number of included participants was smaller in their study compared to ours. Although, an overlap cannot be excluded in the case of an even larger study population.

When assessing the clinical features of the patients with the LVNC phenotype, we found that two-thirds had at least one risk factor requiring regular follow-up and that these patients might be diagnosed with true LVNC (10, 11). The prevalence of positive family history and arrhythmias is similar to that in previous reports; however, chest pain, syncope, and non-ischemic ECG abnormalities were less common in our population (10, 25, 26). Previous studies describing the clinical features of LVNC involved patients who presented to the corresponding study centers due to their symptoms and decreased LV function. In contrast, we included LVNC phenotype patients with good LV ejection fraction; thus, the lower prevalence of clinical findings in our study might be due to differences in the patient populations.

Patients with the LVNC phenotype and at least one clinical feature had a significantly lower LV-CMi value than patients without clinical features. Gebhard et al. described the thinning of the compacted myocardial layer in patients with LVNC using echocardiography (27). Our results might support this criterion; however, it is interesting that no other difference was found between the with and without clinical features subgroups.

One-third of our study's total LVNC phenotype patient population had a negative family history and no symptoms; this prevalence is consistent with the literature (28). According to current knowledge, this "benign form" of LVNC has a good prognosis, and patient follow-up is not necessary (11, 29).

Case reports and previous studies have described the presence of complex ventricular extrasystoles, ventricular tachycardia, and sudden cardiac death in patients with RV non-compaction and some authors have suggested that RV non-compaction is an arrhythmogenic state associated with high mortality (1, 2, 30). However, these patients had either RV dysfunction or congenital cardiac abnormalities that affected the right heart. Furthermore, our study showed that the prevalence of clinical features was similar between patients with RV hypertrabeculation and patients with normal RV trabeculation. Further follow-up studies are necessary to evaluate RV function, clinical features, and major cardiovascular events in the presence of RV hypertrabeculation/non-compaction in patients with LVNC.

To conclude, this study found that almost one-quarter of the patients with the LVNC phenotype had RV trabecular mass values higher than the age and sex-specific reference range. Furthermore, the volumetric, functional, and strain characteristics of the hypertrabeculated RV were similar to these parameters of the LV in LVNC. We described a positive correlation between RV and LV trabeculation, RV trabeculation and RV volumes, and significant inverse relationships between RV and LV trabeculation with RV function. These results suggest that a portion of patients with the LVNC phenotype might also have RV non-compaction, raising further questions about its long-term effect on RV function, clinical manifestation, and

patient prognosis. Further follow-up studies are necessary to answer these questions.

We need to mention that the study's main limitations arise from its retrospective nature and the lack of follow-up information on the patients. We also have to mention the limitations of the threshold-based software. The software currently quantifies ejection fraction and volume using short-axis slices, with an 8 mm standard for spatial resolution in the Z-direction. Trabeculae and the papillary muscles do not cross the slice perfectly perpendicularly, resulting in partial volume effects. Depending on the actual path of the trabeculae, this influences the threshold-based quantification (16, 31). The limitations of the feature-tracking software include the lack of a relevant validation process; thus, its clinical application is questionable. Furthermore, there is high variability in normal strain values between different vendors; thus, there is a lack of an accepted normal reference range (32, 33).

DATA AVAILABILITY STATEMENT

The raw data supporting the conclusions of this article will be made available by the authors, without undue reservation.

ETHICS STATEMENT

The studies involving human participants were reviewed and approved by Central Ethics Committee of Hungary. The patients/participants provided their written informed consent to participate in this study.

AUTHOR CONTRIBUTIONS

ARK: methodology, formal analysis, investigation, resources, data curation, writing—original draft, and visualization. ZG and AP: data curation. LS, ZD, AK, and BL: writing—review and editing. BM: supervision. HV: writing—review and editing and supervision. AS: conceptualization, methodology, investigation, resources, writing—review and editing, supervision, and project administration. All authors contributed to the article and approved the submitted version.

FUNDING

The research was financed by the Thematic Excellence Programme (Tématerületi Kiválósági Program, 2020-4.1.1.-TKP2020) of the Ministry for Innovation and Technology in Hungary within the framework of the Therapeutic Development and Bioimaging Programs of Semmelweis University; by the Development of Scientific Workshops of Medical, Health Sciences and Pharmaceutical Education (Project identification number: EFOP-3.6.3-VEKOP-16-2017-00009); and by the Ministry of Innovation and Technology NRDI Office within the framework of the Artificial Intelligence National Laboratory Program. Project no. NVKP_16-1–2016-0017 (National Heart Program) has been implemented with the support provided by the National Research, Development, and Innovation Fund of Hungary, financed under the NVKP_16 funding scheme.

ACKNOWLEDGMENTS

We thank the technicians who helped perform the cardiac magnetic resonance imaging examinations.

SUPPLEMENTARY MATERIAL

The Supplementary Material for this article can be found online at: https://www.frontiersin.org/articles/10.3389/fcvm.2022.843952/full#supplementary-material

REFERENCES

1. Bekheit S, Karam B, Daneshvar F, Zaidan J, Tabet R, Spagnola J, et al. Sudden cardiac death in isolated right ventricular hypertrabeculation/noncompaction cardiomyopathy. *Ann Noninvasive Electrocardiol.* (2018) 23:e12487. doi: 10.1111/anec.12487
2. Fazio G, Lunetta M, Grassedonio E, Gullotti A, Ferro G, Bacarella D, et al. Noncompaction of the right ventricle. *Pediatr Cardiol.* (2010) 31:576–8. doi: 10.1007/s00246-010-9652-6
3. Aggarwal S, Kalavakunta J, Gupta V. A case of isolated right ventricle noncompaction with ST-elevation chest leads. *Heart Views.* (2016) 17:30–4. doi: 10.4103/1995-705X.182645
4. Kawel N, Nacif M, Arai AE, Gomes AS, Hundley WG, Johnson WC, et al. Trabeculated (noncompacted) and compact myocardium in adults: the multi-ethnic study of atherosclerosis. *Circ Cardiovasc Imaging.* (2012) 5:357–66. doi: 10.1161/CIRCIMAGING.111.971713
5. Stampfli SF, Donati TG, Hellermann J, Anwer S, Erhart L, Gruner C, et al. Right ventricle and outcome in left ventricular non-compaction cardiomyopathy. *J Cardiol.* (2020) 75:20–6. doi: 10.1016/j.jjcc.2019.09.003
6. Zhou X, Ferrara F, Contaldi C, Bossone E. Right ventricular size and function in chronic heart failure: not to be forgotten. *Heart Fail Clin.* (2019) 15:205–17. doi: 10.1016/j.hfc.2018.12.015
7. Berglund F, Pina P, Herrera CJ. Right ventricle in heart failure with preserved ejection fraction. *Heart.* (2020) 106:1798–804. doi: 10.1136/heartjnl-2020-317342
8. Petersen SE, Selvanayagam JB, Wiesmann F, Robson MD, Francis JM, Anderson RH, et al. Left ventricular non-compaction: insights from cardiovascular magnetic resonance imaging. *J Am Coll Cardiol.* (2005) 46:101–5. doi: 10.1016/j.jacc.2005.03.045
9. Jacquier A, Thuny F, Jop B, Giorgi R, Cohen F, Gaubert J-Y, et al. Measurement of trabeculated left ventricular mass using cardiac magnetic resonance imaging in the diagnosis of left ventricular non-compaction. *Eur Heart J.* (2010) 31:1098–104. doi: 10.1093/eurheartj/ehp595
10. Negri F, De Luca A, Fabris E, Korcova R, Cernetti C, Grigoratos C, et al. Left ventricular noncompaction, morphological, and clinical features for an integrated diagnosis. *Heart Fail Rev.* (2019) 24:315–23. doi: 10.1007/s10741-018-9763-3
11. Vergani V, Lazzeroni D, Peretto G. Bridging the gap between hypertrabeculation phenotype, noncompaction phenotype and left ventricular noncompaction cardiomyopathy. *J Cardiovasc Med.* (2020) 21:192–9. doi: 10.2459/JCM.0000000000000924
12. Szucs A, Kiss AR, Suhai FI, Tóth A, Gregor Z, Horváth M, et al. The effect of contrast agents on left ventricular parameters calculated by a threshold-based software module: does it truly matter? *Int J Cardiovasc Imaging.* (2019) 35:1683–9. doi: 10.1007/s10554-019-01587-9

13. Kuetting DL, Dabir D, Homsi R, Sprinkart AM, Luetkens J, Schild HH, et al. The effects of extracellular contrast agent (Gadobutrol) on the precision and reproducibility of cardiovascular magnetic resonance feature tracking. *J Cardiovasc Magn Reson.* (2016) 18:30. doi: 10.1186/s12968-016-0249-y
14. Kiss AR, Gregor Z, Furak A, Szabo LE, Dohy Z, Merkely B, et al. Age- and sex-specific characteristics of right ventricular compacted and non-compacted myocardium by cardiac magnetic resonance. *Front Cardiovasc Med.* (2021) 8:781393. doi: 10.3389/fcvm.2021.781393
15. Pelliccia A, Sharma S, Gati S, Back M, Borjesson M, Caselli S, et al. 2020 ESC Guidelines on sports cardiology and exercise in patients with cardiovascular disease. *Eur Heart J.* (2021) 42:17–96. doi: 10.1093/eurheartj/ehaa605
16. Jaspers K, Freling HG, van Wijk K, Romijn EI, Greuter MJ, Willems TP. Improving the reproducibility of MR-derived left ventricular volume and function measurements with a semi-automatic threshold-based segmentation algorithm. *Int J Cardiovasc Imaging.* (2013) 29:617–23. doi: 10.1007/s10554-012-0130-5
17. Paun B, Bijnens B, Butakoff C. Relationship between the left ventricular size and the amount of trabeculations. *Int J Numer Method Biomed Eng.* (2018) 34:2939. doi: 10.1002/cnm.2939
18. Nucifora G, Aquaro GD, Masci PG, Pingitore A, Lombardi M. Magnetic resonance assessment of prevalence and correlates of right ventricular abnormalities in isolated left ventricular noncompaction. *Am J Cardiol.* (2014) 113:142–6. doi: 10.1016/j.amjcard.2013.08.049
19. Haddad F, Doyle R, Murphy DJ, Hunt SA. Right ventricular function in cardiovascular disease, part II: pathophysiology, clinical importance, and management of right ventricular failure. *Circulation.* (2008) 117:1717–31. doi: 10.1161/CIRCULATIONAHA.107.653584
20. Saleh S, Liakopoulos OJ, Buckberg GD. The septal motor of biventricular function. *Eur J Cardiothorac Surg.* (2006) 29(Suppl.1):S126–38. doi: 10.1016/j.ejcts.2006.02.048
21. Lakatos BK, Nabeshima Y, Tokodi M, Nagata Y, Tosér Z, Otani K, et al. Importance of nonlongitudinal motion components in right ventricular function: three-dimensional echocardiographic study in healthy volunteers. *J Am Soc Echocardiogr.* (2020) 33:995–1005.e1. doi: 10.1016/j.echo.2020.04.002
22. Andre F, Burger A, Lossnitzer D, Buss SJ, Abdel-Aty H, Gianntisis E, et al. Reference values for left and right ventricular trabeculation and non-compacted myocardium. *Int J Cardiol.* (2015) 185:240–7. doi: 10.1016/j.ijcard.2015.03.065
23. Kovács A, Molnár A, Kolossváry M, Szilveszter B, Panajotu A, Lakatos BK, et al. Genetically determined pattern of left ventricular function in normal and hypertensive hearts. *J Clin Hypertens.* (2018) 20:949–58. doi: 10.1111/jch.13271
24. Stampfli SF, Gotschy A, Kiarostami P, Ozkartal T, Gruner C, Niemann M, et al. Right ventricular involvement in left ventricular non-compaction cardiomyopathy. *Cardiol J.* (2020) 36:493–500. doi: 10.5603/CJ.a2020.0095
25. Oechslin EN, Attenhofer Jost CH, Rojas JR, Kaufmann PA, Jenni R. Long-term follow-up of 34 adults with isolated left ventricular noncompaction: a distinct cardiomyopathy with poor prognosis. *J Am Coll Cardiol.* (2000) 36:493–500. doi: 10.1016/S0735-1097(00)00755-5
26. Aras D, Tufekcioglu O, Ergun K, Ozeke O, Yildiz A, Topaloglu S, et al. Clinical features of isolated ventricular noncompaction in adults long-term clinical course, echocardiographic properties, and predictors of left ventricular failure. *J Card Fail.* (2006) 12:726–33. doi: 10.1016/j.cardfail.2006.08.002
27. Gebhard C, Stahli BE, Greutmann M, Biaggi P, Jenni R, Tanner FC. Reduced left ventricular compacta thickness: a novel echocardiographic criterion for non-compaction cardiomyopathy. *J Am Soc Echocardiogr.* (2012) 25:1050–7. doi: 10.1016/j.echo.2012.07.003
28. Brescia ST, Rossano JW, Pignatelli R, Jefferies JL, Price JF, Decker JA, et al. Mortality and sudden death in pediatric left ventricular noncompaction in a tertiary referral center. *Circulation.* (2013) 127:2202–8. doi: 10.1161/CIRCULATIONAHA.113.002511
29. Towbin JA, Lorts A, Jefferies JL. Left ventricular non-compaction cardiomyopathy. *Lancet.* (2015) 386:813–25. doi: 10.1016/S0140-6736(14)61282-4
30. Leung SW, Elayi CS, Charnigo RJ Jr, Syed MA. Clinical significance of right ventricular dysfunction in left ventricular non-compaction cardiomyopathy. *Int J Cardiovasc Imaging.* (2012) 28:1123–31. doi: 10.1007/s10554-011-9925-z
31. Espe EKS, Bendiksen BA, Zhang L, Sjaastad I. Analysis of right ventricular mass from magnetic resonance imaging data: a simple post-processing algorithm for correction of partial-volume effects. *Am J Physiol Heart Circ Physiol.* (2021) 320:H912–H22. doi: 10.1152/ajpheart.00494.2020
32. Bucius P, Erley J, Tanacli R, Zieschang V, Giusca S, Korosoglou G, et al. Comparison of feature tracking, fast-SENC, and myocardial tagging for global and segmental left ventricular strain. *ESC Heart Fail.* (2020) 7:523–32. doi: 10.1002/ehf2.12576
33. Amzulescu MS, De Craene M, Langet H, Pasquet A, Vancraeynest D, Pouleur AC, et al. Myocardial strain imaging: review of general principles, validation, and sources of discrepancies. *Eur Heart J Cardiovasc Imaging.* (2019) 20:605–19. doi: 10.1093/ehjci/jez041

Conflict of Interest: The authors declare that the research was conducted in the absence of any commercial or financial relationships that could be construed as a potential conflict of interest.

frontiers | Frontiers in Cardiovascular Medicine

ORIGINAL RESEARCH
published: 03 May 2022
doi: 10.3389/fcvm.2022.861464

Assessment of Right Ventricular Mechanics by 3D Transesophageal Echocardiography in the Early Phase of Acute Respiratory Distress Syndrome

Bruno Evrard[1,2†], Bálint Károly Lakatos[3†], Marine Goudelin[1,2], Zoltán Tősér[4], Béla Merkely[3], Philippe Vignon[1,2] and Attila Kovács[3†]*

[1] Medical-Surgical ICU, Limoges University Hospital, Limoges, France, [2] Inserm CIC 1435, Limoges, France, [3] Heart and Vascular Center, Semmelweis University, Budapest, Hungary, [4] Argus Cognitive, Inc., Lebanon, NH, United States

Aim: To compare global and axial right ventricular ejection fraction in ventilated patients for moderate-to-severe acute respiratory distress syndrome (ARDS) secondary to early SARS-CoV-2 pneumonia or to other causes, and in ventilated patients without ARDS used as reference.

Methods: Retrospective single-center cross-sectional study including 64 ventilated patients: 21 with ARDS related to SARS-CoV-2 (group 1), 22 with ARDS unrelated to SARS-CoV-2 (group 2), and 21 without ARDS (control group). Real-time three-dimensional transesophageal echocardiography was performed for hemodynamic assessment within 24 h after admission. Contraction pattern of the right ventricle was decomposed along the three anatomically relevant axes. Relative contribution of each spatial axis was evaluated by calculating ejection fraction along each axis divided by the global right ventricular ejection fraction.

Results: Global right ventricular ejection fraction was significantly lower in group 2 than in both group 1 and controls [median: 43% (25–75th percentiles: 40–57) vs. 58% (55–62) and 65% (56–68), respectively: $p < 0.001$]. Longitudinal shortening had a similar relative contribution to global right ventricular ejection fraction in all groups [group 1: 32% (28–39), group 2: 29% (24–40), control group: 31% (28–38), $p = 0.6$]. Radial shortening was lower in group 2 when compared to both group 1 and controls [45% (40–53) vs. 57% (51–62) and 56% (50–60), respectively: $p = 0.005$]. The relative contribution of right ventricular shortening along the anteroposterior axis was not statistically different between groups [group 1: 51% (41–55), group 2: 56% (46–63), control group; 56% (50–64), $p = 0.076$].

Edited by:
Sebastian Kelle, Deutsches Herzzentrum Berlin, Germany

Reviewed by:
Michael Anthony Matthay, University of California, San Francisco, United States
Gamze Babur Guler, Mehmet Akif Ersoy Thoracic and Cardiovascular Surgery Training and Research Hospital, Turkey

***Correspondence:**
Bruno Evrard
bruno.evrard@chu-limoges.fr

† These authors have contributed equally to this work

Specialty section:
This article was submitted to Cardiovascular Imaging, a section of the journal Frontiers in Cardiovascular Medicine

Received: *24 January 2022*
Accepted: *12 April 2022*
Published: *03 May 2022*

Citation:
Evrard B, Lakatos BK, Goudelin M, Tősér Z, Merkely B, Vignon P and Kovács A (2022) Assessment of Right Ventricular Mechanics by 3D Transesophageal Echocardiography in the Early Phase of Acute Respiratory Distress Syndrome. Front. Cardiovasc. Med. 9:861464. doi: 10.3389/fcvm.2022.861464

Conclusion: During early hemodynamic assessment, the right ventricular systolic function appears more impaired in ARDS unrelated to SARS-CoV-2 when compared to early stage SARS-CoV-2 ARDS. Radial shortening appears more involved than longitudinal and anteroposterior shortening in patients with ARDS unrelated to SARS-CoV-2 and decreased right ventricular ejection fraction.

Keywords: acute respiratory distress syndrome—ARDS, right ventricle (RV), myocardial deformation, 3D echocardiography (3DE), COVID-19

INTRODUCTION

Acute respiratory distress syndrome (ARDS) is characterized by diffuse alveolar damage and alterations of the pulmonary microcirculation, which both result in increased pulmonary vascular resistance (1). This abrupt increase of right ventricular (RV) afterload may lead to acute cor pulmonale, which combines the abrupt dilation of the RV cavity and a paradoxical septal motion (2). Acute cor pulmonale can be identified using transesophageal echocardiography (TEE) in 22% of patients under protective mechanical ventilation for moderate-to-severe ARDS (3). When severe, it is an independent predictor of mortality (3, 4). Unfortunately, only few echocardiographic parameters are currently available to detect and quantify RV systolic dysfunction in this clinical setting.

Due to its complex anatomy, RV volumes—hence RV ejection fraction (EF)—can only be measured at the bedside using Real-time three-dimensional echocardiography (RT-3D), which has been validated against cardiac Magnetic Resonance Imaging (5). RV ejection depends on three mechanical components: systolic shortening along the longitudinal axis, the radial axis and the antero-posterior axis (6). Using dedicated software, RT3D echocardiography allows the separate quantification of RV shortening along each of these three spatial axes (7). A recent study measuring axial right ventricular ejection fraction (RVEF) in healthy volunteers suggested that non-longitudinal shortening (i.e., radial and anteroposterior shortening) play a major role in generating global RVEF (8). Certain pulmonary diseases (e.g., pulmonary embolism, pulmonary arterial hypertension) could predominantly reduce RV systolic shortening along specific axes before reducing global RVEF (8). Notably, radial and anteroposterior axial impairment could be easily overlooked by conventional two-dimensional echocardiography. This substantial limitation may result in relevant over- or underestimation of global RV systolic function, according to its axial shortening pattern, especially in ARDS patients with acute cor pulmonale (ACP). There are growing evidence distinguishing SARS-CoV-2-induced ARDS and ARDS of other causes (9). This raises the possibility that severe COVID-19 may result in specific alterations of RV mechanics. We hypothesized that RV systolic function was not uniformly impaired in patients with ARDS and that the relative contribution of shortening along the three spatial axes may differ according to the cause of ARDS.

Accordingly, the objective of the present study was to compare global and axial RVEF in patients under protective ventilation at the early phase of ARDS secondary to SARS-CoV-2 pneumonia with patients ventilated for ARDS unrelated to SARS-CoV-2, and with patients who were ventilated for another reason than ARDS with a normal echocardiography examination who were used as controls.

MATERIALS AND METHODS

Study Design and Settings

This observational retrospective cross-sectional study included ventilated adult patients admitted to the Intensive Care Unit of the Limoges Hospital Centre (Nouvelle-Aquitaine, France) between November 2009 and December 2020. The protocol complied with the Declaration of Helsinki and was approved by the local Ethics Committee (#459-2021-115). Non-opposition was obtained from all participating patients.

Inclusion Criteria

Patients who required a hemodynamic assessment using conventional TEE during the first 24 h following ICU admission for moderate-to-severe ARDS related to SARS-CoV-2 as defined by the Berlin conference consensus (bilateral infiltrates on chest X-ray, PaO2/FiO2 $\leq$ 200 with a positive end-expiratory pressure $\geq$ 5 cm H_2O, and non-elevated left ventricular filling pressure) constituted group 1 (10). Patients ventilated for a moderate-to-severe ARDS unrelated to SARS-CoV-2 who had been included in the ARCOFOP study constituted group 2 (11). Patients ventilated in the ICU for severe head trauma or stroke without lung injury, any cardiopathy, and sex-matched with group 1, were used as controls.

Exclusion Criteria

Patients were not studied if they had a medical history of chronic respiratory failure with oxygen therapy or non-invasive ventilation, or with a known RV disease, or if the RT3D imaging quality was not suitable for accurate analysis using the dedicated software.

Patients' Characteristics

Age, sex, body mass index (BMI), Simplified Acute Physiology Score (SAPS) II, Sequential Organ Failure Assessment (SOFA) score, and vasopressor use were recorded. Body surface area was calculated using the Mosteller formula (12). The causes of ARDS in group 2 were reported. Conventional hemodynamic and ventilatory parameters were collected. Driving pressure was defined as the plateau pressure minus total end-expiratory pressure. Static compliance was defined as the tidal volume

divided by the driving pressure. Ventilatory ratio was defined as follows: measured minute ventilation (mL/min) × $PaCO_2$ measured (mmHg)/predicted minute ventilation × $PaCO_2$ ideal (13).

Echocardiography

All hemodynamic assessments were performed by experts in critical care echocardiography.

Two-Dimensional Echocardiography

Transthoracic Measurements

Conventional transthoracic echocardiography was performed using a Philips EPIQ7 or iE33 upper-end system equipped with a X5-1 transducer (Philips Healthcare, Netherlands). M-mode-derived tricuspid annular plane systolic excursion (TAPSE) and maximal tissue Doppler systolic velocity recorded at the lateral aspect of the tricuspid annulus were measured in the apical four-chamber view.

Transesophageal Measurements

Conventional TEE was performed using a Philips EPIQ7 or iE33 upper-end system equipped with a X7-1 or X8-1 transducer (Philips Healthcare, Netherlands). RV fractional area change (FAC) was measured in the mid-esophageal four-chamber view. Right atrio-ventricular systolic pressure gradient was calculated using the simplified Bernouilli's equation applied to the maximal velocity of the tricuspid regurgitant jet (14). Left ventricular (LV) outflow tract velocity-time integral (VTI) was measured in the transgastric 120° view using pulsed-wave Doppler (15). Moderate RV dilatation was defined by a RV/LV end-diastolic area ratio ≥ 0.6 and < 1 in the four chamber view in the mid-esophagus view of the heart. Severe RV dilatation was defined by a RV/LV end-diastolic area ratio ≥ 1 in the mid-esophagus four chamber view of the heart. ACP was defined by the association of a RV/LV end-diastolic area ratio ≥ 0.6 in the long-axis view of the heart and of a septal paradoxical motion in the short-axis view (15).

All derived of TTE and TEE measurements were performed off-line using the IntelliSpace CardioVascular software (Philips Medical Systems, Version 4.2.1.0, Netherlands).

Real-Time Three-Dimensional Transesophageal Echocardiography

Electrocardiographically gated full-volume 3D data sets reconstructed from four or six cardiac cycles optimized for the RV or for the LV endocardial border detection were recorded and digitally stored for off-line analysis. Image quality was optimized at the bedside, especially to avoid artifacts (6). Measurements were performed on a commercially available workstation using a dedicated software (4D RV-Function, Version 4.6, TomTec Imaging, Unterschleissheim, Germany for the RV and QLAB, Version 13.0, Philips, Amsterdam, Netherlands for the LV). The algorithm automatically detected the endocardial surface and following potential manual corrections, it traced its motion throughout the entire cardiac cycle. We measured the end-diastolic and end-systolic volume indexed to body surface area, and calculated RVEF and LVEF conventionally.

Evaluation of 3D Right Ventricular Mechanics

3D RV models were exported from the TomTec software to a dedicated software to obtain the RV longitudinal, radial, and anteroposterior axial shortening using the ReVISION method (Right VentrIcular Separate wall motIon quantificatiON; Argus Cognitive, Inc., Lebanon, New Hampshire, United States)[1] (7, 16). Briefly, the orientation of the exported 3D RV models is aligned using a standard, automated method to define the anatomically relevant, orthogonal axes (i.e., longitudinal, radial, anteroposterior). Then, the wall motions of the 3D model are split based on the movement of the model's each vertex point along these axes. Shortening in each direction can be selectively switched on and off to assess the contribution of those, which remained enabled to the global RVEF. The method allows to produce such end-systolic 3D models, which contracts along only one axis, while remains "locked" in the other two directions. Thus, volume changes attributable to either longitudinal, radial, or anteroposterior directions can be separately quantified and the corresponding EF values can be calculated. Finally, the relative contribution of the longitudinal, radial, or anteroposterior RV wall motion to global RV pump function can be expressed by the ratio of the given axial RVEF to global RVEF. The absolute volume change of RV chamber is generated by the aggregated contribution of the three motion components. This composition is not additive, and consequentially, the sum of the decomposed volume changes is not equal to the global volume change; in other words, the relative contribution of the motion components do not add up to 100%.

Statistics

According to our recent preliminary study (17), we anticipated a mean global RVEF of 55% in Group 1 and 45% in Group 2, with a standard deviation of 10%. When considering an alpha risk of 0.05 and a beta risk of 0.1, 21 patients were needed in each group. Because of the absence of previous data on TEE axial RVEF, we also studied 21 sex-matched patients without ARDS or cardiopathy as controls.

Continuous data are reported as median and interquartile range. Categorical data are reported as counts and percentages. Comparisons used the Kruskall-Wallis test for continuous variables. When p-value was ≤ 0.05, a paired comparison was performed between groups and p-value was adjusted with a Bonferroni test to consider the multiplicity of tests. Pearson's Chi-squared test was used for comparisons between categorical variables.

To assess the intra-observer reproducibility of global and axial RVEF, the same operator repeated the 3D analysis in a randomly chosen subset of 12 patients, blinded to previous results. Inter-observer reproducibility was determined by a new analysis of the same 12 patients by a second trained operator who performed his measurements independently.

A two-tailed p-value ≤ 0.05 was considered statistically significant. No use of previous value or interpolation rule was used in the presence of missing data. Data were analyzed using R software (version 4.0.2).

[1] www.revisionmethod.com

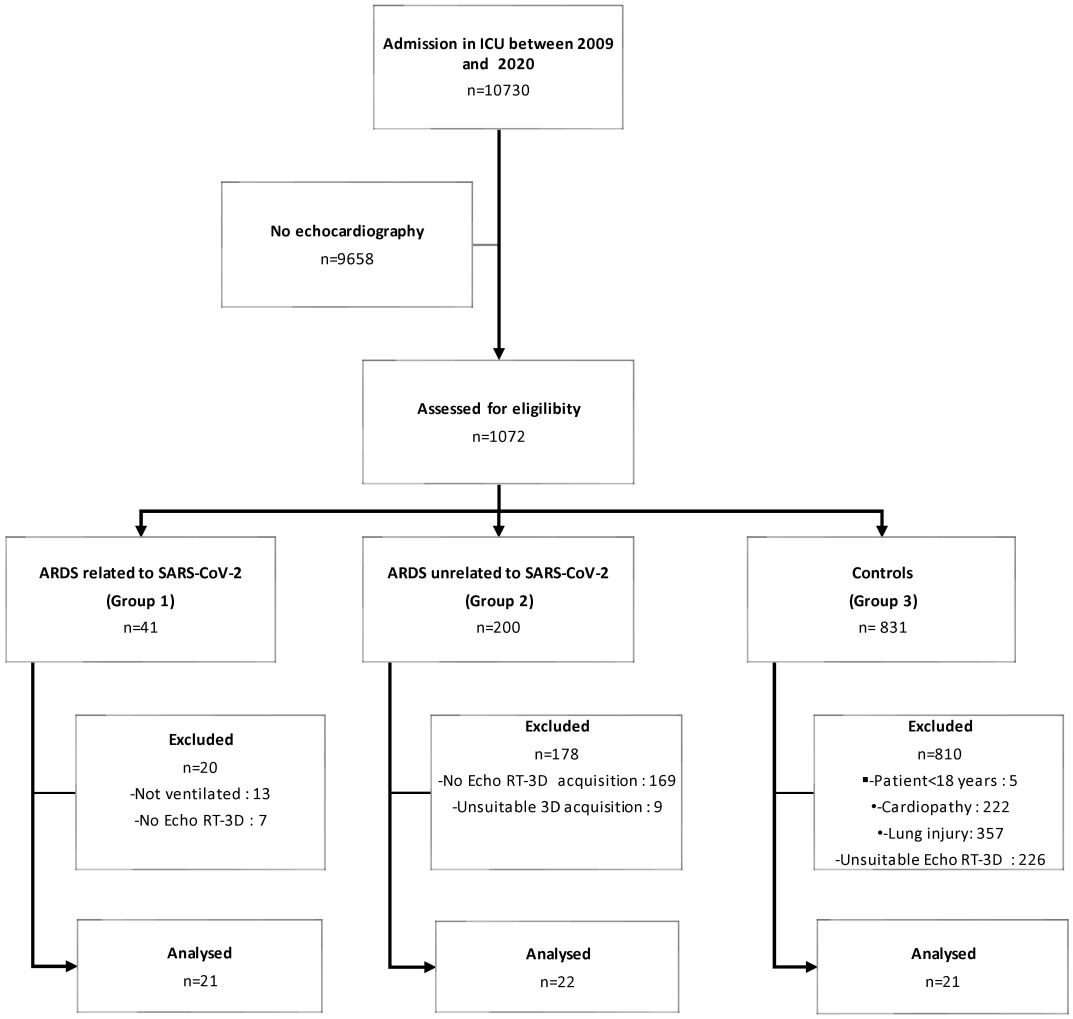

FIGURE 1 | Study flow chart.

RESULTS

Study Population

Among 10,730 patients who were admitted to the ICU between November 2009 and December 2020, 1,072 with echocardiography were assessed for eligibility (group 1: n = 41; group 2: n = 200; control group: n = 831). Among controls, 810 patients were not studied because of underlying cardiopathy (n = 222), lung injury (n = 357), or unavailable RT3D TEE (n = 226). In addition, 7 patients in group 1 and 169 patients in group 2 had no RT3D TEE recorded images (**Figure 1**). Finally, 64 patients were included in the present study [median age: 60 (46–71); male: 48 (75%); SAPSII: 35 (29–46)]: 21 patients were ventilated for an ARDS related to SARS-CoV-2 (group 1), 22 patients sustained an ARDS unrelated to SARS-CoV-2 (group 2), and 21 patients constituted the control group (**Table 1**). Group 2 patients had a higher SOFA score and required more frequently a vasopressor support than patients of group 1 (**Table 1**). SAPS II was not statistically different between group 1 patients and controls, mainly due to a low Glasgow coma scale in controls, and despite the absence of other organ failures (**Table 1**). Main causes of ARDS in group 2 were septic shock (45%), community-acquired pneumonia (18%), and Influenza virus pneumonia (13%). In ARDS patients, PaO2/FiO2 was lower in group 1 than in group 2, the difference being not statistically significant [118 (77–185) vs. 154 (100–181): p = 1.00]. Median $PaCO_2$ and ventilatory ratio were similar in the two ARDS groups (**Table 2**).

Echocardiography

TAPSE and RVFAC were statistically lower in group 2 compared to group 1 and controls, whereas tricuspid S' maximal velocity was not (**Table 3**). These parameters were preserved in patients with ARDS related to SARS-CoV-2, while right atrio-ventricular systolic pressure gradient was not statistically different across groups (**Table 3**). LVEF measured with RT3D TEE was statistically lower in group 1 than in controls, whereas the difference was not statistically

TABLE 1 | Characteristics of the study population.

	ARDS related to SARS-CoV-2 (Group 1)	ARDS unrelated to SARS-CoV-2 (Group 2)	Controls (Group 3)	*p*-value[b]	Paired *p*-value[c]
	n = 21[a]	*n* = 22[a]	*n* = 21[a]		
Age (years)	69 (56 – 74)†	62 (50 – 71)	51 (32 – 59)†	0.006	0.89
Sex (Male)	15 (71%)	19 (86%)	14 (67%)	0.3	–
Body Mass Index (kg/cm^2)	29.0 (26.0 – 33.0)	26.7 (24.5 – 31.6)	27.9 (27.3 – 33.4)	0.2	–
Comorbidity					
Cardiopathy[d]	1 (5%)	1 (5%)	0 (0%)	0.6	–
Hypertension	12 (57%)	8 (36%)	4 (19%)	0.038	–
Diabetes	7 (33%)	1 (5%)	1 (5%)	0.008	–
Obesity	10 (48%)	7 (32%)	6 (29%)	0.4	–
COPD	0 (0%)	1 (5%)	1 (5%)	0.6	–
Norepinephrine	3 (14%)	14 (64%)	0 (0%)	< 0.001	< 0.001
Alive at discharge	15 (71%)	17 (77%)	15 (71%)	0.9	–
SAPSII	34 (28 – 40)	42 (32 – 56)*	31 (24 – 39)*	0.022	0.132
SOFA	4 (3 – 4)	6 (4 – 7)*	3 (2 – 4)*	0.006	0.039
Cause of ARDS					
Septic shock[e]	–	10 (45%)			
Influenza virus	–	3 (13%)	–	–	–
Community acquired pneumonia without septic shock	–	4 (18%)	–	–	–
Pancreatitis	–	2 (9%)	–	–	–
Others	–	3 (13%)	–	–	–

[a] *Median (25-75%); n (%).*
[b] *Kruskal-Wallis rank sum test; Pearson's Chi-squared test.*
[c] *Kruskal-Wallis rank sum test or Pearson's Chi-squared test adjusted with Bonferroni test between ARDS group.*
[d] *Cardiopathy was defined has a past medical history of ischemic, valvular or hypertrophic cardiopathy.*
[e] *Etiology of septic shock: 8 patients with a community acquired pneumonia and 2 patients with a peritonitis.*
† *p-value < 0.05 between Control and Group 1 adjusted with Bonferroni test.*
* *p-value < 0.05 between Control and Group 2 adjusted with Bonferroni test.*
SAPSII, Simplified Acute Physiology Score; SOFA, Sepsis-related Organ Failure Assessment; ARDS, Acute Respiratory Distress Syndrome.

TABLE 2 | Hemodynamic and ventilatory parameters at the time of echocardiography assessment.

	ARDS related to SARS-CoV-2 (Group 1)	ARDS unrelated to SARS-CoV-2 (Group 2)	Controls (Group 3)	*p*-value[b]	Paired *p*-value[c]
	n = 21[a]	*n* = 22[a]	*n* = 21[a]		
Heart rate (bpm)	92 (85 – 113)	94 (84 – 108)	101 (88 – 114)	0.7	–
Systolic arterial pressure (mmHg)	140 (120 – 152)	124 (116 – 128)*	141 (133 – 160)*	0.012	0.087
Mean arterial pressure (mmHg)	95 (84 – 103)	86 (79 – 90)*	96 (91 – 105)*	0.018	0.092
Tidal volume (mL/kg)	6.88 (6.53 – 7.23)	6.51 (5.91 – 7.06)	7.08 (6.69 – 7.71)	0.095	–
PEEP (cm/H_2O)	10.00 (10.00 – 12.00)†	10.50 (9.25 – 12.00)*	8.00 (7.00 – 8.00)*†	0.001	1.00
Plateau pressure (cmH_2O)	25.0 (22.0 – 26.0)†	25.5 (24.0 – 27.8)*	15.5 (15.0 – 16.5)*†	< 0.001	0.52
Driving pressure (cmH_2O)	13.0 (11.0 – 16.0)†	14.5 (13.0 – 16.8)*	8.0 (7.5 – 9.5)*†	< 0.001	0.24
Static compliance (mL/cmH_2O)	34 (30 – 42)†	32 (27 – 36)*	49 (44 – 66)*†	0.002	0.65
PaO_2/FiO_2	118 (77 – 185)†	154 (100 – 181)*	286 (253 – 373)*†	< 0.001	1.00
$PaCO_2$ (mmHg)	44 (36 – 52)	49 (42 – 61)*	35 (32 – 40)*	0.002	0.34
Ventilatory ratio	1.95 (1.63 – 2.15)	2.09 (1.77 – 2.50)	–	–	0.822

[a] *Median (25–75%).*
[b] *Kruskal-Wallis rank sum test.*
[c] *Kruskal-Wallis rank sum test adjusted with Bonferroni test between ARDS group.*
† *p-value < 0.05 between Controls and Group 1 adjusted with Bonferroni test.*
* *p-value < 0.05 between Controls and Group 2 adjusted with Bonferroni test.*
PEEP, Positive end-expiratory pressure.

different between group 2 and controls (**Table 4**). Indexed RV end-diastolic volume was not statistically different between groups. In contrast, indexed RV end-systolic volume was higher in group 2 than in the other groups [35 mL/m^2 (31–40) vs. 23 mL/m^2 (16–29) and 18 mL/m^2 (13–22), respectively: $p < 0.001$]. As a result, RVEF was

TABLE 3 | Two-dimensional echocardiography parameters.

	ARDS related to SARS-CoV-2 (Group 1) $n = 21^a$	ARDS unrelated to SARS-CoV-2 (Group 2) $n = 22^a$	Controls (Group 3) $n = 21^a$	p-value[b]	Paired p-value[c]
Indexed LV end-diastolic volume (mL/m^2)	44.0 (38.5 – 48.7)–	43.2 (36.1 – 47.7)	38.2 (25.8 – 49.2)	0.63	–
Indexed LV end-systolic volume (mL/m^2)	20.6 (18.8 – 27.2)	20.0 (12.5 – 23.5)	13.3 (9.9 – 15.9)	0.087	–
LV ejection fraction (%)	52.0 (47.6 – 62.4)	54.5 (46.0 – 65.8)	62.7 (58.1 – 67.6)	0.016	0.91
LV outflow tract VTI (cm)	21.0 (18.0 – 23.3)	18.0 (16.2 – 20.5)	21.7 (17.0 – 25.9)	0.2	–
Cardiac index (l/min/m^2)	2.7 (2.5 – 3.3)	2.7 (2.5 – 3.4)	3.1 (2.9 – 3.9)	0.3	–
RV/LV end-diastolic area	0.55 (0.53 – 0.69)	0.68 (0.53 – 0.72)*	0.54 (0.46 – 0.58)*	0.044	0.44
RV fractional area change (%)	45 (33 – 50)	28 (25 – 35)*	42 (34 – 50)*	< 0.001	0.003
TAPSE (mm)	24.0 (21.5 – 27.0)	19.3 (15.2 – 20.7)*	26.0 (21.8 – 27.2)*	0.005	0.025
Tricuspid annular S' wave (cm/s)	16.0 (14.3 – 18.1)	15.0 (12.0 – 17.8)	18.3 (15.7 – 22.0)	0.067	–
Vmax tricuspid regurgitation (cm/s)	3.05 (2.65 – 3.48)	2.90 (2.80 – 2.92)	2.70 (2.30 – 2.88)	0.3	–
Right atrio-ventricular systolic pressure gradient (mmHg)	37.2 (28.1 – 48.4)	33.6 (31.4 – 34.1)	29.2 (21.2 – 33.2)	0.3	–
RV dilatation				0.012	
Absent	13 (62%)	7 (32%)	21 (100%)		
Moderate	7 (33%)	14 (64%)	0 (0%)		
Severe	1 (4.8%)	1 (4.5%)	0 (0%)		
Acute cor pulmonale	4 (19%)	11 (50%)	0 (0%)	< 0.001	0.033

[a] *Median (25–75%).*
[b] *Kruskal-Wallis rank sum test.*
[c] *Kruskal-Wallis rank sum test or Pearson's Chi-squared test adjusted with Bonferroni test between ARDS group.*
**p-value < 0.05 between Controls and Group 2 adjusted with Bonferroni test.*
LV, left ventricle; VTI, velocity time integral; RV, right ventricle; TAPSE, tricuspid annular plane systolic excursion; Vmax, maximal velocity.

TABLE 4 | Three-dimensional echocardiography parameters.

	ARDS related to SARS-CoV-2 (Group 1) $n = 21^a$	ARDS unrelated to SARS-CoV-2 (Group 2) $n = 22^a$	Controls (Group 3) $n = 21^a$	p-value[b]	Paired p-value[c]
Indexed LV end-diastolic volume (mL/m^2)	55 (50–64)	58 (52–65)	47 (38–54)	0.069	–
Indexed LV end-systolic volume (mL/m^2)	23 (19–34)†	23 (19–28)*	15 (13–18)*†	0.002	1.00
LV ejection fraction (%)	56 (46–64)†	56 (49–64)	66 (62–71)†	0.017	1.00
Indexed RV end-diastolic volume (mL/m^2)	59 (48–72)	70 (61–72)	54 (40–59)	0.10	–
Indexed RV end-systolic volume (mL/m^2)	23 (16–29)	35 (31–40)*	18 (13–22)*	< 0.001	0.008
RV ejection fraction (%):	58 (55–62)	43 (40–57)*	65 (56–68)*	< 0.001	0.001
Absolute longitudinal RVEF (%)	20 (16–23)	11 (9–18)*	20 (16–24)*	0.014	0.11
Relative contribution of longitudinal axis (%)	32 (28–39)	29 (24–40)	31 (28–38)	0.6	–
Absolute anteroposterior RVEF (%)	29 (25–31)†	25 (18–32)*	36 (32–38)*†	< 0.001	0.57
Relative contribution of anteroposterior axis (%)	51 (41–55)	56 (46–63)	56 (50–64)	0.076	–
Absolute radial RVEF (%)	34 (28–38)	21 (17–28)*	34 (31–40)*	< 0.001	0.001
Relative contribution radial axis (%)	57 (51–62)	45 (40–53)*	56 (50–60)*	0.005	0.007

[a] *Median (25–75%).*
[b] *Kruskal-Wallis rank sum test.*
[c] *Kruskal-Wallis rank sum test adjusted with Bonferroni test between ARDS group.*
[†] *p-value < 0.05 between Control and Group 1 adjusted with Bonferroni test.*
**p-value < 0.05 between Control and Group 2 adjusted with Bonferroni test.*
LV, Left ventricle; RV, Right Ventricle; EF, Ejection fraction; 3D, Three-dimensional.

significantly lower in group 2 than in the other groups [43% (40–57) vs. 58% (55–62) and 65% (56–68), respectively: $p < 0.001$] (**Table 4**).

RVEF along the three spatial axes was uniformly lower in Group 2 (**Table 4** and **Figures 2A,B**, **3**). In group 1, only the anteroposterior RVEF was significantly lower when compared to controls [29% (25–31) vs. 36% (32–38): $p = 0.029$]. Radial RVEF was significantly lower in group 2 than in the other groups (**Table 4** and **Figures 2**, **4**). When considering the relative contribution of each RV axis to the global RVEF, the contribution of RV shortening along the radial axis was the only one reduced in group 2 when compared to the other groups

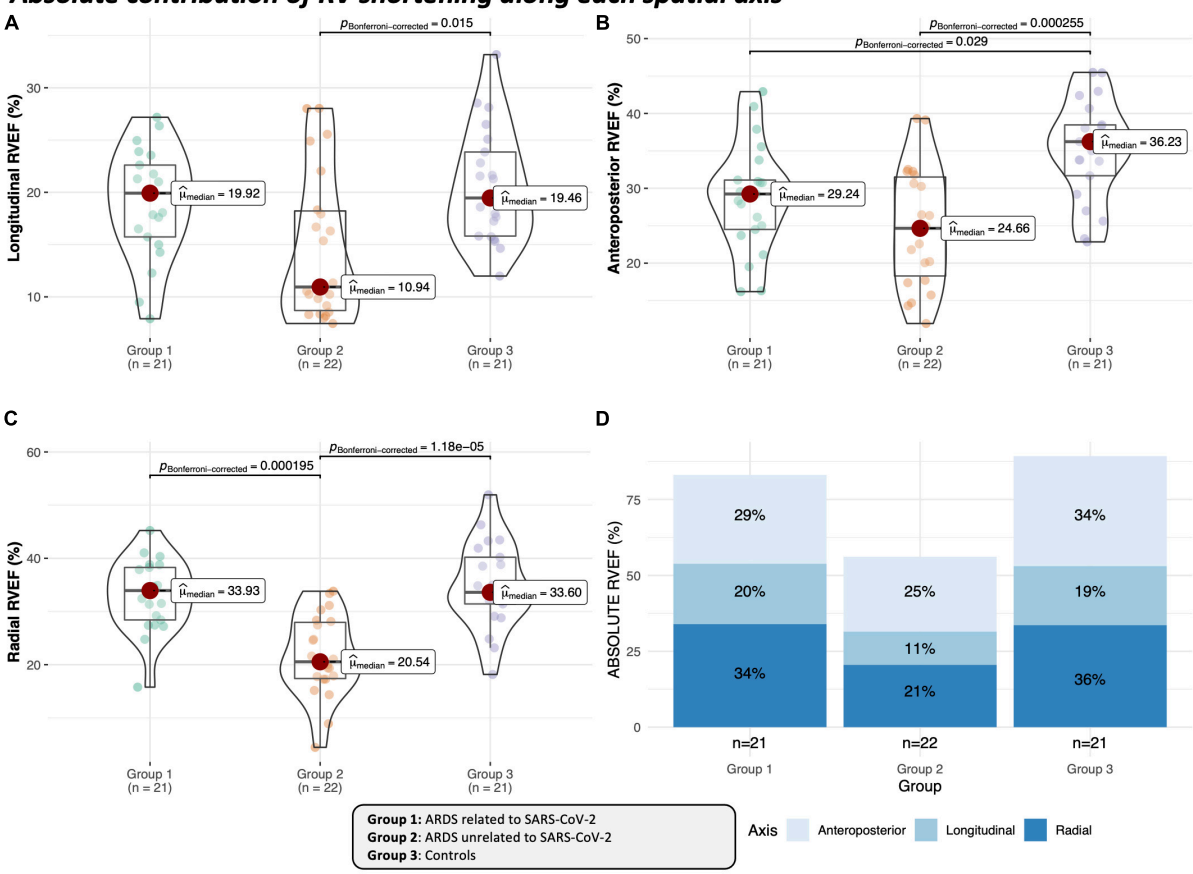

FIGURE 2 | Absolute contribution of RV shortening along each spatial axis to the generation of global ejection fraction in ARDS groups and in the control group. Paired *p*-values are given when significant and were adjusted with Bonferroni test. The sum of the decomposed volume changes and ejection fractions is not equal to the global values due to the non-additive manner of the motion decomposition. Thus, when analyzing RV shortening along a single axis, the contribution of the given motion direction to global RV volume loss is mathematically overestimated. **(A)** Violin plot including box plot depicting median value of the absolute longitudinal RVEF in the different groups. **(B)** Violin plot including boxplot depicting median value of the absolute anteroposterior RVEF in the different groups. **(C)** Violin plot including boxplot depicting median value of the absolute radial RVEF in the different groups. **(D)** Stacked bar plot depicting each cumulated median absolute value (indicated in black) of different axes in the ARDS groups and in the control group.

[45% (40–53) vs. 57% (51–62) and 56% (50–60): $p = 0.007$ and $p < 0.05$, respectively] (**Figures 3**, **4**). In contrast, the relative contribution of RV shortening along both the longitudinal and antero-posterior axes were not statistically different between ARDS groups and controls (**Table 4** and **Figures 3**, **4**).

Intra- and Inter-Observer Reproducibility

Acceptable agreement was found between the repeated measurements by the same operator (intra-observer reproducibility) or by two independent operators (inter-observer reproducibility), with the lowest agreement for the longitudinal RVEF (**Table 5**).

DISCUSSION

In this study assessing for the first time the ability of RT3D TEE to quantify the respective relative contribution of RV shortening along the three anatomically relevant spatial axes to global RVEF in the setting of ARDS, we showed that ventilated patients with ARDS unrelated to SARS-CoV-2 had a lower RVEF related to an impairment of all its mechanical components. In contrast, ventilated patients for an ARDS secondary to SARS-CoV-2 exhibited preserved RVEF, with only a reduced absolute shortening along the anteroposterior axis when compared to controls.

Longitudinal RV shortening has been previously suggested as the major component of RV contraction (18). A previous study using RT3D transthoracic echocardiography in healthy subjects has shown the role of non-longitudinal (i.e., radial and anteroposterior) shortening in generating global RVEF (8). Accordingly, in the present study, patients with ARDS unrelated to SARS-CoV-2 with reduced global RVEF exhibited a uniformly lowered RV shortening along the three spatial axes when compared to controls. Noticeably, the longitudinal RV shortening had a lower contribution to global RVEF

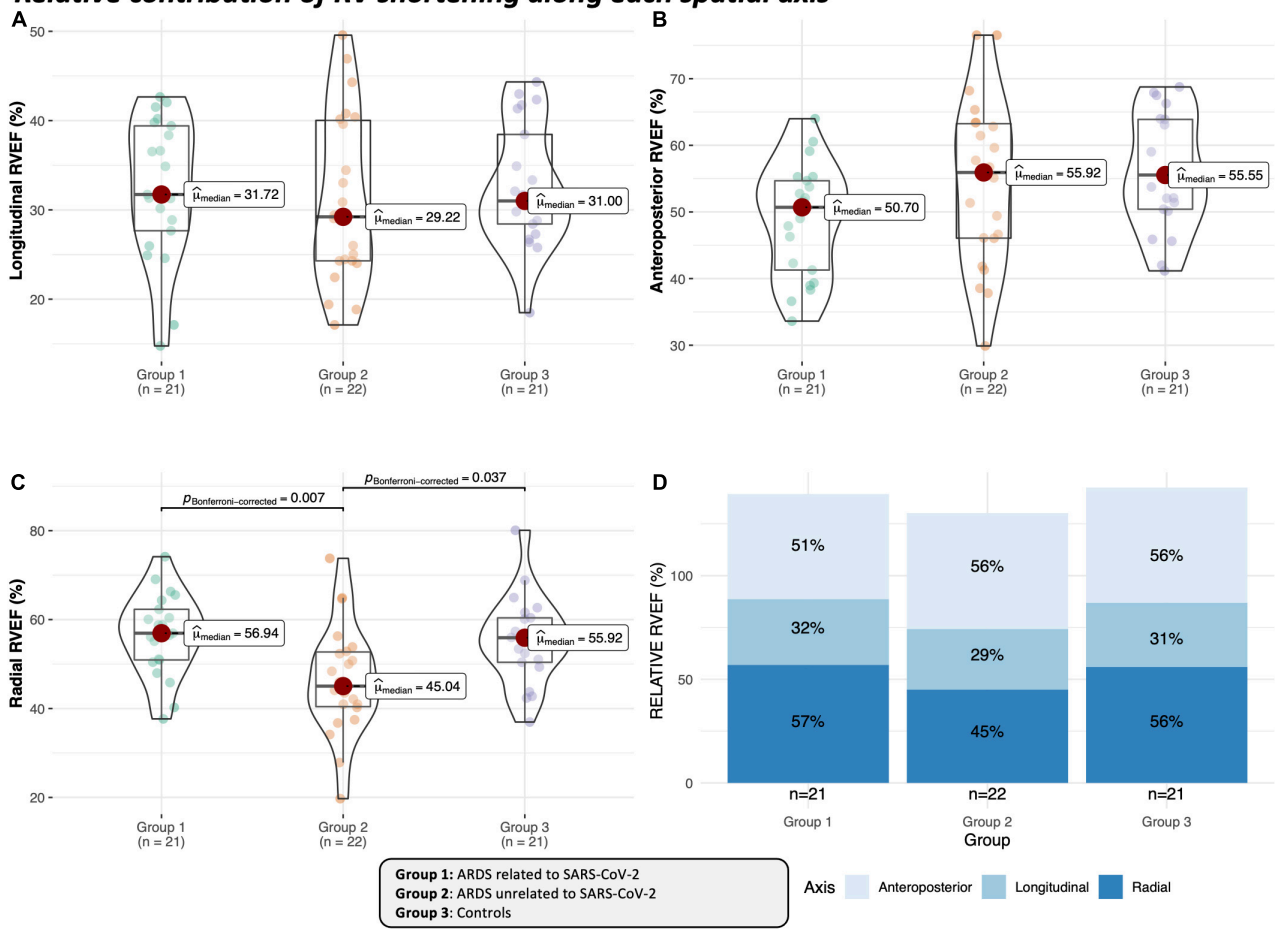

FIGURE 3 | Relative contribution of RV shortening along each spatial axis to the generation of global ejection fraction in ARDS groups and in the control group. Paired *p*-values are given when significant and were adjusted with Bonferroni test. The sum of the decomposed volume changes and ejection fractions is not equal to the global values due to the non-additive manner of the motion decomposition. Thus, when analyzing RV shortening along a single axis, the contribution of the given motion direction to global RV volume loss is mathematically overestimated. **(A)** Violin plot including boxplot depicting median value of the relative longitudinal RVEF in the different groups. **(B)** Violin plot including boxplot depicting median value of the relative anteroposterior RVEF in the different groups. **(C)** Violin plot including boxplot depicting median value of the relative radial RVEF in the different groups. **(D)** Stacked bar plot depicting each cumulated median relative value (indicated in black) of different axes in the ARDS groups and in the control group.

than the radial and anteroposterior shortening, including in controls. Since all our patients were mechanically ventilated, intrathoracic positive pressure have presumably altered RV hemodynamic, in increasing RV afterload and reducing venous return, hence RV preload (19). In addition, RV mechanics has been previously studied in a totally different clinical setting, using RT3D transthoracic echocardiography in normal spontaneously breathing subjects (7, 8).

Patients ventilated for an ARDS unrelated to SARS-CoV-2 had a lower RVFAC and relative contribution of RV radial shortening to global RVEF. In this group, the prevalence of ACP was higher than that in other groups. ACP develops in the presence of excessive RV afterload. This results in a prolonged RV contraction, RV-LV pressure imbalance, and subsequent paradoxical interventricular septal motion (2). It has previously been suggested than increased RV afterload induces a reduction of RV radial shortening (8). Interestingly, transverse wall motion (i.e., RV radial shortening), which is reflected by RVFAC, was a better marker of RVEF than the longitudinal wall motion assessed using TAPSE in patients with pulmonary hypertension (20). RV volume overload states have also been shown to influence the ventricular mechanical pattern (21). The interventricular septum is a major contributor to RV contraction (18): when the LV contracts, septal circumferential myocardial fibers shorten, leading to a RV shortening along both the radial and antero-posterior axes. In the case of a paradoxical septal motion, the septum is unable to efficiently contract, potentially leading to a reduction in RV radial and anteroposterior shortening (22). In the current study, the relative contribution of RV radial shortening was solely identified, but not that of the anteroposterior shortening. RV antero-posterior shortening may reflect the effect of LV contraction

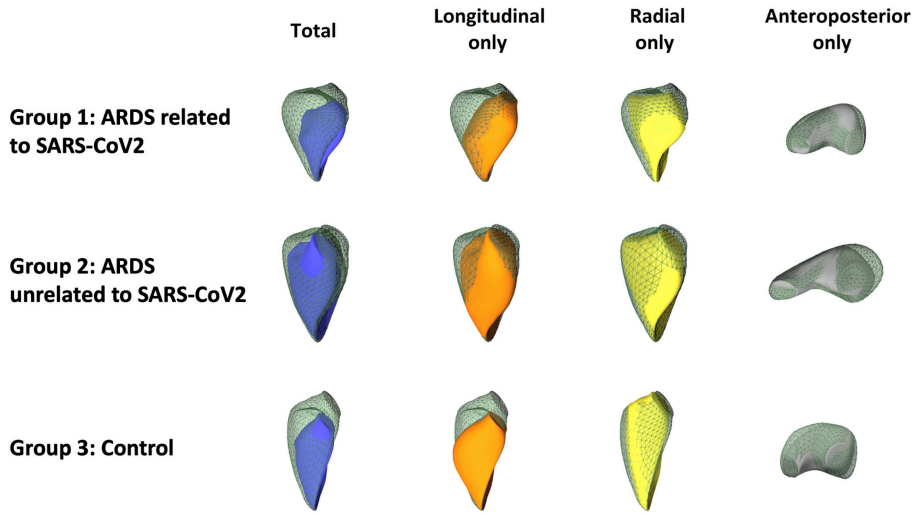

FIGURE 4 | Representative cases depicting the global motion and the three different mechanical components of the right ventricle (RV) from each ARDS group and from the control group. Color represents each isolated axis of right ventricular end systolic volume (Blue for global, Orange for longitudinal, Yellow for radial and Gray for anteroposterior). Right ventricular mechanics can be appreciated by measuring its shortening along the three spatial axes (green mesh, RV end-diastolic volume; blue surface, end-systolic volume related to global right ventricular ejection fraction). By decomposing RV shortening along the three anatomically relevant axes, theoretical RV end-systolic meshes can be generated in which RV motion is "locked" in two directions and enabled along only one axis (orange surface, longitudinal axis only; yellow surface, radial axis only; gray surface, anteroposterior axis only). In the patient from group 1, global RV ejection fraction was preserved with only a decrease in the anteroposterior shortening when compared to the control. In the patient from group 2, both the global and axial RV ejection fractions were decreased when compared to the control, with a particular impairment of radial shortening.

TABLE 5 | Intra and Interobserver variability of 3D RV ejection fraction.

	Intraobserver variability		Interobserver variability	
	CV, %	R^2	CV, %	R^2
Global EF	5.73	0.89	5.81	0.98
Longitudinal EF	12.98	0.67	12.18	0.60
Radial EF	11.55	0.91	8.82	0.83
Anteroposterior EF	13.33	0.73	10.57	0.87

EF, Ejection fraction; CV, Coefficient of variability.

on RV ejection through myocardial fibers entwining the two ventricles (8, 23). In the absence of LV systolic dysfunction, RV anteroposterior shortening could be relatively preserved even in the presence of a paradoxical septal motion. In our ARDS population, RV anteroposterior shortening was lower than in controls, which may be a consequence of a lower LVEF in this specific group. The potential relationship between RV anteroposterior shortening and LV systolic function requires further clinical investigation.

Patients in the two ARDS groups had no statistically different static lung compliance and ventilatory parameters on ICU admission. In addition, the right atrio-ventricular systolic pressure gradient was not significantly different among ARDS patients. Overall, these results suggest that the burden sustained by the RV was similar in these patients. In contrast, patients with SARS-CoV-2 ARDS had a lower incidence of circulatory failure on admission than other ARDS patients, presumably due to the low incidence of primary bacterial infection (24). Indeed, sepsis can induce both a RV systolic dysfunction and dilatation (25). In patients with SARS-CoV-2 ARDS, RV dilatation has been reported in 13.3–49.9% of patients, which is consistent with our findings (26).

RT3D TEE in ventilated ARDS has been shown to become feasible in routine clinical practice (26, 27). The herein reported reproducibility of measurements of the different RVEF components is comparable to previous studies (8), and appears adequate for clinical use. The clinical relevance of this further insight in RV systolic properties remains to be determined.

This study has several limitations. First, ARDS is not a homogeneous syndrome and has multiple phenotypes with different prognosis (28). Accordingly, patients ventilated for an ARDS unrelated to SARS-CoV-2 had heterogeneous associated acute conditions which could have a variable impact on RV contraction pattern (e.g., sepsis). Second, age was not adjusted between groups, especially in the control group which was only sex-matched. Although axial RV shortening is influenced by sex in the normal population, age may also alter it (8). Third, the prevalence of ACP was higher in patients ventilated for ARDS unrelated to SARS-CoV-2 when compared to conventional ARDS population (11). A selection bias cannot be excluded due to the high exclusion rate in this group. Nevertheless, this high prevalence allowed to better evidence the potential role of paradoxical septal motion on RV mechanics. Fourth, we did not compare RT3D acquisitions obtained from both the transthoracic and transesophageal approaches since surface RT3D imaging is technically challenging in patients under positive-pressure ventilation. Fifth, since invasive central venous pressure was not available in all patients, we used the right

atrio-ventricular systolic pressure gradient calculated from the maximal velocity of tricuspid regurgitant jet as a surrogate of systolic pulmonary arterial pressure. Finally, we could not exclude associated pulmonary embolism in our patients who did not undergo systematically a contrast-enhanced chest CT at the time of echocardiography assessment.

In the present study, RV systolic dysfunction was more pronounced in patients ventilated for ARDS unrelated to SARS-CoV-2, and resulted from a homogeneous decrease of RV shortening along the three spatial axes. Radial shortening appeared more involved than RV longitudinal and anteroposterior shortening in patients with ARDS unrelated to SARS-CoV-2 and decreased RVEF. The clinical impact of both the global and axial RV impairment assessed by RT3D echocardiography needs to be determined in future studies.

DATA AVAILABILITY STATEMENT

The raw data supporting the conclusions of this article will be made available by the authors, without undue reservation.

ETHICS STATEMENT

The studies involving human participants were reviewed and approved by Comité d'éthique du CHU de Limoges. Written informed consent for participation was not required for this study in accordance with the national legislation and the institutional requirements.

AUTHOR CONTRIBUTIONS

BE and BL drafted the manuscript and designed the study. MG included patients and reviewed the manuscript. ZT supervised the model development and participated in the interpretation of the results. BM, PV, ZT, and AK reviewed the manuscript. All authors contributed to the article and approved the submitted version.

FUNDING

This work was supported by the Association Limousine d'Aide aux Insuffisants Respiratoires (ALAIR).

REFERENCES

1. Price LC, McAuley DF, Marino PS, Finney SJ, Griffiths MJ, Wort SJ. Pathophysiology of pulmonary hypertension in acute lung injury. *Am J Physiol Lung Cell Mol Physiol.* (2012) 302:L803–15. doi: 10.1152/ajplung.00355.2011
2. Belenkie I, Dani R, Smith ER, Tyberg JV. Ventricular interaction during experimental acute pulmonary embolism. *Circulation.* (1988) 78:761–8. doi: 10.1161/01.cir.78.3.761
3. Mekontso Dessap A, Boissier F, Charron C, Bégot E, Repessé X, Legras A, et al. Acute cor pulmonale during protective ventilation for acute respiratory distress syndrome: prevalence, predictors, and clinical impact. *Intensive Care Med.* (2016) 42:862–70. doi: 10.1007/s00134-015-4141-2
4. Vieillard-Baron A, Naeije R, Haddad F, Bogaard HJ, Bull TM, Fletcher N, et al. Diagnostic workup, etiologies and management of acute right ventricle failure. *Intensive Care Med.* (2018) 44:774–90. doi: 10.1007/s00134-018-5172-2
5. Shimada YJ, Shiota M, Siegel RJ, Shiota T. Accuracy of right ventricular volumes and function determined by three-dimensional echocardiography in comparison with magnetic resonance imaging: a meta-analysis study. *J Am Soc Echocardiogr.* (2010) 23:943–53. doi: 10.1016/j.echo.2010.06.029
6. Addetia K, Muraru D, Badano LP, Lang RM. New directions in right ventricular assessment using 3-dimensional echocardiography. *JAMA Cardiol.* (2019) 4:936. doi: 10.1001/jamacardio.2019.2424
7. Lakatos B, Tősér Z, Tokodi M, Doronina A, Kosztin A, Muraru D, et al. Quantification of the relative contribution of the different right ventricular wall motion components to right ventricular ejection fraction: the ReVISION method. *Cardiovasc Ultrasound.* (2017) 15:8. doi: 10.1186/s12947-017-0100-0
8. Lakatos BK, Nabeshima Y, Tokodi M, Nagata Y, Tősér Z, Otani K, et al. Importance of nonlongitudinal motion components in right ventricular function: three-dimensional echocardiographic study in healthy volunteers. *J Am Soc Echocardiogr.* (2020) 33:995.e–1005.e. doi: 10.1016/j.echo.2020.04.002
9. Gattinoni L, Coppola S, Cressoni M, Busana M, Rossi S, Chiumello D. COVID-19 Does Not Lead to a 'Typical' Acute Respiratory Distress Syndrome. *Am J Respir Crit Care Med.* (2020) 201:1299–300. doi: 10.1164/rccm.202003-0817LE
10. Ards Definition Task Force, Ranieri VM, Rubenfeld GD, Thompson BT, Ferguson ND, Caldwell E, et al. Acute respiratory distress syndrome: the Berlin Definition. *JAMA.* (2012) 307:2526–33. doi: 10.1001/jama.2012.5669
11. Lhéritier G, Legras A, Caille A, Lherm T, Mathonnet A, Frat J-P, et al. Prevalence and prognostic value of acute cor pulmonale and patent foramen ovale in ventilated patients with early acute respiratory distress syndrome: a multicenter study. *Intensive Care Med.* (2013) 39:1734–42. doi: 10.1007/s00134-013-3017-6
12. Mosteller RD. Simplified calculation of body-surface area. *N Engl J Med.* (1987) 317:1098. doi: 10.1056/nejm198710223171717
13. Sinha P, Calfee CS, Beitler JR, Soni N, Ho K, Matthay MA, et al. Physiologic Analysis and Clinical Performance of the Ventilatory Ratio in Acute Respiratory Distress Syndrome. *Am J Respir Crit Care Med.* (2019) 199:333–41. doi: 10.1164/rccm.201804-0692OC
14. Vignon P. Assessment of pulmonary arterial pressure using critical care echocardiography: dealing with the yin and the yang? *Crit Care Med.* (2019) 47:126-8. doi: 10.1097/CCM.0000000000003491
15. Lang RM, Badano LP, Mor-Avi V, Afilalo J, Armstrong A, Ernande L, et al. Recommendations for cardiac chamber quantification by echocardiography in adults: an update from the american society of echocardiography and the european association of cardiovascular imaging. *J Am Soc Echocardiogr.* (2015) 28:1.e–39.e.
16. Tokodi M, Staub L, Budai Á, Lakatos BK, Csákvári M, Suhai FI, et al. Partitioning the right ventricle into 15 segments and decomposing its motion using 3D echocardiography-based models: the updated ReVISION method. *Front Cardiovasc Med.* (2021) 8:622118. doi: 10.3389/fcvm.2021.622118
17. Evrard B, Goudelin M, Montmagnon N, Fedou A-L, Lafon T, Vignon P. Cardiovascular phenotypes in ventilated patients with COVID-19 acute respiratory distress syndrome. *Crit Care.* (2020) 24:236. doi: 10.1186/s13054-020-02958-8
18. Buckberg G, Hoffman JIE. Right ventricular architecture responsible for mechanical performance: unifying role of ventricular septum. *J Thorac Cardiovasc Surg.* (2014) 148:3166.e–71.e. doi: 10.1016/j.jtcvs.2014.05.044
19. Jardin F, Vieillard-Baron A. Right ventricular function and positive pressure ventilation in clinical practice: from hemodynamic subsets to respirator settings. *Intensive Care Med.* (2003) 29:1426–34. doi: 10.1007/s00134-003-1873-1

20. Kind T, Mauritz G-J, Marcus JT, van de Veerdonk M, Westerhof N, Vonk-Noordegraaf A. Right ventricular ejection fraction is better reflected by transverse rather than longitudinal wall motion in pulmonary hypertension. *J Cardiovasc Magn Reson.* (2010) 12:35. doi: 10.1186/1532-429X-12-35
21. Kovács A, Lakatos B, Tokodi M, Merkely B. Right ventricular mechanical pattern in health and disease: beyond longitudinal shortening. *Heart Fail Rev.* (2019) 24:511–20. doi: 10.1007/s10741-019-09778-1
22. Sanz J, Sánchez-Quintana D, Bossone E, Bogaard HJ, Naeije R. Anatomy, Function, and Dysfunction of the Right Ventricle: JACC State-of-the-Art Review. *J Am Coll Cardiol.* (2019) 73:1463–82. doi: 10.1016/j.jacc.2018.12.076
23. Surkova E, Kovács A, Tokodi M, Lakatos BK, Merkely B, Muraru D, et al. Contraction Patterns of the Right Ventricle Associated with Different Degrees of Left Ventricular Systolic Dysfunction. *Circ Cardiovasc Imaging.* (2021) 14:e012774. doi: 10.1161/CIRCIMAGING.121.012774
24. Covid-Icu Group on behalf of the Reva Network and the Covid-Icu Investigators. Clinical characteristics and day-90 outcomes of 4244 critically ill adults with COVID-19: a prospective cohort study. *Intensive Care Med.* (2021) 47:60–73. doi: 10.1007/s00134-020-06294-x
25. Beesley SJ, Weber G, Sarge T, Nikravan S, Grissom CK, Lanspa MJ, et al. Septic Cardiomyopathy. *Crit Care Med.* (2018) 46:625–34.
26. Lan Y, Liu W, Zhou Y. Right ventricular damage in COVID-19: association between myocardial injury and COVID-19. *Front Cardiovasc Med.* (2021) 8:606318. doi: 10.3389/fcvm.2021.606318
27. Evrard B, Goudelin M, Fedou AL, Vignon P. Hemodynamic response to prone ventilation in COVID-19 patients assessed with 3D transesophageal echocardiography. *Intensive Care Med.* (2020) 46:2099–101. doi: 10.1007/s00134-020-06217-w
28. Calfee CS, Delucchi K, Parsons PE, Thompson BT, Ware LB, Matthay MA. Subphenotypes in acute respiratory distress syndrome: latent class analysis of data from two randomised controlled trials. *Lancet Respir Med.* (2014) 2:611–20. doi: 10.1016/S2213-2600(14)70097-9

Conflict of Interest: ZT was a cofounder and CEO of Argus Cognitive, Inc. (the company developing the ReVISION software), held equity in the company, and received financial compensation for his work. BL and AK served as medical consultants to Argus Cognitive and received financial compensation for their work.

The remaining authors declare that the research was conducted in the absence of any commercial or financial relationships that could be construed as a potential conflict of interest.

Publisher's Note: All claims expressed in this article are solely those of the authors and do not necessarily represent those of their affiliated organizations, or those of the publisher, the editors and the reviewers. Any product that may be evaluated in this article, or claim that may be made by its manufacturer, is not guaranteed or endorsed by the publisher.

frontiers | Frontiers in Cardiovascular Medicine

ORIGINAL RESEARCH
published: 03 May 2022
doi: 10.3389/fcvm.2022.843606

Echocardiographic Evaluation of Initial Ambrisentan Plus Phosphodiesterase Type 5 Inhibitor on Right Ventricular Pulmonary Artery Coupling in Severe Pulmonary Arterial Hypertension Patients

Wei-Fang Lan[1], Yan Deng[1], Bin Wei[2], Kai Huang[2], Ping Dai[1], Shan-Shan Xie[1] and Dan-dan Wu[1]*

[1] Department of Ultrasound, First Affiliated Hospital of Guangxi Medical University, Nanning, China, [2] Department of Cardiology, First Affiliated Hospital of Guangxi Medical University, Nanning, China

Introduction: ambrisentan and phosphodiesterase type 5 inhibitor (PDE5i) have been approved for treating patients with pulmonary arterial hypertension (PAH). Echocardiographic right ventricular pulmonary artery coupling (RVPAC) has been shown to be a valid non-invasive and alternative measurement method to assess the predicted outcomes in PAH patients. The aim of this study was to study the effect and clinical correlates of initial ambrisentan plus PDE5i combination therapy on RVPAC in patients with severe PAH.

Method and Results: We retrospectively studied and analyzed comprehensive clinical data, hemodynamics, and echocardiography in 27 patients with severe PAH before and after 6 months of initial combination therapy. Compared with the baseline, significant improvements in RVPAC ratios were observed, including RVFAC/PASP (0.31 ± 0.10 vs. 0.44 ± 0.15%/mmHg, $p < 0.001$), TAPSE/PASP (0.15 ± 0.05 vs. 0.21 ± 0.06 mm/mmHg, $p = 0.001$), S'/PASP (0.10 ± 0.03 vs. 0.14 ± 0.05 cm/s•mmHg, $p = 0.001$), and RVSV/RVESV (0.79 ± 0.22 vs. 1.02 ± 0.20, $p < 0.001$). Functional status indices [World Health Organization functional classifications (WHO-FC) and 6 min walk distance (6MWD) and N-terminal pro B-type natriuretic peptide (NT-proBNP) levels] showed significant improvements. Right heart catheterization (RHC) evaluations for hemodynamic measurements between baseline and the 6–12 month follow-up were sPAP (96 ± 22 vs. 86 ± 24 mmHg, $p = 0.002$), mPAP (64 ± 18 vs. 56 ± 17 mmHg, $p < 0.001$) and TPVR (17.3 ± 6.7 vs. 12.1 ± 5.4 WU, $p = 0.001$). Simultaneously, significant associations between RVPAC ratios and NT-proBNP levels and WHO-FC and 6MWD were observed.

Conclusion: Ambrisentan plus PDE-5i combination therapy resulted in a significant improvement in RVPAC in severe PAH. Importantly, RVPAC parameters correlated with known prognostic markers of PAH.

Keywords: pulmonary arterial hypertension, right ventricular pulmonary arterial coupling, echocardiography, combination therapy, right ventricular remodeling

OPEN ACCESS

Edited by:
Attila Kovacs,
Semmelweis University, Hungary

Reviewed by:
Mohammad Abdelghani,
Al-Azhar University, Egypt
Balint Karoly Lakatos,
Semmelweis University, Hungary

***Correspondence:**
Yan Deng
190662044@qq.com

Specialty section:
This article was submitted to Cardiovascular Imaging, a section of the journal Frontiers in Cardiovascular Medicine

Received: *26 December 2021*
Accepted: *11 April 2022*
Published: *03 May 2022*

Citation:
Lan W-F, Deng Y, Wei B, Huang K, Dai P, Xie S-S and Wu D-d (2022) Echocardiographic Evaluation of Initial Ambrisentan Plus Phosphodiesterase Type 5 Inhibitor on Right Ventricular Pulmonary Artery Coupling in Severe Pulmonary Arterial Hypertension Patients. Front. Cardiovasc. Med. 9:843606. doi: 10.3389/fcvm.2022.843606

INTRODUCTION

Pulmonary arterial hypertension (PAH) is a severe clinical syndrome characterized by increasing pulmonary vascular resistance resulting in chronic pressure overload of the right ventricle (RV) and ultimately leading to right heart failure and death (1, 2).

The treatment goal in PAH patients is to achieve good exercise capacity, reduce the RV afterload, keep the patient in WHO-FC II and maintain low mortality rates whenever possible (3). Current research studies on potential therapeutic targets and the development of new PAH-targeted therapies focused on the endothelium, nitric oxide, and prostacyclin pathways have contributed to improved survival in patients with PAH (2, 3). Ambrisentan is an endothelin-specific receptor antagonist (ERA) approved for the treatment of PAH. Phosphodiesterase type 5 inhibitor (PDE-5i), such as sildenafil, are available therapies to influence the nitric oxide pathway. Initial or early combination therapy (generally ambrisentan and PDE-5i) is an attractive option and is currently recommended for treating patients with PAH, especially severe PAH (3, 4).

The main prognostic factor of symptoms and outcome in PAH is related to RV function (3, 5). However, merely assessing RV function can provide limited insight into RV adaptation and chronic volume overload and does not take into account the effects of pulmonary circulation (6). Right ventricular pulmonary arterial coupling (RVPAC) based on the matching of RV function and its vascular circulation can early and precisely reflect the status of overloaded RV function (6, 7). The gold standard of assessing RVPAC is the ratio of end-systolic elastance to pulmonary arterial elastances (Ees/Ea), which has been evaluated by invasive right heart catheterization (RHC). Ideally, coupling is maintained at resting conditions in patients with adaptive RV. Only in the late stages of pressure overload does uncoupling occur (6, 8).

Echocardiography is a non-invasive ultrasound technique and provides RV function parameters such as tricuspid annular plane systolic excursion (TAPSE), right ventricular fractional area change (RVFAC), tricuspid annular peak systolic tissue Doppler velocity (TASV or S') and pulmonary artery systolic pressure (PASP) for estimating hemodynamic characteristics or improving RV function in patients with PAH (3, 9). Recently, some studies demonstrated that the ratios of TAPSE to pulmonary artery systolic pressure (PASP) were closely related to prognostic markers and have been considered a surrogate of Ees/Ea (10–14). The TASV/RVSP ratio, as a determinant of poor prognosis, is associated with short-term and long-term mortality (15). In addition, another ratio of RV stroke volume (RVSV) to RV end-systolic volume (RVESV), measured by 3-dimensional echocardiography (3-DE), has the same capacity and is a significant predictor of adverse clinical events for pediatric patients with PAH (16). However, data concerning the evaluation of right ventricular function and RVPAC in severe PAH patients after ambrisentan and PDE-5i combination therapy are scarce.

Our study aims to (1) determine changes in RV function and RVPAC in response to combination therapy with initial ambrisentan plus PDE-5i in patients with severe PAH and (2) evaluate the relationship between RVPAC and clinical parameters.

MATERIALS AND METHODS

Study Population

A retrospective study was conducted in treatment-naive patients and their medical records from June 2019 to February 2022 were collected and reviewed at the First Affiliated Hospital of Guangxi Medical University. The patients' diagnoses were confirmed by RHC, and confirmed by criteria such as a mean pulmonary artery pressure (mPAP) $>$ 25 mmHg, a pulmonary vascular resistance (PVR) $>$ 5 Wood Units (WU), and pulmonary arterial wedge pressure (PAWP) or left ventricular end diastolic pressure of $<$ 15 mmHg (3). Based on relevant literature, at least two experts confirmed, through a comprehensive data review of severe PAH-related assessments, severe PAH in patients with reduced RV function as assessed by echocardiography and right heart catheterization (higher right atrial pressure, lower cardiac index, increased pulmonary vascular resistance index), a WHO FC III or IV, and a significantly elevated N-terminal-Pro-Brain-Natriuretic Peptide (NT-proBNP) level (3, 4, 17). Disease progression and the presence or absence of signs of right heart failure were also considered. They were treated with an upfront combination of ambrisentan and PDE-5i.

The following were exclusion criteria: (1) total lung capacity of pulmonary function test was lower than the 60% estimated value; (2) suffering from interstitial lung disease, pulmonary hypertension due to lung diseases or chronic thromboembolic disease; (3) pulmonary hypertension due to left heart disease, including left ventricular systolic or diastolic dysfunction, valvular disease (moderate to severe stenosis or insufficiency confirmed by echocardiography), cardiomyopathies; (4) pulmonary valve or pulmonary arterial stenosis; and (5) autonomic hypotension, severe hepatic and renal impairment.

Patients who fulfilled the above criteria and had PAH confirmed by RHC but who had not yet received PAH-specific therapy were enrolled.

Clinical Data

At the baseline, patient demographics, clinical status and treatment strategies were collected by review of electronic medical records. Heart function was assessed by World Health Organization functional classifications (WHO-FC). A 6 min walk distance (6MWD) was performed according to American Thoracic Society guidelines (18).

Biochemical markers were obtained, and the level of plasma N-terminal pro B-type natriuretic peptide (NT-proBNP) was measured by an enzyme-linked immunosorbent assay using a COBAS 6000 E601 immunoassay analyzer and an Elecsys proBNP II reagent kit (Roche Diagnostics GmbH, Mannheim, Germany).

Right Heart Catheterization

Right heart catheterization was performed using a balloon wedge catheter through the femoral vein or internal jugular

vein by standard methods at the first diagnosis of PAH (19). At the follow-up, RHC was performed using MPA2 angiographic catheter (6F, Cordis Corporation, Miami Lakes, FL, United States) under fluoroscopic guidance. Hemodynamic measurements obtained by RHC included mean pulmonary arterial pressure (mPAP), systolic pulmonary arterial pressure (sPAP), diastolic pulmonary arterial pressure (dPAP), mean right ventricular pressure (mRVP), systolic right ventricular pressure (sRVP), diastolic right ventricular pressure (dRVP), mean right atrial pressure (mRAP), heart rate and pulmonary arterial wedge pressure (PAWP). Cardiac output (CO) was divided by heart rate to obtain stroke volume. The cardiac index (CI) was divided by body surface area (BSA) to CO. Total pulmonary vascular resistance (TPVR) was divided by CO to mPAP. Pulmonary vascular resistance (PVR) was calculated as (mPAP − PAWP)/CO.

Transthoracic Echocardiography

Transthoracic echocardiography was performed on all patients with an available echocardiographic Philips EPIC 7C (Philips Healthcare, Andover, MA, United States), and 3DE RV data were digitally analyzed using an advanced data quality quantification system (Philips Healthcare, Andover, MA, United States). All parameters were performed both at baseline and after 6 months of combination therapy in patients with severe PAH according to the recommendations for echocardiographic assessment of the right heart by the American Society of Echocardiography chamber guidelines (9, 20).

TAPSE was defined as the difference between the displacement of the RV lateral annulus from end-diastole to end-systole obtained by M-mode imaging in the apical four-chamber view centered on the RV. S' was defined as tricuspid annular systolic velocity derived from tissue Doppler transthoracic echocardiography. PASP was calculated using the maximal tricuspid regurgitation velocity obtained from continuous wave Doppler and integrated into the modified Bernoulli equation [PASP = 4 $(TRV)^2$ + RAP]. Right atrial pressure was estimated through the inferior vena cava (IVC) size and variability with respiration. RAP is equal to 3 mmHg when the IVC size $\leq$ 2.1 cm and variability with respiration (> 50% diameter change with inspiration), equal to 8 mmHg when the IVC size > 2.1 cm and variability with respiration (> 50% diameter change with inspiration), and equal to 15 mmHg when the IVC size > 2.1 cm and variability with respiration (< 50% diameter change with inspiration), according to the guidelines (20).

The 3D data were transferred and analyzed using an advanced data quality quantification system (QLAB version 12.0; Philips Healthcare) to automatically generate RV volumes and functional indices. Specifically, there were acquired in 3 steps. First, the RV basal short-axis and apical two- and four-chamber views were extracted by an advanced data quality quantification system equipped with 3D viewer software, and the software initially identified RV long-axis landmarks in end-diastole in the apical two- and four-chamber views. Next, the tricuspid valve annulus hinge points and the RV endocardial surfaces were automatically defined and tracked throughout the cardiac cycle (inclusion of papillary muscles and trabeculae in the cavity volume). The automatic tracings were manually adjusted if correction was needed. Finally, the RV volume–time curve was automatically constructed, and RV volumes and functional indices were obtained, including 3D RV end-diastolic volume (RVEDV), RV end-systolic volume (RVESV), RV stroke volume (RVSV), and RV ejection fraction (RVEF) was calculated using the standard formula: RVEF = (RVEDV-RVESV)/RVEDV (20). RV fractional area change (RVFAC) was defined as the percentage of the RV area from end-diastolic to end-systolic obtained by 3DE in the apical four-chamber view centered on the RV.

These measurements were performed at baseline and after 6 to 12 months of combination therapy.

Variability Analysis of 3DE Right Ventricle Measurements

Intraobserver and interobserver variability of the newer measures of RV volume and function assessment were evaluated in 10 randomly selected patients by 2 different investigators. For variability analysis, similar views were used but not necessarily the same beat, each blinded to the results obtained by the other. For intraobserver variability, RV measurements were repeated by the same investigator 6 months later. Reproducibility of the RV measurements was assessed using intraclass correlation coefficients. An intraclass correlation coefficient > 0.9 was considered to represent a high degree of reliability of the strain measurements.

Assessment of Right Ventricular Function and Right Ventricular Pulmonary Artery Coupling

RV systolic function was evaluated using RVFAC, S', TAPSE and RVEF. RV diastolic function was evaluated by the Doppler velocity of the transtricuspid flow (E), lateral tricuspid annular diastolic tissue Doppler velocity (E') and tricuspid annular E/E' ratio. The TAPSE/PASP, RVFAC/PASP, RVSV/RVESV and S'/PASP ratios were considered indices of RVPAC (10–16).

Statistical Analysis

Statistical analyses were performed utilizing SPSS statistical software (version 26, IBM Corporation, Armonk, NY, United States). Normal and non-normal distributions were determined using the Shapiro–Wilk test and visual analysis (P-P plots, Q-Q plots). Continuous variables are presented as the mean ± standard deviation or median and interquartile range (IQR; 25th–75th percentiles), and categorical variables are expressed as numbers and percentages. NT-proBNP values were log-transformed for analyses. The paired Student's *t*-test, chi-square test, and Wilcoxon signed rank tests were used in patients for measurements at 2 time points. RV volumes adjusted for body surface area (BSA). Correlations between RVPAC indices and NT-proBNP, 6MWD, WHO FC were evaluated by the Spearman rank correlation coefficient or Pearson correlation coefficient. For all tests, a p value less than 0.05 was considered statistically significant.

RESULTS

Baseline Demographic and Clinical Characteristics

We retrospectively reviewed 27 patients (median age 37 years, 85% female) who were provided with comprehensive data in this study, including idiopathic PAH (n = 15, 55%), congenital heart disease-associated PAH (n = 8, 30%) and systemic lupus erythematosus-associated PAH (n = 4, 15%). During the follow-up period, 21 patients were treated with ambrisentan plus tadalafil, and 6 patients were treated with ambrisentan plus sildenafil. In patients who had WHO FC IV at baseline, there were 4 patients treated with ambrisentan and PDE5i for intermediate risk (3), 2 patients for high risk were inoperable with initial combination therapy including i.v. prostacyclin because of the expensive price. The demographics and baseline characteristics of the study patients are shown in **Table 1**.

Clinical Status Change

After 6 months of combination therapy, the majority of patients improved their WHO FC, and 20 patients (74%) reached WHO-FC I or II (**Table 2**). NT-proBNP levels were significantly decreased from 1,690.0 (510.3–3,568.0) to 112.0 (1 9.85–1,936.0) pg/mL ($p < 0.001$). Simultaneously, a statistically significant difference was observed in the 6MWD (baseline 323 ± 125 vs. 391 ± 115 m after treatment, $p = 0.004$) (**Table 2**).

Hemodynamic Improvement

The effects of combination therapy on hemodynamics are presented in **Table 2** and **Figure 1**. Patients showed significant hemodynamics improvements after 6 months of initial combination therapy. Significant improvements in mPAP, sPAP and TPVR were observed ($p < 0.001$, $p = 0.002$, $p = 0.001$, respectively). We did not observe any significant changes in CI ($p = 0.110$). We observed a baseline median cardiac index of 2.5 L/min/m^2, which was indicative of RV dysfunction. At the same time, we did not observe any significant changes in mRAP (baseline 9 ± 3 mmHg vs. 8 ± 5 mmHg after treatment, $p = 0.948$).

Right Ventricular Function and Pulmonary Artery Systolic Pressure Improvement

Routine RV echocardiographic parameters differenced with respect to ambrisentan plus PDE-5i combination therapy are summarized in **Table 3** and **Figure 2**. RV systolic function was significantly improved in patients with severe PAH compared to the baseline, as assessed by S' ($p < 0.001$), TAPSE ($p < 0.001$), RVEF ($p < 0.001$), and RVFAC ($p < 0.001$).

RV diastolic function that assessed by the tricuspid annular E/E' ratio was not different compared to the baseline (baseline 7.1 ± 2.6 vs. 6.8 ± 3.0 after treatment, $p = 0.664$) and remained impaired. There was a trend that showed a decrease in RVEDV, whereas RVSV was unchanged after treatment; RVESV significantly decreased. After adjusting for BSA, RVEDVi significantly decreased. At the same time, an RV echocardiography performed at 6 months revealed slightly

TABLE 1 | Baseline demographics and clinical characteristics.

Total cohort	
Patients, n	27
Age, y	37 ± 14
Sex (female), %	23(85)
BSA, m^2	1.49 ± 0.19
SBP, mmHg	108 ± 14
DBP, mmHg	72 ± 10
HR, bpm	90 ± 12
Clinical presentation, n	
Exercise-induced symptoms	26 (96)
Syncope	3 (11)
Peripheral edema	9 (33)
Chronic cough	10 (37)
Hemoptysis	1 (4)
Clinical signs, n	
Enlargement of the heart	16 (59)
Accentuation of the P2	25 (93)
Right heart failure signs	12 (44)
Cardiac murmur	19 (70)
Cyanopathy	5 (19)
Electrocardiogram, n	
Right ventricular hypertrophy	12 (44)
Right bundle branch block	8 (30)
Arrhythmia	4 (15)
ST -T change	11 (41)
Normal	8 (30)
LVEF, %	71 ± 8

BSA, body surface area; SBP, systolic blood pressure; DBP, diastolic blood pressure; HR, heart rate; P2, pulmonary component of the second heart sound; LVEF, left ventricular ejection fraction.

TABLE 2 | Functional status, hemodynamic at baseline and follow-up.

Variables	**Baseline**	**Follow-up**	***P* value**
Functional status (n = 27)			
WHO FC I/II/III/IV, n	4/6/11/6	7/13/5/2	0.002
6MWD, m	323 ± 125	391 ± 115	0.004
NT-proBNP, pg/mL	1690.0 (510.3–3,568.0)	112.0 (19.85–1,936.0)	<0.001
Right heart catheterization (n = 23)			
mPAP, mmHg	64 ± 18	56 ± 17	<0.001
sPAP, mmHg	96 ± 22	86 ± 24	0.002
mRAP, mmHg	9 ± 4	9 ± 5	0.948
TPVR, WU	17.3 ± 6.7	12.1 ± 5.4	0.001
PAWP, mmHg	8 ± 2	–	–
PVR, WU	13 ± 6	–	–
CI, L/min/m^2	2.5 (2.0–3.5)	3.0 (2.5–4.0)	0.110

WHO-FC, World Health Organization functional class; 6MWD, 6 min walk distance; NT-proBNP, N-terminal pro B-type natriuretic peptide; sPAP, systolic pulmonary artery pressure; mPAP, mean pulmonary artery pressure; mRAP, mean right atrial pressure; PAWP, pulmonary arterial wedge pressure; (T) PVR, (total) pulmonary vascular resistance; CI, cardiac index.

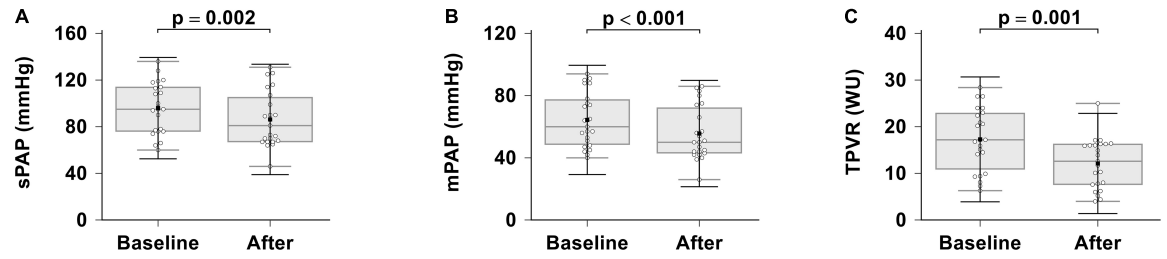

FIGURE 1 | Effects of ambrisentan plus PDE-5i combination therapy on hemodynamics. **(A)** sPAP; **(B)** mPAP; **(C)** TPVR. sPAP, systolic pulmonary artery pressure; mPAP, mean pulmonary artery pressure; TPVR, total pulmonary vascular resistance.

significant reduction in TRV (p = 0.021) and estimated PASP (p = 0.022) but not in tricuspid regurgitation (p = 0.166).

Right Ventricular Pulmonary Artery Coupling Improvement

In this study, we looked for RVPAC changes induced by ambrisentan plus PDE-5i combination therapy (**Table 4** and **Figure 3**). All RVPAC ratios (RVFAC/PASP, $p < 0.001$; RVSV/RVESV, $p < 0.001$; TAPSE/PASP, $p = 0.001$; S'/PASP, $p = 0.001$) were significantly increased. This indicates that combination therapy may result in significant improvements in RV function and decreases in RVPAC for patients with severe PAH.

TABLE 3 | Echocardiographic parameters at baseline and follow-up.

Variables (n = 27)	Baseline	Follow-up	P value
RV wall thickness, mm	8 (6–8)	7 (6–8)	0.713
S', cm/s	9.8 ± 1.8	12.2 ± 2.3	<0.001
E, cm/s	55.0 (42.0–80.0)	57.0 (42.0–77.0)	0.770
E', cm/s	9.4 (6.9–12.3)	9.0 (7.1–14.6)	0.259
E/E' ratio	7.1 ± 2.6	6.8 ± 3.0	0.664
TAPSE, mm	14.6 ± 2.1	17.5 ± 2.4	<0.001
TRV, cm/s	4.8 ± 0.7	4.4 ± 0.7	0.021
Tricuspid regurgitation, n (mild, moderate, severe)	12/9/6	15/8/4	0.166
PASP, mmHg	103 ± 29	90 ± 25	0.022
RVSV, mL	47 ± 18	49 ± 17	0.523
RVESV, mL	63 ± 24	51 ± 23	0.010
RVEDV, mL	110 ± 39	98 ± 38	0.076
RVSVi, mL/m^2	32 ± 2	33 ± 2	0.622
RVESVi, mL/m^2	42 ± 16	34 ± 14	0.004
RVEDVi, mL/m^2	74 ± 5	66 ± 4	0.041
RVCO, L/min	4.1 ± 1.8	4.5 ± 2.0	0.232
RVEF, %	43 ± 6	51 ± 5	<0.001
RVFAC, %	30 ± 6	37 ± 6	<0.001

S', tricuspid annular systolic velocity; E/e, tricuspid early diastolic transmitral flow velocity to averaged annular early diastolic velocity ratio; TAPSE, tricuspid annular plane systolic excursion; TRV, tricuspid regurgitation velocity; PASP, systolic pulmonary artery pressure; RVEDV, right ventricular end-diastolic volume; RVESV, right ventricular end-systolic volume; RVSV, right ventricular stroke volume; RVEDVi, right ventricular end-diastolic volume indexed; RVESVi, right ventricular end-systolic volume indexed; RVSVi, right ventricular stroke volume indexed; RVCO, right ventricular cardiac output; RVEF, right ventricular ejection fraction; RVFAC, right ventricular fractional area change.

Relationship Between Clinical Parameters and Right Ventricular Pulmonary Artery Coupling

The correlations between 6MWD, NT-proBNP levels, WHO-FC and RVPAC parameters were showed in **Table 5** and **Figure 4**. At the baseline, NT-proBNP levels had a significantly negative correlation with the SV/ESV and RVFAC/PASP ratio (p = 0.008, p = 0.037, respectively). The rest of measures had no significant correlation with the baseline functional parameters.

After treatment, NT-proBNP levels still had a significantly negative correlation with the SV/ESV ratio ($r = -0.560$; p = 0.003), but had no significant correlation with the TAPSE/PASP, RVFAC/PASP, S'/PASP ratios. WHO-FC was significantly negatively correlated with the TAPSE/PASP, RVFAC/PASP, S'/PASP ratios (p = 0.039, p = 0.031 and p = 0.027, respectively), but had no significant correlation with SV/ESV ratio. The 6MWD was significantly positively correlated with the TAPSE/PASP, RVFAC/PASP, S'/PASP ratio (p = 0.013, p = 0.011 and p = 0.012, respectively), but had no significant correlation with the SV/ESV ratio.

Interestingly, the improvement in TAPSE/PASP, S'/PASP, RVSV/RVESV correlated with a reduction in NT-proBNP levels and an increase in the 6MWD. But there is not any relationship between the baseline coupling and follow-up functional state.

Reproducibility

The results for the intraobserver and interobserver variability for 3DE RV volume and function assessment upon repeated measurements in 10 random patients were shown in **Table 6**. ICC values were higher for intraobserver and interobserver variability when the same images were analyzed by the two different cardiologists.

DISCUSSION

In the present study, a significant improvement in hemodynamics, RV function and RVPAC was demonstrated

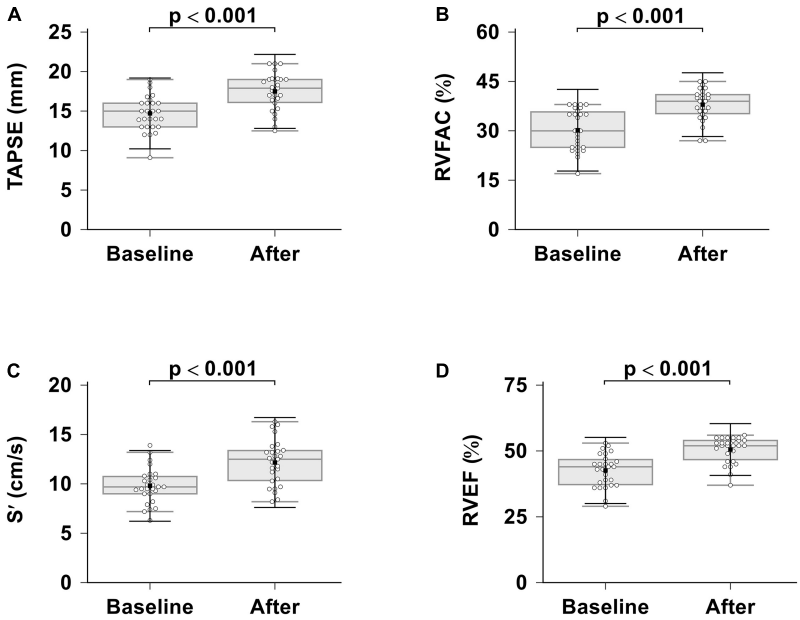

FIGURE 2 | Effects of ambrisentan plus PDE-5i combination therapy on RV systolic function. **(A)** TAPSE; **(B)** RVFAC; **(C)** S'; **(D)** RVEF. TAPSE, tricuspid annular plane systolic excursion; RVFAC, right ventricular fractional area change; S', tricuspid annular systolic velocity; RVEF, right ventricular ejection fraction.

TABLE 4 | Right ventricular pulmonary arterial coupling at baseline and follow-up.

RVPAC	Baseline	Follow-up	*P* value
RVFAC/PASP, %/mmHg	0.31 ± 0.10	0.44 ± 0.15	<0.001
TAPSE/PASP, mm/mmHg	0.15 ± 0.05	0.21 ± 0.06	0.001
S'/PASP, cm/s•mmHg	0.10 ± 0.03	0.14 ± 0.05	0.001
RVSV/RVESV	0.79 ± 0.22	1.02 ± 0.20	<0.001

RVPAC, Right ventricular pulmonary arterial coupling; S', tricuspid annular systolic velocity; TAPSE, tricuspid annular plane systolic excursion; PASP, systolic pulmonary artery pressure; RVESV, right ventricular end-systolic volume; RVSV, right ventricular stroke volume; RVFAC, right ventricular fractional area change.

as a result of 6 months of initial ambrisentan plus PDE-5i combination therapy. We also demonstrated that RVPAC parameters correlated with various clinical parameters such as the 6MWD, NT-proBNP levels and WHO-FC.

Current therapeutic options targeting prostacyclin, nitric oxide, or the endothelin pathway are involved in PAH patients. With regard to the updated treatment for PAH, the latest guidelines give a strong recommendation for the use of combination therapy, even for patients with milder WHO-FC II–III PAH (3). Previous reports offered important evidence and manifested a statistically significant greater decrease in hemodynamics and an enhancement in functional overall survival rates after initial combination therapy (21–25). Several studies showed the effect of combination therapy on afterload and RV reverse remodeling in PAH (25–29). Similar as previous studies, we observed a prominent elevation in RV function, including the S', RVEF, RVFAC, TAPSE and RVPAC ratios, a reduction in pulmonary artery pressure and RV afterload after combination therapy. In addition, 6 patients had WHO FC IV at baseline, and the current guidelines emphasize the initiation of prostacyclin analog therapy for these patients. The initial combination therapy strategy based on the comprehensive risk assessment in guidelines for the diagnosis and treatment of pulmonary hypertension (3). The patients can be classified as low risk, intermediate risk or high risk for clinical worsening or death. There were 4 patients treated with ambrisentan and PDE5i for intermediate risk, 2 patients for high risk were inoperable with initial triple combination therapy including i.v. treprostinil. D'Alto et al. showed that triple upfront combination therapy with ambrisentan, tadalafil, and subcutaneous treprostinil in severe non-reversible PAH is associated with considerable clinical and hemodynamic improvement and RV reverse remodeling.

Compared with the baseline, our study showed differences in WHO-FC and 6MWD after 6–12 months of initial combination therapy. This finding is consistent with the results of the AMBITION trial in which significant differences were observed in favor of combination therapy (21, 24). Furthermore, the differences in CI and mRAP were not significant. In our study, patients had a baseline median CI of 2.5 L/min/m^2, undifferentiated mRAP and a median follow-up E/E' of 6.8, which was indicative of RV dysfunction (3, 9). The reason CI was not improved may be that there was a subset of patients with severe tricuspid regurgitation. Our results did not show an improvement in tricuspid regurgitation. A previous report showed that tricuspid regurgitation progression was associated with worsening pulmonary hypertension and adverse RV and TV apparatus remodel in patients with PAH (30).

Regarding cardiac volumes, we observed decreases in RVEDVi and RVESVi, while RVSVi remained unchanged after treatment. These findings are partly similar to those found in previous research (26), Van de Veerdonk et al. showed that RV volumes (RVSV, RVESV, RVEDV) improved after

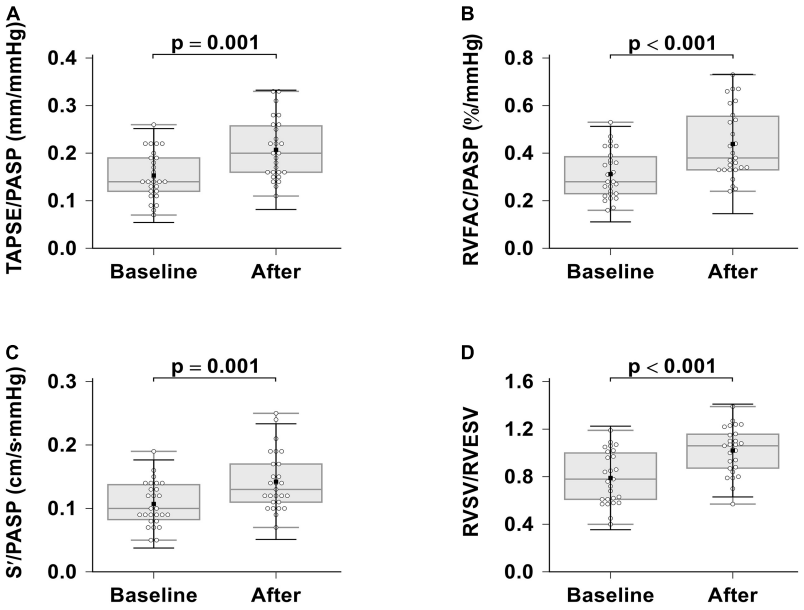

FIGURE 3 | Effects of ambrisentan plus PDE-5i combination therapy on right ventricular pulmonary arterial coupling. **(A)** TAPSE/PASP; **(B)** RVFAC/PASP; **(C)** S'/PASP; **(D)** RVSV/RVESV. TAPSE, tricuspid annular plane systolic excursion; RVFAC, right ventricular fractional area change, S', tricuspid annular systolic velocity; PASP, systolic pulmonary artery pressure, RVEF, right ventricular ejection fraction; RVESV, right ventricular end-systolic volume; RVSV, right ventricular stroke volume.

TABLE 5 | Correlation of right ventricular pulmonary arterial coupling to functional status.

RVPAC	Correlation with NT-proBNP		Correlation with WHO FC		Correlation with 6MWD	
	R	*P* value	R	*P* value	R	*P* value
Baseline RVPAC vs. baseline functional status						
TAPSE/PASP	−0.274	0.167	−0.010	0.962	0.210	0.294
RVFAC/PASP	−0.403	0.037	−0.020	0.923	0.207	0.300
S'/PASP	−0.231	0.247	−0.007	0.965	0.202	0.312
RVSV/RVESV	−0.501	0.008	−0.181	0.366	0.270	0.173
Follow-up RVPAC vs. follow-up functional status						
TAPSE/PASP	−0.129	0.521	−0.399	0.039	0.468	0.013
RVFAC/PASP	−0.177	0.377	−0.417	0.031	0.482	0.011
S'/PASP	−0.310	0.116	−0.425	0.027	0.474	0.012
RVSV/RVESV	−0.560	0.003	−0.020	0.920	0.236	0.235
Changes in RVPAC vs. changes in functional status						
ΔTAPSE/PASP	0.446	0.020	0.015	0.940	0.445	0.020
ΔRVFAC/PASP	0.359	0.066	0.076	0.706	0.306	0.117
ΔS'/PASP	0.430	0.025	0.240	0.906	0.431	0.025
ΔRVSV/RVESV	0.416	0.031	0.046	0.818	0.552	0.003

Correlation between right ventricular pulmonary arterial coupling ratios and functional status was evaluated by the Spearman rank correlation coefficient or Pearson correlation coefficient.

Δ, change; 6MWD, 6 min walk distance; WHO-FC, World Health Organization functional class; NT-proBNP, N-terminal pro B-type natriuretic peptide. RVPAC, Right ventricular pulmonary arterial coupling; S', tricuspid annular systolic velocity; TAPSE, tricuspid annular plane systolic excursion; PASP, systolic pulmonary artery pressure; RVESV, right ventricular end-systolic volume; RVSV, right ventricular stroke volume; RVFAC, right ventricular fractional area change.

combination therapy compared with the monotherapy group. Although reverse remodeling of the right heart is associated with functional improvement, moderate improvements in RV function may not result in a decrease in right heart size (31). We hypothesize that the consequence in this study may be due to the RV maladaptive remodeling that occurred in our severe PAH patients compared to those in an earlier stage of PAH. Usually, RV remodeling in PAH differentiates 2 patterns of ventricular remodeling: adaptive and maladaptive remodeling (32). Adaptive remodeling resembles the fetal RV phenotype and is characterized by concentric hypertrophy with slight eccentric dilatation and fibrosis, preserved systolic

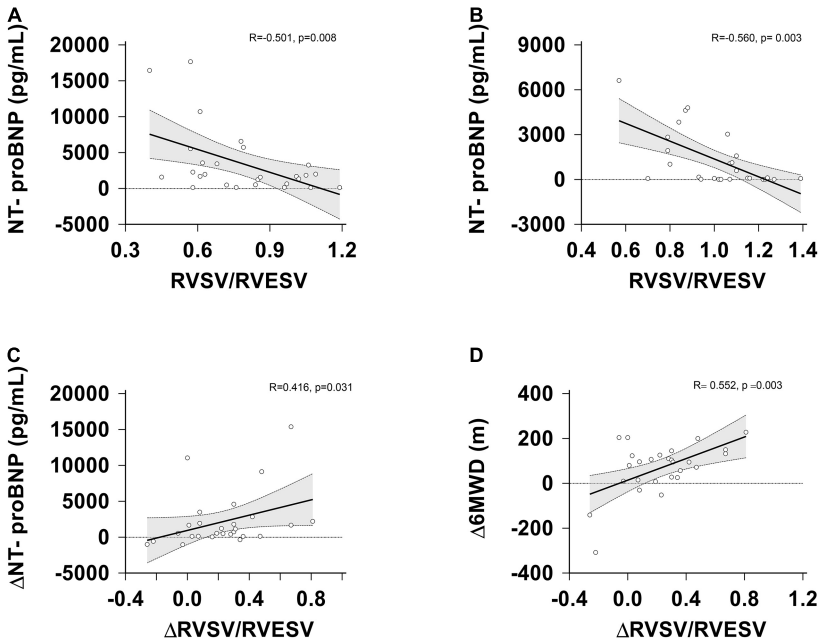

FIGURE 4 | Correlation between RVSV/RVESV, △RVSV/RVESV, NT-proBNP, △NT-proBNP and △6MWD at the baseline and follow-up assessment. **(A)** RVSV/RVESV vs. NT-proBNP levels at the baseline; **(B)** RVSV/RVESV vs. NT-proBNP levels at the follow-up; **(C)** changes in RVSV/RVESV vs. changes in NT-proBNP levels. **(D)** changes in RVSV/RVESV vs. changes in the 6MWD. △, change; RVESV, right ventricular end-systolic volume; RVSV, right ventricular stroke volume; NT-proBNP, N-terminal pro B-type natriuretic peptide.

TABLE 6 | ICCs for intra- and interobserver variability for 3DE RV measurements.

Variable	Interobserver variability		Intraobserver variability	
	ICC	95% CI	ICC	95% CI
RVEDV	0.990	0.960–0.997	0.991	0.965–0.998
RVESV	0.975	0.909–0.998	0.993	0.972–0.998
RVSV	0.991	0.910–0.994	0.972	0.888–0.993
RVEF	0.935	0.746–0.984	0.949	0.802–0.987
RVCO	0.988	0.952–0.997	0.987	0.947–0.997

ICC, intraclass correlation coefficient; RVEDV, right ventricular end-diastolic volume; RVESV, right ventricular end-systolic volume; RVSV, right ventricular stroke volume; RVCO, right ventricular cardiac output; RVEF, right ventricular ejection fraction.

and diastolic function, and maintained of normal cardiac output and filling pressures (33–35). In these subjects, the RV is more capable of coping with increased RV afterload and is characterized by concentric remodeling, probably because a fetal phenotype is maintained throughout life, therefore developing compensatory hypertrophy over dilatation. Conversely, maladaptive remodeling causes eccentric dilatation, excessive fibrosis and worse systolic and diastolic function, in addition to reducing the ejection fraction, cardiac output and elevating filling pressures (32, 34). A previous report showed that the reversal of RV remodeling in IPAH patients after 1-year of targeted treatment, is difficult and complex (36). We speculate that a potential cause for the lack of improvement in RVSV is most likely related to the relatively small number of patients in our study.

Previous research is limited to estimating routine RV echocardiographic parameters or invasive measurements. No published studies have examined the effects of echocardiographic measures of RVPAC after initial ambrisentan plus PDE-5i combination therapy in severe PAH patients.

The gold-standard method to assess RVPAC in clinical practice should use RHC and was used to assess treatment response in the ERS/ESC guidelines (3). Not all medical institutions set up routine hemodynamic evaluation centers. A number of studies indicate that non-invasive echocardiography may be superior to invasive RHC or relatively expensive cardiac magnetic resonance imaging (CMRI) for routine follow-up of patients with PAH.

In our study, the TAPSE/PASP, RVFAC/PASP, RVSV/RVESV and S'/PASP ratios were considered indices of RVPAC. Some previous studies showed that TAPSE/PASP were crucial surrogates for describing RVPAC and emerged as an independent predictor of Ees/Ea (10, 11, 37). A correlation analysis revealed a significant direct relationship between the TAPSE/PASP ratio and pro-BNP levels. While the TAPSE/PASP ratio has been substantiated in patients with PAH, only a few studies have explored the significance of the other parameters. Several other ratios have been proposed to estimate RVPAC. The FAC/RV systolic pressure (RVSP) or TAPSE/RVSP ratio has been shown to be of superior prognostic value compared with RV systolic function (FAC or TAPSE) in other studies (38–40). Jentzer et al. (15) described the relationship between the lower tricuspid annular systolic velocity (TASV)/RVSP ratio derived from Doppler transthoracic echocardiography and short-term and

long-term mortality in cardiac intensive care unit patients. Similarly, because Ees and Ea share a common pressure term, coupling can be simplified as SV/ESV and is quantifiable with magnetic resonance (41). A cutoff value of approximately 0.54 for SV/ESV prediction has been validated as a predictor of poor outcomes in patients with PH (16). The SV/ESV ratio as a volume estimate of coupling ratio correlates with RV strain and is a strong predictor of adverse clinical events in pediatric PH (33). The SV/ESV ratio was suitable for patients with limited TR signals.

In this study, the mean baseline TAPSE/PASP was fairly low at 0.14 mm/mmHg and had a lower mean baseline RVSV of 47 mL, which suggested a rather sick PAH patient population. However, baseline 3D RV volumes do not seem to be consistent with such a low TAPSE/PASP. According to Telio et al. (37), the patient population had severe PH with a mean Ees/Ea ratio of 0.70, a mean TAPSE/PASP ratio of 0.28 mm/mmHg (0.19–0.42), a TAPSE/PASP cutoff of 0.31 mm/mmHg, an RV end-diastolic volume/body surface area of 111 mL/m^2 (88–144), and RVSV of 71 mL (59–95), which implied that they were already in an RV-PA uncoupling state. Compared with Gerges et al. (42) who examined TAPSE/PASP in patients with combined pre- and postcapillary PH and idiopathic PAH, the mean TAPSE/PASP ratio in that study of patients with idiopathic PAH was 0.14 ± 0.11 mm/mmHg. Whether these results can be extrapolated for patients with other etiologies of PH, as well for different stages of severity of PH, the conclusion is guarded. One possible explanation for this result is that RV volumes tend to reach a minimum as RV progresses. dysfunction. Another possibility that cannot be ruled out is that we overestimated the PASP that was calculated using the modified Bernoulli equation [PASP = 4 (TRV)^2 + RAP].

In addition, NT-proBNP, WHO-FC and 6MWD seem to be stronger predictors of prognosis and survival (3). We found that the SV/ESV ratio had a stronger negative correlation with log-transformed NT-proBNP levels. The ratios of RVFAC/PASP, TAPSE/PASP and S'/PASP were correlated with WHO-FC and 6MWD. In contrast, our results failed to demonstrate a correlation between the TAPSE/PASP ratio and NT-proBNP levels. However, we remain firmly convinced of the importance of the TAPSE/PASP ratio in RV function and clinical outcome. Routine measurements are limited because of the complex shape of the RV and the interaction between the RV and pulmonary vascular system. While multiple non-invasive parameters to approximate RV function have been studied, one of the more promising methods is the use of the TAPSE/PASP ratio (10). A better RVPAC might reflect both a significant reversible remodeling of the RV and a fixed decrease in pulmonary vascular resistances. Clinically, these patients probably have reversible structural damage and are more prone to benefit from ambrisentan plus PDE-5i combination therapy. The TAPSE/PASP ratio has been validated in patients with PAH; however, the other parameters have not and there are minimal data on many of them. The means by which to interpret these other parameters are unclear, and their relevance is questionable. Non-invasive imaging of RV structure and function is essential to monitoring patients with PAH and appraising the RV response to pulmonary vascular remodeling. Our study attempts to provide potential useful parameters of RV-PA coupling for characterizing RV function and clinical improvement from a new perspective.

No prior study has reported on the effects of ambrisentan plus PDE-5i combination therapy on RV remodeling and RVPAC in severe PAH patients by non-invasive echocardiography, which provides important information about the effectiveness of combination therapy. Our study indicate that ambrisentan plus PDE-5i combination therapy may result in significant improvements in RV systolic function and RVPAC for severe PAH patients. Most importantly, RVPAC parameters were related to the 6MWD, NT-proBNP levels and WHO FC, which established prognostic markers in PAH.

Strengths and Limitations

The advantage of the current study lies in detailed information, including clinical functional status, laboratory data, and invasive hemodynamic and non-invasive echocardiography data. There are several limitations to this study. First, the present study was performed as a retrospective observational, single-center cohort, small population study. Due to the small sample size, we were unable to perform quantitative analysis and identify risk factors. Second, considering the high cost of, balloon wedge catheter, pulmonary arterial wedge pressure (PAWP) during RHC was only performed at the first diagnosis (i.e., baseline) in our study. At follow-up measurements, RHC was performed using more economical MPA2 angiographic catheter under fluoroscopic guidance, in 23 patients. and it is different to further analyze the relationship between hemodynamic Ees/Ea and echocardiographic RVPAC. Then, a mix of therapies dose showed in the study. Finally, long-term follow-up was not conducted, however, large-scale, long-term, multicenter prospective studies are needed or confirmation.

CONCLUSION

In conclusion, ambrisentan plus PDE-5i combination therapy resulted in a significant improvement in RV systolic function and RVPAC in patients with severe PAH. These findings provide insight into the hemodynamic and RV effects of ambrisentan plus PDE-5i combination therapy. More importantly, the RVPAC correlated with known prognostic markers of PAH. RVPAC may be an accurate non-invasive and sensitive marker of RV function and clinical improvement in response to combination therapy. Considering multiple factors such as a small number of patients, the conclusion is guarded. Therefore, future prospective studies are required to determine whether or how long combination therapy optimizes RV reverse remodeling and to evaluate treatment outcomes based on a long-term follow-up patients of severe PAH to provide further insights into clinical practice.

DATA AVAILABILITY STATEMENT

The original contributions presented in the study are included in the article/supplementary material, further inquiries can be directed to the corresponding author/s.

ETHICS STATEMENT

The studies involving human participants were reviewed and approved by the Ethics Committee of First Affiliated Hospital of Guangxi Medical University. The patients/participants provided their written informed consent to participate in this study. Written informed consent was obtained from the individual(s) for the publication of any potentially identifiable images or data included in this article.

AUTHOR CONTRIBUTIONS

W-FL: conception, methodology, data curation, formal analysis, writing-original draft, and writing-review and editing. YD: conceptualization, methodology, design, and writing-review and editing. BW, KH, PD, S-SX, and D-DW: data curation. All authors have read and approved the final manuscript.

FUNDING

This study was supported by grants from National Natural Science Foundation of China (Grant no. 82060051); the projects of Guangxi medical and health appropriate technology development and promotion application (Grant no. S2020030); the Precision Medicine Foundation of Guangxi Key Laboratory of Cardio-cerebrovascular Disease (Grant no. GXXNXG202001); Guangxi medical "139" Program for Training High-level Backbone Talents (Grant no. G201903053) and Project of training one thousand young and middle aged backbone teachers of Guangxi.

REFERENCES

1. Hoeper MM, Ghofrani HA, Grunig E, Klose H, Olschewski H, Rosenkranz S. Pulmonary hypertension. *Dtsch Arztebl Int.* (2017) 114:73–84.
2. Thenappan T, Ormiston ML, Ryan JJ, Archer SL. Pulmonary arterial hypertension: pathogenesis and clinical management. *BMJ.* (2018) 360:j5492. doi: 10.1136/bmj.j5492
3. Galie N, Humbert M, Vachiery JL, Gibbs S, Lang I, Torbicki A, et al. 2015 ESC/ERS Guidelines for the diagnosis and treatment of pulmonary hypertension: the joint task force for the diagnosis and treatment of pulmonary hypertension of the European society of cardiology (ESC) and the European respiratory society (ERS): endorsed by: association for European paediatric and congenital cardiology (AEPC), international society for heart and lung transplantation (ISHLT). *Eur Heart J.* (2016) 37:67–119. doi: 10.1093/eurheartj/ehv317
4. Galiè N, Channick RN, Frantz RP, Grünig E, Jing ZC, Moiseeva O, et al. Risk stratification and medical therapy of pulmonary arterial hypertension. *Eur Respir J.* (2019) 53:1801889. doi: 10.1183/13993003.01889-2018
5. Beshay S, Sahay S, Humbert M. Evaluation and management of pulmonary arterial hypertension. *Respir Med.* (2020) 171:106099.
6. Vonk Noordegraaf A, Westerhof BE, Westerhof N. The relationship between the right ventricle and its load in pulmonary hypertension. *J Am Coll Cardiol.* (2017) 69:236–43. doi: 10.1016/j.jacc.2016.10.047
7. Tello K, Dalmer A, Axmann J, Vanderpool R, Ghofrani HA, Naeije R, et al. Reserve of right ventricular-arterial coupling in the setting of chronic overload. *Circ Heart Fail.* (2019) 12:e005512. doi: 10.1161/CIRCHEARTFAILURE.118.005512
8. Vonk Noordegraaf A, Chin KM, Haddad F, Hassoun PM, Hemnes AR, Hopkins SR, et al. Pathophysiology of the right ventricle and of the pulmonary circulation in pulmonary hypertension: an update. *Eur Respir J.* (2019) 53:1801900. doi: 10.1183/13993003.01900-2018
9. Rudski LG, Lai WW, Afilalo J, Hua L, Handschumacher MD, Chandrasekaran K, et al. Guidelines for the echocardiographic assessment of the right heart in adults: a report from the American society of echocardiography endorsed by the european association of echocardiography, a registered branch of the European society of cardiology, and the Canadian society of echocardiography. *J Am Soc Echocardiogr.* (2010) 23:685–713; quiz86–8. doi: 10.1016/j.echo.2010.05.010
10. Bashline MJ, Simon MA. Use of tricuspid annular plane systolic excursion/pulmonary artery systolic pressure as a non-invasive method to assess right ventricular-PA coupling in patients with pulmonary hypertension. *Circ Cardiovasc Imaging.* (2019) 12:e009648. doi: 10.1161/CIRCIMAGING.119.009648
11. Vriz O, Pirisi M, Bossone E, Fadl ElMula FEM, Palatini P, Naeije R. Right ventricular-pulmonary arterial uncoupling in mild-to-moderate systemic hypertension. *J Hypertens.* (2020) 38:274–81. doi: 10.1097/HJH.0000000000002238
12. Forton K, Motoji Y, Caravita S, Faoro V, Naeije R. Exercise stress echocardiography of the pulmonary circulation and right ventricular-arterial coupling in healthy adolescents. *Eur Heart J Cardiovasc Imaging.* (2021) 22:688–94. doi: 10.1093/ehjci/jeaa085
13. Braganca B, Trepa M, Santos R, Silveira I, Fontes-Oliveira M, Sousa MJ, et al. Echocardiographic assessment of right ventriculo-arterial coupling: clinical correlates and prognostic impact in heart failure patients undergoing cardiac resynchronization therapy. *J Cardiovasc Imaging.* (2020) 28:109–20. doi: 10.4250/jcvi.2019.0094
14. Tello K, Axmann J, Ghofrani HA, Naeije R, Narcin N, Rieth A, et al. Relevance of the TAPSE/PASP ratio in pulmonary arterial hypertension. *Int J Cardiol.* (2018) 266:229–35. doi: 10.1016/j.ijcard.2018.01.053
15. Jentzer JC, Anavekar NS, Reddy YNV, Murphree DH, Wiley BM, Oh JK, et al. Right ventricular pulmonary artery coupling and mortality in cardiac intensive care unit patients. *J Am Heart Assoc.* (2021) 10:e019015. doi: 10.1161/JAHA.120.019015
16. Jone PN, Schafer M, Pan Z, Ivy DD. Right ventricular-arterial coupling ratio derived from 3-dimensional echocardiography predicts outcomes in pediatric pulmonary hypertension. *Circ Cardiovasc Imaging.* (2019) 12:e008176. doi: 10.1161/CIRCIMAGING.118.008176
17. Corris P, Degano B. Severe pulmonary arterial hypertension: treatment options and the bridge to transplantation. *Eur Respir Rev.* (2014) 23:488–97. doi: 10.1183/09059180.00007214
18. Agarwala P, Salzman SH. Six-minute walk test: clinical role, technique, coding, and reimbursement. *Chest.* (2020) 157:603–11. doi: 10.1016/j.chest.2019.10.014
19. Krishnan A, Markham R, Savage M, Wong YW, Walters D. Right heart catheterisation: how to do it. *Heart Lung Circ.* (2019) 28:e71–8. doi: 10.1016/j.hlc.2018.08.005
20. Lang RM, Badano LP, Mor-Avi V, Afilalo J, Armstrong A, Ernande L, et al. Recommendations for cardiac chamber quantification by echocardiography in adults: an update from the American society of echocardiography and the European association of cardiovascular imaging. *J Am Soc Echocardiogr.* (2015) 28:e14.
21. Galie N, Barbera JA, Frost AE, Ghofrani HA, Hoeper MM, McLaughlin VV, et al. Initial use of ambrisentan plus tadalafil in pulmonary arterial hypertension. *N Engl J Med.* (2015) 373:834–44. doi: 10.1056/NEJMoa1413687
22. Sitbon O, Sattler C, Bertoletti L, Savale L, Cottin V, Jaïs X, et al. Initial dual oral combination therapy in pulmonary arterial hypertension. *Eur Respir J.* (2016) 47:1727–36. doi: 10.1183/13993003.02043-2015
23. Sitbon O, Jaïs X, Savale L, Cottin V, Bergot E, Macari EA, et al. Upfront triple combination therapy in pulmonary arterial hypertension: a pilot study. *Eur Respir J.* (2014) 43:1691–7. doi: 10.1183/09031936.00116313
24. Sitbon O, Cottin V, Canuet M, Clerson P, Gressin V, Perchenet L, et al. Initial combination therapy of macitentan and tadalafil in pulmonary arterial hypertension. *Eur Respir J.* (2020) 56:2000673. doi: 10.1183/13993003.00673-2020

25. D'Alto M, Badagliacca R, Argiento P, Romeo E, Farro A, Papa S, et al. Risk reduction and right heart reverse remodeling by upfront triple combination therapy in pulmonary arterial hypertension. *Chest.* (2020) 157:376–83. doi: 10.1016/j.chest.2019.09.009
26. van de Veerdonk MC, Huis In T Veld AE, Marcus JT, Westerhof N, Heymans MW, Bogaard HJ, et al. Upfront combination therapy reduces right ventricular volumes in pulmonary arterial hypertension. *Eur Respir J.* (2017) 49:1700007. doi: 10.1183/13993003.00007-2017
27. Taran IN, Belevskaya AA, Saidova MA, Martynyuk TV, Chazova IE. Initial riociguat monotherapy and transition from sildenafil to riociguat in patients with idiopathic pulmonary arterial hypertension: influence on right heart remodeling and right ventricular-pulmonary arterial coupling. *Lung.* (2018) 196:745–53. doi: 10.1007/s00408-018-0160-4
28. Huis In't Veld AE, Oosterveer FPT, De Man FS, Marcus JT, Nossent EJ, Boonstra A, et al. Hemodynamic effects of pulmonary arterial hypertension-specific therapy in patients with heart failure with preserved ejection fraction and with combined post- and precapillay pulmonary hypertension. *J Card Fail.* (2020) 26:26–34. doi: 10.1016/j.cardfail.2019.07.547
29. Badagliacca R, D'Alto M, Ghio S, Argiento P, Bellomo V, Brunetti ND, et al. Risk reduction and hemodynamics with initial combination therapy in pulmonary arterial hypertension. *Am J Respir Crit Care Med.* (2021) 203:484–92. doi: 10.1164/rccm.202004-1006OC
30. Medvedofsky D, Aronson D, Gomberg-Maitland M, Thomeas V, Rich S, Spencer K, et al. Tricuspid regurgitation progression and regression in pulmonary arterial hypertension: implications for right ventricular and tricuspid valve apparatus geometry and patients outcome. *Eur Heart J Cardiovasc Imaging.* (2017) 18:86–94. doi: 10.1093/ehjci/jew010
31. Badagliacca R, Papa S, Matsubara H, Lang IM, Poscia R, Manzi G, et al. The importance of right ventricular evaluation in risk assessment and therapeutic strategies: raising the bar in pulmonary arterial hypertension. *Int J Cardiol.* (2020) 301:183–9. doi: 10.1016/j.ijcard.2019.10.043
32. Vonk-Noordegraaf A, Haddad F, Chin KM, Forfia PR, Kawut SM, Lumens J, et al. Right heart adaptation to pulmonary arterial hypertension: physiology and pathobiology. *J Am Coll Cardiol.* (2013) 62:D22–33.
33. Sanz J, Sanchez-Quintana D, Bossone E, Bogaard HJ, Naeije R. Anatomy, Function, and dysfunction of the right ventricle: JACC state-of-the-art review. *J Am Coll Cardiol.* (2019) 73:1463–82. doi: 10.1016/j.jacc.2018.12.076
34. Prins KW, Thenappan T. World health organization group I pulmonary hypertension: epidemiology and pathophysiology. *Cardiol Clin.* (2016) 34:363–74. doi: 10.1016/j.ccl.2016.04.001
35. Guimaron S, Guihaire J, Amsallem M, Haddad F, Fadel E, Mercier O. Current knowledge and recent advances of right ventricular molecular biology and metabolism from congenital heart disease to chronic pulmonary hypertension. *Biomed Res Int.* (2018) 2018:1981568. doi: 10.1155/2018/1981568
36. Naeije R, Manes A. The right ventricle in pulmonary arterial hypertension. *Eur Respir Rev.* (2014) 23:476–87.
37. Tello K, Wan J, Dalmer A, Vanderpool R, Ghofrani HA, Naeije R, et al. Validation of the tricuspid annular plane systolic excursion/systolic pulmonary artery pressure ratio for the assessment of right ventricular-arterial coupling in severe pulmonary hypertension. *Circ Cardiovasc Imaging.* (2019) 12:e009047.
38. Egbe AC, Kothapalli S, Miranda WR, Pislaru S, Ammash NM, Borlaug BA, et al. Assessment of right ventricular-pulmonary arterial coupling in chronic pulmonary regurgitation. *Can J Cardiol.* (2019) 35:914–22. doi: 10.1016/j.cjca.2019.03.009
39. Hussain I, Mohammed SF, Forfia PR, Lewis GD, Borlaug BA, Gallup DS, et al. Impaired right ventricular-pulmonary arterial coupling and effect of sildenafil in heart failure with preserved ejection fraction: an ancillary analysis from the phosphodiesterase-5 inhibition to improve clinical status and exercise capacity in diastolic heart failure (RELAX) trial. *Circ Heart Fail.* (2016) 9:e002729. doi: 10.1161/CIRCHEARTFAILURE.115.002729
40. Vanderpool RR, Pinsky MR, Naeije R, Deible C, Kosaraju V, Bunner C, et al. RV-pulmonary arterial coupling predicts outcome in patients referred for pulmonary hypertension. *Heart.* (2015) 101:37–43. doi: 10.1136/heartjnl-2014-306142
41. Sanz J, García-Alvarez A, Fernández-Friera L, Nair A, Mirelis JG, Sawit ST, et al. Right ventriculo-arterial coupling in pulmonary hypertension: a magnetic resonance study. *Heart.* (2012) 98:238–43. doi: 10.1136/heartjnl-2011-300462
42. Gerges M, Gerges C, Pistritto AM, Lang MB, Trip P, Jakowitsch J, et al. Pulmonary hypertension in heart failure. Epidemiology, right ventricular function, and survival. *Am J Respir Crit Care Med.* (2015) 192:1234–46. doi: 10.1164/rccm.201503-0529OC

Conflict of Interest: The authors declare that the research was conducted in the absence of any commercial or financial relationships that could be construed as a potential conflict of interest.

frontiers | Frontiers in Cardiovascular Medicine

TYPE Original Research
PUBLISHED 16 February 2023
DOI 10.3389/fcvm.2023.1082725

OPEN ACCESS

EDITED BY
Andreas Rolf,
Kerckhoff Klinik, Germany

REVIEWED BY
Eleonora Avenatti,
Houston Methodist Hospital, United States
Sebastian Kelle,
German Heart Center Berlin, Germany

*CORRESPONDENCE
Attila Kovács
✉ attila.kovacs@med.semmelweis-univ.hu

†These authors have contributed equally to this work

SPECIALTY SECTION
This article was submitted to Cardiovascular Imaging, a section of the journal Frontiers in Cardiovascular Medicine

RECEIVED 28 October 2022
ACCEPTED 30 January 2023
PUBLISHED 16 February 2023

CITATION
Tolvaj M, Fábián A, Tokodi M, Lakatos B, Assabiny A, Ladányi Z, Shiida K, Ferencz A, Schwertner W, Veres B, Kosztin A, Szijártó Á, Sax B, Merkely B and Kovács A (2023) There is more than just longitudinal strain: Prognostic significance of biventricular circumferential mechanics.
Front. Cardiovasc. Med. 10:1082725.
doi: 10.3389/fcvm.2023.1082725

There is more than just longitudinal strain: Prognostic significance of biventricular circumferential mechanics

Máté Tolvaj, Alexandra Fábián, Márton Tokodi, Bálint Lakatos, Alexandra Assabiny, Zsuzsanna Ladányi, Kai Shiida, Andrea Ferencz, Walter Schwertner, Boglárka Veres, Annamária Kosztin, Ádám Szijártó, Balázs Sax, Béla Merkely† and Attila Kovács*†

Semmelweis University Heart and Vascular Center, Budapest, Hungary

Introduction: Despite the significant contribution of circumferential shortening to the global ventricular function, data are scarce concerning its prognostic value on long-term mortality. Accordingly, our study aimed to assess both left (LV) and right ventricular (RV) global longitudinal (GLS) and global circumferential strain (GCS) using three-dimensional echocardiography (3DE) to determine their prognostic importance.

Methods: Three hundred fifty-seven patients with a wide variety of left-sided cardiac diseases were retrospectively identified (64 ± 15 years, 70% males) who underwent clinically indicated 3DE. LV and RV GLS, and GCS were quantified. To determine the prognostic power of the different patterns of biventricular mechanics, we divided the patient population into four groups. Group 1 consisted of patients with both LV GLS and RV GCS above the respective median values; Group 2 was defined as patients with LV GLS below the median while RV GCS above the median, whereas in Group 3, patients had LV GLS values above the median, while RV GCS was below median. Group 4 was defined as patients with both LV GLS and RV GCS below the median. Patients were followed up for a median of 41 months. The primary endpoint was all-cause mortality.

Results: Fifty-five patients (15%) met the primary endpoint. Impaired values of both LV GCS (HR, 1.056 [95% CI, 1.027–1.085], $p < 0.001$) and RV GCS (1.115 [1.068–1.164], $p < 0.001$) were associated with increased risk of death by univariable Cox regression. Patients with both LV GLS and RV GCS below the median (Group 4) had a more than 5-fold increased risk of death compared with those in Group 1 (5.089 [2.399–10.793], $p < 0.001$) and more than 3.5-fold compared with those in Group 2 (3.565 [1.256–10.122], $p = 0.017$). Interestingly, there was no significant difference in mortality between Group 3 (with LV GLS above the median) and Group 4, but being categorized into Group 3 versus Group 1 still held a more than 3-fold risk (3.099 [1.284–7.484], $p = 0.012$).

Discussion: The impaired values of both LV and RV GCS are associated with long-term all-cause mortality, emphasizing the importance of assessing biventricular circumferential mechanics. Reduced RV GCS is associated with significantly increased risk of mortality even if LV GLS is preserved.

KEYWORDS

speckle tracking echocardiography, 3D echocardiography, global longitudinal strain, global circumferential strain, heart failure

Introduction

Longitudinal strain (LS) of the left (LV) and right ventricles (RV) is a well-established biomarker of ventricular dysfunction, having a robust predictive power to future adverse outcomes in numerous cardiac diseases (1, 2). In contrast to ejection fraction (EF), a global measure of pump function, LS enables the quantification of ventricular deformation along their long axis. As many cardiac disease processes primarily affect the mainly longitudinally-oriented subendocardial layer, the measurement of LS is more sensitive to subtle changes and possesses added prognostic power compared to EF (2, 3).

Besides longitudinal shortening, also circumferential deformation contributes significantly to the ventricular pump function (4, 5). Thus, global ventricular function is the resultant of these two distinct but interconnected deformation components. Despite the unequivocal importance of circumferential shortening in biventricular function, data are scarce concerning its prognostic value on long-term mortality.

The advantages of three-dimensional echocardiography (3DE) over conventional echocardiography opens the door for a more thorough understanding and quantification of the ventricular structure and function, including the measurement of the circumferential strain of both the LV and the RV.

Although the detailed assessment of RV function is commonly neglected in left-sided heart diseases, it has been proved that patients who develop RV dysfunction are more symptomatic and carry a higher risk for long-term adverse outcomes than those who do not (6). Importantly, the prognostic value of RV function was also found to be independent of LV function in these patients (7). Therefore, the detailed assessment of the RV mechanics has increasing importance in identifying patients at risk for developing right heart failure and subsequent adverse outcomes.

Accordingly, we aimed to assess LV and RV GLS and GCS using 3DE to determine their prognostic relevance.

Methods

Study design and population

Clinically and hemodynamically stable patients with an established diagnosis of left-sided cardiac disease were identified from the previously published RVENet dataset [https://rvenet.github.io/dataset/], which comprises of individuals underwent clinically indicated 2D and 3D transthoracic echocardiography at our Center between November 2013 and March 2021. Exclusion criteria were 1) suspicion or presence of any primary right-sided cardiac disease at the first report or during the review process of the previously acquired datasets and 2) suboptimal LV and RV 3D dataset image quality for the respective 3D analysis. Demographic and clinical data (age, body surface area, body mass index, systolic and diastolic blood pressure, heart rate, cardiovascular risk factors, comorbidities, medical history, and laboratory parameters) were retrieved from the electronic clinical records. Obtaining written informed consent was waived due to the retrospective nature of the analysis. Our study protocol follows the Declaration of Helsinki and it was approved by the Semmelweis University Regional and Institutional Committee of Science and Research Ethics (approval No. 190/2020).

Two- and three-dimensional echocardiography

Transthoracic echocardiographic examinations were performed on commercially available ultrasound systems (E95, 4Vc-D probe, GE Vingmed Ultrasound, Horten, Norway, and EPIQ 7, X5-1 probe, Philips Medical Systems, Best, the Netherlands). A standard acquisition protocol consisting of 2D loops from parasternal, apical, and subxiphoid views was applied. LV internal diameters, wall thicknesses, relative wall thickness, and mass; left atrial (LA) 2D end-systolic volume; mitral inflow velocities such as early (E) and late diastolic (A) peak velocities, their ratio, and E wave deceleration time; systolic (s'), early diastolic (e'), and atrial (a') velocities of the mitral lateral and septal annulus; average E/e'; RV basal short-axis diameter, tricuspid annular plane systolic excursion (TAPSE), fractional area change (FAC); right ventricular systolic pressure (RVSP) and right atrial (RA) 2D end-systolic volume were measured according to current guidelines (8).

Beyond conventional echocardiographic examination, ECG-gated full-volume 3D datasets reconstructed from four cardiac cycles optimized for the left or the right heart were obtained for further analysis on a separate workstation. 3D datasets focused on the left heart were processed using semiautomated, commercially available software (4D LV-Analysis 3, TomTec Imaging, Unterschleissheim, Germany). We determined LV end-diastolic volume index (EDVi), end-systolic volume index (ESVi), stroke volume index (SVi), and mass index (Mi). To assess global LV function, ejection fraction (EF), 3D global longitudinal strain (GLS), and 3D global circumferential strain (GCS) were also calculated. Concerning the right heart, we quantified 3D RV EDVi, ESVi, SVi, EF, and septal and free wall two-dimensional longitudinal strain as well (4D RV-Function 2, TomTec Imaging). Using the ReVISION software (Argus Cognitive, Inc., Lebanon, NH, USA), we have quantified 3D RV GLS and GCS as previously described (9). By convention, GLS and GCS values are negative, meaning that less negative values refer to more impaired ventricular function.

Study outcomes

The patients were followed up for a maximum of 6 years. Follow-up data (status [dead or alive], date of death) was obtained from Hungary's National Health Insurance Database. The primary endpoint of our study was all-cause mortality.

Statistical analysis

Statistical analysis was performed using SPSS (v22, IBM, Armonk, NY, USA) and R (version 3.6.2, R Foundation for Statistical Computing, Vienna, Austria). Continuous variables are expressed as mean ± standard deviation (SD), whereas categorical variables were reported as frequencies and percentages. After verifying the normal distribution of variables using the Shapiro-Wilk test, the clinical and echocardiographic characteristics were compared with unpaired Student's *t*-test or Mann-Whitney *U*-test for continuous variables, and Chi-squared or Fisher's exact test for categorical variables, as appropriate. Multiple group comparisons (>2) were performed using

ANOVA (with Tukey *post-hoc* test) or Kruskal-Wallis test (with Dunn *post-hoc* test) and $\chi 2$ or Fisher exact test, as appropriate. Using univariable Cox regression, we identified factors associated with all-cause mortality. Targeting a maximum of 1 covariate per 10 events, we built several sequential multivariable Cox proportional hazards models. First, we constructed a baseline model including only clinical and laboratory parameters, and then in two consecutive steps, we added different LV and RV functional parameters to the model. As the final step, the constructed multivariable models were compared based on Akaike Information Criterion (AIC) to determine which one is the best fit for our data. Collinearity was tested using the variance inflation factor (excessive if variance inflation factor >3). Survival of the subgroups was visualized *via* Kaplan-Meier curves and compared using log-rank tests. Cox proportional hazards models were used to compute hazard ratios (HRs) with 95% confidence intervals (95% CIs) between the groups. Receiver-operating characteristic (ROC) curves were constructed to investigate the discriminative power of 2D and 3D echocardiographic parameters with regards to the primary endpoint. Metrics having more than 10% of missing values were not included in these analyses. Intraobserver and interobserver variability were also tested: the first reader repeated the analysis in a randomly chosen subset of patients ($n = 15$) blinded to previous results. A second reader also analyzed this patient subset in a blinded fashion. Intraclass correlation coefficient values were calculated. A two-sided P-value of <0.05 was considered statistically significant.

Results

Baseline clinical characteristics

Three hundred fifty-seven patients (age: 64 ± 15 years, 70% males) with established left-sided cardiac disease and 3DE recordings suitable for LV and RV analysis were identified from the RVENet dataset (444 patients were initially identified of whom we excluded 80 due to inadequate 3D image quality for RV analysis, and further 7 due to inadequate image quality for LV analysis). During the median follow-up time of 41 months (interquartile range 20–52), 55 (15%) patients died. Demographics and clinical characteristics of the study cohort and a comparison of patients alive vs. those who died are presented in Table 1.

Ninety-five subjects (27%) were heart failure with reduced ejection fraction (HFrEF) patients, of whom 81 patients were referred to our electrophysiology department for assessment prior to device implantation (pacemaker/implantable cardioverter defibrillator [ICD]/cardiac resynchronization therapy [CRT]). Fourteen patients were investigated for candidacy for a long-term LV assist device (LVAD) implantation. Ninety-one subjects (26%) were heart transplant recipients (HTX) with a median of 157 days after the operation (ranging from 8 to 6,571 days). Sixty-seven subjects (19%) were patients with severe primary mitral valve regurgitation (MVR) enrolled in a previous prospective study (10). Seventy-nine patients (22%) were investigated to evaluate aortic stenosis severity (moderate or severe). Twenty-five patients (7%) with a history of atrial fibrillation were referred for evaluation before a potential catheter ablation. The most frequently observed comorbidities were hypertension (73%), diabetes (28%), coronary artery disease (22%), and atrial fibrillation (33%).

Patients who died were older, had a higher prevalence of coronary artery disease and atrial fibrillation, and more frequently underwent ICD implantation in their medical history. Importantly, these patients had higher serum creatinine values than those who survived (Table 1).

Echocardiographic characteristics

2D echocardiographic parameters are summarized in Supplementary Table 1. Interestingly, conventional morphological parameters of the LV, the LA, and the RV did not differentiate between patients who died vs. those who survived. Mitral annular velocities by TDI, both in systole and diastole, were more impaired in those patients who died. However, E/e' was similar. The right atrial size was larger in those patients who died, along with a more impaired RV longitudinal function (TAPSE, free wall longitudinal strain); however, RV systolic pressure and FAC were similar.

3DE parameters are summarized in Table 2. Patients who died had larger LV and RV volumes, along with a more impaired systolic function. Notably, LV SVi and RV SVi were similar. In terms of longitudinal and circumferential biventricular strains, both LV and RV GLS and GCS were more impaired in patients who died.

Using univariable Cox regression, we identified variables associated with all-cause mortality (Supplementary Table 2). Then, we created several multivariable Cox models with a maximum of 5 predictors by adding covariates to a baseline model in a sequential manner (Figure 1). This analysis comprised three consecutive steps. In the first step, we created a baseline model (Model 0) that included age, sex, and serum creatinine level, as that latter was found to be a significant predictor during univariable analysis. In the second step, we added LVEF, LV GLS, or LV GCS to the baseline model one by one (Model 1, Model 2, and Model 3, respectively), and we found that the model with LV GLS (Model 2) had the lowest AIC among the constructed models (Figure 1A). In the third step, we built Models 4, 5, and 6 by adding RV EF, RV GLS, or RV GCS to Model 2, respectively. Among these models, the one with RV GCS (Model 6) exhibited the lowest AIC (Figure 1B and Supplementary Table 3). In this model, age and RV GCS were independent predictors of all-cause mortality, whereas sex, creatinine level, and LV GLS were not (Table 3). We have confirmed that our approach identified the best combination of covariates by constructing multivariable models with all possible combination of the LV and RV parameters (Supplementary Table 4). In multivariable models including the medical history of coronary artery disease or atrial fibrillation instead of sex, RV GCS remained an independent predictor of all-cause mortality (Supplementary Tables 5, 6). On ROC analysis, LV GLS had the highest discriminative power among LV functional parameters (area under the ROC curve: 0.644 [95% CI: 0.561–0.726, $p < 0.001$]), nevertheless, RV GCS had the highest discriminative power among all the investigated 2D and 3D echocardiographic parameters (0.690 [95% CI: 0.614–0.765, $p < 0.001$], Supplementary Table 7).

Subgroup analysis

As the model, which included LV GLS and RV GCS, was identified as the best among the evaluated models, we created four subgroups

10.3389/fcvm.2023.1082725

TABLE 1 Demographic and clinical characteristics.

	Overall ($n = 357$)	Alive ($n = 302$)	Dead ($n = 55$)	p
Baseline demographic characteristics				
Age (years)	64.2 ± 14.5	63.4 ± 14.6	68.6 ± 13.1	**0.014**
Male, *n* (%)	249 (69.7)	211 (69.9)	38 (69.1)	0.908
BSA (m^2)	1.93 ± 0.22	1.93 ± 0.22	1.91 ± 0.22	0.494
BMI (kg/m^2)	26.8 ± 4.2	27.0 ± 4.3	26.0 ± 3.6	0.288
Systolic blood pressure (mmHg)	126.5 ± 18.4	126.1 ± 17.2	128.0 ± 23.2	0.585
Diastolic blood pressure (mmHg)	74.6 ± 15.3	74.0 ± 15.9	77.4 ± 12.3	0.230
Heart rate (bpm)	77.6 ± 14.6	77.7 ± 15.0	77.4 ± 12.5	0.935
Risk factors and medical history				
Hypertension, *n* (%)	260 (72.8)	218 (72.2)	42 (76.4)	0.522
History of smoking, *n* (%)	82 (23.0)	66 (21.9)	16 (29.1)	0.241
COPD, *n* (%)	40 (11.2)	33 (10.9)	7 (12.7)	0.735
Diabetes, *n* (%)	99 (27.7)	78 (25.8)	21 (38.2)	0.060
History of atrial fibrillation, *n* (%)	116 (32.5)	89 (29.5)	27 (49.1)	**0.005**
PM, *n* (%)	49 (13.7)	38 (12.6)	11 (20.0)	0.159
ICD, *n* (%)	33 (9.2)	23 (7.6)	10 (18.2)	**0.015**
CRT, *n* (%)	15 (4.2)	12 (4.0)	3 (5.5)	0.637
CAD, *n* (%)	77 (21.6)	55 (18.2)	22 (40.0)	**<0.001**
Previous CABG, *n* (%)	19 (5.3)	13 (4.3)	6 (10.9)	**0.045**
Previous PCI, *n* (%)	67 (18.8)	49 (16.2)	18 (32.7)	**0.004**
Previous AMI, *n* (%)	48 (13.4)	34 (11.3)	14 (25.5)	**0.005**
Laboratory parameters				
GFR ($mL/min/1.73m^2$)	61.0 ± 19.4	62.1 ± 19.1	56.3 ± 20.2	0.056
Creatinine (μmol/L)	101.1 ± 41.7	99.1 ± 38.6	112.1 ± 54.5	**0.035**
Hgb (g/dL)	12.9 ± 2.1	12.9 ± 2.1	12.6 ± 2.2	0.385
CRP (mg/L)	6.7 ± 11.9	6.3 ± 12.1	9.0 ± 10.5	0.134

Continuous variables are presented as means ± SD, categorical variables are reported as frequencies (%). AMI, acute myocardial infarction; BMI, body mass index; BSA, body surface area; CABG, coronary artery bypass grafting; CAD, coronary artery disease; COPD, chronic obstructive pulmonary disease; CRP, C-reactive protein; CRT, cardiac resynchronization therapy; GFR, glomerular filtration rate; Hgb, hemoglobin; ICD, implantable cardioverter defibrillator; PCI, percutaneous coronary intervention; PM, pacemaker. Bold values mean significant *p* values (below 0.05).

based on the median values of LV GLS and RV GCS (−15.9 and −17.9%, respectively). In Group 1, patients had both LV GLS and RV GCS above the median, while in Group 4, both LV GLS and RV GCS were below the median. Group 2 patients had LV GLS values below the median while RV GCS above the median. Group 3 had patients with LV GLS above the median and RV GCS below the median.

Out of the 125 patients in Group 1, 37 (30%) were HTX recipients, 19 (15%) were evaluated before atrial fibrillation ablation, 18 (14%) had aortic stenosis, and 51 (41%) had mitral valve disease. Group 2 consisted of 53 patients, of whom 16 (30%) had HFrEF, 11 (21%) were HTX recipients, 6 (11%) were evaluated before atrial fibrillation ablation, and 20 (38%) had aortic stenosis. Group 3 had 54 patients in total, one (2%) with HFrEF, 30 (56%) HTX recipients, 8 (15%) with aortic stenosis, and 15 (28%) with mitral valve disease. Group 4 was composed of 125 patients and had 78 (62%) HFrEF patients, 13 (10%) HTX recipients, 33 (26%) patients with aortic stenosis, and 1 (1%) with mitral valve disease.

In Group 1, 7.2% of the patients died during the follow-up, while 7.5% died in Group 2. Group 3 and Group 4 patients experienced adverse outcomes more frequently, with 20.3% mortality in the former and 24.8% in the latter. These differences in the outcomes between patient subgroups were visualized *via* Kaplan-Meier curves (Figure 2). Patients with both LV GLS and RV GCS below the median (Group 4) had a more than 5-fold increased risk of death compared with those in Group 1 and more than 3.5-fold compared with those in Group 2. Interestingly, there was no significant difference in mortality between Group 3 (with LV GLS above the median) and Group 4, but being categorized into Group 3 vs. Group 1 still held a more than 3-fold risk (Supplementary Table 8).

Regarding the baseline characteristics of these groups, Group 4 patients were older, presented with lower systolic blood pressure, more frequently had diabetes and coronary artery disease, and had ICD implantation in their medical history (Supplementary Table 9). Their creatinine levels were also the highest among the groups. On the contrary, in Group 3, there were relatively younger patients, less

TABLE 2 3D echocardiographic parameters.

	Overall ($n = 357$)	Alive ($n = 302$)	Dead ($n = 55$)	p
Left ventricle				
LV EDVi (ml/m^2)	82.2 ± 32.2	80.3 ± 32.3	91.9 ± 30.3	**0.019**
LV ESVi (ml/m^2)	44.5 ± 30.4	42.2 ± 30.0	56.3 ± 30.0	**0.003**
LV SVi (ml/m^2)	37.7 ± 14.6	38.1 ± 15.1	35.6 ± 11.2	0.269
LV Mi (g/m^2)	102.5 ± 36.8	100.4 ± 35.1	113.4 ± 43.0	**0.023**
LV EF (%)	49.0 ± 15.7	50.2 ± 15.3	42.3 ± 16.1	**0.001**
LV GLS (%)	−15.2 ± 6.0	−15.7 ± 5.9	−12.5 ± 6.2	**<0.001**
LV GCS (%)	−23.9 ± 9.1	−24.6 ± 9.0	−20.2 ± 9.3	**0.001**
Right ventricle				
RV EDVi (ml/m^2)	70.2 ± 23.5	68.9 ± 23.1	76.6 ± 24.6	**0.033**
RV ESVi (ml/m^2)	37.4 ± 18.7	36.0 ± 17.8	44.4 ± 21.3	**0.003**
RV SVi (ml/m^2)	32.7 ± 9.0	32.8 ± 9.3	32.2 ± 7.5	0.648
RV EF (%)	48.3 ± 9.4	49.1 ± 9.2	44.1 ± 9.5	**<0.001**
RV GLS (%)	−16.4 ± 5.1	−16.9 ± 5.0	−13.8 ± 4.6	**<0.001**
RV GCS (%)	−17.7 ± 6.1	−18.3 ± 5.9	−14.3 ± 6.2	**<0.001**

Continuous variables are presented as means ± SD, categorical variables are reported as frequencies (%). EDVi, end-diastolic volume index; EF, ejection fraction; ESVi, end-systolic volume index; GCS, global circumferential strain; GLS, global longitudinal strain; LV, left ventricle; Mi, mass index; RV, right ventricle; SVi, stroke volume index. Bold values mean significant p values (below 0.05).

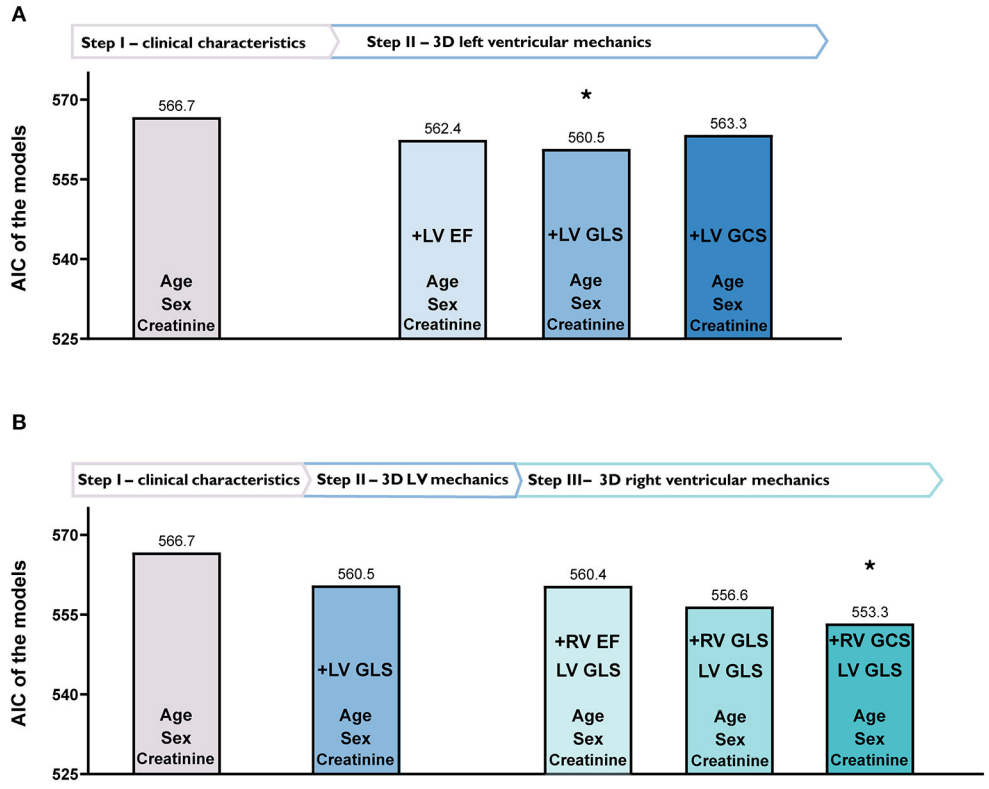

FIGURE 1
Identification of the best-fit models, including left (LV) and right ventricular (RV) functional parameters by multivariable Cox regression analysis based on Akaike Information Criterion (AIC). **(A)** Depicts different models with only clinical characteristics (Step I) and 3D LV mechanical parameters added one by one (Step II). In Step II, adding LV global longitudinal strain (GLS) to the model resulted in the lowest (best) AIC value. **(B)** Shows the added value of 3D RV mechanical parameters (Step III). In Step III, adding RV global circumferential strain (GCS) to the previously established model in Step II (clinical characteristics and LV GLS) resulted in the best fit to our data as confirmed by the lowest AIC value.

10.3389/fcvm.2023.1082725

TABLE 3 Independent predictors of all-cause mortality identified using multivariable cox regression.

Multivariable cox regression		
	HR [95% CI]	*p*
Age	1.036 [1.011–1.061]	**0.004**
Sex	0.690 [0.376–1.266]	0.231
Creatinine[#]	1.005 [0.999–1.012]	0.087
LV GLS	1.017 [0.963–1.075]	0.543
RV GCS	1.091 [1.032–1.152]	**0.002**

[#]Creatinine levels were available in 341 patients.

CI, confidence interval; HR, hazard ratio; LV GLS, left ventricular global longitudinal strain; RV GCS, right ventricular global circumferential strain. Bold values mean significant *p* values (below 0.05).

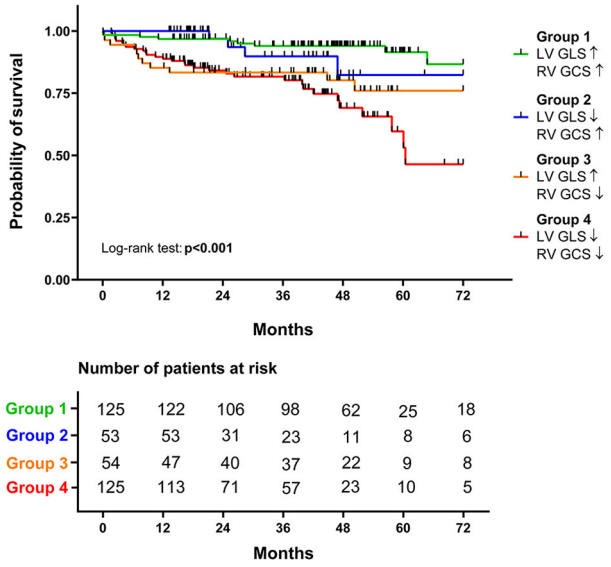

FIGURE 2
Survival analysis of the different groups. Based on the respective median values of left ventricular global longitudinal strain (LV GLS, −15.9%) and right ventricular global circumferential strain (RV GCS, −17.9%), patients were divided into four groups. The survival of the four groups is visualized on Kaplan-Meier curves, and the log-rank test was performed for comparison.

frequently with diabetes, coronary artery disease, or atrial fibrillation in their medical history. Group 4 patients were presented with the highest LV, RV, and RA dimensions and E/e', while LAVi or RV systolic pressure did not differ between the four subgroups (Supplementary Table 10).

The 3DE parameters of the four groups are demonstrated in Supplementary Table 11. Beyond the aforementioned significant chamber dilation and biventricular functional impairment seen in Group 4 patients, Group 3 patients had the lowest LV Mi with a preserved average LV and RV EF (60 ± 5 and 49 ± 6%, respectively).

Reproducibility

Intraclass correlation coefficient values were lower but still acceptable for RV GCS compared with RVEF and RV GLS (Supplementary Table 12).

Discussion

To the best of our knowledge, our study is the first that specifically aimed to assess the prognostic value of both LV and RV circumferential shortening using 3DE. Our main findings can be summarized as follows: (1) Impaired values of both LV and RV GCS were associated with all-cause mortality in univariable Cox models. (2) Among the evaluated multivariable models, the one with LV GLS and RV GCS fitted our data the best. Interestingly, however, only RV GCS was found to be an independent predictor of mortality, whereas LV GLS and creatinine levels were not. (3) Based on the median values of LV GLS and RV GCS, we created four groups that differed significantly in terms of all-cause mortality. Importantly, reduced RV GCS was associated with worse outcomes even if LV GLS was maintained (Figure 3).

Recent advances in echocardiographic hardware and software environment enabled the automated and accurate quantification of myocardial mechanics. First and foremost, GLS by 2D speckle tracking echocardiography has emerged as a mainstay parameter of LV systolic function. Due to the representation of subendocardial longitudinally-oriented myofibers, LV GLS is more sensitive to subtle functional impairment in various clinical scenarios than conventional echocardiographic parameters (i.e., LV EF). A meta-analysis comprising 16 published articles provided strong evidence about the prognostic value of LV GLS, which appeared to be superior to LV EF for predicting major adverse cardiac events in patients with different underlying cardiac abnormalities. GLS is now a well-validated and reproducible metric for the quantification of LV longitudinal deformation, and its integration into routine clinical practice is about to be completed in the upcoming years (2).

Nevertheless, besides longitudinal shortening, circumferential shortening also contributes significantly to the global systolic function of both ventricles. A mathematical model showed that LV GCS contributes more than twice as much to LV EF than LV GLS, and a small increase in LV GCS could compensate for a significant reduction of LV GLS (5). LV EF was shown to be quadratically dependent on circumferential shortening and only linearly dependent on longitudinal shortening. Previously, numerous publications reported global circumferential strain by 2D echocardiography; however, due to its complicated calculation (3 levels of parasternal short-axis view are needed to be acquired and analyzed) and poor reproducibility, the majority of software vendors discontinued the possibility of its measurement (11, 12). Using 3DE, a single acquisition (and the same cardiac cycle) can be used to calculate both GCS and GLS; thus, it may overcome the limitations of 2D-based calculations.

Importantly, circumferential shortening contributes substantially to global RV pump function, which can be measured only by using 3DE. Notably, the circumferential motion may also hold particular importance in the global RV function: even subtle deterioration in the circumferential shortening of the large RV free wall may result in significant global functional damage (13). Circumferential shortening is composed of the inward motion of the RV free wall (radial shortening) and the traction of the free wall insertion lines toward each other by the LV contraction (anteroposterior shortening) (14). Beyond the latter functional connection of the two ventricles, evidence suggests that LV-RV interactions exist on many layers: alterations of geometry, loading conditions, and contractility of

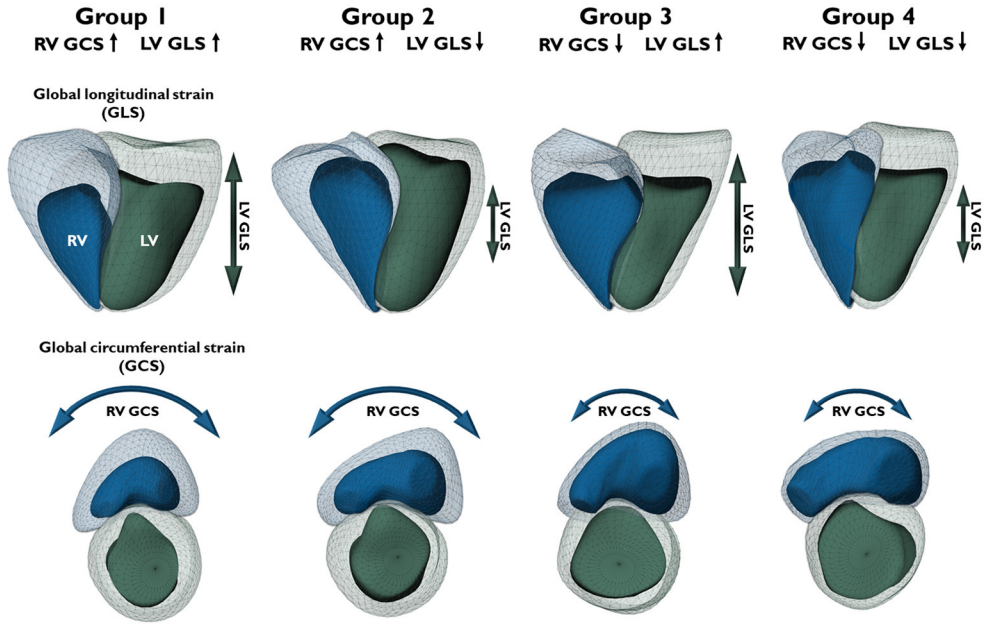

FIGURE 3
Three-dimensional schematic models depict representative cases of different biventricular mechanical patterns in patients from the respective groups. The four groups were divided based on the median values of left ventricular global longitudinal strain (LV GLS, −15.9%) and right ventricular global circumferential strain (RV GCS, −17.9%). Upward arrows represent strain values better than the median (more negative), downward arrows represent strain values worse than the median (less negative). Light green mesh – left ventricular end-diastolic volume; dark green surface – left ventricular end-systolic volume; green arrow – LV longitudinal shortening (GLS); light blue mesh – right ventricular end-diastolic volume; dark blue surface – right ventricular end-systolic volume; blue arrow – RV circumferential shortening (GCS).

a ventricle will significantly influence its counterpart (15). This complex interplay underpins that practically every disease process may have consequences on both sides of the interventricular septum, with potential importance in terms of diagnosis and outcomes.

With the constantly increasing recognition of the left-right heart interaction, a detailed assessment of the right ventricle gains more and more momentum. This approach is hugely facilitated by the advancements of 3DE imaging, allowing real-time examination of the right ventricle, free of geometrical assumptions. 3D RV analysis enables the calculation of RV volumes and, therefore, RV EF. 3D RV EF by itself holds an established added clinical value: as of today, multiple clinical studies have demonstrated the independent prognostic importance of the parameter. Surkova et al. performed their retrospective study on a large cohort of patients with different cardiovascular diseases (7). Their study found that reduced RV EF was independently associated with all-cause mortality and cardiac death after adjusting for clinical and echocardiographic parameters. RV EF also demonstrated higher sensitivity and specificity for predicting all-cause mortality than conventional parameters of RV systolic function (TAPSE and FAC), and its impairment carried a significantly higher risk of mortality independent of LV EF. They also divided patients into four groups with maintained or reduced LV EF and/or RV EF. The four groups had significantly different survival: both all-cause mortality and cardiac death in patients with reduced RV EF and normal LV EF were significantly higher than in those with reduced LV EF and normal RV EF and did not differ significantly from patients with reduced EF of both ventricles (7). In a secondary analysis of the Atherosclerosis Risk in Communities (ARIC) 3DE substudy, lower RV EF was independently associated with incident heart failure or death in patients free of heart failure at baseline (16). Our group has recently performed a meta-analysis in which we sought to compare the prognostic power of RV EF to conventional echocardiographic parameters (TAPSE, FWLS, FAC). We found that 1 SD reduction in RV EF was robustly associated with adverse cardiopulmonary outcomes, and importantly, RV EF had a superior predictive value compared to the other three parameters (17). Thus, 3DE-derived RV EF seems to be the best parameter among the "standard" echocardiographic metrics of RV function. Nonetheless, similarly to the left ventricle, the assessment of the RV deformation may exceed the added diagnostic and prognostic value of even RV EF. Small cohort studies with various RV pathologies, such as pulmonary hypertension, atrial septal defect, or patients following cardiac surgery, unveiled distinct changes in RV mechanics; still, they were using simple 2D-derived measures of RV function (18–20).

The ReVISION method allows the calculation of the relative contributions of longitudinal, radial, and anteroposterior motion components to global RV function and also 3D longitudinal and circumferential strain, using 3DE-derived models (9). By investigating 300 healthy volunteers using 3DE, Lakatos et al. showed that circumferential EF indexed to global RV EF was clearly dominant compared with longitudinal EF. In contrast to the traditional viewpoint, they found that the relative contribution of the radial and anteroposterior motion directions may be of comparable significance with that of longitudinal shortening in determining global RV function, and standard parameters referring only to longitudinal shortening of the right ventricle may be inadequate to characterize RV function thoroughly (4).

Using the same approach, two studies have already shown the added prognostic value of the RV non-longitudinal functional measures. Kitano et al. examined a relatively large cohort of patients

with diverse cardiac diseases, demonstrating that RV 3D strains were associated with the occurrence of hard endpoints even by adjusting for multiple clinical variables (1). Surkova and colleagues enrolled consecutive patients with left-sided heart disease. Even in patients with maintained LV EF, the anteroposterior component of total EF was a significant and independent predictor of outcome (21). Our results add another layer to the evidence about the importance of RV non-longitudinal shortening from a diagnostic and a prognostic point of view. As a previously neglected marker of ventricular systolic performance, circumferential deformation may be able to describe a novel aspect of RV systolic function with established prognostic value. RV GCS may represent a robust, universal biomarker of the status of the entire cardiopulmonary system as it overpowers conventional echocardiographic metrics and is associated with adverse clinical outcomes not just in "classical" right-heart diseases, but also in primary left-heart diseases. The exact pathophysiological processes (ventricular interdependence, RV pressure overload, etc.) that result in the deterioration of circumferential shortening and the potential usefulness of RV GCS for screening purposes remain to be investigated.

Limitations

Our study has several limitations that have to be acknowledged. First, an inherent limitation is its retrospective, single-center nature. The mixed cohort of patients with some etiologies of left-sided cardiac diseases might not represent the actual patient population treated at a tertiary clinic. However, patients with HFrEF and valvular heart diseases were dominantly included, who are of crucial clinical importance. HTX recipients may represent a unique population in this regard, therefore, we have performed further calculations (see Supplementary Results) to confirm that they do not bias our results. Second, 3DE-based quantifications are not the gold standard; nevertheless, the software packages are well-validated clinically and against cardiac MRI. Calculating RV circumferential strain is quite a novel approach; therefore, literature data are scarce. Third, due to the lack of cause-specific mortality data, we could not investigate the association between the 3DE-derived parameters and cardiac death. The event number has limited the number of covariates in the multivariate models. Lastly, the validity of our results should be tested in prospective outcome studies in different clinical scenarios.

Conclusions

Biventricular circumferential shortening holds important prognostic value to adverse clinical outcomes. RV GCS is a powerful and independent predictor of all-cause mortality in patients with left-sided cardiac disease. Our study highlights the clinical value of 3DE-derived parameters of myocardial mechanics.

Data availability statement

The raw data supporting the conclusions of this article will be made available by the authors, without undue reservation.

Ethics statement

The studies involving human participants were reviewed and the study was approved by the Semmelweis University Regional and Institutional Committee of Science and Research Ethics (approval no. 190/2020). Written informed consent for participation was not required for this study in accordance with the national legislation and the institutional requirements.

Author contributions

MTol, AFá, and AKov performed measurements, interpreted results, and drafted the manuscript. MTok, ZL, KS, and AFe performed measurements. MTok, BL, AA, ZL, KS, AFe, WS, BV, AKos, ÁS, BS, and BM reviewed and approved the manuscript. BL, AA, WS, BV, AKos, BS, and AKov enrolled, followed-up, and investigated patients. AKov and BM secured grant support. AFá, MTok, and ÁS performed statistical analysis. AFá prepared figures. All authors contributed to the article and approved the submitted version.

Funding

MTol was supported by the EFOP-3.6.3-VEKOP-16-2017-00009 project. Project no. RRF-2.3.1-21-2022-00003 has been implemented with the support provided by the European Union. This project was also supported by a grant from the National Research, Development and Innovation Office (NKFIH) of Hungary (FK 142573 to AKov).

Conflict of interest

AFá, MTok, BL, ÁS, and AKov report personal fees from Argus Cognitive, Inc., outside the submitted work.

The remaining authors declare that the research was conducted in the absence of any commercial or financial relationships that could be construed as a potential conflict of interest.

Publisher's note

Supplementary material

The Supplementary Material for this article can be found online at: https://www.frontiersin.org/articles/10.3389/fcvm.2023.1082725/full#supplementary-material

References

1. Kitano T, Kovacs A, Nabeshima Y, Tokodi M, Fabian A, Lakatos BK, et al. Prognostic value of right ventricular strains using novel three-dimensional analytical software in patients with cardiac disease. *Front Cardiovasc Med.* (2022) 9:837584. doi: 10.3389/fcvm.2022.837584

2. Kalam K, Otahal P, Marwick TH. Prognostic implications of global LV dysfunction: a systematic review and meta-analysis of global longitudinal strain and ejection fraction. *Heart.* (2014) 100:1673–80. doi: 10.1136/heartjnl-2014-305538

3. Rothschild E, Baruch G, Kaplan A, Laufer-Perl M, Beer G, Kapusta L, et al. The prognostic value of right ventricular strain and mechanical dispersion on mortality in patients with normal left ventricle function. *Int J Cardiol.* (2023) 372:130–7. doi: 10.1016/j.ijcard.2022.11.040

4. Lakatos BK, Nabeshima Y, Tokodi M, Nagata Y, Tosér Z, Otani K, et al. Importance of nonlongitudinal motion components in right ventricular function: three-dimensional echocardiographic study in healthy volunteers. *J Am Soc Echocardiogr.* (2020) 33:995–1005.e1. doi: 10.1016/j.echo.2020.04.002

5. Stokke TM, Hasselberg NE, Smedsrud MK, Sarvari SI, Haugaa KH, Smiseth OA, et al. Geometry as a confounder when assessing ventricular systolic function: comparison between ejection fraction and strain. *J Am Coll Cardiol.* (2017) 70:942–54. doi: 10.1016/j.jacc.2017.06.046

6. Konstam MA, Kiernan MS, Bernstein D, Bozkurt B, Jacob M, Kapur NK, et al. Evaluation and management of right-sided heart failure: a scientific statement from the American Heart Association. *Circulation.* (2018) 137:e578–622. doi: 10.1161/CIR.0000000000000560

7. Surkova E, Muraru D, Genovese D, Aruta P, Palermo C, Badano LP. Relative prognostic importance of left and right ventricular ejection fraction in patients with cardiac diseases. *J Am Soc Echocardiogr.* (2019) 32:1407–15 e3. doi: 10.1016/j.echo.2019.06.009

8. Lang RM, Badano LP, Mor-Avi V, Afilalo J, Armstrong A, Ernande L, et al. Recommendations for cardiac chamber quantification by echocardiography in adults: an update from the American Society of Echocardiography and the European Association of Cardiovascular Imaging. *J Am Soc Echocardiogr.* (2015) 28:1–39.e14. doi: 10.1016/j.echo.2014.10.003

9. Tokodi M, Staub L, Budai Á, Lakatos BK, Csákvári M, Suhai FI, et al. Partitioning the right ventricle into 15 segments and decomposing its motion using 3D echocardiography-based models: the updated ReVISION method. *Front Cardiovasc Med.* (2021) 8:622118. doi: 10.3389/fcvm.2021.622118

10. Tokodi M, Németh E, Lakatos BK, Kispál E, Tosér Z, Staub L, et al. Right ventricular mechanical pattern in patients undergoing mitral valve surgery: a predictor of post-operative dysfunction? *ESC Heart Fail.* (2020) 7:1246–56. doi: 10.1002/ehf2.12682

11. Kovacs A, Tapolyai M, Celeng C, Gara E, Faludi M, Berta K, et al. Impact of hemodialysis, left ventricular mass and FGF-23 on myocardial mechanics in end-stage renal disease: a three-dimensional speckle tracking study. *Int J Cardiovasc Imaging.* (2014) 30:1331–7. doi: 10.1007/s10554-014-0480-2

12. Lee HF, Hsu LA, Chan YH, Wang CL, Chang CJ, Kuo CT. Prognostic value of global left ventricular strain for conservatively treated patients with symptomatic aortic stenosis. *J Cardiol.* (2013) 62:301–6. doi: 10.1016/j.jjcc.2013.05.001

13. Buckberg G, Hoffman JI. Right ventricular architecture responsible for mechanical performance: unifying role of ventricular septum. *J Thorac Cardiovasc Surg.* (2014) 148:3166–71.e1-4. doi: 10.1016/j.jtcvs.2014.05.044

14. Lakatos B, Tosér Z, Tokodi M, Doronina A, Kosztin A, Muraru D, et al. Quantification of the relative contribution of the different right ventricular wall motion components to right ventricular ejection fraction: the ReVISION method. *Cardiovasc Ultrasound.* (2017) 15:8. doi: 10.1186/s12947-017-0100-0

15. Friedberg MK. Imaging right-left ventricular interactions. *JACC Cardiovasc Imaging.* (2018) 11:755–71. doi: 10.1016/j.jcmg.2018.01.028

16. Nochioka K, Querejeta Roca G, Claggett B, Biering-Sørensen T, Matsushita K, Hung CL, et al. Right ventricular function, right ventricular-pulmonary artery coupling, and heart failure risk in 4 US communities: the Atherosclerosis Risk in Communities (ARIC) Study. *JAMA Cardiol.* (2018) 3:939–48. doi: 10.1001/jamacardio.2018.2454

17. Sayour AA, Tokodi M, Celeng C, Takx RAP, Fábián A, Lakatos BK, et al. Association of right ventricular functional parameters with adverse cardiopulmonary outcomes - a meta-analysis. *J Am Soc Echocardiogr.* (In Press). doi: 10.1016/j.echo.2023.01.018

18. Swift AJ, Rajaram S, Capener D, Elliot C, Condliffe R, Wild JM, et al. Longitudinal and transverse right ventricular function in pulmonary hypertension: cardiovascular magnetic resonance imaging study from the ASPIRE registry. *Pulm Circ.* (2015) 5:557–64. doi: 10.1086/682428

19. Jategaonkar SR, Scholtz W, Butz T, Bogunovic N, Faber L, Horstkotte D. Two-dimensional strain and strain rate imaging of the right ventricle in adult patients before and after percutaneous closure of atrial septal defects. *Eur J Echocardiogr.* (2009) 10:499–502. doi: 10.1093/ejechocard/jen315

20. Raina A, Vaidya A, Gertz ZM, Susan C, Forfia PR. Marked changes in right ventricular contractile pattern after cardiothoracic surgery: implications for post-surgical assessment of right ventricular function. *J Heart Lung Transplant.* (2013) 32:777–83. doi: 10.1016/j.healun.2013.05.004

21. Surkova E, Kovacs A, Tokodi M, Lakatos BK, Merkely B, Muraru D, et al. Contraction patterns of the right ventricle associated with different degrees of left ventricular systolic dysfunction. *Circ Cardiovasc Imaging.* (2021) 14:e012774. doi: 10.1161/CIRCIMAGING.121.012774

frontiers | Frontiers in Cardiovascular Medicine

TYPE Original Research
PUBLISHED 05 May 2023
DOI 10.3389/fcvm.2023.1137814

OPEN ACCESS

EDITED BY
Márton Tokodi,
Semmelweis University, Hungary

REVIEWED BY
Alisa Arunamata,
Stanford University, United States
Mitsuru Seki,
Jichi Medical University, Japan

*CORRESPONDENCE
David M. Harrild
david.harrild@cardio.chboston.org

RECEIVED 04 January 2023
ACCEPTED 19 April 2023
PUBLISHED 05 May 2023

CITATION
Ferraro AM, Bonello K, Sleeper LA, Lu M, Shea M, Marx GR, Powell AJ, Geva T and Harrild DM (2023) A comparison between the apical and subcostal view for three-dimensional echocardiographic assessment of right ventricular volumes in pediatric patients. Front. Cardiovasc. Med. 10:1137814. doi: 10.3389/fcvm.2023.1137814

A comparison between the apical and subcostal view for three-dimensional echocardiographic assessment of right ventricular volumes in pediatric patients

Alessandra M. Ferraro[1,2,3], Kristin Bonello[1,2], Lynn A. Sleeper[1,2], Minmin Lu[1], Melinda Shea[1], Gerald R. Marx[1,2], Andrew J. Powell[1,2], Tal Geva[1,2] and David M. Harrild[1,2]*

[1]Department of Cardiology, Boston Children's Hospital, Boston, MA, United States, [2]Department of Pediatrics, Harvard Medical School, Boston, MA, United States, [3]PhD Program in Angio-Cardio-Thoracic Pathophysiology and Imaging, Sapienza University of Rome, Rome, Italy

Background: Accurate measurement of ventricular volumes is an important clinical imaging goal. Three-dimensional echocardiography (3DEcho) is used increasingly as it is more available and less costly than cardiac magnetic resonance (CMR). For the right ventricle (RV), the current practice is to acquire 3DEcho volumes from the apical view. However, in some patients the RV may be better seen from the subcostal view. Therefore, this study compared RV volume measurements from the apical vs. the subcostal view, using CMR as a reference standard.

Methods: Patients <18 years old undergoing a clinical CMR examination were prospectively enrolled. 3DEcho was performed on the day of the CMR. 3DEcho images were acquired with Philips Epic 7 ultrasound system from apical and subcostal views. Offline analysis was performed with TomTec 4DRV Function for 3DEcho images and cvi42 for CMR ones. RV end-diastolic volume and end-systolic volume were collected. Agreement between 3DEcho and CMR was assessed with Bland-Altman analysis and the intraclass correlation coefficient (ICC). Percentage (%) error was calculated using CMR as the reference standard.

Results: Forty-seven patients were included in the analysis (age range 10 months to 16 years). The ICC was moderate to excellent for all volume comparisons to CMR (subcostal vs. CMR: end-diastolic volume 0.93, end-systolic volume 0.81; apical vs. CMR: end-diastolic volume 0.94, end-systolic volume 0.74).The 3DEcho mean % error vs. CMR for end-systolic volume was 25% for subcostal and 31% for apical; for end-diastolic volume it was 15% for subcostal and 16% for apical. The % error was not significantly different between apical vs. subcostal views for end-systolic and end-diastolic volume measurements.

Conclusions: For apical and subcostal views, 3DEcho-derived ventricular volumes agree well with CMR. Neither echo view has a consistently smaller error when compared to CMR volumes. Accordingly, the subcostal view can

Abbreviations
bSSFP, balanced steady-state free precession; CMR, cardiac magnetic resonance; EDV, end-diastolic volume; ESV, end-systolic volume; ICC, interclass correlation coefficient; RV, right ventricular; ToF, Tetralogy of Fallot; 3DEcho, three-dimensional echocardiography.

be used as an alternative to the apical view when acquiring 3DEcho volumes in pediatric patients, particularly when the image quality from this window is superior.

KEYWORDS

three-dimensional echocardiography, right ventricular volumes, congenital heart disease, pediatrics, apical view, subcostal view

Introduction

Measures of right ventricular (RV) volumes are critically important from a clinical perspective in the fields of pediatric and adult congenital heart disease (1–7), particularly in conditions providing a volume-loaded RV such as in the setting of an atrial septal defect or dysfunction of the pulmonary or tricuspid valves (7). Accurate measurement of these volumes is essential in the setting of tetralogy of Fallot (ToF), a common condition among pediatric patients (1, 3, 5, 6). In addition, RV volumes, together with RV function, are important parameters in patients status post Fontan palliation due to their correlation with mortality and heart transplant outcomes (8). Similarly, 3DEcho RV volume assessment was able to predict the severity of outcomes in patients with pulmonary hypertension (9). As well, 3DEcho RV volume assessment was the method used to assess differences in RV size and function after either Blalock-Taussig or Sano shunt in a multicenter study (9).

Cardiac magnetic resonance (CMR) is currently considered the reference standard for the measurement of ventricular volumes (10). However, this technology is relatively expensive and time-consuming. As an alternative, three-dimensional echocardiography (3DEcho) for the measurement of ventricular volumes is an emerging technique which has wider availability and lower expense relative to CMR, in addition to the fact that it may be used for patients with a contraindication to CMR. As well, 3DEcho images have a shorter acquisition time and time for analysis (with current semi-automated tools) as little as 3 min (11).

Traditionally, 3DEcho volumes have been acquired from an apical four-chamber view (12–18). However, there are limitations to this view including difficulty visualizing portions of the RV, particularly the outflow, and especially when ventricular dilation is present. These limitations result, in part, from the anterior position of the RV and its location just posterior to the sternum and rib cage (19, 20). Based on these challenges, recent data have called into question the practice of deriving 3DEcho RV volumes images based on apical view (20). An alternative to the apical view is the subcostal view. The potential advantage of this view is access to the entire RV, including the outflow, by avoiding acoustic shadowing from the sternum and rib cage (20, 21). On the other hand, it might happen that patients do not have adequate quality images from this view while having good apical ones. Therefore, in this study we sought to compare 3DEcho RV volume measurements from the apical vs. subcostal view, using contemporaneously acquired CMR measurements as a reference standard.

Materials and methods

Study design

Patients who were referred for a clinical CMR were approached prospectively for acquisition of 3DEcho images immediately prior to or following the CMR examination. Inclusion criteria were age ≤18 years old, both a right and left ventricle were present, and adequate apical and subcostal imaging windows. The study protocol was approved by the local Institutional Review Board (IRB-P00033035). Informed consent was obtained from the patient's parent. The 3DEcho was acquired on the same day as the CMR in all cases.

Image acquisition and analysis

Echocardiography images were obtained using the Philips EPIQ system (Philips Healthcare, Cambridge, MA, USA). Some patients were sedated for CMR for clinical indications and, in these cases, 3DEcho images were acquired while the patient was recovering from anesthesia; no additional sedation was administered for the 3DEcho images. The X5-1 or X-7-2 transducers were used based upon the patient's size. Images were acquired using standard techniques from subcostal and apical views by sonographers with expertise in 3DEcho (**Figure 1**). When possible, patients were instructed to hold their breath to minimize "stitch artifact" during imaging reconstruction. A 4 or 6 beat acquisition method was used in all cases.

Deidentified images were stored in Digital Imaging and Communications in Medicine format. Offline volumetric analysis was carried out with 4D RV Function version 3 (TomTec, Unterschleißheim, Germany) according to the manufacturer's recommendations and prior descriptions (22). Manual adjustments of the endocardial borders as well as the tricuspid and pulmonary valves landmarks were made following the generation of the semi-automatic tracing (**Figure 2**). Custom bookmark tools were constructed to optimize the consistency of image alignment acquired from the subcostal view (**Figure 3**). End-diastolic volume (EDV) and end-systolic volume (ESV) were recorded. Intra- and inter-observer reproducibility was assessed for 10 randomly selected patients. For inter-observer measurements, the second analysis was performed at least 2 weeks after the first.

All CMR images were obtained from a 1.5 Tesla CMR scanner (Achieva, Phillips Healthcare, Best, the Netherlands). Imaging included a 12–14 slice stack (slice thickness 8–10 mm) of breath hold, ECG-gated, balanced steady-state free precession (bSSFP) cine acquisitions in the short-axis plane. Ventricular volumes were measured using commercially available software (cvi42,

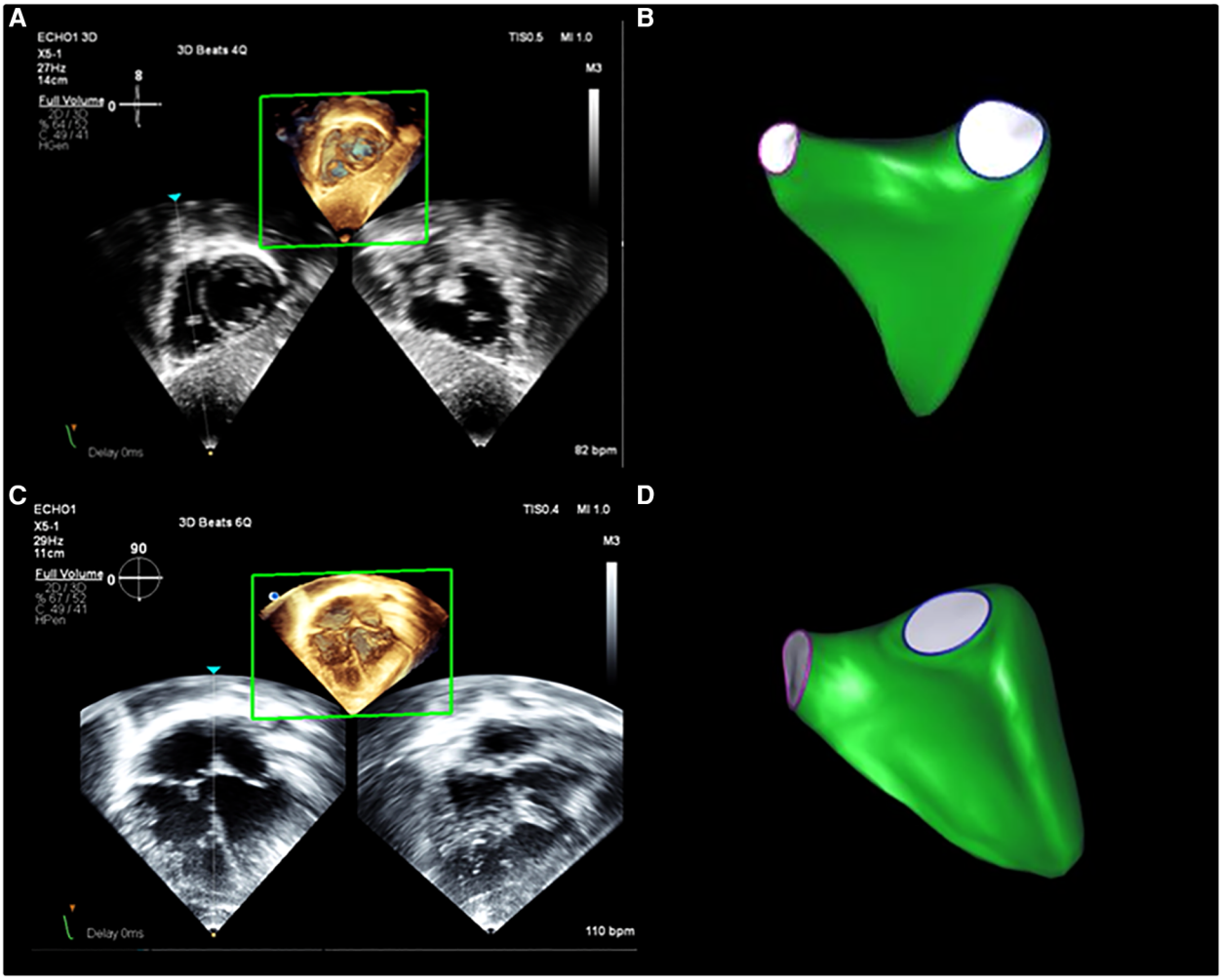

FIGURE 1
3DEcho RV volume assessment. Example of RV volumes acquired from (**A**) subcostal and (**C**) apical views from a normal patient, as well as examples of the 3D surface resulting from analysis with the post-processing software from subcostal (**B**) and apical (**D**) views.

Circle Cardiovascular Imaging Inc., Calgary, Alberta, Canada; and QMass, Medis Medical Imaging Systems, Leiden, the Netherlands). Horizontal (four-chamber) and vertical (two-chamber) long-axis images were used as cross-references to aid with the identification of the ventricular myocardium to be included as chamber volume. The left ventricular papillary muscles and major trabeculations of the RV (e.g., septal band) were excluded from the blood pool and considered part of the myocardial mass as previously described (1, 2, 3).

Statistical analysis

Agreement between 3DEcho and CMR was assessed with Bland-Altman analysis and the intraclass correlation coefficient (ICC). To study if age may have an impact on agreement, we additionally divided our cohort in three age groups: <6 years old, 6–2 years old, and >12 years old. Percentage (%) error was calculated as [|(Echo − CMR)|/mean of Echo and CMR] × 100. Differences in raw values and % error for apical vs. subcostal views were compared with a paired *t*-test. In addition, differences in cardiac output using ventricular volumes calculated with apical vs. subcostal views were assessed using a Wilcoxon signed rank exact test.

Intra- and inter-observer reproducibility was assessed with a one-sample *t*-test and ICC. The Bland-Altman plots were used to display agreement between two readings (from the same observer) and between two readings (from different observers). Descriptive statistics include mean ± standard deviation and median with interquartile range. A p value 0.05 was considered to be statistically significant.

Results

Study participants

Fifty patients were consented for the study; in 3 of these, however, 3DEcho image quality from one of the views was

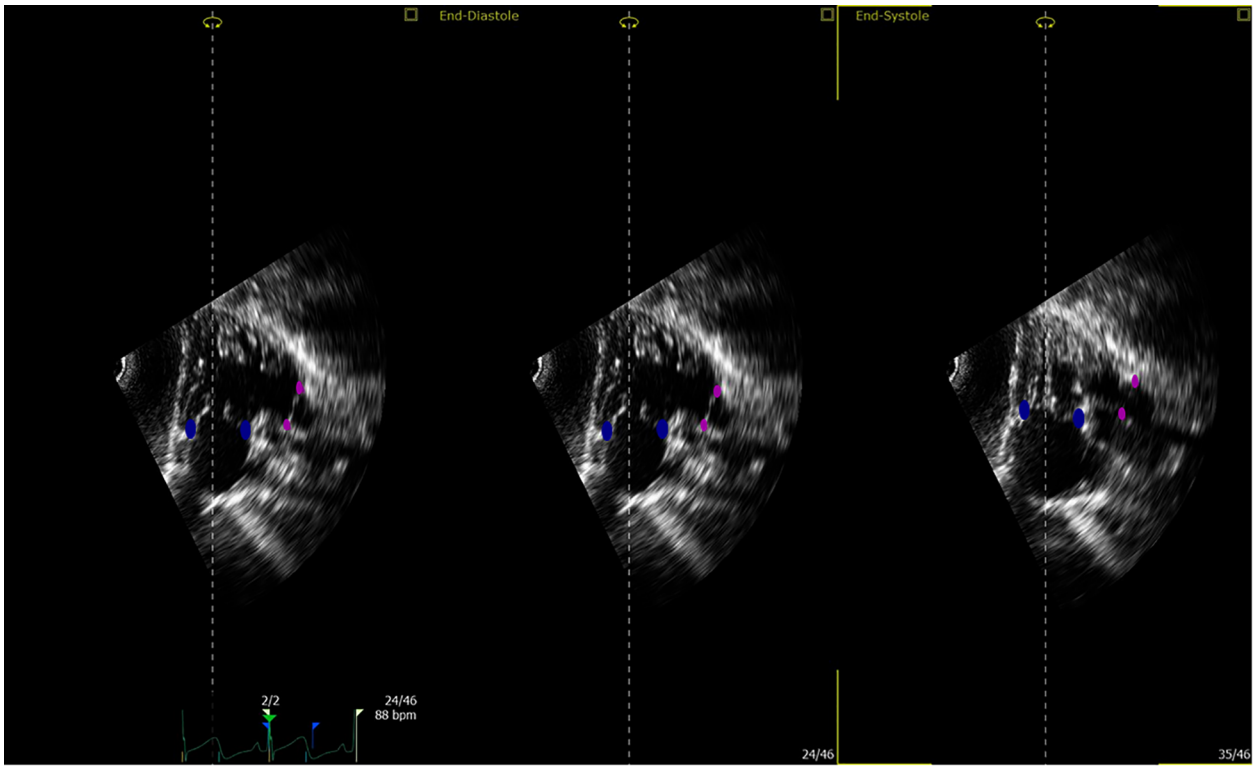

FIGURE 2
Tricuspid and pulmonary valve landmarks. Blue points define the tricuspid valve annulus; magenta points define the pulmonary valve annulus (this is true for both apical and subcostal views).

judged to be inadequate for analysis upon subsequent review (apical view 1, subcostal view 2). Hence, the analytic cohort size for apical vs. subcostal comparisons was 47 patients. Demographic and clinical characteristics are presented in Table 1. Ages ranged from 10 months to 16 years. Eighteen patients underwent general anesthesia for CMR. Indications for CMR were for suspected or established congenital heart disease in nearly all patients ($n = 43$).

Comparison of volume measurements by 3DEcho apical and subcostal views to CMR

Bland-Altman plots for 3DEcho vs. CMR measurements of ventricular volumes for the two echo views are presented in Figure 4. In addition, differences in cardiac output using ventricular volumes calculated with apical vs. subcostal views were assessed using a Wilcoxon signed rank exact test. The biases were not significantly different for the comparison of end-diastolic measurements (panel A vs. panel C) (p value = 0.36), but they were different for end-systolic (panel B vs. panel D) (p-value <0.05). The biases were negative for all volume comparisons, reflecting an underestimation of 3DEcho ventricular volumes compared to CMR. Figure 5 presents box plots for the volume data analyzed in a grouped fashion. Volumes measured from the apical windows were significantly smaller than the CMR values (p values for EDV = 0.05 and ESV <0.001); the volumes measured by subcostal windows and the CMR values were not statistically different. When comparing mean volumes from subcostal to apical view: EDV volume from apical (98.5 ml) and subcostal (101.5 ml) views did not differ from each other, $p = 0.36$; ESV volume from apical (37.0 ml) and subcostal (43.9 ml) views differed one from the other ($p < 0.05$). Table 2 presents mean difference data between the two views compared to CMR, both as a raw value and as a percent error. The % error was not statistically different between apical vs. subcostal views for ESV and EDV measurements. Agreement as assessed by the ICC between 3DEcho and CMR for each view was high (ICC >0.7 for all), and higher for EDV compared to ESV (Table 2). When stratified by age, the patients in the middle age group (6 to 12 years) had a lower ICC than patients in both the youngest (<6 years) and oldest (>12 years) age groups. A factor contributing to these differences may be variations in patient diagnoses among the three patient groups; for example, the 6–12 year old cohort had a higher prevalence of patients with small left-sided structures than the other two.

The median and interquartile range for cardiac output were: subcostal view, 4,312 (2,893–5,711) ml/min; apical view, 4,296 (2,802–6,078) ml/min; these did not differ statistically ($p = 0.42$).

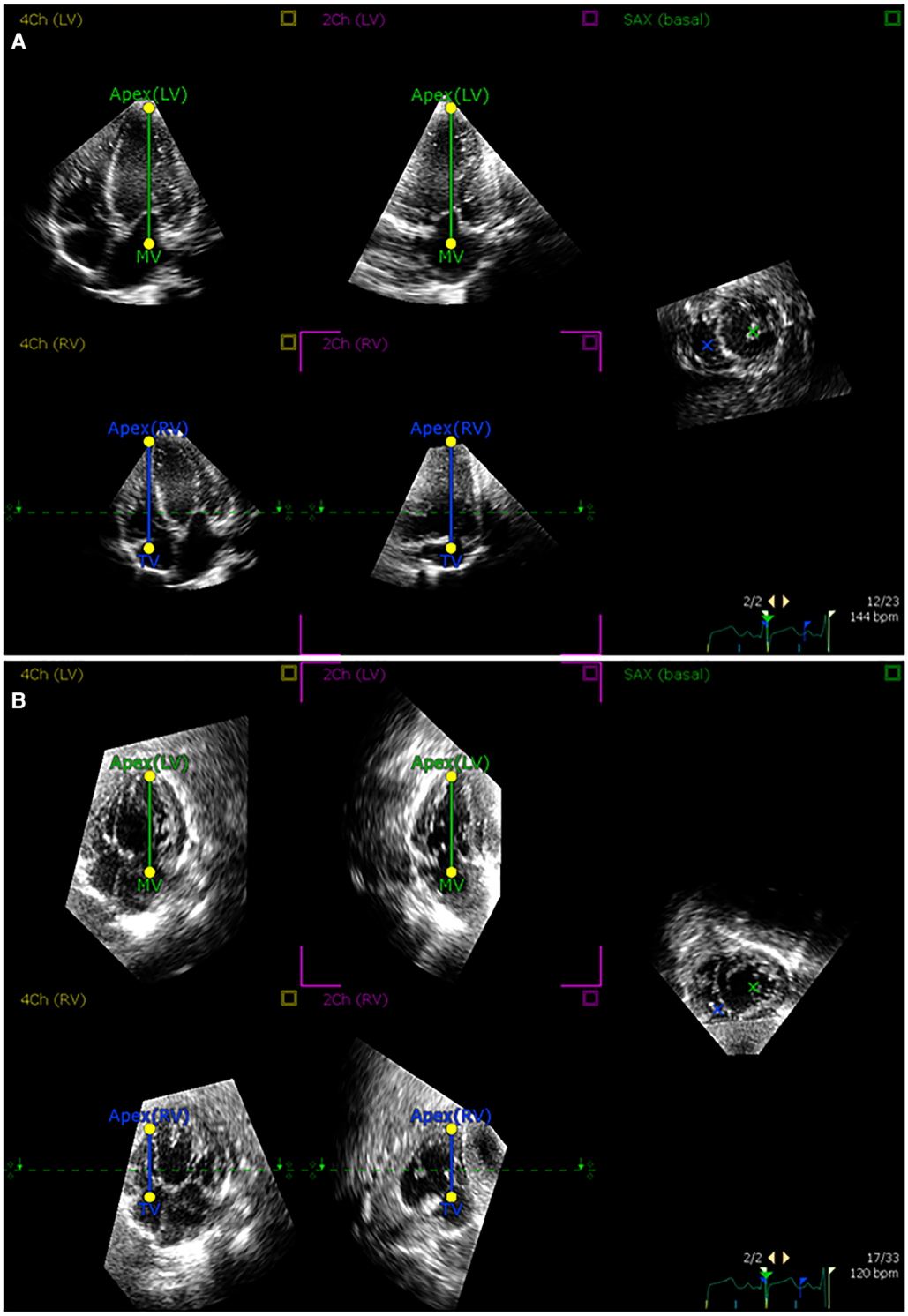

FIGURE 3
Alignment of 3D echocardiographic images from apical and subcostal views. An example of alignment of (A) apical and (B) subcostal views in the postprocessing software according to prespecified landmarks.

TABLE 1 Patient demographics ($n = 47$).

Characteristics	Value
Age (years) (median and range)	9.5 (0.8–16)
Female (%)	29% (14)
Body surface area (m^2)	1 (0.7–1.3)
Body mass index (kg/m^2)	16.5 (15.5–19.2)
Height (cm)	131.0 (109.3–149.0)
Heart rate (bpm)	80 (73.0–96.0)
CMR	
RV EDV, ml	92.7 (67.5–123.7)
RV ESV, ml	42.7 (26.7–56.7)
Diagnosis	
Aortic stenosis	6
Atrioventricular canal defect	4
Atrial septal defect	3
Ventricular septal defect	3
Shone syndrome	3
Double outlet right ventricle	2
Partial anomalous pulmonary venous return	2
Coarctation of the aorta	2
Tetralogy of Fallot	2
Other congenital heart disease	10
Other non-congenital heart disease	10

Data are presented as median and interquartile ranges (except for age). EDV, end-diastolic volume; ESV, end-systolic volume. Other congenital heart disease includes: dysplastic tricuspid valve; double chamber right ventricle; hypoplastic left heart syndrome; left ventricular non-compaction; mitral valve prolapse; pulmonary valve stenosis and atresia; transposition of the great arteries. Other non-congenital heart disease includes: alpha and beta thalassemia; hepatoblastoma; lymphatic malformation; Loeys-Dietz syndrome; multi-inflammatory disease syndrome in children; pulmonary hypertension; sickle cell disease; ventricular ectopy. Two patients were judged to have normal cardiac structure and function.

Assessment of 3DEcho volume measurement reproducibility

Inter- and intra-observer reproducibility data for RV EDV and RV ESV volume measurements using the two views are presented in Table 3. ICC values are in the good to excellent range (all >0.75) with slightly higher values for all EDV volumes measurements compared to ESV. The mean difference between the two measurements was statistically significant only for inter-observer subcostal RV ESV ($p = 0.03$).

Discussion

In this study, we compared 3DEcho RV volume measurements from subcostal vs. apical views using CMR as the reference standard in a pediatric population. Overall, the volumes derived from echocardiography agreed well with those from CMR, for both systolic and diastolic measurements. In addition, we found no significant difference in the percent error of the measured volumes between the two views relative to CMR, thus, neither view clearly emerged as consistently inferior relative to the other.

Apical and subcostal view

The great majority of descriptions of 3DEcho RV volume acquisitions have used the apical view in a wide range of ages, in both normal and abnormal hearts (13–15, 20, 22, 24–26). In the pediatric population, the feasibility of quantifying 3D RV volumes from this view has varied widely with reported ranges between 20% (20) to 91% (14). 3DEcho RV volumes acquired from the apical view have been reported to correlate well with CMR (14, 22); however, there are limitations to acquisition from this view. For example, when the RV is dilated, portions of the ventricle may be incompletely captured from apical imaging, particularly the region of the heart adjacent to the transducer and the right ventricular outflow (14). In these cases, the 3D RV volumes may be significantly underestimated (13) (for example, inconsistent representation of the outflow tract). To overcome this issue, the subcostal view has been proposed as an alternative view for acquiring 3D RV volumes (20). In one early report describing its use in a pediatric cohort, the authors describe that analysis was feasible in 44% of the patients using this view, with only 20% feasibility in the same patients using the apical window. In our study, the feasibility of analysis was not examined; nearly all images could be analyzed as subjects had been preselected for having good-quality images from both views.

Comparison of 3D RV volumes to CMR

Comparisons of 3DEcho-based RV to CMR have been reported in multiple studies and nearly all have used the apical view for the echo-based quantification. For example, Dragulescu et al. compared 3DEcho RV volume images to CMR in 36 pediatric patients ages 7–18 years. They found that 3D RV EDV and ESV correlated very well with CMR (correlation coefficients were 0.99 for both EDV and ESV). In their report, Dragulescu et al. highlighted the importance of manually adjusting the endocardial borders and landmarks (such as tricuspid and pulmonary valves) to increase correlation of 3DEcho (14); this was similar to the techniques which we used in the current study. In a later report, Laser et al. (22) also found that 3DEcho RV volumes (EDV, ESV) were highly correlated to CMR (r values 0.98 for both volumes). Similarly, Muraru et al., in a cohort of congenital heart disease patients that included both pediatric and adult patients, showed that 3DEcho RV volumes correlated highly with CMR values ($r = 0.92$ and 0.93 for ESV and EDV, respectively) (11). Similar to these descriptions, our EDV measurements, from the apical view, agreed well with the CMR (ICC 0.94). ESV measurements, however, were less reliable (ICC 0.74). Some of the difference in our findings and those reported in the literature might be explained by differences in patient size and age, and the nature of the congenital heart disease in the included cohort, with variations in the degree of dilation of the portions of the RV that are particularly difficult to image by 3DEcho.

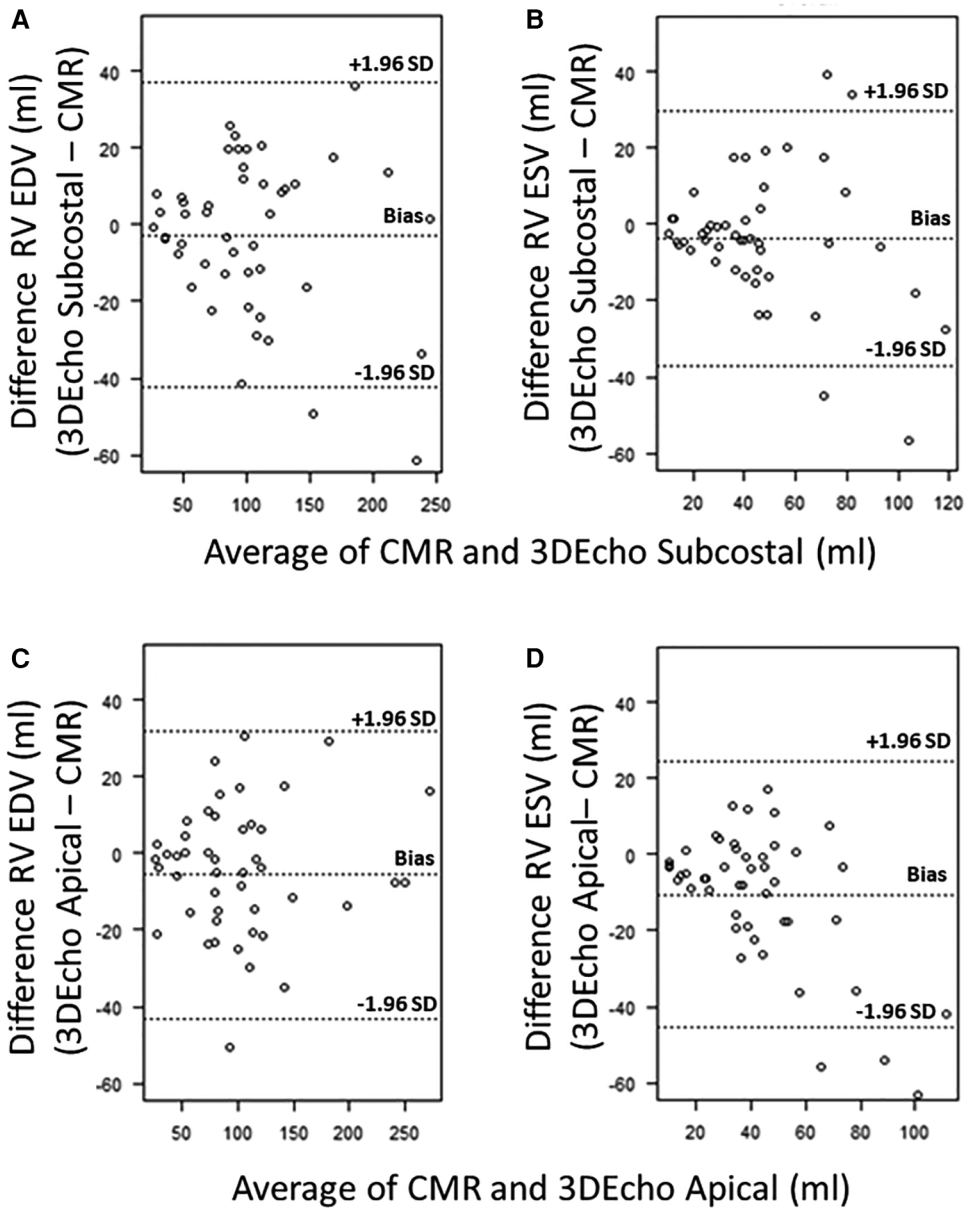

FIGURE 4
Bland–Altman plots for 3DEcho vs. CMR volumetric measurements ($N = 47$). Bland–Altman plots for 3DEcho vs. CMR for: end-diastolic measurements (panels **A**,**C**); end-systolic measurements (panels **B**,**D**). CMR, cardiac magnetic resonance; EDV, end diastolic volume; ESV, end systolic volume; ml, milliliter; RV, right ventricular.

To the best of our knowledge, the only other study that has compared 3DEcho RV volumes acquired from the subcostal view to CMR measurements was also from our group (27). In this report, we studied a pediatric population ages 2 to 8 years with a variety of forms of single ventricle congenital heart disease. EDV and ESV agreed well with CMR values (ICCs 0.95 and 0.94, respectively) (27). In the current study, 3DEcho-based EDV from the subcostal view also agreed well with CMR (ICC = 0.93). ESV agreement was good (ICC 0.81) but somewhat less robust. In a subgroup analysis, agreement was best in the youngest cohort, perhaps reflecting enhanced image quality in this group of patients relative to the older cohort.

Reproducibility

Prior reports of RV volume measurements (both EDV and ESV) have described good to excellent intra- and inter-observer reproducibility with less reproducibility for intra-observer readings (14, 17, 18, 20, 27, 28). Our results for intra- and intra-observer reproducibility follow a similar pattern with ICC values reflecting good agreement. Values were generally higher for intra-observer measurements, compared to inter-observer, as is typically the case, and were higher for end-diastolic volume compared to end-systolic volume. The latter finding is likely a reflection of the highly trabeculated nature of the RV leading to

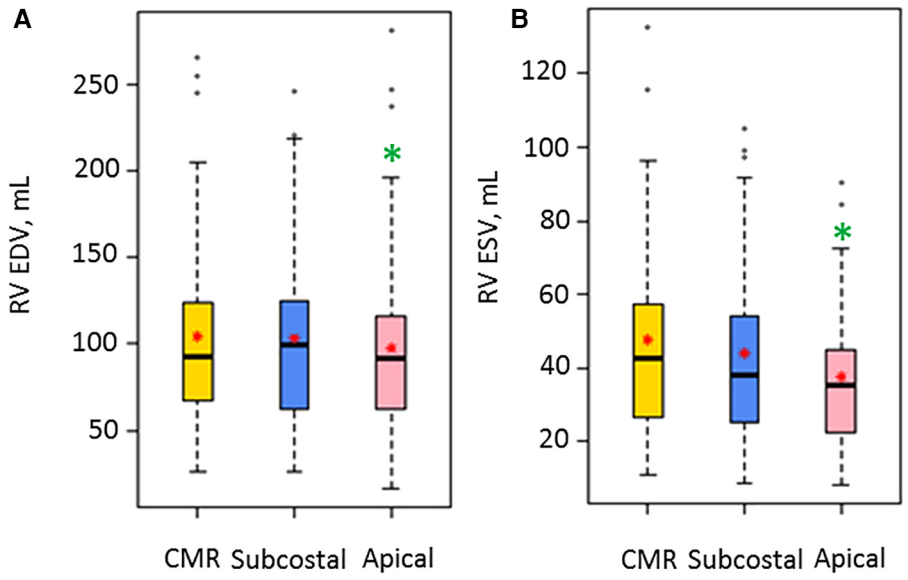

FIGURE 5
Box plots for volume measurements by CMR and the two 3D Echo views ($N = 47$). EDV, end diastolic volume; ESV, end systolic volume; ml, milliliter; RV, right ventricular. A red star indicates the mean value, and a solid box line indicates the median value. A green asterisk shows significant differences for the 3DEcho view relative to CMR.

difficulty identifying the optimal location for placing the end-systolic contour.

Study limitations

While CMR was considered a reference standard, this technology itself has a certain amount of intrinsic variability in volume measurement. However, CMR is considered the most reliable imaging modality for the assessment of ventricular volumes. Our patients did not have the echo and CMR performed at precisely the same time. However, 3DEcho was performed soon before or after the CMR to mitigate change in patient conditions as much as possible. Finally, while differences are reported as "statistically significant", these differences may not necessarily have clinical importance.

Conclusions

3DEcho measurements of RV volumes based on either subcostal or apical views agree well with corresponding values from CMR. There were no significant differences in the errors calculated by either view relative to CMR. These results support the use of the subcostal view as an alternative to the apical view when acquiring 3DEcho volumes in pediatric patients with good subcostal views, particularly if the RV outflow is not well seen in the apical view. These findings may encourage the use of 3DEcho

TABLE 2 Comparisons of RV volumes calculated by 3DEcho views vs. CMR; mean values, absolute percent error, and ICC.

	Mean difference	Absolute %error	ICC			
	All		All	<6 years	6–12 years	>12 years
	($n = 47$)			$n = 14$	$n = 21$	$n = 12$
Subcostal vs. CMR						
EDV, ml	−2.8 ± 20.2	15.2 ± 9.4	0.93	0.92	0.61	0.89
ESV, ml	−3.7 ± 17.1	25.0 ± 16.7	0.81	0.91	0.36	0.79
Apical vs. CMR						
EDV, ml	−5.7 ± 19.1	15.6 ± 15.3	0.94	0.82	0.61	0.95
ESV, ml	−10.6 ± 17.76	30.7 ± 21.1	0.74	0.67	0.34	0.61

CMR, cardiac magnetic resonance; EDV, end-diastolic volume; ESV, end-systolic volume; ICC, interclass correlation coefficient.

TABLE 3 Intra and inter-observer reproducibility for 3D Echo according to view ($n = 10$).

	Mean difference O2–O1 95% CI	Paired test p	Absolute % error O2–O1	ICC (95%CI)
Intra-observer				
Subcostal				
RV EDV	−2.5 ± 15.2 (−32.4 to 27.3)	0.61	13.8 ± 9.6	0.96 (0.94, 0.98)
RV ESV	2.9 ± 10.4 (−17.5 to 23.2)	0.41	17.2 ± 16.6	0.89 (0.82, 0.94)
Apical				
RV EDV	3.8 ± 17.8 (−31.2 to 38.7)	0.52	13.8 ± 14.4	0.96 (0.93, 0.98)
RV ESV	6.5 ± 9.7 (−12.5 to 25.5)	0.06	23.9 ± 16.7	0.90 (0.84, 0.94)
Inter-observer				
Subcostal				
RV EDV	9.49 ± 26.25 (−41.96, 60.94)	0.28	20.8 ± 21.0	0.88 (0.80, 0.93)
RV ESV	13.11 ± 15.90 (−18.05, 44.26)	**0.03**	36.2 ± 18.8	0.76 (0.61, 0.85)
Apical				
RV EDV	8.73 ± 23.65 (−37.62, 55.09)	0.27	18.8 ± 15.6	0.92 (0.87, 0.96)
RV ESV	8.11 ± 13.28 (−17.91, 34.13)	0.09	33.4 ± 17.9	0.82 (0.70, 0.89)

EDV, end diastolic volume; ESV, end systolic volume; O1 and O2, observer 1 and 2; RV, right ventricular.

measurement of RV volumes in the pediatric population, particularly when access to CMR is limited.

Data availability statement

The raw data supporting the conclusions of this article will be made available by the authors, without undue reservation. The data and materials from this study will be available upon request and following approval from our Institutional Review Board.

Ethics statement

The studies involving human participants were reviewed and approved by Institutional Review Board—Boston Children's Hospital. Written informed consent to participate in this study was provided by the participants' legal guardian/next of kin.

Author contributions

All authors provided substantial contribution to the conception of the study; AMF and DMH designed the study; AMF and KB collected data; AMF, ML, LAS, DMH analyzed and interpreted data; AMF, ML, and LAS prepared figures; AMF and DMH drafted the manuscript. All authors contributed to the article and approved the submitted version.

Funding

We would like to acknowledge funding from the Higgins Family Research Fund.

Acknowledgements

The authors would like to thank the sonographers who helped in acquiring the 3DEchos: Isabella Andrade, Efe Clode, Kathryn Cronin, Brenna Hardiman, Sara Keyser, Manouk Kirakosian, Linda Le, Rose Lipinski, Kaitlyn Lozier, Rebecca Odour, Stephen O'Neil, Stephanie Quealy, Nicole Rabideau, Marga Rivera, Ingrid Roth, Matthew Schildmeier, Eugenya Stantcheva, Stephanie Strout, Xiahong Su, Bridget Weygand, and Kara Zammito. In addition, we thank Dr. Sonal Jhaveri for her dedication in teaching scientific writing and for editing an early version of the manuscript.

Conflict of interest

The authors declare that the research was conducted in the absence of any commercial or financial relationships that could be construed as a potential conflict of interest.

Publisher's note

References

1. Geva T. Repaired tetralogy of Fallot: the roles of cardiovascular magnetic resonance in evaluating pathophysiology and for pulmonary valve replacement decision support. *J Cardiovasc Magn Reson.* (2011) 13(1):9. doi: 10.1186/1532-429X-13-9

2. Williams RG, Pearson GD, Barst RJ, Child JS, del Nido P, Gersony WM, et al. Report of the national heart, lung, and blood institute working group on research in adult congenital heart disease. *J Am Coll Cardiol.* (2006) 47(4):701–7. doi: 10.1016/j.jacc.2005.08.074

3. Oosterhof T, van Straten A, Vliegen HW, Meijboom FJ, van Dijk AP, Spijkerboer AM, et al. Preoperative thresholds for pulmonary valve replacement in patients with corrected tetralogy of Fallot using cardiovascular magnetic resonance. *Circulation.* (2007) 116(5):545–51. doi: 10.1161/CIRCULATIONAHA.106.659664

4. Knauth AL, Gauvreau K, Powell AJ, Landzberg MJ, Walsh EP, Lock JE, et al. Ventricular size and function assessed by cardiac MRI predict major adverse clinical outcomes late after tetralogy of Fallot repair. *Heart.* (2008) 94(2):211–6. doi: 10.1136/hrt.2006.104745

5. Geva T, Sandweiss BM, Gauvreau K, Lock JE, Powell AJ. Factors associated with impaired clinical status in long-term survivors of tetralogy of Fallot repair evaluated by magnetic resonance imaging. *J Am Coll Cardiol*. (2004) 43(6):1068–74. doi: 10.1016/j.jacc.2003.10.045

6. Shimazaki Y, Kawashima Y, Mori T, Kitamura S, Matsuda H, Yokota K. Ventricular volume characteristics of single ventricle before corrective surgery. *Am J Cardiol*. (1980) 45(4):806–10. doi: 10.1016/0002-9149(80)90125-3

7. Davlouros PA, Niwa K, Webb G, Gatzoulis MA. The right ventricle in congenital heart disease. *Heart*. (2006) 92(Suppl 1):i27–38. doi: 10.1136/hrt.2005.077438

8. Piran S, Veldtman G, Siu S, Webb GD, Liu PP. Heart failure and ventricular dysfunction in patients with single or systemic right ventricles. *Circulation*. (2002) 105(10):1189–94. doi: 10.1161/hc1002.105182

9. Marx GR, Shirali G, Levine JC, Guey LT, Cnota JF, Baffa JM, et al. Multicenter study comparing shunt type in the Norwood procedure for single-ventricle lesions: three-dimensional echocardiographic analysis. *Circ Cardiovasc Imaging*. (2013) 6 (6):934–42. doi: 10.1161/CIRCIMAGING.113.000304

10. Kilner PJ, Geva T, Kaemmerer H, Trindade PT, Schwitter J, Webb GD. Recommendations for cardiovascular magnetic resonance in adults with congenital heart disease from the respective working groups of the European society of cardiology. *Eur Heart J*. (2010) 31(7):794–805. doi: 10.1093/eurheartj/ehp586

11. Muraru D, Spadotto V, Cecchetto A, Romeo G, Aruta P, Ermacora D, et al. New speckle-tracking algorithm for right ventricular volume analysis from three-dimensional echocardiographic data sets: validation with cardiac magnetic resonance and comparison with the previous analysis tool. *Eur Heart J Cardiovasc Imaging*. (2016) 17(11):1279–89. doi: 10.1093/ehjci/jev309

12. Laser KT, Horst JP, Barth P, Kelter-Klöpping A, Haas NA, Burchert W, et al. Knowledge-based reconstruction of right ventricular volumes using real-time three-dimensional echocardiographic as well as cardiac magnetic resonance images: comparison with a cardiac magnetic resonance standard. *J Am Soc Echocardiogr*. (2014) 27(10):1087–97. doi: 10.1016/j.echo.2014.05.008

13. Khoo NS, Young A, Occleshaw C, Cowan B, Zeng IS, Gentles TL. Assessments of right ventricular volume and function using three-dimensional echocardiography in older children and adults with congenital heart disease: comparison with cardiac magnetic resonance imaging. *J Am Soc Echocardiogr*. (2009) 22(11):1279–88. doi: 10.1016/j.echo.2009.08.011

14. Dragulescu A, Grosse-Wortmann L, Fackoury C, Mertens L. Echocardiographic assessment of right ventricular volumes: a comparison of different techniques in children after surgical repair of tetralogy of Fallot. *Eur Heart J Cardiovasc Imaging*. (2012) 13(7):596–604. doi: 10.1093/ejechocard/jer278

15. Sato T, Calderon RJ, Klas B, Pedrizzetti G, Banerjee A. Simultaneous volumetric and functional assessment of the right ventricle in hypoplastic left heart syndrome after fontan palliation, utilizing 3-dimensional speckle-tracking echocardiography. *Circ J*. (2020) 84(2):235–44. doi: 10.1253/circj.CJ-19-0926

16. Kamińska H, Małek Ł A, Barczuk-Falęcka M, Werner B. Usefulness of three-dimensional echocardiography for the assessment of ventricular function in children: comparison with cardiac magnetic resonance, with a focus on patients with arrhythmia. *Cardiol J*. (2021) 28(4):549–57. doi: 10.5603/CJ.a2019.0026

17. Jone PN, Schäfer M, Pan Z, Bremen C, Ivy DD. 3D Echocardiographic evaluation of right ventricular function and strain: a prognostic study in paediatric pulmonary hypertension. *Eur Heart J Cardiovasc Imaging*. (2018) 19(9):1026–33. doi: 10.1093/ehjci/jex205

18. Bell A, Rawlins D, Bellsham-Revell H, Miller O, Razavi R, Simpson J. Assessment of right ventricular volumes in hypoplastic left heart syndrome by real-time three-dimensional echocardiography: comparison with cardiac magnetic resonance imaging. *Eur Heart J Cardiovasc Imaging*. (2014) 15(3):257–66. doi: 10.1093/ehjci/jet145

19. Wu VC, Takeuchi M. Echocardiographic assessment of right ventricular systolic function. *Cardiovasc Diagn Ther*. (2018) 8(1):70–9. doi: 10.21037/cdt.2017.06.05

20. Renella P, Marx GR, Zhou J, Gauvreau K, Geva T. Feasibility and reproducibility of three-dimensional echocardiographic assessment of right ventricular size and function in pediatric patients. *J Am Soc Echocardiogr*. (2014) 27(8):903–10. doi: 10.1016/j.echo.2014.04.008

21. Kurath-Koller S, Koestenberger M, Hansmann G, Cantinotti M, Tissot C, Sallmon H. Subcostal echocardiographic imaging in neonatal and pediatric intensive care. *Front Pediatr*. (2021) 9:471558. doi: 10.3389/fped.2021.471558

22. Laser KT, Karabiyik A, Körperich H, Horst JP, Barth P, Kececioglu D, et al. Validation and reference values for three-dimensional echocardiographic right ventricular volumetry in children: a multicenter study. *J Am Soc Echocardiogr*. (2018) 31(9):1050–63. doi: 10.1016/j.echo.2018.03.010

23. Alfakih K, Plein S, Thiele H, Jones T, Ridgway JP, Sivananthan MU. Normal human left and right ventricular dimensions for MRI as assessed by turbo gradient echo and steady-state free precession imaging sequences. *J Magn Reson Imaging*. (2003) 17(3):323–9. doi: 10.1002/jmri.10262

24. Nagata Y, Wu VC, Kado Y, Otani K, Lin FC, Otsuji Y, et al. Prognostic value of right ventricular ejection fraction assessed by transthoracic 3D echocardiography. *Circ Cardiovasc Imaging*. (2017) 10(2):e005384. doi: 10.1161/CIRCIMAGING.116.005384

25. Grewal J, Majdalany D, Syed I, Pellikka P, Warnes CA. Three-dimensional echocardiographic assessment of right ventricular volume and function in adult patients with congenital heart disease: comparison with magnetic resonance imaging. *J Am Soc Echocardiogr*. (2010) 23(2):127–33. doi: 10.1016/j.echo.2009.11.002

26. Medvedofsky D, Addetia K, Patel AR, Sedlmeier A, Baumann R, Mor-Avi V, et al. Novel approach to three-dimensional echocardiographic quantification of right ventricular volumes and function from focused views. *J Am Soc Echocardiogr*. (2015) 28(10):1222–31. doi: 10.1016/j.echo.2015.06.013

27. Soriano BD, Hoch M, Ithuralde A, Geva T, Powell AJ, Kussman BD, et al. Matrix-array 3-dimensional echocardiographic assessment of volumes, mass, and ejection fraction in young pediatric patients with a functional single ventricle: a comparison study with cardiac magnetic resonance. *Circulation*. (2008) 117 (14):1842–8. doi: 10.1161/CIRCULATIONAHA.107.715854

28. Vogel M, Gutberlet M, Dittrich S, Hosten N, Lange PE. Comparison of transthoracic three dimensional echocardiography with magnetic resonance imaging in the assessment of right ventricular volume and mass. *Heart*. (1997) 78(2):127–30. doi: 10.1136/hrt.78.2.127

frontiers | Frontiers in Cardiovascular Medicine

TYPE Original Research
PUBLISHED 03 August 2023
DOI 10.3389/fcvm.2023.1141027

OPEN ACCESS

EDITED BY
Andreas Rolf,
Kerckhoff Klinik, Germany

REVIEWED BY
Piet Claus,
KU Leuven, Belgium
Jayant Shyam Jainandunsing,
University Medical Center Groningen,
Netherlands

*CORRESPONDENCE
Attila Kovacs
attila.kovacs@med.semmelweis-univ.hu
David M. Harrild
David.harrild@cardio.chboston.org

†These authors have contributed equally to this work and share first authorship

‡These authors have contributed equally to this work and share last authorship

RECEIVED 09 January 2023
ACCEPTED 04 July 2023
PUBLISHED 03 August 2023

CITATION
Valle C, Ujvari A, Elia E, Lu M, Gauthier N, Hoganson D, Marx G, Powell AJ, Ferraro A, Lakatos B, Tősér Z, Merkely B, Kovacs A and Harrild DM (2023) Right ventricular contraction patterns in healthy children using three-dimensional echocardiography.
Front. Cardiovasc. Med. 10:1141027.
doi: 10.3389/fcvm.2023.1141027

Right ventricular contraction patterns in healthy children using three-dimensional echocardiography

Christopher Valle[1,2†], Adrienn Ujvari[3†], Eleni Elia[1,2,4], Minmin Lu[1,2], Naomi Gauthier[1,2], David Hoganson[5], Gerald Marx[1,2], Andrew J. Powell[1,2], Alessandra Ferraro[1,2], Bálint Lakatos[3], Zoltán Tősér[6], Béla Merkely[3], Attila Kovacs[3,6*‡] and David M. Harrild[1,2*‡]

[1]Department of Cardiology, Boston Children's Hospital, Boston, MA, United States, [2]Department of Pediatrics, Harvard Medical School, Boston, MA, United States, [3]Heart and Vascular Center, Semmelweis University, Budapest, Hungary, [4]School of Engineering, Computing and Mathematics, Oxford Brookes University, Oxford, United Kingdom, [5]Department of Cardiac Surgery, Boston Children's Hospital, Boston, MA, United States, [6]Argus Cognitive, Inc., Lebanon, NH, United States

Background: The right ventricle (RV) has complex geometry and function, with motion along three separate axes—longitudinal, radial, and anteroposterior. Quantitative assessment of RV function by two-dimension echocardiography (2DE) has been limited as a consequence of this complexity, whereas newer three dimensional (3D) analysis offers the potential for more comprehensive assessment of the contributors to RV function. The aims of this study were to quantify the longitudinal, radial and anteroposterior components of global RV function using 3D echocardiography in a cohort of healthy children and to examine maturational changes in these parameters.

Methods: Three-dimensional contours of the RV were generated from a cohort of healthy pediatric patients with structurally normal hearts at two centers. Traditional 2D and 3D echo characteristics were recorded. Using offline analysis of 3D datasets, RV motion was decomposed into three components, and ejection fractions (EF) were calculated (longitudinal-LEF; radial-REF; and anteroposterior-AEF). The individual decomposed EF values were indexed against the global RVEF. Strain values were calculated as well.

Results: Data from 166 subjects were included in the analysis; median age was 13.5 years (range 0 to 17.4 years). Overall, AEF was greater than REF and LEF ($29.2 \pm 6.2\%$ vs. $25.1 \pm 7.2\%$ and $25.7 \pm 6.0\%$, respectively; $p < 0.001$). This remained true when indexed to overall EF ($49.8 \pm 8.7\%$ vs. $43.3 \pm 11.6\%$ and $44.4 \pm 10\%$, respectively; $p < 0.001$). Age-related differences were present for global RVEF, REF, and all components of RV strain.

Conclusions: In healthy children, anteroposterior shortening is the dominant component of RV contraction. Evaluation of 3D parameters of the RV in children is feasible and enhances the overall understanding of RV function, which may allow improvements in recognition of dysfunction and assessment of treatment effects in the future.

KEYWORDS

right ventricle, three dimensional echocardiography, ventricular mechanics, myocardial deformation, pediatric cardiology

Abbreviations

2D, two-dimensional; 3D, three-dimensional; AEF, anteroposterior ejection fraction; BMI, body mass index; BSA, body surface area; EF, ejection fraction; FAC, fractional area change; GAS, global area strain; GCS, global circumferential strain; GLS, global longitudinal strain; ICC, intraclass correlation coefficient; LEF, longitudinal ejection fraction; LV, left ventricle; REF, radial ejection fraction; RV, right ventricle; SD, standard deviation; TAPSE, tricuspid annular plane systolic excursion.

Introduction

Accurate assessment of RV morphology and function are of critical importance in cardiovascular disease in children and adolescents, particularly in complex congenital heart disease involving systemic RV physiology (1–3), obstructive right-sided heart disease (4, 5) and pulmonary hypertension (6, 7). However, compared to the established tools and techniques developed for assessment of the LV, evaluation of the complex anatomy and contraction of the RV by two-dimensional (2D) echocardiography remains significantly limited in clinical practice. Recently, however, three-dimensional echocardiography (3DE) has been shown to be able to produce excellent quantification of RV volumes and has been validated against gold-standard modalities such as cardiac magnetic resonance imaging, even in children with complex congenital heart disease (8–10).

The pattern of right ventricular (RV) contraction is dictated by its complex structure on both gross and microscopic levels. In the normal RV, two myofiber layers are present: a subendocardial layer that consists primarily of longitudinally aligned fibers and a subepicardial layer that consists primarily of circumferentially oriented fibers (11–14). This arrangement results in three primary contributors to RV ejection: (1) traction of the tricuspid annulus toward the apex leading to longitudinal shortening; (2) a "bellows"-like inward movement of the RV free wall leading to radial shortening; and (3) traction of the RV free wall associated with left ventricular (LV) deformation, leading to anteroposterior shortening (15, 16).

Accordingly, the aim of this study was to use a novel 3DE-based analysis technique to develop foundational data describing the relative contributions of longitudinal, radial, and anteroposterior motion components of global RV function in a cohort of healthy children with structurally normal hearts. Specifically, we sought to examine differences in the relative contributions of the 3 components of ejection fraction in children and to look for changes in the contribution of these components as a function of age.

Methods

Healthy children age <18 years were included from two centers: Boston Children's Hospital, Boston, MA, USA; and the Heart and Vascular Center of the Semmelweis University, Budapest, Hungary. Subjects at the Boston site were identified retrospectively from an existing database of 3DE images with accompanying clinical and demographic information. Patients in this database had presented to the outpatient clinic between 2014 and 2020 for evaluation of a common cardiac condition (most frequently murmur, chest pain, syncope, or family history of cardiac condition), were judged to have a structurally and functionally normal heart, and were discharged from further follow-up. Exclusion criteria included structural abnormalities other than patent foramen ovale or trivial branch pulmonary stenosis (maximum instantaneous gradient < 15 mmHg within the first two years of life); arrhythmia (other than rare atrial or ventricular premature beats) including sinus bradycardia or tachycardia (heart rate z-score < -2 or $> +2$ for age), acquired heart disease (cardiomyopathy, chemotherapy exposure, and Kawasaki disease), or co-morbidities with a potential impact on ventricular size and function (i.e., hypertension, renal failure, anemia, history of prematurity, chronic lung disease, pulmonary hypertension, obstructive sleep apnea, and connective tissue disorder).

Healthy volunteers at the Semmelweis site were recruited from local schools; no individuals were identified subsequently with significant cardiac abnormalities revealed by echocardiography, electrocardiography, blood pressure measurement, or review of medical history. Study protocols were approved by both centers' institutional review boards. Given the retrospective nature of recruitment at Boston Children's Hospital, informed consent was waived at that site. At Semmelweiss University, families of all participants provided written informed consent to participate in the study.

Blood pressure, height, and weight were recorded for all subjects. Body surface area (BSA) was calculated using the Mosteller formula (17).

2D and 3d echocardiography

Echocardiographic acquisitions were performed using the Philips (IE33 and Epiq, Philips, Cambridge, MA) and GE (E95, GE Healthcare, Horten, Norway) ultrasound systems, in accordance with the American Society of Echocardiography (ASE) standards for performing a pediatric echocardiogram (18). Parameters recorded from the 2D echo images included tricuspid annular plane systolic excursion (TAPSE), RV length, fractional area change (FAC), and qualitative assessment of the degree of tricuspid regurgitation. LV volumes were calculated from the $5/6 \times \text{area} \times \text{length}$ formula and presented in raw fashion, as well as being indexed to BSA.

In addition to the standard 2D echocardiographic protocol, electrocardiographically gated full-volume 3D data sets reconstructed from four or six cardiac cycles optimized for RV views were obtained for offline analysis. At the Semmelweiss site, images were obtained from the apical window using the 4Vc-D transducer (GE Healthcare, Horten, Norway). At the Boston site, images were obtained from the apical or subcostal window using the X5 probe (Philips, Cambridge, MA) in a patient-specific fashion (i.e., the window providing better image quality was used). Image quality was verified at the bedside to minimize stitching and dropout artifacts of the 3D data; breath-holding manuevers were used as appropriate for the developmental age of the child.

3D datasets were analyzed off-line using dedicated software (4D RV-Function; TomTec Imaging, Unterschleissheim, Germany). The algorithm detects the endocardial surface of the RV and, following manual correction, traces its motion throughout the cardiac cycle. End-diastolic volume, end-systolic volume, stroke volume, and free wall longitudinal strain were recorded.

Analysis of 3D components of right ventricular contraction

The 3D RV deformation analysis used has been previously described in detail (19, 20). Briefly, the constructed 3D meshes

were exported from TomTec 4D RV Function. Then, using the ReVISION software (Argus Cognitive, Lebanon, New Hampshire), the workflow consists of the following steps: (1) standardization of the 3D mesh orientation, (2) movement decomposition, and (3) calculation of volumes and strain values. Orientation adjustment was performed by a rule-based, automated method to define longitudinal, radial and anteroposterior directions as described in tetail elsewere (20). Motion decomposition along the aforementioned, orthogonal, anatomically relevant axes is performed in a vertex-based manner. By the decomposition of the model's motion along the three anatomically relevant orthogonal axes, the volume change of the RV attributable to each specific direction was determined (**Figure 1**).

Therefore, we measured component EF values (longitudinal EF—LEF, radial EF—REF, and anteroposterior EF—AEF). These raw decomposed EF values were then indexed to global RVEF (i.e., indexed AEF = AEF/global RVEF) to genertate the longitudinal EF index (LEFi), radial EF index (REFi), and anteroposterior EF index (AEFi). These measures quantify the relative contribution of the given direction to global RV performance. Note that the absolute volume change of the chamber is generated by the aggregated contribution of the three motion components. This composition is not additive, and consequentially, the sum of the decomposed volume changes is not equal to the global volume change; in other words, the relative contribution of the motion components do not add up to 100%. Global and decomposed volumes are calculated using the signed tetrahedron method (19).

To assess myocardial deformation, predefined longitudinally and circumferentially-oriented contours were used, and 3D global longitudinal strain (GLS) and global circumferential strain (GCS) were computed as previously described (20). 3D global area strain (GAS) was also calculated by the relative change of the endocardial surface between end-diastole and end-systole.

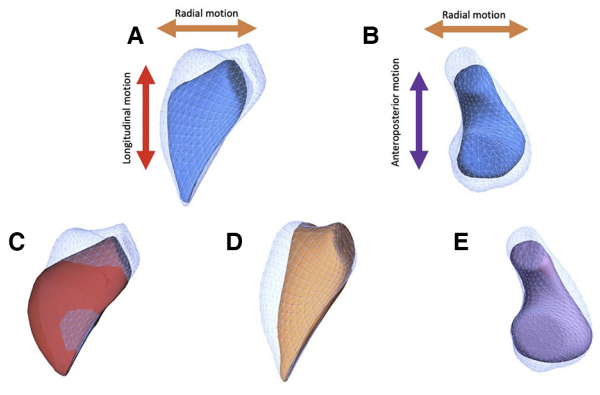

FIGURE 1
The three different components of right ventricular contraction from a representative subject. In the figure the global motion of the right ventricle is shown from anterior (A) and superior (B) views (blue mesh, RV end-diastolic volume; blue surface, RV end-systolic volume). RV end-systolic meshes can be generated by "locking" the RV motion in two directions, permitting motion in only a single axis and thus revealing the impact of decomposed contraction components. Thus, the change in ventricular volume attributable to shortening along the longitudinal (C, red surface), radial (D, orange surface) and anteroposterior (E, purple surface) can be separately quantified.

Statistical analysis

Continuous data were presented as mean ± standard deviation (SD) or median and interquartile range. Categorical data were presented as counts and percentages (% of total population). Outcomes were summarized according to age groups representing different categories of patient body size: *Infants*: <1 year, *Toddlers* >1–5 years, *School-Aged*: >5–10 years, *(Pre)Teens* > 10–18 years. One-way ANOVA or the Kruskal Wallis H test was performed to compare the distribution of parameters by age group as appropriate. Wilcoxon signed-rank test was used to assess for differences in the contribution of LEF, REF, and AEF within each pre-specified age group, with Bonferroni correction applied (i.e., level of statistical significance set at $p < 0.017$). In order to assess the impact of patient sex on the ejection fraction parameters, a general linear model was used to compare EF means by sex with adjustment for age to produce least-squares means.

To assess intercenter reproducibility, one operator from the Boston site and one from the Semmelweis site each reviewed a subset of 30 patients, blinded to the other's results. The strength of agreement was assessed by intraclass correlation coefficients (ICC) along with the Bland Altman plot.

Data analyses were performed with SAS software (version 9.4, SAS Institute Inc., Cary, North Carolina) and R 4.1.2 (2021 The R Foundation for Statistical Computing Platform). *P* values <0.05 were used to indicate statistical significance.

Results

The study population included 166 subjects (Boston = 76; Semmelweis = 90). Demographic and clinical characteristics of the study population are summarized in **Table 1**. The median age of subjects was 13.8 years (IQR 8.6 to 15.3), with a skewed distribution towards the oldest age group (as a consequence of the recruitment strategy at the Semmelweis site). The population was majority male ($n = 131$, 79%), driven by a male-predominant population recruited at the Semmelweiss site ($n = 81$, 90%).

Conventional echocardiographic measures of RV and LV function are presented in **Table 2**. Tricuspid annular plane systolic excursion (TAPSE) increased significantly with age. Most subjects had either no (92, 53%) or trivial (72, 42%) tricuspid regurgitation. There were no differences between groups in terms of RV FAC. Age-related variation in 2D free wall longitudinal strain was present, with the largest absolute values seen in the toddler and school-aged groups.

Table 3 presents 3D RV volumes and contraction patterns. RV volumes, global RVEF, REF and REFi, longitudinal and circumferential 3D strain parameters significantly differ by age group. Age-related differences were present for global RVEF, REF and REFi. Additionally, age-related differences were seen for all components of RV strain. **Supplementary Table S1** presents

TABLE 1 Patient characteristics.

	All ($n = 166$)	Infants ($n = 13$)	Toddlers ($n = 11$)	School-Aged ($n = 21$)	(Pre)Teens ($n = 121$)	*p*-value
Age, year	13.8 (8.6, 15.3)	0.1 (0.05, 0.1)	3.6 (3.3, 4.1)	6.3 (5.2, 7.9)	14.4 (13.6,15.7)	<0.001
Female [*n* (%)]	35 (21%)	7 (54%)	5 (45%)	7 (33%)	16 (13%)	
Height, m	1.49 ± 0.38	0.53 ± 0.07	1.00 ± 0.08	1.21 ± 0.11	1.69 ± 0.14	<0.001
Weight, kg	47.7 ± 23.8	4.2 ± 2.0	16.6 ± 3.2	23.3 ± 5.9	59.4 ± 15.3	<0.001
BMI, kg/m^2	19.1 ± 3.5	14.3 ± 2.0	16.3 ± 1.4	15.5 ± 1.5	20.5 ± 3.0	<0.001
BSA, m^2	1.39 ± 0.54	0.25 ± 0.07	0.68 ± 0.09	0.88 ± 0.14	1.66 ± 0.29	<0.001
SBP, mm Hg	117 ± 19	92 ± 14	100 ± 10	100 ± 10	125 ± 16	<0.001
DBP, mm Hg	65 ± 12	53 ± 11	53 ± 6	56 ± 8	68 ± 10	<0.001
HR, beats/min	80 ± 20	130 ± 13	89 ± 12	84 ± 14	73 ± 12	<0.001

Continuous data are expressed as mean ±SD, with the exception of age which are presented as median (IQR).
BMI, body mass index; BSA, body surface area; DBP, diastolic blood pressure; HR, heart rate; SBP, systolic blood pressure.

TABLE 2 Conventional echocardiographic characteristics.

	All ($n = 166$)	Infants ($n = 13$)	Toddlers ($n = 11$)	School-Aged ($n = 21$)	(Pre)Teens ($n = 121$)	*p*-value
TAPSE, mm	21.8 (16.9, 26.1)	6.2 (4.5, 9.0)	14.3 (12.0, 19.7)	17.1 (15.3, 19.6)	23.7 (20.9, 27.8)	<.001
RV FAC, %	48.8 (45.3, 52.4)	46.5 (42.9, 51.2)	51.3 (44.7, 54.2)	50.7 (48.7, 54.2)	48.5 (45.3, 52.2)	0.161
RV 2D FWLS, %	−30.4 (−33.7, −26.2)	−29.8 (−31.8, −23.2)	−34.8 (−39.0, −28.4)	−32.1 (−36.6, −30.9)	−29.4 (−33.0, −26.2)	0.016
2D LVEDV, ml	113.9 (74.6, 145.6)	9.4 (7.7, 11.1)	48.6 (39.0, 55.9)	62.8 (55.7, 74.6)	135.0 (110.9, 154.6)	<.001
2D LVEDVi, ml/m^2	77.2 (67.1, 85.8)	42.7 (35.0, 43.5)	70.8 (60.9, 75.5)	70.4 (66.8, 79.3)	79.8 (73.0, 88.9)	<.001
2D LVESV, ml	45.2 (26.3, 60.9)	3.7 (3.0, 3.9)	17.3 (12.5, 18.2)	21.3 (20.1, 26.3)	54.8 (42.5, 66.1)	<.001
2D LVESVi, ml/m^2	30.1 (24.9, 35.4)	14.6 (12.7, 16.5)	23.4 (21.1, 25.8)	25.3 (23.4, 26.8)	32.7 (28.1, 36.7)	<.001
LV EF, %	60.4 (57.0, 63.9)	61.5 (59.0, 64.3)	65.9 (64.0, 67.9)	64.0 (62.6, 67.0)	58.9 (56.3, 62.0)	<.001

Data are expressed as median (Q1, Q3).
2D, two-dimensional; EF, ejection fraction; FAC, fractional area change; FWLS, free wall longitudinal strain; LVEDVi, indexed left ventricular end-diastolic volume; LVESVi, indexed left ventricular end-systolic volume; RV, right ventricular; TAPSE, tricuspid annulus plane systolic excursion.

TABLE 3 Three-dimensional echocardiographic analysis of right ventricular size and ejection fraction components.

	All ($n = 166$)	Infants ($n = 13$)	Toddlers ($n = 11$)	School-aged ($n = 21$)	(Pre)Teens ($n = 121$)	*p*-value
3D RVEDV, ml	115.3 (66.0, 149.6)	9.4 (8.0, 10.0)	43.5 (37.5, 47.7)	56.3 (52.4, 64.3)	133.4 (107.2, 157.0)	**<.001**
3D RVEDVi, ml/m^2	74.8 (64.4, 87.3)	40.7 (38.0, 43.1)	64.4 (59.4, 67.9)	66.4 (59.9, 73.8)	80.1 (71.0, 89.9)	**<.001**
3D RVESV, ml	47.1 (25.6, 63.3)	3.9 (3.3, 4.9)	16.4 (15.2, 19.5)	22.4 (18.4, 25.6)	56.8 (43.0, 70.3)	**<.001**
3D RVESVi, ml/m^2	31.6 (24.6, 37.4)	16.0 (14.9, 18.8)	24.6 (22.2, 28.1)	25.8 (23.4, 27.4)	33.8 (28.8, 39.4)	**<.001**
RV EF, %	58.1 (54.6, 61.4)	55.1 (52.7, 61.1)	59.3 (55.0, 65.0)	62.1 (58.4, 64.6)	57.3 (54.3, 61.0)	**0.008**
LEF, %	25.8 (22.1, 29.8)	23.0 (19.3, 27.2)	27.6 (22.7, 35.8)	28.0 (23.4, 29.8)	25.8 (21.3, 29.7)	0.345
REF, %	25.3 (20.3, 30.6)	28.7 (22.6, 32.2)	26.8 (22.3, 31.7)	28.2 (25.7, 32.2)	24.1 (19.5, 29.7)	**0.020**
AEF, %	28.8 (24.8, 32.9)	27.6 (24.1, 33.8)	31.2 (27.2, 37.5)	32.6 (25.1, 36.4)	28.3 (24.7, 32.2)	0.109
LEFi, %	43.8 (39.1, 50.2)	43.0 (33.7, 43.7)	43.7 (40.8, 57.5)	43.7 (42.1, 51.1)	44.9 (38.2, 49.9)	0.436
REFi, %	43.7 (35.3, 51.3)	48.2 (42.8, 53.6)	45.8 (33.8, 59.2)	48.0 (43.4, 50.8)	42.4 (34.0, 51.1)	0.055
AEFi, %	50.7 (43.1, 55.6)	52.2 (41.5, 54.4)	57.2 (46.6, 60.9)	53.0 (42.1, 58.2)	50.5 (43.5, 54.0)	0.353
3D GAS, %	−40.3 (−43.7, −37.3)	−37.6 (−43.8, −34.4)	−43.8 (−44.8, −37.7)	−43.1 (−45.0, −39.0)	−40.1 (−42.7, −37.0)	**0.046**
3D GLS, %	−22.9 (−25.8, −20.5)	−18.9 (−23.7, −17.5)	−25.9 (−26.8, −22.7)	−24.5 (−25.8, −21.1)	−22.8 (−25.6, −20.9)	**0.029**
3D GCS, %	−23.6 (−26.6, −19.9)	−24.9 (−26.9, −20.9)	−25.6 (−27.0, −17.1)	−26.6 (−29.1, −22.5)	−22.7 (−25.9, −19.7)	**0.031**

Data are expressed as median (Q1, Q3).
3D, three-dimensional; AEF, anteroposterior ejection fraction; EF, ejection fraction; GAS, global area strain; GCS, global circumferential strain; GLS, global longitudinal strain; LEF, longitudinal ejection fraction; REF, radial ejection fraction; RVEDVi, indexed right ventricular end-diastolic volume; RVESVi, indexed right ventricular end-systolic volume.
Bolded values are statistically significant ($p < 0.05$).

sex-specific age-adjusted mean values for the ejection fraction parameters; no differences were identified between male and female subgroups.

Figure 2 shows the ejection fraction components for the entire cohort as well as broken down by age group. For the entire cohort, the AEF was greater than the other two components; the same pattern was observed for the oldest group. For the school-aged cohort, the AEF was greater than the LEF. No significant differences were observed among any components in the infants and toddlers.

There was excellent inter-center reproducibility with intraclass correlation coefficients of 0.97 (95% CI 0.94–0.98) for RV end-

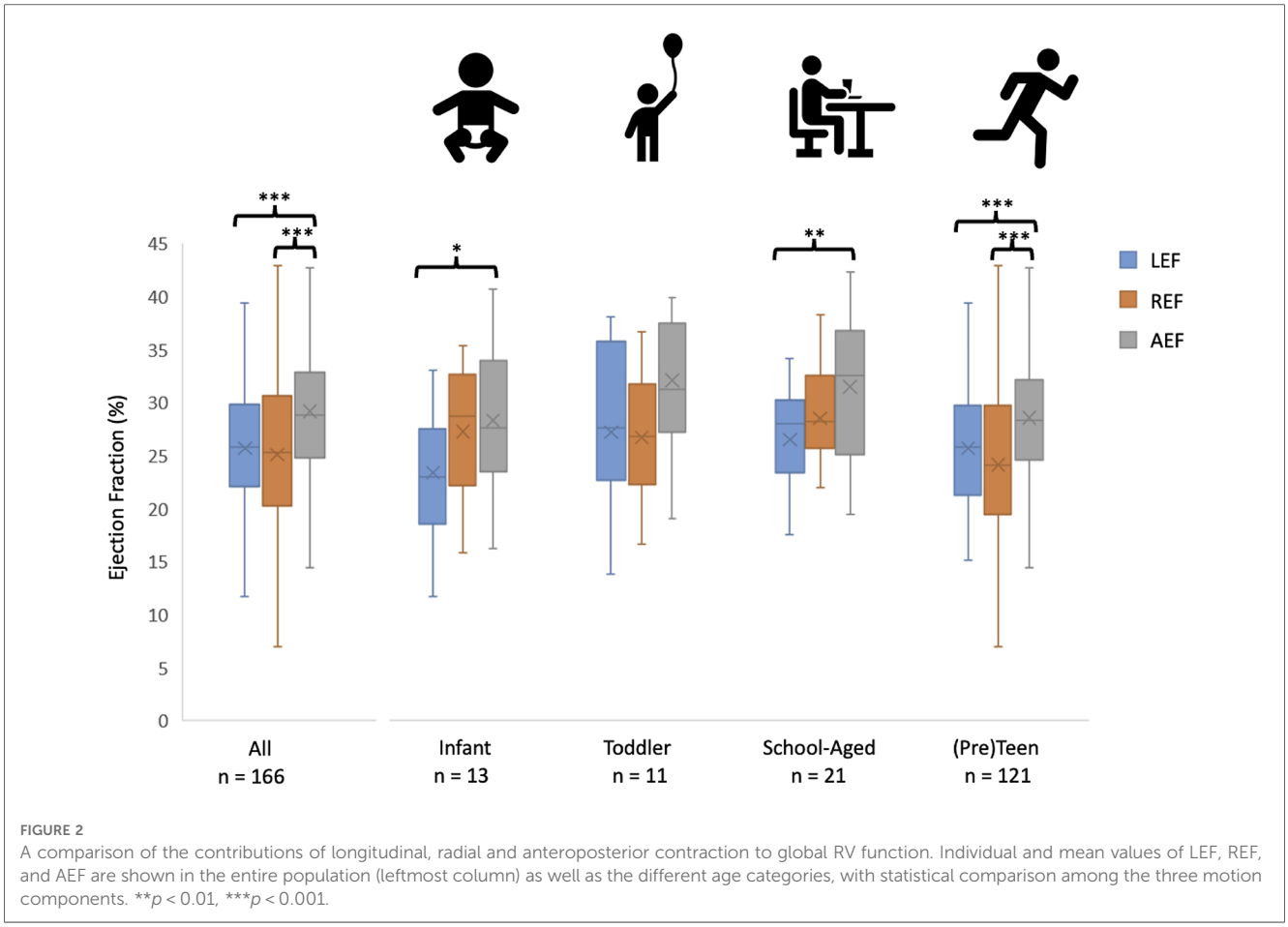

FIGURE 2
A comparison of the contributions of longitudinal, radial and anteroposterior contraction to global RV function. Individual and mean values of LEF, REF, and AEF are shown in the entire population (leftmost column) as well as the different age categories, with statistical comparison among the three motion components. $^{**}p < 0.01$, $^{***}p < 0.001$.

diastolic volume and 0.94 (95% CI 0.89–0.97) for RV end-systolic volume. Bland Altman plots are presented as **Supplementary Figure S1**. As the ReVISION method is a fully automated technique, it adds no further variability in addition to that represented in these volume comparisons.

Discussion

The primary aim of this two-center study was to define the specific contributions of longitudinal, radial and anteroposterior contraction to global RV function in a cohort of healthy children using 3D echocardiographic images and advanced analytical software. As well, we sought to describe the maturational changes that occur in each of the components of RV function, in addition to the global value. Our major finding was that whereas the contributions of the longitudinal and radial components were similar, a predominance for AP contraction was present in the overall cohort. Moreover, age-related differences were present for global RVEF, REF, REFi, and all compenents fof RV strain.

There are three primary mechanisms of RV contraction: longitudinal shortening with traction of the tricuspid valve annulus toward the apex, inward (radial) movement of the free wall, and anteroposterior directed motion of the RV wall related to LV deformation (15, 21). In this study, we identified the predominance of anteroposterior shortening in nearly every age group. Typical 2D parameters of RV function have relied upon simple, linear measurements which incompletely reflect the complex mechanics of RV function. For example, TAPSE is a measure of the longitudinal motion of the chamber, has been shown to correlate with global RVEF, and has been described in children with pulmonary hypertension with and without congenital heart disease (22). FAC is a measurement of both the radial contraction of the free wall as well as longitudinal traction of the tricuspid annulus and has been associated with changes in RV function in patients with Ebstein anomaly undergoing the cone procedure (23). While these techniques offer some degree of quantitative analysis of RV function, they are imperfect in that they do not account for RV function in all axes, failing to fully quantify the complex RV mechanics. Moreover, they do not meaningfully assess the anteroposterior contraction, which predominated in our study.

Prior groups have used 2D echocardiography to show that the contraction pattern of the RV in children changes over the first year of life as children transition from fetal circulation in which the RV faces a high afterload to post-natal circulation in which the pulmonary vascular resistance gradually declines over the first few months of life. One group used measurements of

TAPSE and a surrogate marker of radial contraction to demonstrate a clear transition from predominantly radial contraction to more longitudinal contraction around 4 months of age (24). While likely underpowered to detect significant differences between the contribution of radial contraction in neonates (i.e., under 1 month of age) and older children, we did find differences in the contribution of radial shortening with increasing age. Others have used 2D speckle-tracking strain analysis to demonstrate that longitudinal contraction increases in this first year of life in premature infants (24), whereas our study suggests that pattern of longitudinal shortening may be complex, with an early increase in magnitude followed by a later return to baseline values. Moreover, we are the first to describe anteroposterior contraction patterns in children. The anteroposterior contraction is determined in large part by the circumferential shortening of the LV mid-layer myofibers, which draw the RV free-wall insertion lines towards each other. It has been shown previously that AEF is strongly associated with LVEF in both healthy volunteers and those with congenital heart disease resulting in a systemic RV (25, 26).

The maturational differences in directional contraction of the RV identified in this work emphasize the importance of using advanced techniques to assess RV contraction patterns in children with simple and complex congenital heart disease. Prior studies have demonstrated the prognostic value of global RV function in children with congenital heart disease (27, 28). Even in the face of preserved global RV function, important variations in the relative contributions of the three main components can be seen, as in the case of adults undergoing mitral valve surgery as well as those with either volume-loading or pressure-loading lesions on the right side of the heart (25, 29, 30). Understanding and quantifying the relative contribution of each component of RV contraction could have potential applications across multiple subsets of RV pathology by providing insights into the long-term effects of (1) pressure-load on the RV in children with chronic RV outflow tract obstruction (i.e., children with tetralogy of Fallot, congenital pulmonic stenosis, idiopathic pHTN), (2) volume-load in children with long-standing left-right shunt (i.e., partial anomalous pulmonary venous connections, atrial septal defects), (3) primary RV myopathy (i.e., arrhythmogenic cardiomyopathy) and finally (4) complex anatomy leading to the use of the right ventricle as the systemic ventricle in either a single ventricle circulation (i.e., hypoplastic left heart syndrome) or a biventricular circulation (i.e., "congenitally corrected" transposition of the great arteries). A more refined understanding of the evolution and progression of changes in RV contraction could help providers identify the effects of medical therapy and better define the optimal timing for procedural interventions.

Limitations

Our study group was limited by smaller number of subjects in the younger age groups, which is of particular importance in considering the significant hemodynamic changes to which the RV is subjected in the first weeks to months of life. Moreover, the differing recruitment methods contributed to a predominance of males in the oldest age group, with all but 9 subjects at the Semmelweiss site being male. As a consequence, our exploratory analysis intended to identify sex-specific differences in ejection fraction parameters among various age groups was likely underpowered. Apart from the limitations to the study population itself, there is no "gold standard" for comparison of our specific results because there is, at present, no reference method for assessing the relative components of RV motion.

Conclusions

In healthy children, analysis of the components of right ventricular contraction is feasible and reliable. In this pediatric cohort, the anteroposterior component of RV contraction was greater than the radial and longitudinal contributions. Additionally, there were age-related differences for both global RVEF and the radial component of RV contraction. Future 3DE-based study of the contraction patterns of the pediatric right ventricle, especially in children with congenital heart disease, may facilitate enhanced recognition of dysfunction and assessment of treatment effects.

Data availability statement

The raw data supporting the conclusions of this article will be made available by the authors, without undue reservation.

Ethics statement

The studies involving human participants were reviewed and approved by Semmelweis University, Heart and Vascular Institute and Boston Children's Hospital, Institutional Review Board. Written informed consent to participate in this study was provided by the participants' legal guardian/next of kin.

Author contributions

CV and AU: were equally responsible for data collection at their representative institutions. CV: was additionally responsible for research design and manuscript writing. EE, KG and ML: performed statistical analyses. DH and AK: provided oversight of research design and conduct as well as critical review of the manuscript. All authors contributed to the article and approved the submitted version.

Funding

Project no. RRF-2.3.1-21-2022-00003 has been implemented with the support provided by the European Union. This project was also supported by a grant from the National Research,

Development, and Innovation Office (NKFIH) of Hungary (FK 142573 to AK). In addition, this work was supported by the Higgins Family Noninvasive Imaging Research Fund at Boston Children's Hospital.

Conflict of interest

ZT and AK are employees of Argus Cognitive, Inc., and receive financial compensation for their work. BM reports grants from Boston Scientific and Medtronic and personal fees from Biotronic, Abbott, Astra Zeneca, Novartis, and Boehringer-Ingelheim, outside the submitted work.

The remaining authors declare that the research was conducted in the absence of any commercial or financial relationships that could be construed as a potential conflict of interest.

Publisher's note

Supplementary material

The Supplementary Material for this article can be found online at: https://www.frontiersin.org/articles/10.3389/fcvm.2023.1141027/full#supplementary-material

References

1. Diller GP, Radojevic J, Kempny A, Alonso-Gonzalez R, Emmanouil L, Orwat S, et al. Systemic right ventricular longitudinal strain is reduced in adults with transposition of the great arteries, relates to subpulmonary ventricular function, and predicts adverse clinical outcome. *Am Heart J*. (2012) 163(5):859–66. doi: 10.1016/j.ahj.2012.01.038

2. Shafer KM, Mann N, Hehn R, Ubeda Tikkanen A, Valente AM, Geva T, et al. Relationship between exercise parameters and noninvasive indices of right ventricular function in patients with biventricular circulation and systemic right ventricle. *Congenit Heart Dis*. (2015) 10(5):457–65. doi: 10.1111/chd.12248

3. Filippov AA, del Nido PJ, Vasilyev N. Management of systemic right ventricular failure in patients with congenitally corrected transposition of the great arteries. *Circulation*. (2016) 134(17):1293–302. doi: 10.1161/circulationaha.116.022106

4. Valente AM, Gauvreau K, Assenza GE, Babu-Narayan S, Schreier J, Gatzoulis MA, et al. Contemporary predictors of death and sustained ventricular tachycardia in patients with repaired tetralogy of fallot enrolled in the INDICATOR cohort. *Heart*. (2014) 100(3):247–53. doi: 10.1136/heartnjl-2013-304958

5. Geva T, Mulder B, Gauvreau K, Babu-Narayan S, Wald RM, Hickey K, et al. Preoperative predictors of death and sustained ventricular tachycardia after pulmonary valve replacement in patients with repaired tetralogy of fallot enrolled in the indicator cohort. *Circulation*. (2018) 138(19):2106–15. doi: 10.1161/circulationaha.118.034740

6. Driessen MMP, Meijboom FJ, Hui W, Dragulescu A, Mertens L, Friedberg MK. Regional right ventricular remodeling and function in children with idiopathic pulmonary arterial hypertension vs those with pulmonary valve stenosis: insights into mechanics of right ventricular dysfunction. *Echocardiography*. (2017) 34 (6):888–97. doi: 10.1111/echo,13529

7. Jone PN, Duchateau N, Pan Z, Ivy DD, Moceri P. Right ventricular area strain from 3-dimensional echocardiography: mechanistic insight of right ventricular dysfunction in pediatric pulmonary hypertension. *J Heart Lung Transplant*. (2021) 40(2):138–48. doi: 10.1016/j.healun.2020.11.005

8. Riehle TJ, Mahle WT, Parks WJ, Sallee D, Fyfe DA. Real-time three-dimensional echocardiographic acquisition and quantification of left ventricular indices in children and young adults with congenital heart disease: comparison with magnetic resonance imaging. *J Am Soc Echocardiogr*. (2008) 21(1):78–83. doi: 10.1016/j.echo,2007.05.021

9. van der Zwaan HB, Helbing WA, McGhie JS, Geleijnse ML, Luijnenburg SE, Roos-Hesselink JW, et al. Clinical value of real-time three-dimensional echocardiography for right ventricular quantification in congenital heart disease: validation with cardiac magnetic resonance imaging. *J Am Soc Echocardiogr*. (2010) 23(2):134–40. doi: 10.1016/j.echo.2009.12.001

10. Khoo NS, Young A, Occleshaw C, Cowan B, Zeng ISL, Gentles TL. Assessments of right ventricular volume and function using three-dimensional echocardiography in older children and adults with congenital heart disease: comparison with cardiac magnetic resonance imaging. *J Am Soc Echocardiogr*. (2009) 22(11):1279–88. doi: 10.1016/j.echo.2009.08.011

11. Hsu EW. *Myocardial fiber orientation mapping via MR diffusion tensor imaging. Annual international conference of the IEEE engineering in medicine and biology—proceedings* (2002).

12. Hsu EW, Healy LJ, Einstein DR, Kuprat AP. Imaging-based assessment and modeling of the structures of the myocardium. In: *Computational Cardiovascular Mechanics*. (2010). p. 23–9. doi: 10.1007/978-1-4419-0730-1_2

13. Hsu EW, Muzikant AL, Matulevicius SA, Penland RC, Henriquez CS. Magnetic resonance myocardial fiber-orientation mapping with direct histological correlation. *Am J Physiol Heart Circ Physiol*. (1998) 274(5):H1627–34. doi: 10.1152/ajpheart.1998.274.5.H1627

14. Scollan DF, Holmes A, Winslow R, Forder J. Histological validation of myocardial microstructure obtained from diffusion tensor magnetic resonance imaging. *Am J Physiol Heart Circ Physiol*. (1998) 275(6):H2308–18. doi: 10.1152/ajpheart.1998.275.6.H2308

15. Addetia K, Muraru D, Badano LP, Lang RM. New directions in right ventricular assessment using 3-dimensional echocardiography. *JAMA Cardiology*. (2019) 4 (9):936–44. doi: 10.1001/jamacardio.2019.2424

16. Lakatos BK, Nabeshima Y, Tokodi M, Nagata Y, Tősér Z, Otani K, et al. Importance of nonlongitudinal motion components in right ventricular function: three-dimensional echocardiographic study in healthy volunteers. *J Am Soc Echocardiogr*. (2020) 33(8):995–1005. doi: 10.1016/j.echo.2020.04.002

17. el Edelbi R, Lindemalm S, Eksborg S. Estimation of body surface area in various childhood ages—validation of the mosteller formula. Acta paediatrica. *Int J Paediatr*. (2012) 101(5):540–44. doi: 10.1111/j.1651-2227.2011.02580.x

18. Lai WW, Geva T, Shirali GS, Frommelt PC, Humes RA, Brook MM, et al. Guidelines and standards for performance of a pediatric echocardiogram: a report from the task force of the pediatric council of the American society of echocardiography. *J Am Soc Echocardiogr*. (2006) 19(1):1413–30. doi: 10.1016/j.echo.2006.09.001

19. Lakatos B, Tősér Z, Tokodi M, Doronina A, Kosztin A, Muraru D, et al. Quantification of the relative contribution of the different right ventricular wall motion components to right ventricular ejection fraction: the ReVISION method. *Cardiovasc Ultrasound*. (2017) 15(1):8. doi: 10.1186/s12947-017-0100-0

20. Tokodi M, Staub L, Budai Á, Lakatos BK, Csákvári M, Suhai FI, et al. Partitioning the right ventricle into 15 segments and decomposing its motion using 3D echocardiography-based models: the updated ReVISION method. *Front Cardiovasc Med*. (2021) 8:622118. doi: 10.3389/fcvm.2021.622118

21. Kovács A, Lakatos B, Tokodi M, Merkely B. Right ventricular mechanical pattern in health and disease: beyond longitudinal shortening. *Heart Fail Rev*. (2019) 24 (4):511–20. doi: 10.1007/s10741-019-09778-1

22. Hauck A, Guo R, Ivy DD, Younoszai A. Tricuspid annular plane systolic excursion is preserved in young patients with pulmonary hypertension except when associated with repaired congenital heart disease. *Eur Heart J Cardiovasc Imaging*. (2017) 18(4):459–66. doi: 10.1093/ehjci/jew068

23. Lianza AC, Rodrigues ACT, Mercer-Rosa L, Vieira MLC, de Oliveira WAA, Afonso TR, et al. Right ventricular systolic function after the cone procedure for Ebstein's Anomaly: comparison between echocardiography and cardiac magnetic resonance. *Pediatr Cardiol*. (2020) 41(5):985–95. doi: 10.1007/s00246=020-02347-6

24. Levy PT, EL-Khuffash A, Patel MD, Breatnach CR, James AT, Sanchez AA, et al. Maturational patterns of systolic ventricular deformation mechanics by two-dimensional speckle-tracking echocardiography in preterm infants over the first year of age. *J Am Soc Echocardiogr*. (2017) 30(7):685–98. doi: 10.1016/j.echo.2017.03.003

25. Surkova E, Kovacs A, Tokodi M, Lakatos B, Muraru D, Badano L. Functional adaptation of the right ventricle to different degrees of the left ventricular systolic

dysfunction in patients with left-sided heart disease: a three-dimensional echocardiography study. *Eur Heart J Cardiovasc Imaging*. (2021) 14(10):e012774. doi: 10.1161/CIRCIMAGING.121.012774

26. Surkova E, Kovács A, Lakatos BK, Tokodi M, Fábián A, West C, et al. Contraction patterns of the systemic right ventricle: a three-dimensional echocardiography study. *Eur Heart J Cardiovasc Imaging*. (2021) 23(12):1654–62. doi: 10.1093/ehjci/jeab272

27. Bhatt SM, Goldmuntz E, Elci O, McBride M, Paridon S, Mercer-Rosa L. Rigth ventricular contractile reserve is impaired in children and adolescents with repaired tetralogy of fallot: an exercise strain imaging study. *J Am Soc Echocardiogr*. (2019) 32(1):135–44. doi: 10.1016/j.echo.2018.08.008

28. Maskatia SA, Petit CJ, Travers CD, Goldberg DJ, Rogers LS, Glatz AC, et al. Echocardiographic parameters associated with biventricular circulation and right ventricular growth following right ventricular decompression in patients with pulmonary atresia and intact ventricular septum: results from a multicenter study. *Congenit Heart Dis*. (2018) 13(6):892–902. doi: 10.1111/chd.12671

29. Tokodi M, Lakatos BK, Kispal E, Racz K, Soltesz A, Hartyanski I, et al. Predictive value of right ventricular mechanics on postoperative right ventricular function in patients undergoing mitral valve surgery. *J Am Coll Cardiol*. (2019) 73(9):1952. doi: 10.1016/S0735-1097(19)32558-6

30. Bidviene J, Muraru D, Maffessanti F, Ereminiene E, Kovács A, Lakatos B, et al. Regional shape, global function and mechanics in right ventricular volume and pressure overload conditions: a three-dimensional echocardiography study. *Int J Cardiovasc Imaging*. (2021) 37(4):1289–99. doi: 10.1007/s10554-020-02117-8

frontiers | Frontiers in Cardiovascular Medicine

TYPE Review
PUBLISHED 21 December 2023
DOI 10.3389/fcvm.2023.1263864

OPEN ACCESS

EDITED BY
Márton Tokodi,
Semmelweis University, Hungary

REVIEWED BY
Réka Faludi,
University of Pécs, Hungary
Tetsuji Kitano,
University of Occupational and Environmental Health, Japan
Luigi P. Badano,
University of Milano Bicocca, Italy
Csaba Jenei,
University of Debrecen, Hungary

*CORRESPONDENCE
Karima Addetia
✉ kaddetia@bsd.uchicago.edu

RECEIVED 20 July 2023
ACCEPTED 22 November 2023
PUBLISHED 21 December 2023

CITATION
Randazzo M, Maffessanti F, Kotta A, Grapsa J, Lang RM and Addetia K (2023) Added value of 3D echocardiography in the diagnosis and prognostication of patients with right ventricular dysfunction.
Front. Cardiovasc. Med. 10:1263864.
doi: 10.3389/fcvm.2023.1263864

Added value of 3D echocardiography in the diagnosis and prognostication of patients with right ventricular dysfunction

Michael Randazzo[1], Francesco Maffessanti[2], Alekhya Kotta[3], Julia Grapsa[4], Roberto M. Lang[1] and Karima Addetia[1]*

[1]Department of Medicine, Section of Cardiology, University of Chicago Heart and Vascular Center, Chicago, IL, United States, [2]Maria Cecilia Hospital, GVM Care & Research, Cotignola, Italy, [3]Department of Internal Medicine, Baylor College of Medicine, Houston, TX, United States, [4]Department of Cardiology, Guys and St Thomas NHS Trust, London, United Kingdom

Recent inroads into percutaneous-based options for the treatment of tricuspid valve disease has brought to light how little we know about the behavior of the right ventricle in both health and disease and how incomplete our assessment of right ventricular (RV) physiology and function is using current non-invasive technology, in particular echocardiography. The purpose of this review is to provide an overview of what three-dimensional echocardiography (3DE) can offer currently to enhance RV evaluation and what the future may hold if we continue to improve the 3D evaluation of the right heart.

KEYWORDS

3D echocardiography, right ventricle, prognosis, echocardiography, tricuspid valve

Introduction

The diagnostic and prognostic importance of RV size and function is being increasingly appreciated owing both to the advent of percutaneous procedures targeted to pathologies involving the right heart and the growing interest in prognostication of various disease states that compromise the RV (1). In spite of this, reliable, non-invasive assessment of RV size and function remains elusive.

Despite being the current reference standard for RV size and function assessment, cardiovascular magnetic resonance imaging (CMR) suffers from several critical drawbacks which prevent its ubiquitous use in the clinical space. These drawbacks include, high cost, limited availability, non-portability, dependence on patient cooperation as well as numerous key contraindications and relative contraindications. Echocardiography, therefore, remains the workhorse for initial cardiac evaluation; it is cost-effective, safe, widely accessible, portable and without contraindications. It can be flexibly incorporated across multiple clinical settings. Accurate, reproducible evaluation of the RV, however, with current two-dimensional echocardiography (2DE) techniques is hindered by its anatomical location in the anterior mediastinum, irregular crescentic geometry, complex mechanics, and asymmetric remodeling. Recent advancements in 3DE have helped overcome many of these limitations by avoiding the geometrical assumptions inherent to 2D size and function assessments (2). Using 3DE, a pyramidal dataset of the RV which contains all of the structural components of the chamber including the inflow, outflow, body and apex as well as the tricuspid and pulmonary valves is acquired (**Figure 1**). Access to this data enables comprehensive, quantitative volumetric analysis of the RV (3). RV volume and ejection fraction (RVEF) derived from 3D datasets have been shown to

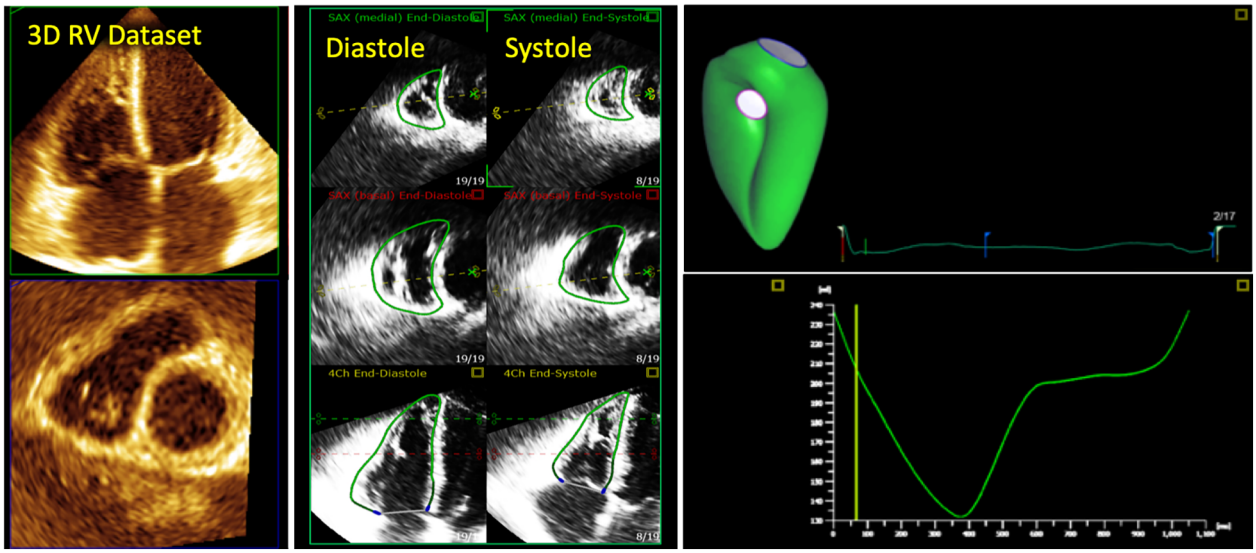

FIGURE 1
3d echocardiographic analysis of the right ventricle. Far left, 3D dataset of the right ventricle depicting the apical four-chamber and short-axis planes using multi-planar reconstruction. Middle panel shows endocardial tracings overlying the diastolic and systolic phases of the 2D short and long-axis cut-planes obtained from the 3D right ventricular dataset. Far right, top panel shows the 3D endocardial rendered surface while bottom panel shows the volumes obtained after automated software analysis throughout the cardiac cycle.

strongly correlate with measurements obtained with CMR as well as adverse cardiopulmonary outcomes (4–6). These findings have recently prompted considerable exploration into the potential utility of 3DE in a vast array of clinical applications. The objective of this review is to describe 3DE acquisition and analysis methods for the RV, summarize their established diagnostic and prognostic value, and outline potential novel utilities for 3D RV imaging on the horizon and for the future.

2D echocardiography: analysis and limitations

2D echocardiographic evaluation of the RV requires integration of multiple imaging planes to enable optimal evaluation of RV size and function (**Figure 2**). Even when all views can be adequately acquired, quantitative analysis remains a regional assessment at best. RV chamber size is typically classified as normal or abnormal according to basal, mid-ventricular, and longitudinal dimensions obtained at end-diastole from the RV-focused apical 4-chamber view (**Figure 3**) (7). Despite this standardized approach, measurements can still vary widely based on minor differences in transducer positioning. Indeed, RV size and functional measurements have been shown to be consistently different in the RV focused view when compared with the apical 4-chamber view (8). Furthermore, volumetric estimations derived from geometric assumptions based on linear dimensions correlate poorly with volumes calculated from CMR and are discouraged (9).

Evaluation of RV systolic function on 2DE involves the integration of multiple parameters, of which the most commonly used include tricuspid annular systolic excursion (TAPSE), tissue Doppler-derived tricuspid lateral annular systolic velocity (S'), fractional area change (FAC), free-wall and four-chamber (free-wall + septal) longitudinal strain (FWS and 4CHLS respectively), and myocardial performance index (MPI) (7). Indeed, utilization of a single, global assessment of function is hindered by the complex mechanism of RV contraction that is unique from the left ventricle. In comparison to the left ventricle, the RV wall is thinner and composed of two muscular layers with longitudinally oriented myocytes in the sub-endocardium and circumferentially oriented myocytes in the sub-epicardial layer. Together, these layers contribute to RV contraction by respectively drawing the tricuspid annulus towards the apex and inwardly moving the free wall (2). Given that there is not one single accepted method for RV quantification, qualitative interpretation is often also used in clinical practice, characterizing dysfunction as mild, moderate, or severe despite poor sensitivity and notable interobserver variability (9). Routine metrics such as TAPSE and S' have demonstrated modest agreement with global RV systolic function obtained by CMR (10). These measures predominantly assess longitudinal excursion of the RV free-wall and thereby omit the contribution of other determinants of RV function. In many instances, longitudinal excursion is the most important determinant of systolic RV function. However, altered contraction mechanics and adverse remodeling in various disease states may result in under- or over-estimation of function using these methods such as in the setting of some types of pulmonary hypertension, post-cardiac surgery where systolic motion is concentrated in the transverse plane, or significant tricuspid regurgitation (TR) which produces exaggerated motion of the base (2). FAC provides a percentage estimate of global function, improving the correlation with CMR but it is highly dependent on identifying a suitable tomographic view that avoids cavity

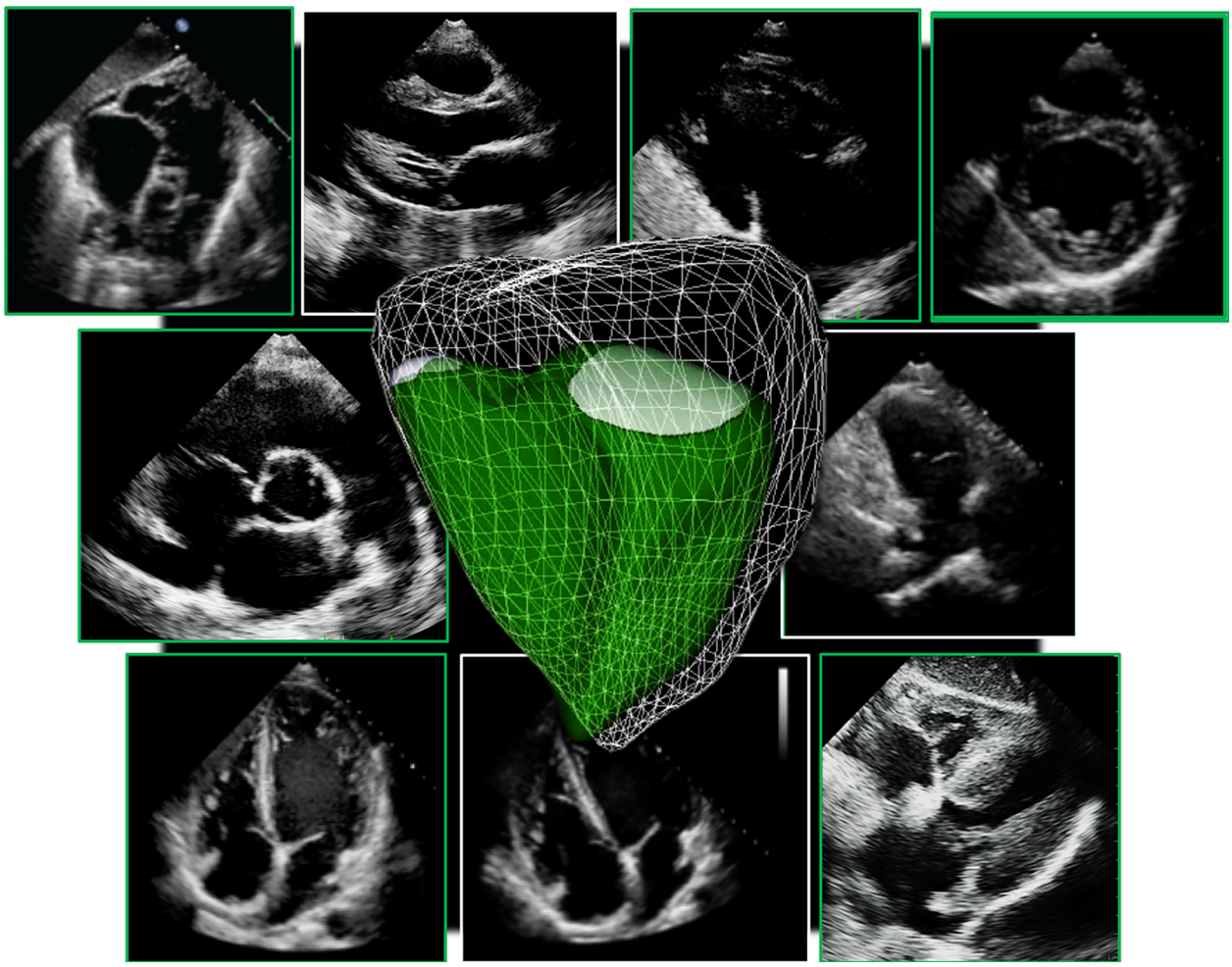

FIGURE 2
Collection of all 2D standard imaging planes used on routine transthoracic echocardiography to assess the right ventricle. A 3D right ventricle endocardial surface is superimposed on top (in green).

foreshortening. This limitation results in poor reproducibility. Additionally, since FAC is measured in the RV focused view, it excludes much of the RV body as well as the RV outflow tract which in itself contributes to 25%–30% of the RV volume (3, 7). Similar to FAC, FWS, a measure of myocardial shortening in the longitudinal plane, fails to incorporate the RV outflow tract and focuses on longitudinal deformation. Unlike TAPSE and RV S', FWS incorporates the entire RV free wall (or free and septal walls in the case of 4CHLS), and therefore correlates better with CMR measurements than either TAPSE or RV S' (11). Finally, MPI, or Tei index, defined as the sum of RV iso-volumetric contraction and relaxation times divided by the RV ejection time, has the ability to account for both systolic and diastolic components of RV function; however, situations such as tachycardia, elevated right atrial pressures, atrial fibrillation, and conduction system disorders prevent its consistent use (2). Overall, conventional 2D parameters (**Figure 3**) necessitate leveraging limited sections of the RV endocardial surface to extrapolate global function, which may subject these measures to inaccuracies. See **Table 1** for an overview of advantages and disadvantages of each 2D parameter.

3D echocardiography of the right heart

Acquisition and analysis of the right ventricle

Acquisition of the 3D RV pyramidal dataset can be achieved using either a single or multi-beat approach from the RV-focused apical 4-chamber view (**Figure 4**). Notably, RV volumes and ejection fractions derived from 3D datasets acquired in the apical four-chamber view strongly correlate with measurements from the RV-focused view providing that the entire RV can be captured within the 3D dateset (12). Four to six beat acquisitions allow for higher temporal and spatial resolution enabling more optimal identification of end-diastolic and end-systolic phases for volumetric calculations (2). Prior validation studies with CMR in

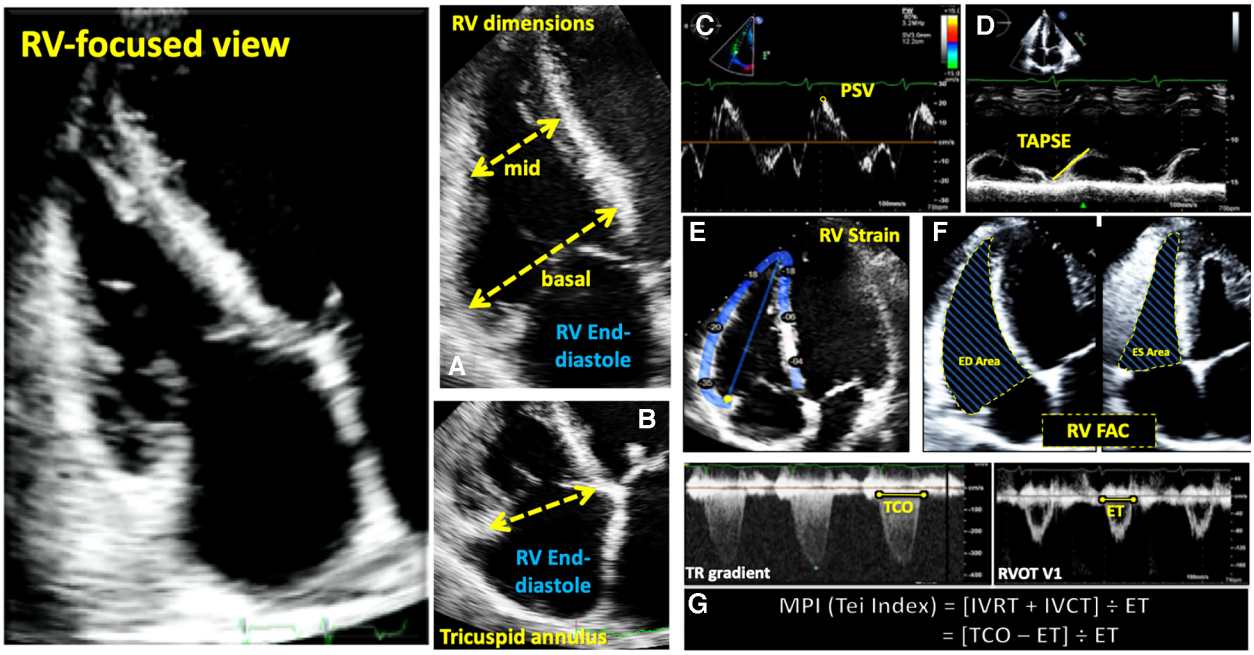

FIGURE 3
Guideline-recommended right ventricular size and function assessment. All measurements are performed in the RV focused apical 4-chamber view (far left panel). (**A**) RV mid-ventricular and basal dimensions obtained at end-diastole in the RV-focused view; (**B**) tricuspid annulus diameter obtained at end-diastole starting at the hinge-point of the non-septal TV leaflet and ending at hinge-point of the septal TV leaflet; (**C**) depiction of doppler-derived tricuspid lateral annular systolic velocity (S') or peak systolic velocity (PSV); (**D**) m-mode is used to measure longitudinal displacement of the lateral tricuspid annulus in systole to yield tricuspid annular systolic excursion (TAPSE); (**E**) region of interest used to guide free-wall and global RV strain assessment; (**F**) RV areas obtained at end-diastole and end-systole to compute fractional area change; (**G**) Calculation of the myocardial performance index (MPI) defined as the sum of isovolumic contraction time the (IVCT) and isovolumic relaxation time (IVRT) divided by ejection time (ET) obtained from the right ventricular outflow tract initial velocity (RVOT V1). The sum of IVCT and IVRT is equal to the difference between the interval from cessation to onset of the tricuspid inflow (TCO) and ET.

both children and adults have demonstrated sufficient frame rates ranging between 20 and 50 volumes per second to ensure reliable identification of cardiac timing (13, 14). Moreover, adequate patient cooperation with breath holding is critical to reduce stitch and dropout artifacts (2). Various clinical factors can adversely impact 3DE data collection including irregular cardiac rhythms, morbid obesity, inability to breath-hold, marked structurally abnormal RVs, mechanical ventilation, and mechanical support devices. In spite of these limitations on acoustic windows, transthoracic 3DE has exhibited exceptional feasibility in several large highly experienced cohorts ranging from 75% to 85% (15–17). The addition of ultrasound-enhancing agents has been shown to further augment performance with respect to reproducibility and correlation with CMR (18). In the World Alliance Society of Echocardiography (WASE) study, a worldwide cohort of centers with variable experience with 3D RV acquisition and analysis, feasibility of 3D RV acquisition dropped to 50%–60% with incomplete RV capture, typically anterior wall or apical drop-out being some of the main reasons for unanalyzable 3D RV data (**Figure 5**) (19). The ability to adequately capture the RV for 3D analysis is highly dependent on individual expertise to both acquire and analyze the 3D dataset. This expertise can vary widely from center to center as shown in the WASE study (**Figure 6**). According to this graph, the feasibility for RV analysis ranged anywhere from 20% to 95% and was dependent on the center in which the data was acquired, suggesting that it is possible to attain a level of expertise such that >80% of captured 3D RV data can be analyzed in patients with adequate 2D images. The major advantage of using 3D RV datasets for size and functional assessment is that this parameter represents the first echocardiography-based global method for RV functional assessment. Current 3D analysis software employs a volumetric approach to compute the total quantity of pixels within the RV endocardial surface in systole and diastole to obtain the respective volumes. This technique removes geometric assumptions and minimizes variability due to acquisition. Accordingly, volumes obtained from 3DE have demonstrated incremental improvements in accuracy and reproducibility compared to 2DE although they still underestimate volumes in comparison to CMR (5, 20). Fully automated methods of volumetric quantification based on machine-learning algorithms have been explored showing accurate, reproducible measurements following minimal revision (21).

The volumetric dataset provides multiple opportunities for post-processing analysis. Particular regions of the wide-angle acquisition can be visualized and interrogated for wall motion abnormalities, hypertrophy, or masses (3). 3D RV datasets enable better characterization of the complex contraction pattern of the RV including alterations caused by various pathologies. One

TABLE 1 Advantages and limitations of one- and two-dimensional analysis techniques for right ventricular functional assessment.

	Definition	Advantages	Limitations
Doppler-derived tricuspid lateral annular systolic velocity (S')	Assessment of the longitudinal excursion velocity of the lateral tricuspid annulus	• Reproducible • Easy to perform • Correlated with radionuclide angiography for functional discrimination • Validated in population-based studies • Does not depend on 2D image quality • Minimal required post-processing	• Assumes regional function is representative of the entire chamber • Angle dependent • Lack of normative data across sex and age
Tricuspid annular systolic excursion (TAPSE)	Measurement of longitudinal displacement of the tricuspid annulus in systole	• Reproducible • Reduced dependence on image quality • Correlated with Simpson's biplane right ventricular ejection fraction • Easy to perform • Minimal required post-processing	• Assumes regional function is representative of the entire chamber • Angle dependent • Varies with loading conditions
Free-wall and global longitudinal strain (FWS & 4CHLS respectively)	Percentage of myocardial shortening in the longitudinal plane	• Accounts for several RV segments • Correlated with CMR assessments • Feasible despite abnormal RV geometry • Load independent	• Angle dependent • High degree of variability across platforms • Requires post-processing with limited accessibility • Lack of normative data • Poor signal-to-noise ratio • Excludes RV outflow tract
Fractional area change (FAC)	Percentage difference between end systolic and end diastolic areas divided by end diastolic area	• Correlated with CMR assessments • Prognostic for heart failure, stroke, and death	• Excludes outflow tract and most of the RV body • High inter-observer variability • Varies with loading conditions • Tedious and time-consuming
Myocardial performance index (MPI)	Summation of RV iso-volumetric contraction and relaxation times divided by the RV ejection time	• Accounts for systolic and diastolic function • Well validated in healthy patients • Feasible despite abnormal RV geometry • Reduced dependence on image quality	• Reduced accuracy in the setting of tachycardia, irregular heart rhythms, and elevated RA pressures

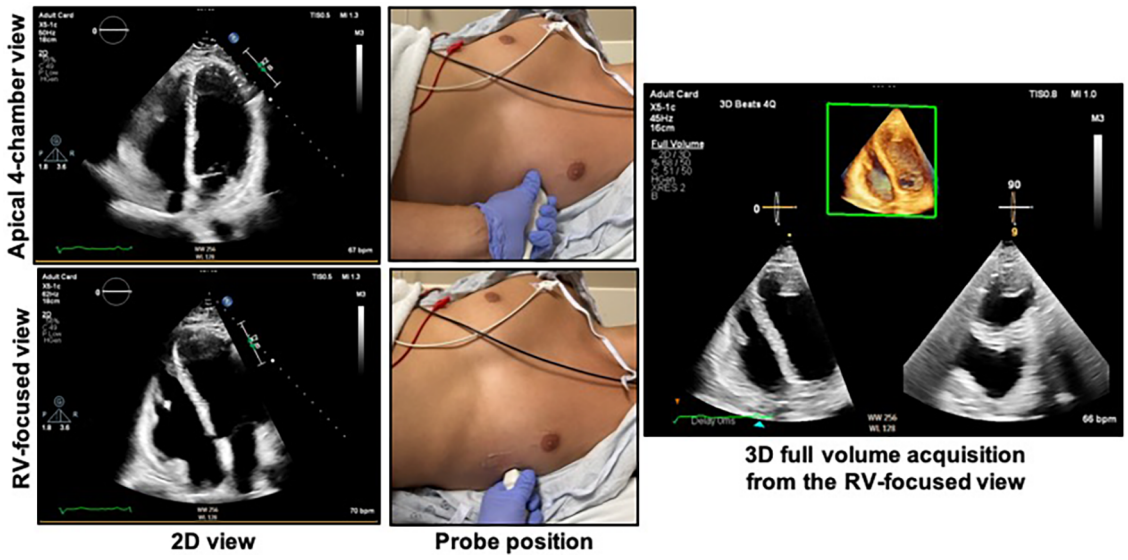

FIGURE 4
Obtaining the right ventricular focused view. The patient should be in the left lateral decubitus position with the left mid-clavicular, fifth intercostal region (approximate apex of the heart) positioned over the cut-out area of the bed if available. The top right shows the apical 4-chamber view as acquired from the probe position at top middle. The bottom left shows the RV-focused view as acquired from a more lateral location as shown in the bottom middle panel. The 3D dataset should be acquired from the RV-focused view to maximize capture of the RV free wall. See Figure 5 for the characteristics of an optimal 3D dataset. RV, right ventricle.

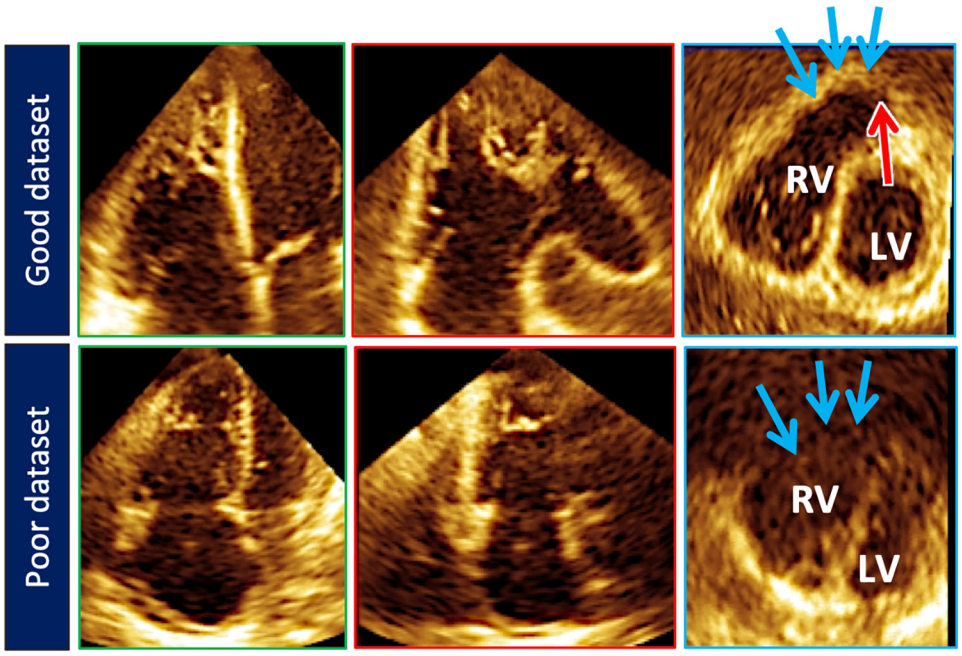

FIGURE 5
Top row illustrates cut planes through the optimal 3D right ventricular dataset. Note that the free-wall and right ventricular outflow tract borders (blue arrows) are well demarcated. Sometimes the pulmonary valve (red arrow) can be seen). Bottom row depicts a less than optimal 3D right ventricular dataset. The right ventricular outflow tract borders (blue arrows) are poorly seen.

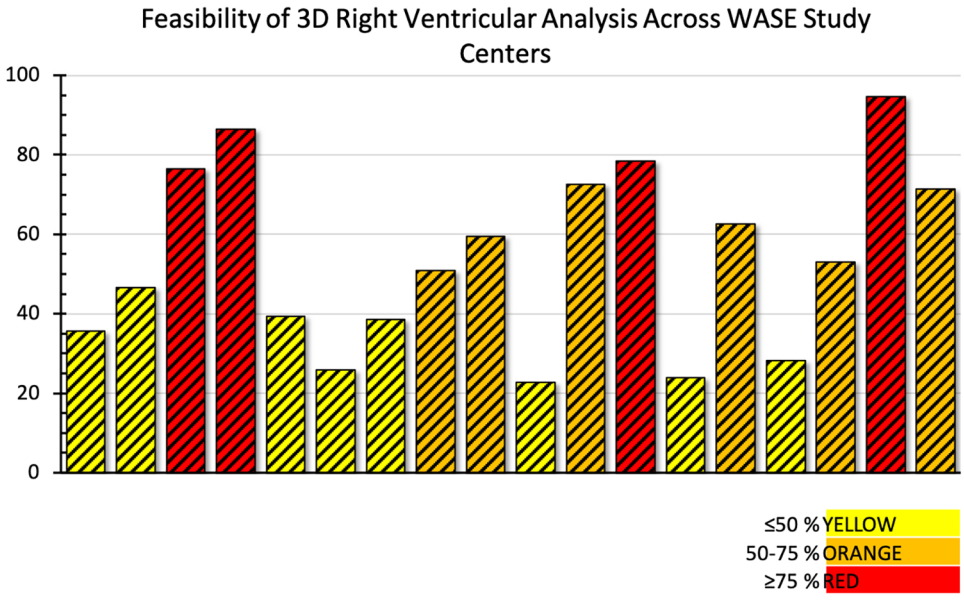

FIGURE 6
Feasibility of adequate 3D right ventricular dataset acquisition around the world. Data from the World Alliance Society of Echocardiography (WASE) study. Each bar represents one of the centers enrolled in the WASE study.

increasingly popular method of 3D RV functional analysis involves the decomposition of the RV ejection fraction into longitudinal, radial, and anteroposterior components in order to investigate modifications in RV function with disease, which cannot be appreciated when studying its longitudinal performance alone. These contraction components have been investigated in patients with left ventricular dysfunction (22), pulmonary hypertension (23), and systemic right ventricles due to transposition of the great arteries (24) using the ReVISION software package (Argus Cognitive Inc., Lebanon, NH) (25, 26).

Conventional echocardiographic measures of RV function including 2D RV functional parameters (TAPSE, S', FAC, RV strain) and 3D RVEF (even if obtained using CMR) are highly load dependent and do not provide a clinically useful assessment of RV function in patients with secondary tricuspid regurgitation or significant pulmonary hypertension. Recent data on outcomes have identified measures of right ventricle-to-pulmonary artery coupling, which better estimate the impact of loading conditions on the RV, as important prognostic markers in these patients. In a recent study, RV volumes from 3D echocardiography were used to compute a surrogate of right ventricle-to-pulmonary artery coupling using the formula total RV forward stroke volume/end-systolic volume. This measure, when applied to patients with more than moderate tricuspid regurgitation, successfully predicted outcomes (including all cause death and hospitalization for heart failure) with better accuracy than RV ejection fraction and other measures of right-ventricle-to-pulmonary artery coupling using combinations of 2D and Doppler parameters raising the possibility that this marker could have a role in the assessment of RV function in patients undergoing percutaneous procedures for the tricuspid valve (27).

Normal reference values for 3D right ventricular size and function parameters

Since its inception, numerous studies have sought to establish reference values for 3D chamber volumes and EF. Initial efforts displayed heterogenous findings, which could be attributed to inconsistencies in frame rates, volumetric analysis algorithms, and 3D imaging technology (28, 29). Recently, a large, multicenter investigation of 507 healthy volunteers evenly distributed across age and sex (17) showed for the first time, using 3DE, that men had larger right ventricular end-diastolic and end-systolic volumes compared to women even after indexation to body surface area, and that aging correlated with a consistent decline in volumes by decade. These results parallel those obtained from CMR in large populations of normal subjects (30, 31). From these findings, normative equations with allometric scaling were derived to assist with recognition of abnormal values. Even more recently, the World Alliance Society of Echocardiography (WASE) study also published normal values for 3D RV size and function parameters on 1,051 healthy volunteers, adding to the repertoire of 3D RV normal values with the added distinction of being the first 3D normal values study on a worldwide multi-ethnic cohort (19) (**Table 2**).

3D tricuspid annulus imaging and analysis

The tricuspid annulus (TA) forms the junction between the right atrium and the right ventricle. Its complex anatomy and dynamic behavior preclude systematic characterization with 2DE. Current guidelines recommend that the TA be measured in the apical 4-chamber view on transthoracic echocardiography. TA size and dynamics, however, are much more complicated (32). With 3DE, comprehensive static and dynamic assessment of the TA is possible (33). Visualization of the TA with 3DE begins with optimization of the RV-focused apical view. Narrow-angle or full volume acquisition from this plane adequately captures the TA. Accurate measurement of TA size and function even with current multi-planar reconstruction techniques is difficult due to the nonplanarity of the annulus necessitating manual or automated initialization of the leaflet hinge points with automated interpretation throughout the cardiac cycle (33, 34). Various programs are in existence or in development to assist with this step. One commercially available 3DE software package dedicated to the tricuspid valve was validated and utilized to develop sex-specific reference ranges for the TA. Importantly, TA sizes were shown to be underestimated by 2DE (35). See **Figure 7** for results from an example software package.

3D of the right atrium

Right atrial (RA) assessment is of paramount importance in patients with diseases affecting the RV including pulmonary hypertension, heart failure (both reduced and preserved etiologies), and tricuspid regurgitation. The RA has been heralded as both "first chamber to live and the last to die" (36). With 3DE, it is possible to assess RA volumes, phasic function, and even remodelling (36, 37). In one study, increasing 3D RA sphericity index was found to be associated with clinical deterioration in patients with pulmonary arterial hypertension (36). Similar to the left atrium, RA physiology can be divided into 3 parts: (1) the reservoir phase, which corresponds to tricuspid valve closure and ventricular systole; (2) the conduit phase which corresponds to tricuspid valve opening and early ventricular diastole, and (3) the contractile or booster phase which reflects right atrial contraction (38). 3D RA volumes have been shown to be larger than the corresponding 2D volumes (37, 39, 40). Normal vales for 3D RA volumes are summarized in **Table 2** (41).

Diagnostic value of 3D echocardiography of the right ventricle

Characterization of tricuspid valve disease

Etiology of tricuspid regurgitation (TR) is closely coupled with right atrial and RV remodeling. Secondary or functional TR represents greater than 80% of TR in clinical practice and can be associated with or without pulmonary hypertension (PH) (42). These two TR categories have distinctive RV remodeling patterns which can be characterized using 3DE. Increases in RV afterload due to elevated pulmonary pressures can lead to spherical RV remodeling, papillary muscle displacement, tricuspid valve leaflet tethering, diminished leaflet coaptation surface, and tricuspid valve incompetence. The TA in these patients is often minimally dilated and may in some cases be normal in size. Flattening of

TABLE 2 Normal three-dimensional right ventricular and right atrial echocardiographic reference values.

	Source	N	Age (mean ± SD or range)	FR (Vol/s)	Analysis method	Tracing	Male (mean ± SD)										Female (mean ± SD)			
							N	EDVi ml/m^2 (mean ± SD)	EDVi + 2SD ml/m^2 upper limit	ESVi ml/m^2 (mean ± SD)	ESVi + 2SD ml/m^2 upper limit	EF % (mean ± SD)	EF % lower limit	N	EDVi ml/m^2	EDVi + 2SD ml/m^2 upper limit	ESVi ml/m^2	ESVi + 2SD ml/m^2 upper limit	EF % (mean ± SD)	EF % lower limit
RV	Gopal et al. (28)	71	56 ± 14	15–18	Short-axis disk summation	Manual	36	75 ± 13	101	38 ± 7	52	49 ± 10	29	37	65 ± 13	91	29 ± 11	51	56 ± 9	38
	Aune et al. (29)	166	29–80	NA	Automated border-detection (Qlab version 6)	Semi-automated	79	42 ± 11	64	17 ± 6	29	60 ± 11	38	87	38 ± 10	58	15 ± 5	25	62 ± 10	42
	Maffessanti et al. (17)	507	46 ± 16	26–40	Automated border-detection (TomTec version 1.2)	Semi-automated	247	59 ± 15	89	24 ± 9	42	60 ± 9	42	260	50 ± 11	72	19 ± 7	33	64 ± 9	46
	Addetia et al. (19)	1,051	47 ± 17	>15	Automated border-detection (TomTec)	Semi-automated	540	82 ± 21	124	37 ± 11	59	55 ± 5	45	511	70 ± 17	104	31 ± 9	49	57 ± 6	45
RA	Peluso et al. (37)	200	43 ± 15	NA	Automated border-detection (TomTec)	Semi-automated	87	12 ± 4	20	31 ± 8	47	61 ± 8	45	113	9 ± 3	15	27 ± 6	39	65 ± 8	49
	Soulat-Dufour et al. (41)	2,008	47 ± 17	NA	Automated border-detection (TomTec)	Semi-automated	1,033	11 ± 4	19	23 ± 7	37	53 ± 7	39	975	10 ± 3	16	21 ± 6	33	53 ± 7	39

Upper limits for volumes and lower limits for Ejection fraction also reported.
EDVi, indexed end-diastolic volume; ESVi, indexed end-systolic volume; EF, ejection fraction; FR, frame rate.

10.3389/fcvm.2023.1263864

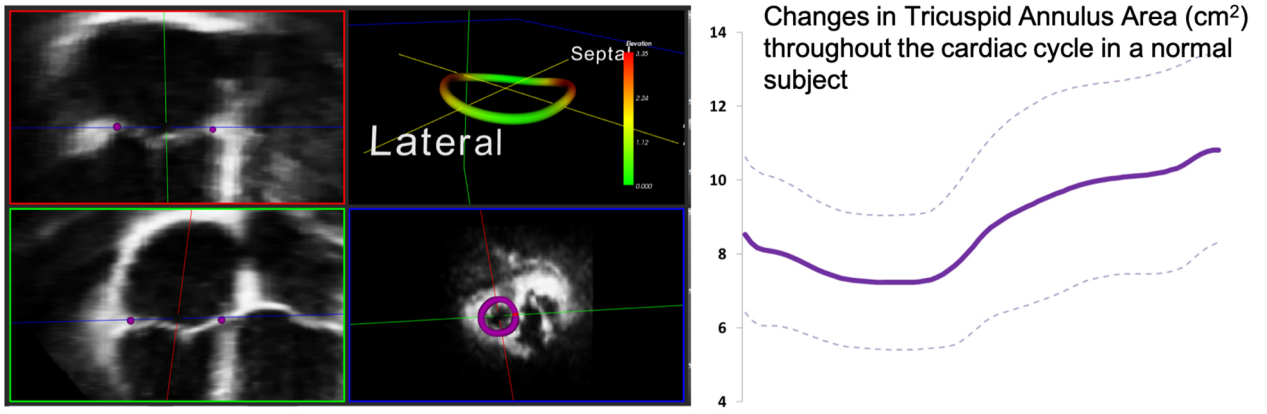

FIGURE 7
One example of customized software used to measure the 3D tricuspid annulus. Purple dots represent the initialization points from which the 3D annulus depiction (left panel, top right) is derived. The annulus is non-planar and therefore better assessed using 3D echocardiography. Dynamic analysis of the annulus allows calculation of changes in area and other parameters throughout the cardiac cycle (see graph right). Images courtesy of Federico Veronesi, PhD.

the interventricular septum, a finding often seen in significant PH, likely also contributes to distortion of the tricuspid apparatus and TR. RV eccentricity index, quantified as the ratio between the long and perpendicular short-axis lengths at the mid- ventricular level in short-axis view has been shown to predict TR severity with high accuracy (43). Functional TR with PH has also been called ventricular functional TR, because the morphological changes in the right heart which sustain TR are seen mostly in the RV (**Figure 8**) (44, 45).

Functional TR without PH is typically seen in older adults with a high incidence of associated atrial fibrillation resulting in RA dilatation with subsequent TA dilatation without leaflet tethering (**Figure 8**). TA dilation results in a diminished leaflet coaptation surface and increased rate of leaflet malcoaptation. In these patients, the RV maintains its normal length but dilates at the base loosely labeled as conical remodeling (42, 44–46). Restoration of sinus rhythm has been shown to improve the degree of TR in some of these patients (47).

Detailed analysis of functional and morphologic changes associated with RV remodeling with 3DE can help to differentiate between the different causes of functional TR and the impact on the RV (44–46). Regional quantitative curvature analysis has previously been implemented to characterize alterations in RV shape attributed to PH using a quantitative approach, demonstrating bulging of the interventricular septum into the left ventricle and greater convexity of the RV free wall throughout the cardiac cycle compared to normal controls. This bulging phenomenon is also known as the "D-shaped left ventricle" or "D-sign", a finding that can also be appreciated on the 2D parasternal short-axis view (**Figure 8**) (48).

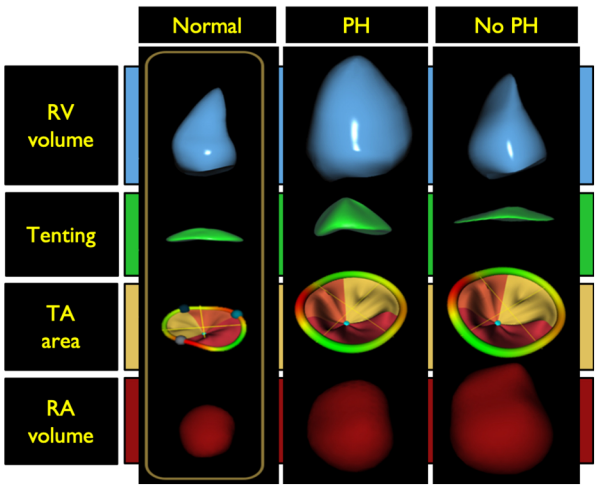

FIGURE 8
Right ventricular morphology changes associated with functional tricuspid regurgitation with and without pulmonary hypertension compared with a normal right ventricle (left panel). Middle panel illustrates the spherical right ventricular remodeling seen in patients with tricuspid regurgitation and pulmonary hypertension. In these patients there is often tricuspid valve leaflet tethering with some right atrial dilatation. The tricuspid annulus is typically minimally dilated and may in some cases be normal in size. The right panel illustrates ventricular remodeling in patients without pulmonary hypertension. This type of remodeling is typically seen in older adults with atrial fibrillation. There is notable right atrial and tricuspid annulus dilatation without leaflet tethering. Tricuspid annular dilation results in a diminished leaflet coaptation surface and increased rates of leaflet malcoaptation. In these patients, the RV dilates at the base, a phenomenon known as conical remodeling. PH, pulmonary hypertension; RV, right ventricle; TA, tricuspid annulus; RA right atrium. (Modified from Muraru D et al. Eur Heart J Cardiovasc Imaging. (2021) May 10;22(6):660–669).

Implantable device lead complications

Device-lead related interference with the tricuspid valve apparatus is a potential complication that is incompletely described by 2DE as the device-lead is really only seen in its entirety in less than 20% of cases (49). The addition of 3D RV imaging has improved non-invasive assessment of the relationship between the tricuspid apparatus and device leads

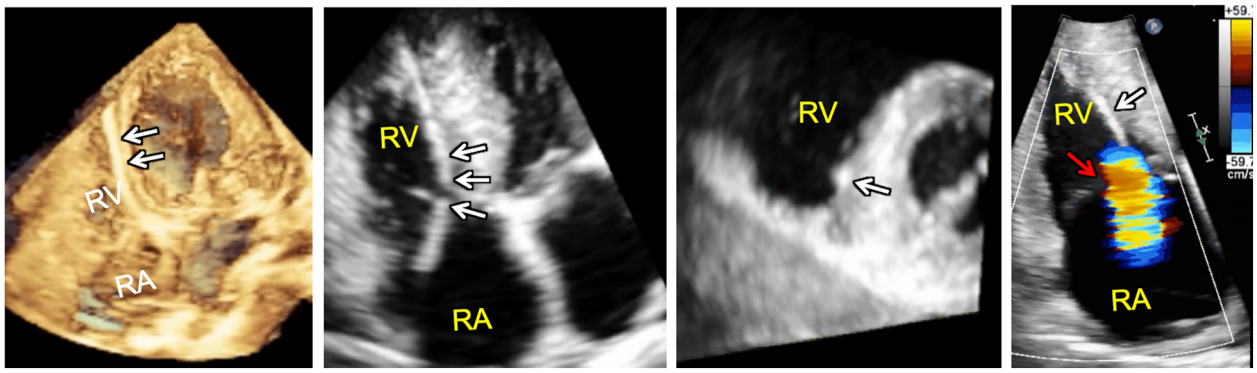

FIGURE 9
3D full volume dataset of the right ventricle (far left) and adjacent cut planes through the 3D dataset (left, middle and right, middle) showing device-lead (white arrows) impinging on the septal leaflet and sub-tricuspid apparatus in the region of the right ventricular septum resulting in tricuspid regurgitation (far right). Note that the tricuspid leaflet coaptation zone (red arrow) is not the origin of tricuspid regurgitation in this case. In fact, tricuspid regurgitation is originating at the point of device-lead contact with the septal leaflet.

enabling direct visualization of the both the TV leaflets and the sub-tricuspid apparatus making it possible to determine the presence or absence of interference in select cases (50–52). According to one study, leads demonstrating leaflet impingement on 3DE were associated with a greater degree of TR with a median vena contracta of 0.62 cm compared to 0.27 cm in patients without 3DE evidence of lead-related leaflet interference. Importantly, positioning of the lead in the commissure resulted in less frequent interaction, suggesting that echocardiographic guidance of or follow-up after lead placement may be beneficial in some cases (52). More recent data suggests that lead-related tricuspid valve interference can be associated with the tricuspid valve leaflet(s) alone, the sub-tricuspid apparatus alone, or both the leaflet(s) and the sub-tricuspid apparatus (**Figure 9**) (53).

Given the increasing interest in percutaneous tricuspid valve repair in patients with heart failure, it is likely that there will be a parallel need to better diagnose lead-related interference with the tricuspid valve apparatus as any associated interference may impact the success of any procedure chosen to repair the tricuspid valve. 3DE shows promise in this area of diagnosis.

Arrhythmogenic right ventricular cardiomyopathy (ARVC)

Echocardiography represents a common first-line imaging modality for both diagnosis and follow-up of ARVC (54). Although CMR is considered the gold standard for meeting the imaging criteria for diagnosis, recent investigations have demonstrated a high concordance in diagnostic performance between 3DE and CMR when either is combined with 2DE. Moreover, 3DE enhances the ability to diagnose wall motion abnormalities and aneurysms which are critical to meeting imaging criteria for the diagnosis of the disease (**Figure 10**) (55, 56). 3DE specifically outperformed 2DE in detection of wall motion abnormalities and exhibited comparable detection rates to CMR (56). These suggest the possibility of 3D echocardiography-guided diagnosis and follow-up of these patients especially in those instances where CMR is not easy to obtain.

Congenital heart disease

The asymmetrical remodeling of the RV often observed in patients with congenital heart disease can limit the efficacy of conventional 2D size and function assessment of the RV due to inaccurate geometric assumptions. These geometric assumptions

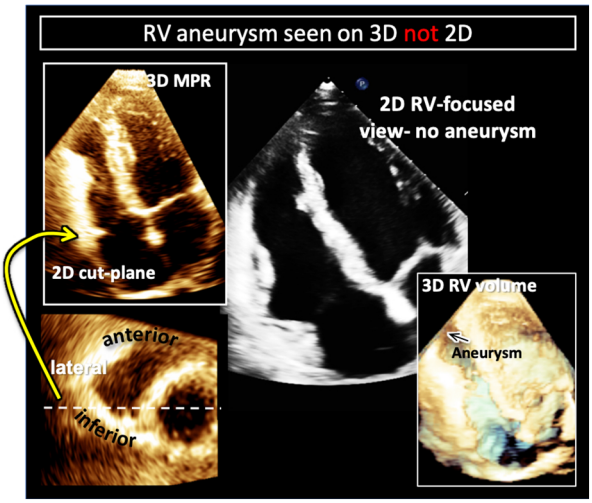

FIGURE 10
Example of right ventricular free-wall aneurysm detection with 3D (left) compared to 2DE in a patient with arrhythmogenic right ventricular cardiomyopathy (ARVC). Two-dimensional cut-planes from a full-volume 3D dataset enables visualization of the apical aneurysm (left) with targeted interrogation of the right ventricular free-wall (left, top) on short-axis imaging planes (left bottom). Here the aneurysm is noted to be on the infero-lateral free wall (white dotted line and yellow arrow). In the same patient the aneurysm is not visualized in the 2D right-ventricular focused view (right, top). Cropping into the 3D full volume also allows visualization of the apical aneurysm (black arrow on right, bottom).

may be overcome by 3DE. Volumes and ejection fractions acquired from 3DE datasets have been shown to correlate well with CMR measurements in addition to demonstrating lower interobserver variability than corresponding measurements obtained on 2DE (57, 58). However, in conditions with progressive RV enlargement including repaired tetralogy of Fallot (TOF) and transposition of the great arteries 3DE has been shown to systematically underestimate volumes while overestimating RVEF (59, 60). These studies were notably performed using earlier software versions that may impact their current applicability. More recent versions of the 3D RV analysis software are easier to use and provide short-axis cut-planes for tracing volumes. A recent investigation in patients with systemic RVs, revealed alterations in contractile mechanisms between patients with transposition of the great arteries (TGA) and congenitally corrected TGA, with motion along the anteroposterior plane dominating RV contraction in TGA and while all components (anteroposterior, longitudinal and radial) contribute equally to ventricular ejection fraction in congenitally corrected TGA (24, 61). 3DE has also facilitated characterization of RV shape and strain changes in conditions that result in chronic pressure and/or volume overload. Patients with TOF exhibited less curvature of the free wall, a more convex intraventricular septum, and significantly impaired RV strain compared to controls (62, 63).

Prognostic value of 3D echocardiography of the RV

Mixed population studies

RV function is reported to have prognostic significance in a variety of cardiovascular diseases including heart failure, PH, and coronary artery disease (**Table 3**) (1, 64–70). Importantly, 2D RV functional assessment can sometimes be inaccurate when used in these disease states. In post-cardiac surgery patients, for instance, due in part to geometrical changes associated with RV protection during bypass or alterations in interventricular septal motion after surgery, the longitudinal excursion of the RV is typically reduced despite preservation of overall RV function (71–74). TAPSE and RV S', therefore, underestimate RV function in this population and cannot be used to assess RV function. This phenomenon extends to at least 1 year post operatively. Global assessment of RV function with 3DE, however, can more accurately measure RV function in these patients suggesting that 3D RV assessment likely has wider applicability than 2DE in the remodeled or abnormal RV (75). 3D RV size and function parameters have been shown to have incremental value in the prediction of outcomes independent of left ventricular ejection fraction (67). In one study, the prevalence of patients with systolic LV dysfunction (left ventricular ejection fraction <52%) increased with worsening 3D RV ejection fraction across a population of consecutive patients with various cardiac conditions who had 3D RV acquisitions performed (68). In another retrospective study of 446 patients over a median follow up of 4.1 years, the authors showed that 3D RV ejection fraction offered incremental value over clinical risk factors and other echocardiographic parameters, including left ventricular systolic and diastolic function, for predicting future adverse outcomes including cardiac death and major adverse cardiac events (MACE) (1). The 3D RV ejection fraction cut-off values to stratify worsened prognosis were 35% for cardiac death and 41% for MACE. A prospective study of 50 patients, with a median follow-up of 16 months, found that 3D RV ejection fraction remained the only independent predictor of MACE after controlling for both clinical and echocardiographic variables, including age, New York Heart Association class, E/e' ratio, and left atrial volume index. By ROC analysis, the optimal RV ejection fraction cut-off value for event prediction was 43.4% (AUC = 0.77, $p = 0.001$), and RV ejection fraction remained an independent predictor in multivariable models when treated as a categorical variable using the cut-off of 43.4%. Categorization of 3D RV ejection fraction into the following partition values: 45%, 40%, and 30% (i.e., very low risk for mortality (RV ejection fraction >45%), low risk (40%< RV ejection fraction ≤45%), moderate risk (30%< RV ejection fraction ≤40%), and high risk (RV ejection fraction ≤30%), stratified the population into high, moderate, and low risk of cardiac death and MACE (68). Furthermore, a recent meta-analysis of ten studies including 1,928 patients identified a robust association between a one standard-deviation reduction in 3D RV ejection fraction and adverse outcomes that was stronger than 2D measures including TAPSE, FAC, and FWS (6).

3D RV parameters have also been shown to have utility in predicting adverse events in patients with heart failure with preserved ejection fraction. Meng et al. found that lower RV ejection fraction and 3D RV longitudinal strain of free wall were associated with heart failure, hospitalization, or death (69).

Pulmonary hypertension

Pulmonary hypertension has garnered a great deal of interest in the study of 3D RV applications, because the entire spectrum of RV remodelling can be documented in this cohort of patients (76). Together with 3D volumes, 3D deformation indices have an important role in the prognosis of PH patients. Specifically, changes in RV function and 3D RV area strain have been shown to be of prognostic importance and correlate more strongly with hemodynamics in RV failure than conventional echo indices (77, 78). In the pediatric PH population, 3D volumes, 3D RV ejection fraction, FAC, and free wall RV longitudinal strain were significantly associated with outcome (79). The ratio of 3D RV stroke volume to end-systolic volume (ESV) ratio as an estimate of RV-arterial coupling correlated with RV strain and was found to be a strong predictor of adverse clinical events in pediatric patients with PH (80).

Secondary tricuspid regurgitation

The ability of 3DE to characterize patterns of chamber remodelling resulting in secondary TR has prompted investigation into the prognostic impact of atrial and

TABLE 3 Studies using RV volumes, EF and strain as prognostic indices.

Publication	Study aim (s)	Parameters studied	Population and methods	Prognostic parameters
Li et al. (86)	To predict adverse clinical outcomes in CTEPH patients with 3D RV indices	RV volumes and EF	• 151 consecutive CTEPH pts Median follow up: 19.7 months	3D analysis of RVEF was a predictor of adverse clinical outcomes [hazard ratio, 1.576; 95% confidence interval (CI), 1.046–2.372; $P = 0.030$]
Meng et al. (69)	To determine whether 3D-STE parameters were the more powerful predictors of poor outcomes in HFpEF patients compared with 2D-STE indices	3D RV volumes, EF and 3D-RVFWS	• 81 consecutive patients with HFpEF After a median follow-up period of 17 months, 39 (48%) patients reached the end point of cardiovascular events	3D-STE parameters are powerful predictors of poor outcomes, providing a similar predictive value as 2D-STE indices in patients with HFpEF
Vîjîiac et al. (66)	To evaluate role of 2D RV strain and 3D RVEF in predicting adverse outcome in patients with non-ischemic dilated cardiomyopathy.	RV global longitudinal strain, RV FWS, 3DRVEF	• 50 eligible patients Median follow-up of 16 months, 29 patients reached the primary endpoint	3D RVEF is an independent predictor of major adverse cardiovascular events in patients with dilated cardiomyopathy
Wang et al. (103)	To investigate whether 2D strain and 3DE could identify impaired RV function after anthracycline exposure	RV 4CHLS, RV FWS, 3D RVEF	61 patients with diffuse large B-cell lymphoma treated with anthracycline were studied	2D STE and 3D echocardiography are valuable methods for evaluating anthracycline-related impairment of RV function in DLBCL patients receiving chemotherapy. RV FWLS and RVEF are reliable predictors of RV systolic dysfunction
Liu et al. (104)	To explore the value of RV parameters detected by 3DE in risk stratification in PAH patients	RV volumes, EF, RV FWS	91 PAH patients (34 ± 12 years, 25 males) were enrolled, among which, 42 were classified into low-risk group, while 49 were intermediate-high risk group	RV volumes, EF and free wall strain detected by 3DE were independent predictors of intermediate-high risk stratification in PAH patients, among which, RVEF showed the best predictive capacity
Tokodi et al. (73)	To explore the association between RV contraction patterns pre mitral valve surgery and post-operative RV dysfunction	3D RVEF, radial and longitudinal components of function	• 42 patients (63 ± 11 years) undergoing MV surgery Patients had pre-operative, at-discharge, and 6-months post-operative TTE's	There was a shift in RV contraction mechanics from longitudinal contraction predominance pre- and radial pre-dominance in the first 6 months post MV surgery. Pre-operative LVEF predicted post-operative RV dysfunction in patients undergoing MV surgery
Nagata et al. (1)	To determine whether 3DRVEF predicts future cardiovascular events	RV volumes, EF	446 patients with various cardiovascular diseases	3D TTE-determined RV EF was independently associated with cardiac outcomes. 3D RVEF offered incremental value over clinical risk factors and other echocardiographic parameters including LV systolic and diastolic function for predicting adverse outcome
Tamborini et al. (105)	To assess RA, RV and TA geometry and function in patients undergoing MV repair +/− TV annuloplasty	3D RA, RV volumes and tricuspid annulus	103 patients undergoing MV surgery without (54 cases) or with (49 cases) concomitant TV annuloplasty and 40 healthy controls	Patients undergoing MV surgery and TV annuloplasty had an increased TA dimensions and a more advanced remodelling of right heart chambers reflecting more advanced disease
Vitarelli et al. (70)	To investigate whether 2D, 3D RV assessment could result in better correlation with hemodynamic variables indicative of heart failure	2D and 3D volumes, EF and strain	• 73 patients (53 ± 13 years; 44% male) with chronic PH of different etiologies were studied by cardiac catheterization and echocardiography 25 precapillary PH, 23 obstructive pulmonary heart disease, 23 postcapillary PH from mitral regurgitation and 30 healthy controls	ROC curves: detecting hemodynamic signs of RV failure were 39% for 3D-RVEF (AUC 0.89), −17% for 3DGFW-RVLS (AUC 0.88), −18% for GFW-RVLS (AUC 0.88), −16% for apical-free-wall longitudinal strain (AUC 0.85), 16 mm for TAPSE (AUC 0.67), and 38% for RV-FAC (AUC 0.62)

3D, 3-dimensional; CTEPH, chronic thromboembolic pulmonary hypertension; DLBCL, doxorubicin chemotherapy; HFpEF, heart failure with preserved ejection fraction; EF, ejection fraction; MV, mitral valve; RA, right atrial; RV, right ventricular; RVFWS, right ventricular free wall strain; STE, strain echocardiography; TA, tricuspid annulus; TV, tricuspid valve; TTE, transthoracic echocardiography; PAH, pulmonary arterial hypertension.

ventricular TR. In a population of patients with moderate-severe TR, patients with atrial TR comparably exhibited a lower rate of all-cause death and hospitalization due to heart failure (81). Categorization of TR severity as mild, moderate, and severe based on 3DE-derived regurgitant volume and effective regurgitant orifice area (82) revealed progressively higher rates of all-cause death and hospitalization due to heart failure with increasing TR severity, imparting the importance of the severity grading (81, 83). As aforementioned, estimation of right ventricular-to-pulmonary artery coupling in these patients can be challenging and therefore surrogate measures derived from 3DE have been investigated. In one study, a ratio between RV

forward stroke volume and end-systolic volume less than 0.40 was associated with a higher risk of death and heart failure hospitalization (27).

It is important to note that structural tricuspid valve procedures and trials do not yet employ 3D indices of the right ventricle or tricuspid valve for decision-making (84). Data on the utility of 3D RV analysis in this space should become available shortly from the TRILUMINATE trial imaging sub-study. Additionally, there are two other studies incorporating 3D of the tricuspid valve which are currently recruiting patients: NCT05130775 and NCT05747404. The results of these studies are highly anticipated.

Pulmonary embolism/chronic thromboembolic pulmonary hypertension

Understanding the impact of a pulmonary embolism on the RV is essential in determining severity and in assessing recovery in follow-up. Here, 3DE of the RV has been shown to have the potential to serve as a useful adjunctive tool in both the acute and chronic settings. In the case of acute sub-massive pulmonary embolism, a reduced 3D RV ejection fraction was noted to be the most sensitive predictor of adverse events and signified a longer time for recovery of function at follow-up compared to 2D parameters (85). In an adult population of patients with chronic thromboembolic disease, a machine learning-based calculation of RV ejection fraction from 3D RV datasets, with a determined cut-off of approximately 31%, was a significant predictor of adverse events these in patients (86). Multiple studies utilizing 3DE have sought to characterize RV function before and after pulmonary thromboendarterectomy for management of chronic thromboembolic pulmonary hypertension. Findings revealed a consistent trend of significantly reduced chamber volume and improved systolic performance post-operatively that persisted at long-term follow-up (87–89).

Future directions

While, in the last decade, speckle tracking analysis of left ventricular performance has significantly fueled the investigation of LV mechanics and its prognostic value, the exploration of 3D RV strain has not advanced. The complex morphology of the RV chamber, the difficulty associated with imaging this chamber and the lack of dedicated software are all factors that have contributed to the sparse interest in 3D RV mechanics. More recently, with the development of different software solutions, characterization of 3D RV mechanics in healthy volunteers (90), and a variety of cardiac diseases (91) has been initiated by some investigators. 3D RV strain has been shown to be independently associated with short-term outcomes in patients undergoing cardiac surgery (73, 92), the severity of obstructive sleep apnea (93), prognostication in heart failure with preserved ejection fraction (69) and pulmonary hypertension (94, 95).

Studies performed on the left ventricle have indicated that its shape carries information independent from conventional functional measurements and is related to prognosis (96, 97). Alterations in 3D left ventricular shape have also been cited as an early manifestation of remodeling in patients with severe mitral regurgitation and normal left ventricular ejection fraction (98). Unlike the left ventricle, the peculiar morphology of the RV does not allow its shape to be simplified to resemble a simple geometrical model. For this reason, RV shape has largely been studied in terms of regional curvedness. Subtle changes in the physiological condition is reflected by local adaptation of the RV wall which can be quantitatively measured by its curvature, for example, a more locally convex or concave wall. RV curvature is altered as a consequence of the remodeling induced by pathological conditions, such as pulmonary hypertension (48, 99), volume overload (62), but also in the settings of congenital heart disease (63) and in patients with mechanical circulatory support (100).

While it has been established that 3D RV measurements are more accurate and prognostic than 2D parameters, it is notable that in the vast majority of centers around the world 3D RV dataset acquisition is not able to meet the requirements to perform a reliable quantitative analysis (19). Indeed, even when data is adequate, quantitative analysis is usually time consuming and requires well-trained echocardiographers to ensure adequate accuracy and reproducibility. This paradox produces a challenge for image-guided artificial intelligence systems of the future to predict, display, and guide echocardiographers and sonographers during image acquisition with the goal to increase the feasibility rate of subsequent 3D RV analysis. This ability already exists in a rudimentary form to guide novices to acquire and display diagnostic quality 2D images (101). Artificial intelligence solutions could also be developed with the potential to fully automate the identification and segmentation of the RV. Fusion of data obtained from different imaging planes/probe positions could theoretically be used to, for instance, address the problem of acquiring a complete dataset in abnormal and large RVs. Deep learning algorithms have already shown promise in accurately predicting 3D RV ejection fractions from two-dimensional images, identifying RV dysfunction with an accuracy equivalent to an expert (78%) and with the additional potential to predict major adverse cardiac events (102). If this combination of AI-guided algorithm allowing quality controlled acquisition, automated segmentation and multiparametric—functional, morphological and mechanical and even hemodynamic (if acquisition of invasive RV pressures and 3D echocardiographic datasets could be acquired simultaneously to develop pressure-volume loops)—quantitative analysis becomes available, it would become an important, accurate and reproducible tool for the assessment and understanding of RV pathophysiology (**Figure 11**).

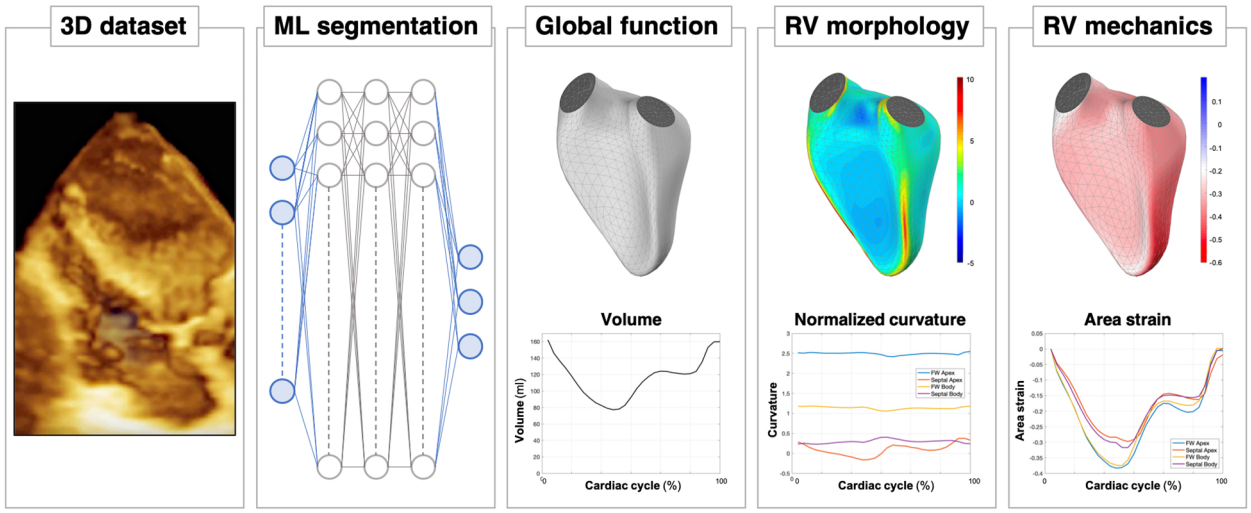

FIGURE 11
A look into the future of right ventricular assessment by 3D echocardiography: after the acquisition of the 3D dataset of the RV chamber, eventually supported by artificial intelligence (AI)-guided systems, a machine learning (ML) algorithm will be able to obtain a rapid, accurate and reproducible segmentation of the RV cavity. Based on these time-evolving surfaces, a comprehensive analysis of the RV will be automatically carried out, from conventional functional analysis (volumes and ejection fraction) to more sophisticated quantitative analyses, including morphological analysis in terms of local curvature or local mechanical function, as assessed by displacement and strain measurements.

Conclusions

3D echocardiography offers substantial advantages for comprehensively evaluating the right ventricle compared to conventional 2D echocardiographic assessment. The growth of 3DE has corresponded with an increasing number of diagnostic applications requiring global chamber assessments as well as considerable investigation into the prognostic significance of 3DE measures. Novel analysis techniques including RV strain and shape combined with automated interpretations may further expand the role of 3DE in clinical practice.

Author contributions

MR: Conceptualization, Data curation, Methodology, Writing – original draft, Writing – review & editing. FM: Conceptualization, Methodology, Writing – review & editing, Visualization. AK: Methodology, Writing – review & editing, Data curation. JG: Writing – review & editing, Conceptualization, Writing – original draft. RL: Conceptualization, Writing – original draft, Writing – review & editing, Methodology. KA: Conceptualization, Methodology, Writing – original draft, Writing – review & editing, Data curation, Resources, Supervision, Visualization.

Funding

The author(s) declare that no financial support was received for the research, authorship, and/or publication of this article.

Conflict of interest

The authors declare that the research was conducted in the absence of any commercial or financial relationships that could be construed as a potential conflict of interest.

The author(s) declared that they were an editorial board member of Frontiers, at the time of submission. This had no impact on the peer review process and the final decision.

Publisher's note

References

1. Nagata Y, Wu VCC, Kado Y, Otani K, Lin FC, Otsuji Y, et al. Prognostic value of right ventricular ejection fraction assessed by transthoracic 3D echocardiography. *Circ Cardiovasc Imaging*. (2017) 10:1–10. doi: 10.1161/CIRCIMAGING.116.005384

2. Addetia K, Muraru D, Badano LP, Lang RM. New directions in right ventricular assessment using 3-dimensional echocardiography. *JAMA Cardiol*. (2019) 4:936–44. doi: 10.1001/jamacardio.2019.2424

3. Badano LP, Addetia K, Pontone G, Torlasco C, Lang RM, Parati G, et al. Advanced imaging of right ventricular anatomy and function. *Heart*. (2020) 106:1469–76. doi: 10.1136/heartjnl-2019-315178

4. Sugeng L, Mor-Avi V, Weinert L, Niel J, Ebner C, Steringer-Mascherbauer R, et al. Multimodality comparison of quantitative volumetric analysis of the right ventricle. *JACC Cardiovasc Imaging*. (2010) 3:10–8. doi: 10.1016/j.jcmg.2009.09.017

5. Shimada YJ, Shiota M, Siegel RJ, Shiota T. Accuracy of right ventricular volumes and function determined by three-dimensional echocardiography in comparison with magnetic resonance imaging: a meta-analysis study. *J Am Soc Echocardiogr*. (2010) 23:943–53. doi: 10.1016/j.echo.2010.06.029

6. Sayour AA, Tokodi M, Celeng C, Takx RAP, Fábián A, Lakatos BK, et al. Association of right ventricular functional parameters with adverse cardiopulmonary outcomes: a meta- analysis. *J Am Soc Echocardiogr*. (2023) 36:624–33.e8. doi: 10.1016/j.echo.2023.01.018

7. Rudski LG, Lai WW, Afilalo J, Hua L, Handschumacher MD, Chandrasekaran K, et al. Guidelines for the echocardiographic assessment of the right heart in adults: a report from the American society of echocardiography. Endorsed by the European association of echocardiography, a registered branch of the European society of cardiology, and the Canadian society of echocardiography. *J Am Soc Echocardiogr*. (2010) 23:685–713. doi: 10.1016/j.echo.2010.05.010

8. Genovese D, Mor-Avi V, Palermo C, Muraru D, Volpato V, Kruse E, et al. Comparison between four-chamber and right ventricular–focused views for the quantitative evaluation of right ventricular size and function. *J Am Soc Echocardiogr*. (2019) 32:484–94. doi: 10.1016/j.echo.2018.11.014

9. Mertens LL, Friedberg MK. Imaging the right ventricleg-current state of the art. *Nat Rev Cardiol*. (2010) 7:551–63. doi: 10.1038/nrcardio.2010.118

10. Anavekar NS, Gerson D, Skali H, Kwong RY, Kent Yucel E, Solomon SD. Two-dimensional assessment of right ventricular function: an echocardiographic-MRI correlative study. *Echocardiography*. (2007) 24:452–6. doi: 10.1111/j.1540-8175.2007.00424.x

11. Focardi M, Cameli M, Carbone SF, Massoni A, De Vito R, Lisi M, et al. Traditional and innovative echocardiographic parameters for the analysis of right ventricular performance in comparison with cardiac magnetic resonance. *Eur Heart J Cardiovasc Imaging*. (2015) 16:47–52. doi: 10.1093/ehjci/jeu156

12. Namisaki H, Nabeshima Y, Kitano T, Otani K, Takeuchi M. Prognostic value of the right ventricular ejection fraction, assessed by fully automated three-dimensional echocardiography: a direct comparison of analyses using right ventricular–focused views versus apical four-chamber views. *J Am Soc Echocardiogr*. (2021) 34:117–26. doi: 10.1016/j.echo.2020.09.016

13. Laser KT, Karabiyik A, Körperich H, Horst JP, Barth P, Kececioglu D, et al. Validation and reference values for three-dimensional echocardiographic right ventricular volumetry in children: a multicenter study. *J Am Soc Echocardiogr*. (2018) 31:1050–63. doi: 10.1016/j.echo.2018.03.010

14. Muraru D, Spadotto V, Cecchetto A, Romeo G, Aruta P, Ermacora D, et al. New speckle-tracking algorithm for right ventricular volume analysis from three-dimensional echocardiographic data sets: validation with cardiac magnetic resonance and comparison with the previous analysis tool. *Eur Heart J Cardiovasc Imaging*. (2016) 17:1279–89. doi: 10.1093/ehjci/jev309

15. Medvedofsky D, Addetia K, Patel AR, Sedlmeier A, Baumann R, Mor-Avi V, et al. Novel approach to three-dimensional echocardiographic quantification of right ventricular volumes and function from focused views. *J Am Soc Echocardiogr*. (2015) 28:1222–31. doi: 10.1016/j.echo.2015.06.013

16. Tamborini G, Brusoni D, Torres Molina JE, Galli CA, Maltagliati A, Muratori M, et al. Feasibility of a new generation three-dimensional echocardiography for right ventricular volumetric and functional measurements. *Am J Cardiol*. (2008) 102:499–505. doi: 10.1016/j.amjcard.2008.03.084

17. Maffessanti F, Muraru D, Esposito R, Gripari P, Ermacora D, Santoro C, et al. Age-, body size-, and sex-specific reference values for right ventricular volumes and ejection fraction by three-dimensional echocardiography: a multicenter echocardiographic study in 507 healthy volunteers. *Circ Cardiovasc Imaging*. (2013) 6:700–10. doi: 10.1161/CIRCIMAGING.113.000706

18. Medvedofsky D, Mor-Avi V, Kruse E, Guile B, Ciszek B, Weinert L, et al. Quantification of right ventricular size and function from contrast-enhanced three-dimensional echocardiographic images. *J Am Soc Echocardiogr*. (2017) 30:1193–202. doi: 10.1016/j.echo.2017.08.003

19. Addetia K, Miyoshi T, Amuthan V, Citro R, Daimon M, Gutierrez Fajardo P, et al. Normal values of three-dimensional right ventricular size and function measurements: results of the world alliance societies of echocardiography study. *J Am Soc Echocardiogr*. (2023) 36:858–66.e1. doi: 10.1016/j.echo.2023.04.011

20. van der Zwaan HB, Geleijnse ML, McGhie JS, Boersma E, Helbing WA, Meijboom FJ, et al. Right ventricular quantification in clinical practice: two-dimensional vs. Three-dimensional echocardiography compared with cardiac magnetic resonance imaging. *Eur J Echocardiogr*. (2011) 12:656–64. doi: 10.1093/ejechocard/jer107

21. Genovese D, Rashedi N, Weinert L, Narang A, Addetia K, Patel AR, Prater D, et al. Machine learning–based three-dimensional echocardiographic quantification of right ventricular size and function: validation against cardiac magnetic resonance. *J Am Soc Echocardiogr*. (2019) 32:969–77. doi: 10.1016/j.echo.2019.04.001

22. Surkova E, Kovács A, Tokodi M, Lakatos BK, Merkely B, Muraru D, et al. Contraction patterns of the right ventricle associated with different degrees of left ventricular systolic dysfunction. *Circ Cardiovasc Imaging*. (2021) 14:E012774. doi: 10.1161/CIRCIMAGING.121.012774

23. Rako ZA, Yogeswaran A, Lakatos BK, Fábián A, Yildiz S, da Rocha BB, et al. Clinical and functional relevance of right ventricular contraction patterns in pulmonary hypertension. *J Heart Lung Transplant*. (2023) 42:1518–28. doi: 10.1016/j.healun.2023.07.004

24. Surkova E, Kovács A, Lakatos BK, Tokodi M, Fábián A, West C, et al. Contraction patterns of the systemic right ventricle: a three-dimensional echocardiography study. *Eur Heart J Cardiovasc Imaging*. (2022) 23:1654–62. doi: 10.1093/ehjci/jeab272

25. Tokodi M, Staub L, Budai Á, Lakatos BK, Csákvári M, Suhai FI, et al. Partitioning the right ventricle into 15 segments and decomposing its motion using 3D echocardiography- based models: the updated ReVISION method. *Front Cardiovasc Med*. (2021) 8:1–18. doi: 10.3389/fcvm.2021.622118

26. Lakatos B, Tősér Z, Tokodi M, Doronina A, Kosztin A, Muraru D, et al. Quantification of the relative contribution of the different right ventricular wall motion components to right ventricular ejection fraction: the ReVISION method. *Cardiovasc Ultrasound*. (2017) 15:1–9. doi: 10.1186/s12947-017-0100-0

27. Gavazzoni M, Badano LP, Cascella A, Heilbron F, Tomaselli M, Caravita S, et al. Clinical value of a novel three-dimensional echocardiography–derived index of right ventricle–pulmonary artery coupling in tricuspid regurgitation. *J Am Soc Echocardiogr*. (2023) 36:1154–66.e3. doi: 10.1016/j.echo.2023.06.014

28. Gopal AS, Chukwu EO, Iwuchukwu CJ, Katz AS, Toole RS, Schapiro W, et al. Normal values of right ventricular size and function by real-time 3-dimensional echocardiography: comparison with cardiac magnetic resonance imaging. *J Am Soc Echocardiogr*. (2007) 20:445–55. doi: 10.1016/j.echo.2006.10.027

29. Aune E, Baekkevar M, Rodevand O, Otterstad JE. The limited usefulness of real-time 3-dimensional echocardiography in obtaining normal reference ranges for right ventricular volumes. *Cardiovasc Ultrasound*. (2009) 7:1–9. doi: 10.1186/1476-7120-7-35

30. Xie E, Yu R, Ambale-Venkatesh B, Bakhshi H, Heckbert SR, Soliman EZ, et al. Association of right atrial structure with incident atrial fibrillation: a longitudinal cohort cardiovascular magnetic resonance study from the multi-ethnic study of atherosclerosis (MESA). *J Cardiovasc Magn Reson*. (2020) 22:1–10. doi: 10.1186/s12968-020-00631-1

31. Kawel-Boehm N, Maceira A, Valsangiacomo-Buechel ER, Vogel-Claussen J, Turkbey EB, Williams R, et al. Normal values for cardiovascular magnetic resonance in adults and children. *J Cardiovasc Magn Reson*. (2015) 17:1–34. doi: 10.1186/s12968-015-0111-7

32. Naser JA, Kucuk HO, Ciobanu AO, Jouni H, Oguz D, Thaden JJ, et al. Atrial fibrillation is associated with large beat-to-beat variability in mitral and tricuspid annulus dimensions. *Eur Heart J Cardiovasc Imaging*. (2021) 22:1362–73. doi: 10.1093/ehjci/jeab033

33. Addetia K, Muraru D, Veronesi F, Jenei C, Cavalli G, Besser SA, et al. 3-dimensional echocardiographic analysis of the tricuspid Annulus provides new insights into tricuspid valve geometry and dynamics. *JACC Cardiovasc Imaging*. (2019) 12:401–12. doi: 10.1016/j.jcmg.2017.08.022

34. Muraru D, Hahn RT, Soliman OI, Faletra FF, Basso C, Badano LP. 3-dimensional echocardiography in imaging the tricuspid valve. *JACC Cardiovasc Imaging*. (2019) 12:500–15. doi: 10.1016/j.jcmg.2018.10.035

35. Muraru D, Gavazzoni M, Heilbron F, Mihalcea DJ, Guta AC, Radu N, et al. Reference ranges of tricuspid annulus geometry in healthy adults using a dedicated three-dimensional echocardiography software package. *Front Cardiovasc Med*. (2022) 9:1–15. doi: 10.3389/fcvm.2022.1011931

36. Grapsa J, Gibbs JSR, Cabrita IZ, Watson GF, Pavlopoulos H, Dawson D, et al. The association of clinical outcome with right atrial and ventricular remodelling in patients with pulmonary arterial hypertension: study with real-time three-dimensional echocardiography. *Eur Heart J Cardiovasc Imaging*. (2012) 13:666–72. doi: 10.1093/ehjci/jes003

37. Peluso D, Badano LP, Muraru D, Dal Bianco L, Cucchini U, Kocabay G, et al. Right atrial size and function assessed with three-dimensional and speckle-tracking echocardiography in 200 healthy volunteers. *Eur Heart J Cardiovasc Imaging*. (2013) 14:1106–14. doi: 10.1093/ehjci/jet024

38. Lang RM, Cameli M, Sade LE, Faletra FF, Fortuni F, Rossi A, et al. Imaging assessment of the right atrium: anatomy and function. *Eur Heart J Cardiovasc Imaging*. (2022) 23:867–84. doi: 10.1093/ehjci/jeac011

39. Ferrara F, Gargani L, Ruohonen S, Vriz O, Scalese M, Russo V, et al. Reference values and correlates of right atrial volume in healthy adults by two-dimensional echocardiography. *Echocardiography*. (2018) 35:1097–107. doi: 10.1111/echo.14015

40. Kou S, Caballero L, Dulgheru R, Voilliot D, De Sousa C, Kacharava G, et al. Echocardiographic reference ranges for normal cardiac chamber size: results from the NORRE study. *Eur Heart J Cardiovasc Imaging*. (2014) 15:680–90. doi: 10.1093/ehjci/jet284

41. Soulat-Dufour L, Addetia K, Miyoshi T, Citro R, Daimon M, Fajardo PG, et al. Normal values of right atrial size and function according to age, sex, and ethnicity: results of the world alliance societies of echocardiography study. *J Am Soc Echocardiogr*. (2021) 34:286–300. doi: 10.1016/j.echo.2020.11.004

42. Prihadi EA, Delgado V, Leon MB, Enriquez-Sarano M, Topilsky Y, Bax JJ. Morphologic types of tricuspid regurgitation: characteristics and prognostic implications. *JACC Cardiovasc Imaging*. (2019) 12:491–9. doi: 10.1016/j.jcmg.2018.09.027

43. Kim HK, Kim YJ, Park JS, Kim KH, Kim KB, Ahn H, et al. Determinants of the severity of functional tricuspid regurgitation. *Am J Cardiol*. (2006) 98:236–42. doi: 10.1016/j.amjcard.2006.01.082

44. Florescu DR, Muraru D, Florescu C, Volpato V, Caravita S, Perger E, et al. Right heart chambers geometry and function in patients with the atrial and the ventricular phenotypes of functional tricuspid regurgitation. *Eur Heart J Cardiovasc Imaging*. (2022) 23:930–40. doi: 10.1093/ehjci/jeab211

45. Topilsky Y, Khanna A, Le Toumeau T, Park S, Michelena H, Suri R, et al. Clinical context and mechanism of functional tricuspid regurgitation in patients with and without pulmonary hypertension. *Circ Cardiovasc Imaging*. (2012) 5:314–23. doi: 10.1161/CIRCIMAGING.111.967919

46. Utsunomiya H, Itabashi Y, Mihara H, Berdejo J, Kobayashi S, Siegel RJ, et al. Functional tricuspid regurgitation caused by chronic atrial fibrillation: a real-time 3-dimensional transesophageal echocardiography study. *Circ Cardiovasc Imaging*. (2017) 10:1–11. doi: 10.1161/CIRCIMAGING.116.004897

47. Soulat-Dufour L, Lang S, Addetia K, Ederhy S, Adavane-Scheuble S, Chauvet-Droit M, et al. Restoring sinus rhythm reverses cardiac remodeling and reduces valvular regurgitation in patients with atrial fibrillation. *J Am Coll Cardiol*. (2022) 79:951–61. doi: 10.1016/j.jacc.2021.12.029

48. Addetia K, Maffessanti F, Yamat M, Weinert L, Narang A, Freed BH, et al. Three-dimensional echocardiography-based analysis of right ventricular shape in pulmonary arterial hypertension. *Eur Heart J Cardiovasc Imaging*. (2016) 17:564–75. doi: 10.1093/ehjci/jev171

49. Seo Y, Ishizu T, Nakajima H, Sekiguchi Y, Watanabe S, Aonuma K. Clinical utility of 3-dimensional echocardiography in the evaluation of tricuspid regurgitation caused by pacemaker leads. *Circ J*. (2008) 72:1465–70. doi: 10.1253/circj.CJ-08-0227

50. Cheng Y, Gao H, Tang L, Li J, Yao L. Clinical utility of three-dimensional echocardiography in the evaluation of tricuspid regurgitation induced by implantable device leads. *Echocardiography*. (2016) 33:1689–96. doi: 10.1111/echo.13314

51. Poorzand H, Tayyebi M, Hosseini S, Bakavoli AH, Keihanian F, Jarahi L, et al. Predictors of worsening TR severity after right ventricular lead placement: any added value by post-procedural fluoroscopy versus three–dimensional echocardiography? *Cardiovasc Ultrasound*. (2021) 19:1–9. doi: 10.1186/s12947-021-00267-w

52. Mediratta A, Addetia K, Yamat M, Moss JD, Nayak HM, Burke MC, et al. 3D echocardiographic location of implantable device leads and mechanism of associated tricuspid regurgitation. *JACC Cardiovasc Imaging*. (2014) 7:337–47. doi: 10.1016/j.jcmg.2013.11.007

53. Henry M, Abutaleb AR, Jeevanandam V, Smith H, Belkin M, Husain A, et al. Anatomic description of tricuspid apparatus interference from implantable intracardiac devices. *JACC Cardiovasc Imaging*. (2022) 15:361–5. doi: 10.1016/j.jcmg.2020.12.016

54. Malik N, Mukherjee M, Wu KC, Zimmerman SL, Zhan J, Calkins H, et al. Multimodality imaging in arrhythmogenic right ventricular cardiomyopathy. *Circ Cardiovasc Imaging*. (2022) 15:e013725. doi: 10.1161/CIRCIMAGING.121.013725

55. Prakasa KR, Dalal D, Wang J, Bomma C, Tandri H, Dong J, et al. Feasibility and variability of three dimensional echocardiography in arrhythmogenic right ventricular dysplasia/cardiomyopathy. *Am J Cardiol*. (2006) 97:703–9. doi: 10.1016/j.amjcard.2005.11.020

56. Addetia K, Mazzanti A, Maragna R, Monti L, Yamat M, Kukavica D, et al. Value of 3D echocardiography in the diagnosis of arrhythmogenic right ventricular cardiomyopathy. *Eur Heart J Cardiovasc Imaging*. (2023) 24:664–77. doi: 10.1093/ehjci/jeac172

57. van der Zwaan HB, Helbing WA, McGhie JS, Geleijnse ML, Luijnenburg SE, Roos-Hesselink JW, et al. Clinical value of real-time three-dimensional echocardiography for right ventricular quantification in congenital heart disease: validation with cardiac magnetic resonance imaging. *J Am Soc Echocardiogr*. (2010) 23:134–40. doi: 10.1016/j.echo.2009.12.001

58. Grewal J, Majdalany D, Syed I, Pellikka P, Warnes CA. Three-dimensional echocardiographic assessment of right ventricular volume and function in adult patients with congenital heart disease: comparison with magnetic resonance imaging. *J Am Soc Echocardiogr*. (2010) 23:127–33. doi: 10.1016/j.echo.2009.11.002

59. Dragulescu A, Grosse-Wortmann L, Fackoury C, Mertens L. Echocardiographic assessment of right ventricular volumes: a comparison of different techniques in children after surgical repair of tetralogy of fallot. *Eur Heart J Cardiovasc Imaging*. (2012) 13:596–604. doi: 10.1093/ejechocard/jer278

60. Crean AM, Maredia N, Ballard G, Menezes R, Wharton G, Forster J, et al. 3D echo systematically underestimates right ventricular volumes compared to cardiovascular magnetic resonance in adult congenital heart disease patients with moderate or severe RV dilatation. *J Cardiovasc Magn Reson*. (2011) 13:1–9. doi: 10.1186/1532-429X-13-78

61. Surkova E, Kovács A, Lakatos BK, Li W. Anteroposterior contraction of the systemic right ventricle: underrecognized component of the global systolic function. *JACC Case Rep*. (2021) 3:728–30. doi: 10.1016/j.jaccas.2021.02.029

62. Bidviene J, Muraru D, Maffessanti F, Ereminiene E, Kovács A, Lakatos B, et al. Regional shape, global function and mechanics in right ventricular volume and pressure overload conditions: a three-dimensional echocardiography study. *Int J Cardiovasc Imaging*. (2021) 37:1289–99. doi: 10.1007/s10554-020-02117-8

63. Moceri P, Duchateau N, Gillon S, Jaunay L, Baudouy D, Squara F, et al. Three-dimensional right ventricular shape and strain in congenital heart disease patients with right ventricular chronic volume loading. *Eur Heart J Cardiovasc Imaging*. (2021) 22:1174–81. doi: 10.1093/ehjci/jeaa189

64. Magunia H, Dietrich C, Langer HF, Schibilsky D, Schlensak C, Rosenberger P, et al. 3D echocardiography derived right ventricular function is associated with right ventricular failure and mid-term survival after left ventricular assist device implantation. *Int J Cardiol*. (2018) 272:348–55. doi: 10.1016/j.ijcard.2018.06.026

65. Kiernan MS, French AL, Denofrio D, Parmar YJ, Pham DT, Kapur NK, et al. Preoperative three-dimensional echocardiography to assess risk of right ventricular failure after left ventricular assist device surgery. *J Card Fail*. (2015) 21:189–97. doi: 10.1016/j.cardfail.2014.12.009

66. Vîjiiac A, Onciul S, Guzu C, Verinceanu V, Bătăilă V, Deaconu S, et al. The prognostic value of right ventricular longitudinal strain and 3D ejection fraction in patients with dilated cardiomyopathy. *Int J Cardiovasc Imaging*. (2021) 37:3233–44. doi: 10.1007/s10554-021-02322-z

67. Surkova E, Muraru D, Genovese D, Aruta P, Palermo C, Badano LP. Relative prognostic importance of left and right ventricular ejection fraction in patients with cardiac diseases. *J Am Soc Echocardiogr*. (2019) 32:1407–15.e3. doi: 10.1016/j.echo.2019.06.009

68. Muraru D, Badano LP, Nagata Y, Surkova E, Nabeshima Y, Genovese D, et al. Development and prognostic validation of partition values to grade right ventricular dysfunction severity using 3D echocardiography. *Eur Heart J Cardiovasc Imaging*. (2020) 21:10–21. doi: 10.1093/ehjci/jez233

69. Meng Y, Zhu S, Xie Y, Zhang Y, Qian M, Gao L, et al. Prognostic value of right ventricular 3D speckle-tracking strain and ejection fraction in patients with HFpEF. *Front Cardiovasc Med*. (2021) 8:1–10. doi: 10.3389/fcvm.2021.694365

70. Vitarelli A, Mangieri E, Terzano C, Gaudio C, Salsano F, Rosato E, et al. Three-dimensional echocardiography and 2D-3D speckle-tracking imaging in chronic pulmonary hypertension: diagnostic accuracy in detecting hemodynamic signs of right ventricular (RV) failure. *J Am Heart Assoc*. (2015) 4:1–14. doi: 10.1161/JAHA.114.001584

71. Keyl C, Schneider J, Beyersdorf F, Ruile P, Siepe M, Pioch K, et al. Right ventricular function after aortic valve replacement: a pilot study comparing surgical and transcatheter procedures using 3D echocardiography. *Eur J Cardiothorac Surg*. (2016) 49:966–71. doi: 10.1093/ejcts/ezv227

72. Raina A, Vaidya A, Gertz ZM, Chambers S, Forfia PR. Marked changes in right ventricular contractile pattern after cardiothoracic surgery: implications for post-surgical assessment of right ventricular function. *J Heart Lung Transplant*. (2013) 32:777–83. doi: 10.1016/j.healun.2013.05.004

73. Tokodi M, Németh E, Lakatos BK, Kispál E, Tősér Z, Staub L, et al. Right ventricular mechanical pattern in patients undergoing mitral valve surgery: a predictor of post-operative dysfunction? *ESC Heart Fail*. (2020) 7:1246–56. doi: 10.1002/ehf2.12682

74. Lakatos BK, Tokodi M, Assabiny A, Tősér Z, Kosztin A, Doronina A, et al. Dominance of free wall radial motion in global right ventricular function of heart transplant recipients. *Clin Transplant*. (2018) 32:1–10. doi: 10.1111/ctr.13192

75. Tamborini G, Muratori M, Brusoni D, Celeste F, Maffessanti F, Caiani EG, et al. Is right ventricular systolic function reduced after cardiac surgery? A two- and three-dimensional echocardiographic study. *Eur J Echocardiogr*. (2009) 10:630–4. doi: 10.1093/ejechocard/jep015

76. Grapsa J, Gibbs JSR, Dawson D, Watson G, Patni R, Athanasiou T, et al. Morphologic and functional remodeling of the right ventricle in pulmonary hypertension by real time three dimensional echocardiography. *Am J Cardiol*. (2012) 109:906–13. doi: 10.1016/j.amjcard.2011.10.054

77. Moceri P, Duchateau N, Baudouy D, Squara F, Bun SS, Ferrari E, et al. Additional prognostic value of echocardiographic follow-up in pulmonary hypertension-role of 3D right ventricular area strain. *Eur Heart J Cardiovasc Imaging*. (2022) 23:1562–72. doi: 10.1093/ehjci/jeab240

78. Smith BCF, Dobson G, Dawson D, Charalampopoulos A, Grapsa J, Nihoyannopoulos P. Three-dimensional speckle tracking of the right ventricle: toward optimal quantification of right ventricular dysfunction in pulmonary hypertension. *J Am Coll Cardiol*. (2014) 64:41–51. doi: 10.1016/j.jacc.2014.01.084

79. Jone PN, Schäfer M, Pan Z, Bremen C, Ivy DD. 3D echocardiographic evaluation of right ventricular function and strain: a prognostic study in paediatric pulmonary hypertension. *Eur Heart J Cardiovasc Imaging*. (2018) 19:1026–33. doi: 10.1093/ehjci/jex205

80. Jone PN, Schäfer M, Pan Z, Ivy DD. Right ventricular-arterial coupling ratio derived from 3-dimensional echocardiography predicts outcomes in pediatric pulmonary hypertension. *Circ Cardiovasc Imaging*. (2019) 12:e008176. doi: 10.1161/CIRCIMAGING.118.008176

81. Gavazzoni M, Heilbron F, Badano LP, Radu N, Cascella A, Tomaselli M, et al. The atrial secondary tricuspid regurgitation is associated to more favorable outcome

than the ventricular phenotype. *Front Cardiovasc Med*. (2022) 9:1–11. doi: 10.3389/fcvm.2022.1022755

82. Tomaselli M, Badano LP, Menè R, Gavazzoni M, Heilbron F, Radu N, et al. Impact of correcting the 2D PISA method on the quantification of functional tricuspid regurgitation severity. *Eur Heart J Cardiovasc Imaging*. (2022) 23:1459–70. doi: 10.1093/ehjci/jeac104

83. Muraru D, Previtero M, Ochoa-Jimenez RC, Guta AC, Figliozzi S, Gregori D, et al. Prognostic validation of partition values for quantitative parameters to grade functional tricuspid regurgitation severity by conventional echocardiography. *Eur Heart J Cardiovasc Imaging*. (2021) 22:155–65. doi: 10.1093/ehjci/jeaa282

84. Sorajja P, Whisenant B, Hamid N, Naik H, Makkar R, Tadros P, et al. Transcatheter repair for patients with tricuspid regurgitation. *N Engl J Med*. (2023) 388:1833–42. doi: 10.1056/NEJMoa2300525

85. Vitarelli A, Barillà F, Capotosto L, D'Angeli I, Truscelli G, De Maio M, et al. Right ventricular function in acute pulmonary embolism: a combined assessment by three-dimensional and speckle-tracking echocardiography. *J Am Soc Echocardiogr*. (2014) 27:329–38. doi: 10.1016/j.echo.2013.11.013

86. Li Y, Liang L, Guo D, Yang Y, Gong J, Zhang X, et al. Right ventricular function predicts adverse clinical outcomes in patients with chronic thromboembolic pulmonary hypertension: a three-dimensional echocardiographic study. *Front Med*. (2021) 8:1–11. doi: 10.3389/fmed.2021.697396

87. Waziri F, Mellemkjær S, Clemmensen TS, Hjortdal VE, Ilkjær LB, Nielsen SL, et al. Long-term changes of resting and exercise right ventricular systolic performance in patients with chronic thromboembolic pulmonary hypertension following pulmonary thromboendarterectomy – A two-dimensional and three-dimensional echocardiographic study. *Echocardiography*. (2019) 36:1656–65. doi: 10.1111/echo.14456

88. Cronin B, O'Brien EO, Gu W, Banks D, Maus T. Intraoperative 3-dimensional echocardiography–derived right ventricular volumetric analysis in chronic thromboembolic pulmonary hypertension patients before and after pulmonary thromboendarterectomy. *J Cardiothorac Vasc Anesth*. (2019) 33:1498–503. doi: 10.1053/j.jvca.2018.09.038

89. Menzel T, Kramm T, Brückner A, Mohr-Kahaly S, Mayer E, Meyer J. Quantitative assessment of right ventricular volumes in severe chronic thromboembolic pulmonary hypertension using transthoracic three-dimensional echocardiography: changes due to pulmonary thromboendarterectomy. *Eur J Echocardiogr*. (2002) 3:67–72. doi: 10.1053/euje.2001.0129

90. Lakatos BK, Nabeshima Y, Tokodi M, Nagata Y, Tősér Z, Otani K, et al. Importance of nonlongitudinal motion components in right ventricular function: three-dimensional echocardiographic study in healthy volunteers. *J Am Soc Echocardiogr*. (2020) 33:995–1005.e1. doi: 10.1016/j.echo.2020.04.002

91. Kitano T, Kovács A, Nabeshima Y, Tokodi M, Fábián A, Lakatos BK, et al. Prognostic value of right ventricular strains using novel three-dimensional analytical software in patients with cardiac disease. *Front Cardiovasc Med*. (2022) 9:1–12. doi: 10.3389/fcvm.2022.837584

92. Keller M, Heller T, Duerr MM, Schlensak C, Nowak-Machen M, Feng YS, et al. Association of three-dimensional mesh-derived right ventricular strain with short-term outcomes in patients undergoing cardiac surgery. *J Am Soc Echocardiogr*. (2022) 35:408–18. doi: 10.1016/j.echo.2021.11.008

93. Chetan IM, Gergely-Domokos B, Beyer R, Tomoaia R, Cabau G, Vulturar D, et al. The role of 3D speckle tracking echocardiography in the diagnosis of obstructive sleep apnea and its severity. *Sci Rep*. (2022) 12:1–11. doi: 10.1038/s41598-022-26940-2

94. Satriano A, Pournazari P, Hirani N, Helmersen D, Thakrar M, Weatherald J, et al. Characterization of right ventricular deformation in pulmonary arterial hypertension using three-dimensional principal strain analysis. *J Am Soc Echocardiogr*. (2019) 32:385–93. doi: 10.1016/j.echo.2018.10.001

95. Jone PN, Duchateau N, Pan Z, Ivy DD, Moceri P. Right ventricular area strain from 3-dimensional echocardiography: mechanistic insight of right ventricular dysfunction in pediatric pulmonary hypertension. *J Heart Lung Transplant*. (2021) 40:138–48. doi: 10.1016/j.healun.2020.11.005

96. Douglas PS, Morrow R, Ioli A, Reichek N. Left ventricular shape, afterload and survival in idiopathic dilated cardiomyopathy. *JACC*. (1989) 13:311–5. doi: 10.1016/0735-1097(89)90504-4

97. Tischler MD, Niggel J, Borowski DT, Lewinter MM. Relation between left ventricular shape and exercise capacity in patients with left ventricular dysfunction. *J Am Coll Cardiol*. (1993) 22:751–7. doi: 10.1016/0735-1097(93)90187-6

98. Maffessanti F, Caiani EG, Tamborini G, Muratori M, Sugeng L, Weinert L, et al. Serial changes in left ventricular shape following early mitral valve repair. *Am J Cardiol*. (2010) 106:836–42. doi: 10.1016/j.amjcard.2010.04.044

99. Sciancalepore MA, Maffessanti F, Patel AR, Gomberg-Maitland M, Chandra S, Freed BH, et al. Three-dimensional analysis of interventricular septal curvature from cardiac magnetic resonance images for the evaluation of patients with pulmonary hypertension. *Int J Cardiovasc Imaging*. (2012) 28:1073–85. doi: 10.1007/s10554-011-9913-3

100. Addetia K, Uriel N, Maffessanti F, Sayer G, Adatya S, Kim GH, et al. 3D morphological changes in LV and RV during LVAD ramp studies. *JACC Cardiovasc Imaging*. (2018) 11:159–69. doi: 10.1016/j.jcmg.2016.12.019

101. Narang A, Bae R, Hong H, Thomas Y, Surette S, Cadieu C, et al. Utility of a deep-learning algorithm to guide novices to acquire echocardiograms for limited diagnostic use. *JAMA Cardiol*. (2021) 6:624–32. doi: 10.1001/jamacardio.2021.0185

102. Tokodi M, Magyar B, Soós A, Takeuchi M, Tolvaj M, Lakatos BK, et al. Deep learning-based prediction of right ventricular ejection fraction using 2D echocardiograms. *JACC Cardiovasc Imaging*. (2023) 16:1005–18. doi: 10.1016/j.jcmg.2023.02.017

103. Wang B, Yu Y, Zhang Y, Hao X, Yang S, Zhao H, et al. Right ventricular dysfunction in patients with diffuse large B-cell lymphoma undergoing anthracycline-based chemotherapy: a 2D strain and 3D echocardiography study. *Int J Cardiovasc Imaging*. (2021) 37:1311–9. doi: 10.1007/s10554-020-02120-z

104. Liu K, Zhang C, Chen B, Li M, Zhang P. Association between right atrial area measured by echocardiography and prognosis among pulmonary arterial hypertension: a systematic review and meta-analysis. *BMJ Open*. (2020) 10:1–8. doi: 10.1136/bmjopen-2019-031316

105. Tamborini G, Fusini L, Muratori M, Gripari P, Ghulam Ali S, Fiorentini C, et al. Right heart chamber geometry and tricuspid annulus morphology in patients undergoing mitral valve repair with and without tricuspid valve annuloplasty. *Int J Cardiovasc Imaging*. (2016) 32:885–94. doi: 10.1007/s10554-016-0846-8

Frontiers in
Cardiovascular Medicine

Innovations and improvements in cardiovascular treatment and practice

Focuses on research that challenges the status quo of cardiovascular care, or facilitates the translation of advances into new therapies and diagnostic tools.

Discover the latest Research Topics

See more →

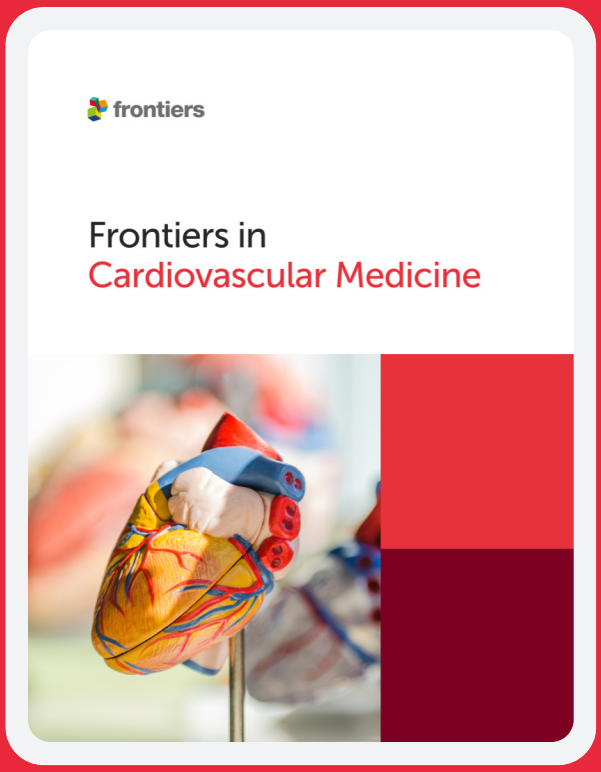

Frontiers

Avenue du Tribunal-Fédéral 34
1005 Lausanne, Switzerland
frontiersin.org

Contact us

+41 (0)21 510 17 00
frontiersin.org/about/contact